

© 2012 by Gavin Kumar Ananda Krishnan. All rights reserved.

AERODYNAMIC PERFORMANCE OF LOW-TO-MODERATE ASPECT RATIO WINGS AT
LOW REYNOLDS NUMBERS

BY

GAVIN KUMAR ANANDA KRISHNAN

THESIS

Submitted in partial fulfillment of the requirements
for the degree of Master of Science in Aerospace Engineering
in the Graduate College of the
University of Illinois at Urbana-Champaign, 2012

Urbana, Illinois

Adviser:

Professor Michael Selig

Abstract

This thesis presents wind tunnel results of wings of low-to-moderate aspect ratio ($2 \leq A \leq 5$) tested at low Reynolds numbers (40,000 to 160,000). All models tested had a chord length of 3 in and a wingspan of 7 to 17.5 in. Experiments were conducted in the low-turbulence wind tunnel in the Subsonic Aerodynamics Research Laboratory at the University of Illinois at Urbana-Champaign (UIUC). An external three-component platform force balance was designed, fabricated and assembled to perform the experiments. The balance design methodology, calibration methodology, experimental setup, wing mounting setup validation and historical data comparisons are described in detail. Low Reynolds number tests performed on a rectangular wing having an aspect ratio of 4 and using the Wortmann FX 63-137 airfoil showed the existence of a critical Reynolds number of 90,000 for which a jump in performance characteristics was observed. Pre-stall and post-stall hysteresis was captured at the critical Reynolds number. Flow visualization photographs for the Wortmann wing at different angles of attack are presented. Finally, aerodynamic performance measurements taken for ten flat-plate rectangular and tapered wings are also presented and discussed. A detailed analysis of trends from aerodynamic performance measurements taken for the ten flat-plate wings showed a number of interesting effects with respect to Reynolds number, aspect ratio, and taper ratio. No critical Reynolds number and aerodynamic hysteresis was however found for the flat-plate wings in the Reynolds number range tested.

To mummy, papa and Anu

Acknowledgments

First and foremost, I would like to take this opportunity to thank my parents for their unconditional love and support throughout my life. Never wavering in supplying me and my sister with every opportunity possible to pursue our dreams, their belief in me has made it possible to complete my masters at UIUC.

I would like to greatly acknowledge the contributions of my adviser, Prof. Michael Selig. With nothing but my assurances and belief, he wholly trusted and supported me in creating a new low Reynolds number three-component wind tunnel balance. I have his learned and experienced guidance to thank for turning my paper dreams into a reality.

To Pritam Sukumar, without your help with the endless hours of summer machining and a trip to the emergency room, the fabrication and assembly of the wind tunnel balance would not have been possible. To Rob Deters, your guidance in teaching me about the LSATs rig, the wind tunnel testing methodology and providing help with any concerns helped me greatly in designing the wind tunnel balance and performing wind tunnel tests. I would like to acknowledge the contributions of the following individuals of whom have contributed greatly to the long hours of calibration and wind tunnel testing: Agrim Sareen, Andrew Jang, Arjun Rao, Chinmay Sapre, Gregory Williamson, Harshit Parolia, Pritam Sukumar and Shreyas Narsipur. I would also like to express my gratitude to Scott McDonald, Greggory Bennett and David Switzer from the ECE Machine shop for their help and guidance in helping me machine the components of the wind tunnel balance.

Finally, to Amrita, words can't express how thankful I am to have your presence in my life. You have given me the extra impetus and motivation to do the best I can in everything I do.

Table of Contents

	Page
List of Figures	vii
List of Tables	xi
Nomenclature	xii
Chapter 1 Introduction	1
Chapter 2 Low Reynolds Number Aerodynamics	3
2.1 Fundamentals of Fluid Dynamics	3
2.2 Two-Dimensional Aerodynamics	4
2.2.1 Laminar Separation Bubble	4
2.2.2 Boundary Layer Management	7
2.3 Three-Dimensional Aerodynamics	8
2.3.1 High Aspect Ratio Wings	8
2.3.2 Low Aspect Ratio Wings	9
2.4 Motivation for Testing	11
Chapter 3 Testing Facility and Experimental Techniques	13
3.1 Experimental Facility	13
3.2 Force Balance	15
3.2.1 Design	15
3.2.2 Fabrication and Assembly	19
3.2.3 Alignment and Installation	20
3.3 Measurement Techniques	23
3.3.1 Data Acquisition System	23
3.3.2 Lift, Drag, and Pitching Moment Measurements	23
3.3.3 Freestream Velocity Measurements	24
3.3.4 Angle of Attack Measurements	25
3.4 Force and Moment Calibration	27
3.4.1 Linear Calibration (Lift and Drag)	27
3.4.2 Non-linear Calibration (Moment)	30
3.5 Wind Tunnel Models	32
3.6 Flow Visualization Technique	36
3.7 Tare and Interference Determination	38
3.8 Data Correction	41
3.8.1 Buoyancy Effects	41

3.8.2	Solid Blockage	41
3.8.3	Wake Blockage	42
3.8.4	Final Blockage Corrections	42
3.8.5	Streamline Curvature	43
3.9	Uncertainty Analysis	44
3.9.1	Uncertainty Equations	44
3.9.2	Example Test Case Uncertainty Calculation	47
Chapter 4 Data Validation	49
4.1	Wortmann FX 63-137 Wing (Check Standard) Validation	49
4.2	\mathcal{R} -3 Rectangular Flat-Plate Wing Validation	53
4.3	Repeatability of Measurements	56
Chapter 5 Experimental Results	58
Chapter 6 Discussion of Results	101
6.1	Wortmann FX 63-137 Wing Results	101
6.2	Flat-Plate Wing Results	105
6.2.1	Reynolds Number Effects	105
6.2.2	Aspect Ratio Effects	111
6.2.3	Taper Ratio Effects	113
6.3	Performance Comparison of \mathcal{R} -4 Rectangular Wings	114
Chapter 7 Summary, Conclusions, and Future Work	116
7.1	Summary and Conclusions	116
7.2	Future Work	117
Appendix A Tabulated Airfoil Coordinates	119
Appendix B Tabulated Drag Polar Data	120
Appendix C Tabulated Lift and Moment Data	150
Appendix D LRN-FB Drawings	180
References	215

List of Figures

Figure	Page
2.1 Boundary layer over a flat plate.	4
2.2 Structure of laminar separation bubble (taken from Ref. 20).	5
2.3 Low Reynolds number airfoil hysteresis effects (taken from Ref. 19).	6
2.4 Low Reynolds number airfoil performance (taken from Ref. 18).	6
2.5 Effect of laminar separation bubble on lift-drag polar (taken from Ref. 18).	7
2.6 Schematic of flowfield for a rectangular planform wing at low Reynolds numbers (taken from Ref. 32).	9
2.7 Leading-edge flow conditions (taken from Ref. 36).	10
2.8 Micro air vehicle designs (taken from Ref. 1).	11
 3.1 UIUC low-speed subsonic wind tunnel.	14
3.2 Photograph of wind tunnel fan and stators (photograph by Gregory Williamson). .	14
3.3 Photograph of wind tunnel inlet showing the honeycomb (photograph by Gregory Williamson).	15
3.4 UIUC LRN-FB setup in tunnel test section.	16
3.5 Side view of UIUC LRN-FB experimental setup.	17
3.6 LRN-FB lift and drag force balance platform.	17
3.7 Annotated LRN-FB lift and drag platforms.	19
3.8 Annotated LRN-FB pitching moment and angle-of-attack setup side and sectional view.	20
3.9 UIUC LRN-FB CAD model and photograph.	21
3.10 UIUC LRN-FB components.	22
3.11 Angle-of-attack alignment method.	26
3.12 LRN-FB calibration setup.	28
3.13 Airfoils of wings tested: Wortmann FX 63-137 airfoil (smooth) and 5-to-1 elliptical leading edge, 10-to-1 elliptical trailing edge flat plate.	34
3.14 Isometric view of all wings tested.	35
3.15 Upper surface oil flow visualization of major flow features on the Wortmann FX 63-137 \mathcal{R} -4 rectangular wing ($\alpha = 9$ deg, $Re = 90,000$).	37
3.16 Experimental setup for mirror sting interference tests.	39
3.17 Upper surface oil flow visualization photographs.	40
 4.1 Lift comparison results for the Wortmann FX 63-137 airfoil and \mathcal{R} -4 rectangular wing.	51
4.2 Drag comparison results for the Wortmann FX 63-137 \mathcal{R} -4 rectangular wing. . . .	52

4.3	Moment comparison results for the Wortmann FX 63-137 airfoil and \mathcal{R} -4 rectangular wing.	52
4.4	Lift comparison results for the \mathcal{R} -3 rectangular flat-plate wing at a Reynolds number of 80,000.	53
4.5	Drag comparison results for the \mathcal{R} -3 rectangular flat-plate wing at a Reynolds number of 80,000.	54
4.6	Moment comparison results for the \mathcal{R} -3 rectangular flat-plate wing at a Reynolds number of 80,000.	55
4.7	Drag polar comparison results for the \mathcal{R} -3 rectangular flat-plate wing at a Reynolds number of 80,000.	55
4.8	Repeatability of the Wortmann FX 63-137 \mathcal{R} -4 rectangular wing at a Reynolds number of 100,000.	56
4.9	Repeatability for the \mathcal{R} -3 rectangular flat-plate wing at a Reynolds number of 100,000.	57
5.1	Drag polar for the Wortmann FX 63-137 wing with an \mathcal{R} of 4 and λ of 1.00.	61
5.2	Drag polar for the 5-to-1 LE, 10-to-1 TE flat-plate wing with an \mathcal{R} of 2 and λ of 0.50.	62
5.3	Drag polar for the 5-to-1 LE, 10-to-1 TE flat-plate wing with an \mathcal{R} of 2 and λ of 0.75.	63
5.4	Drag polar for the 5-to-1 LE, 10-to-1 TE flat-plate wing with an \mathcal{R} of 2 and λ of 1.00.	64
5.5	Drag polar for the 5-to-1 LE, 10-to-1 TE flat-plate wing with an \mathcal{R} of 3 and λ of 0.50.	65
5.6	Drag polar for the 5-to-1 LE, 10-to-1 TE flat-plate wing with an \mathcal{R} of 3 and λ of 0.75.	66
5.7	Drag polar for the 5-to-1 LE, 10-to-1 TE flat-plate wing with an \mathcal{R} of 3 and λ of 1.00.	67
5.8	Drag polar for the 5-to-1 LE, 10-to-1 TE flat-plate wing with an \mathcal{R} of 4 and λ of 0.50.	68
5.9	Drag polar for the 5-to-1 LE, 10-to-1 TE flat-plate wing with an \mathcal{R} of 4 and λ of 0.75.	69
5.10	Drag polar for the 5-to-1 LE, 10-to-1 TE flat-plate wing with an \mathcal{R} of 4 and λ of 1.00.	70
5.11	Drag polar for the 5-to-1 LE, 10-to-1 TE flat-plate wing with an \mathcal{R} of 5 and λ of 1.00.	71
5.12	Flat plate comparison results for a fixed Re of 60,000 and λ of 0.50.	72
5.13	Flat plate comparison results for a fixed Re of 60,000 and λ of 0.75.	73
5.14	Flat plate comparison results for a fixed Re of 60,000 and λ of 1.00.	74
5.15	Flat plate comparison results for a fixed Re of 80,000 and λ of 0.50.	75
5.16	Flat plate comparison results for a fixed Re of 80,000 and λ of 0.75.	76
5.17	Flat plate comparison results for a fixed Re of 80,000 and λ of 1.00.	77
5.18	Flat plate comparison results for a fixed Re of 100,000 and λ of 0.50.	78
5.19	Flat plate comparison results for a fixed Re of 100,000 and λ of 0.75.	79
5.20	Flat plate comparison results for a fixed Re of 100,000 and λ of 1.00.	80
5.21	Flat plate comparison results for a fixed Re of 120,000 and λ of 0.50.	81
5.22	Flat plate comparison results for a fixed Re of 120,000 and λ of 0.75.	82
5.23	Flat plate comparison results for a fixed Re of 120,000 and λ of 1.00.	83

5.24	Flat plate comparison results for a fixed Re of 140,000 and λ of 0.75.	84
5.25	Flat plate comparison results for a fixed Re of 140,000 and λ of 1.00.	85
5.26	Flat plate comparison results for a fixed Re of 60,000 and \mathcal{R} of 3.	86
5.27	Flat plate comparison results for a fixed Re of 60,000 and \mathcal{R} of 4.	87
5.28	Flat plate comparison results for a fixed Re of 60,000 and \mathcal{R} of 5.	88
5.29	Flat plate comparison results for a fixed Re of 80,000 and \mathcal{R} of 2.	89
5.30	Flat plate comparison results for a fixed Re of 80,000 and \mathcal{R} of 3.	90
5.31	Flat plate comparison results for a fixed Re of 80,000 and \mathcal{R} of 4.	91
5.32	Flat plate comparison results for a fixed Re of 80,000 and \mathcal{R} of 5.	92
5.33	Flat plate comparison results for a fixed Re of 100,000 and \mathcal{R} of 2.	93
5.34	Flat plate comparison results for a fixed Re of 100,000 and \mathcal{R} of 3.	94
5.35	Flat plate comparison results for a fixed Re of 100,000 and \mathcal{R} of 4.	95
5.36	Flat plate comparison results for a fixed Re of 100,000 and \mathcal{R} of 5.	96
5.37	Flat plate comparison results for a fixed Re of 120,000 and \mathcal{R} of 2.	97
5.38	Flat plate comparison results for a fixed Re of 120,000 and \mathcal{R} of 3.	98
5.39	Flat plate comparison results for a fixed Re of 120,000 and \mathcal{R} of 4.	99
5.40	Flat plate comparison results for a fixed Re of 140,000 and \mathcal{R} of 2.	100
6.1	Upper surface oil flow visualization of major flow features on the Wortmann FX 63-137 \mathcal{R} -4 rectangular wing at a Re of 90,000.	103
6.2	$C_{D_{min}}$ as a function of Reynolds number for flat-plate wings.	106
6.3	$(C_L/C_D)_{max}$ as a function of Reynolds number for flat-plate wings.	107
6.4	$(C_L^{3/2}/C_D)_{max}$ as a function of Reynolds number for flat-plate wings.	108
6.5	$C_{L_{max}}$ as a function of Reynolds number for flat-plate wings.	109
6.6	$C_{L\alpha}$ as a function of Reynolds number for flat-plate wings.	110
6.7	$C_{L\alpha}$ as a function of \mathcal{R} for flat-plate wings.	112
6.8	Maximum range ($(C_L/C_D)_{max}$) as a function of Reynolds number for the \mathcal{R} -4, $\lambda = 1$ wings.	114
6.9	Maximum endurance ($(C_L^{3/2}/C_D)_{max}$) as a function of Reynolds number for the \mathcal{R} -4, $\lambda = 1$ wings.	115
D.1	LRN-FB rig base.	182
D.2	LRN-FB lift base.	183
D.3	LRN-FB drag base.	184
D.4	LRN-FB absolute optical encoder base.	185
D.5	LRN-FB top roller-bearing base.	186
D.6	LRN-FB lift mounting bracket.	187
D.7	LRN-FB drag mounting bracket.	188
D.8	LRN-FB encoder mounting bracket.	189
D.9	LRN-FB load cell bracket mounting bracket.	190
D.10	LRN-FB lift pivot arm.	191
D.11	LRN-FB drag pivot arm.	192
D.12	LRN-FB encoder base arm.	193
D.13	LRN-FB DC motor mount.	194
D.14	LRN-FB worm shaft mounting bracket.	195
D.15	LRN-FB lower tapered bearing fitting.	196
D.16	LRN-FB flex-pivot fitting.	197
D.17	LRN-FB torque sensor to flex-pivot fitting.	198

D.18	LRN-FB worm gear to torque sensor fitting.	199
D.19	LRN-FB worm gear to optical encoder fitting.	200
D.20	LRN-FB lift platform stiffener.	201
D.21	LRN-FB drag platform stiffener.	202
D.22	LRN-FB lift load cell base mounting 1.	203
D.23	LRN-FB lift load cell base mounting 2.	204
D.24	LRN-FB drag load cell base mounting 1.	205
D.25	LRN-FB drag load cell base mounting 2.	206
D.26	LRN-FB pre-loading mounting bracket.	207
D.27	LRN-FB pre-loading mount 1.	208
D.28	LRN-FB pre-loading mount 2.	209
D.29	LRN-FB pre-loading l-shape bracket.	210
D.30	LRN-FB lift platform locking bracket.	211
D.31	LRN-FB pre-loading corner bracket.	212
D.32	LRN-FB main sting (connected to flexure).	213
D.33	LRN-FB secondary sting.	214

List of Tables

Table	Page
3.1 Force balance aerodynamic loads	22
3.2 Flat-plate model test matrix.	34
3.3 Uncertainty equation table	45
3.4 Force uncertainty equation table	46
3.5 Pressure transducer characteristics	47
3.6 Temperature sensor characteristics	47
3.7 Given constants	48
3.8 Known uncertainties	48
3.9 Flow condition uncertainties	48
3.10 Force balance uncertainties	48
5.1 Test matrix and run number index.	59
5.1 Continued.	60
D.1 LRN-FB machining list	180
D.1 Continued.	181

Nomenclature

Symbols

A_{ss}	settling-section (inlet) area
A_{ts}	test-section area
\mathcal{R}	aspect ratio
b	wingspan
\bar{c}	wing mean aerodynamic chord
C	tunnel test-section area
C_{d_0}	airfoil zero-lift drag coefficient
$C1$	linear coefficient matrix
$C2$	quadratic coefficient matrix
$C3$	interaction coefficient matrix
C_D	wing drag coefficient ($= D / \frac{1}{2} \rho V_\infty^2 S_{ref}$)
$C_{D_{min}}$	wing minimum drag coefficient
C_{D_i}	wing induced drag coefficient
C_L	wing lift coefficient ($= L / \frac{1}{2} \rho V_\infty^2 S_{ref}$)
$C_{L\alpha}$	wing lift curve slope
$C_{l\alpha}$	airfoil lift curve slope
C_M	wing moment coefficient ($= M / \frac{1}{2} \rho V_\infty^2 S_{ref} \bar{c}$)
C_m	airfoil moment coefficient ($= m / \frac{1}{2} \rho V_\infty^2 \bar{c}^2$)
D	wing drag force, intermediate calculation matrix
E	intermediate calculation matrix
H	wind tunnel test-section height, true load matrix

H_D	true drag load
H_L	true lift load
H_M	true moment load
$H1$	true load matrix
$H2$	squared true load matrix
$H3$	interaction true load matrix
K	linear fit coefficient matrix
K_1	body shape factor
K^{-1}	linear calibration matrix
$K_{i,j}$	linear fit coefficient of a i reading due to a j applied load
L	wing lift force
l	characteristic length
M	wing moment
MSF	model span fraction ($= b/H$)
P_{amb}	ambient pressure
P_{ss}	tunnel settling-section (inlet) static pressure
P_{ts}	tunnel test-section static pressure
q_∞	freestream dynamic pressure ($= \frac{1}{2}\rho V_\infty^2$)
R	ideal gas constant, output as a function of several measured values (x)
Rdg	load reading matrix
Rdg_D	drag load cell reading
Rdg_L	lift load cell reading
Rdg_M	moment load cell reading
Re	Reynolds number based on mean aerodynamic chord ($= V_\infty \bar{c}/\nu$)
S	Sutherland temperature (constant), wing surface area
S_{ref}	wing reference area
T_0	reference temperature
T_{amb}	ambient temperature
t	airfoil thickness

t/c	airfoil thickness-to-chord ratio
U_R	experimental uncertainty associated with output R
$U_{x,RSS}$	uncertainty of a combination of multiple uncertainties calculated from root-sum-square method
V_∞	freestream velocity
W	wind tunnel test-section width
α	angle of attack
∂	partial derivative
δ	boundary correction factor
ϵ_{sb}	solid blockage correction
ϵ_{wb}	wake blockage correction
ϵ_T	final blockage correction
λ	taper ratio
μ	dynamic viscosity
μ_0	reference dynamic viscosity at the reference temperature
ρ	density
ρ_{amb}	ambient density
τ_1	correction factor related to the tunnel test-section and <i>MSF</i>
τ_2	downwash correction factor

Subscripts

c	corrected
$c/4$	quarter-chord
i	lift (L), drag (D) or moment (M) reading
j	lift (L), drag (D) or moment (M) load
n	iteration number, number of measured values
u	uncorrected
x	measured values, x_1, x_2, \dots, x_n

Abbreviations

AC	alternating current
CAD	computer-aided design
DARPA	Defense Advanced Research Projects Agency
ECE	Electrical and Computer Engineering
LAR	low aspect ratio
LSATs	low-speed airfoil tests
LRN	low Reynolds number
LRN-FB	UIUC low Reynolds number force balance
LSB	laminar separation bubble
MAV	micro air vehicle
MDF	medium density fiberboard
NRL	Naval Research Laboratory
RC	radio control
RSS	root-sum-square
SEI	serial encoder interface
SLA	stereolithography
SUPAERO	Ecole Nationale Supérieure de l'Aéronautique et de l'Espace
UAV	unmanned aerial vehicle
UIUC	University of Illinois at Urbana-Champaign
VTOL	vertical take-off and landing

Chapter 1

Introduction

With the emergence of large unmanned aerial vehicle (UAV) platforms as an integral part of the military, there has been a push to reduce the size of these vehicles to serve platoon level roles and other forms of civilian aerial surveillance and reconnaissance missions. As noted by Mueller [1], the research and development of small UAVs has exploded in the past 20 years due to breakthroughs in miniature electronics (i.e. sensors, cameras, control, and power generation technologies) and a large-scale military backed interest. This interest spawned the field of low Reynolds number aerodynamic research. Prior to this, due to its lack of practicality, scientific engagement in this area was infrequent. However, with the increasing use of UAVs (i.e. Predator, Global Hawk, etc.), small back-packable UAVs are becoming more viable and sought after both for military and commercial use. The current level of technology has produced a plethora of small-UAVs (i.e. man-portable UAVs and hand launch UAVs) that are in service both in military and civilian environments. Most of the UAVs (i.e. Lockheed Martin's Desert Hawk, Aerovironment's Wasp III and Raven, etc.) in this category are of low-to-moderate aspect ratios ($2 \leq AR \leq 7$) and operate at Reynolds numbers between 50,000 and 300,000.

Similar to large scale aircraft, the aerodynamic performance of small UAV airfoil sections and wing planforms is of fundamental importance as it relates critically to the flight characteristics of the vehicle. It is commonly noted [2, 3] that, with a few exceptions [4–9], there is a lack of experimental data related to low-to-moderate aspect ratio ($2 \leq AR \leq 7$) UAV flight at low Reynolds numbers. As a result, two-dimensional experimental data [10–14] is used in the small UAV design process. However, the mutual interaction between the three-dimensional finite wing and low Reynolds number effects plays a key role. Therefore, it is essential to have a comprehensive understanding of low Reynolds number wing characteristics in order to push the envelope of small UAV capabilities.

The goal of this thesis is to address the issues discussed here-to-fore. Aerodynamic performance measurements for low-to-moderate aspect ratio wings taken using a custom-designed and fabricated low Reynolds number wind tunnel balance are presented. Lift, drag, and moment calibration and validation for the balance were performed and results presented. In addition, conclusions and resulting trends are drawn from the aerodynamic performance data collected for a Wortmann FX 63-137 wing and ten flat-plate wings of varying aspect ratio and taper ratio.

The thesis is organized as follows. Chapter 2 details an overview of two-dimensional and three-dimensional low Reynolds number aerodynamics. A detailed literature review of the current state of low Reynolds number aerodynamic research is also presented. Chapter 3 contains details of the testing facility and experimental techniques. The design methodology and capabilities of the custom-fabricated three-component force balance is discussed and presented. The calibration methodology and results for the balance are also detailed. Chapter 4 presents historical lift, drag and moment comparisons for two separate wings to validate the balance. Aerodynamic measurements for the Wortmann FX 63-137 wing and ten flat-plate wings of varying aspect ratio and taper ratio are presented in Chapter 5. Chapter 6 discusses and presents trends from the results obtained from Chapter 5. In addition, flow visualization performed on the Wortmann FX 63-137 wing are presented to further aid in understanding low Reynolds number flow characteristics over low-to-moderate aspect ratio wings. Finally, in Chapter 7 conclusions are realized and the scope for future work is presented.

Chapter 2

Low Reynolds Number Aerodynamics

2.1 Fundamentals of Fluid Dynamics

Prior to describing the characteristics of low Reynolds number aerodynamics, it is imperative to understand the fundamentals of fluid dynamics over a given airfoil or flat plate. The Reynolds number (Re) of a fluid flow is a non-dimensional value that characterizes the ratio of magnitudes of inertial and viscous forces acting on a fluid and is given by

$$Re = \frac{\rho V_\infty l}{\mu} \quad (2.1)$$

where ρ is the density of the fluid, l is the characteristic length, V_∞ is the freestream velocity, and μ is the dynamic viscosity. The dynamic viscosity needed to calculate Reynolds number is temperature dependent and can be calculated using Sutherland's viscosity [15] law as shown in

$$\frac{\mu}{\mu_0} = \left(\frac{T_{amb}}{T_0} \right)^{3/2} \left(\frac{T_0 + S}{T_{amb} + S} \right) \quad (2.2)$$

where μ_0 is the reference dynamic viscosity at the reference temperature T_0 , and S is a constant defined as the Sutherland temperature. For the wind tunnel experiments performed in this research, Sutherland viscosity law was used to determine the test section dynamic viscosity.

In flows with $Re \gg 1$, the inertial forces of a fluid are much larger than its viscous forces. This characteristic allows the use of an inviscid fluid assumption where the fluids viscous effects are discarded. However, as alluded to by Batchelor [16], with the introduction of a stationary body (i.e. airfoil or flat plate) and its associated no-slip condition, the inviscid flow assumption is rendered inappropriate for most cases. The ‘no-slip’ condition states that the tangential velocity of the fluid flow is zero as the solid boundary of a stationary body is approached. As a result, there exists a

thin region close to the boundary of the body where the tangential velocity of the flow is retarded with respect to the fluid as a whole. This region of fluid is called the boundary layer and was initially discovered by Ludwig Prandtl in 1904.

The boundary layer of a fluid is divided into three separate regions, a steady laminar region, the transition region, and an unsteady turbulent region as shown in Fig. 2.1. With an oncoming steady flow, a laminar boundary layer initially grows from the forward stagnation point of a body (airfoil or flat plate). As the flow proceeds farther downstream, there exists a transition point that is dependent on the local Reynolds number of the flow and the surface quality of the body. As stated by Kuethe and Chow [17], downstream of this critical Reynolds number, the boundary layer becomes unstable and any small disturbances in the flow results in a turbulent boundary layer forming. The relationship between the critical Reynolds number and smoothness of the body was demonstrated famously by Osborne Reynolds in 1883.

2.2 Two-Dimensional Aerodynamics

2.2.1 Laminar Separation Bubble

Low Reynolds number airfoil flows are principally distinguished by their associated laminar separation bubbles. A laminar separation bubble (LSB) is formed when the laminar boundary layer of a body encounters an adverse pressure gradient that is too large for it to overcome, resulting in the separation of the boundary layer from the surface of the body. For airfoils operating at $Re > 70,000$, conditions can exist for reattachment of the separated boundary layer. In these con-

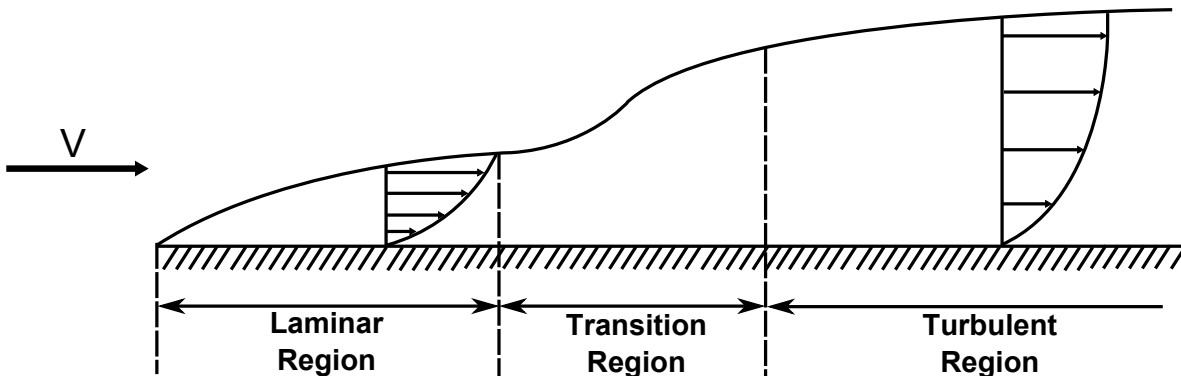


Fig. 2.1: Boundary layer over a flat plate.

ditions, the separated boundary layer rapidly undergoes transition to turbulent flow. The increased entrainment due to turbulence causes the reattachment of the boundary layer onto the body as shown in Fig. 2.2. As stated by Lissaman [18], the LSB formed is dependent upon the airfoil shape and Reynolds number. At $Re \approx 100,000$, the LSB generally extends over 20–30% of the airfoil and significantly changes the pressure distribution by altering the effective shape of the airfoil. At higher Reynolds numbers, the LSB shortens. This short bubble represents the transition-forcing mechanism, and as long as its length is minimized, its effect on airfoil performance is limited. As angle of attack increases however, the LSB grows and requires a greater pressure recovery for reattachment. Eventually the bubble "bursts" causing an abrupt stall and sudden deterioration in airfoil performance.

An additional characteristic of this regime are its hysteresis effects as noted by Selig [19] and others. When the airfoil stalls due to its LSB bursting, a reduction in the angle of attack does not immediately "unburst" the bubble. This characteristic is mainly due to the inherent instability of the LSB. An example of these hysteresis effects on airfoil performance are shown in Fig. 2.3.

As shown in Fig. 2.4, for smooth low Reynolds number airfoils there exists a performance jump in

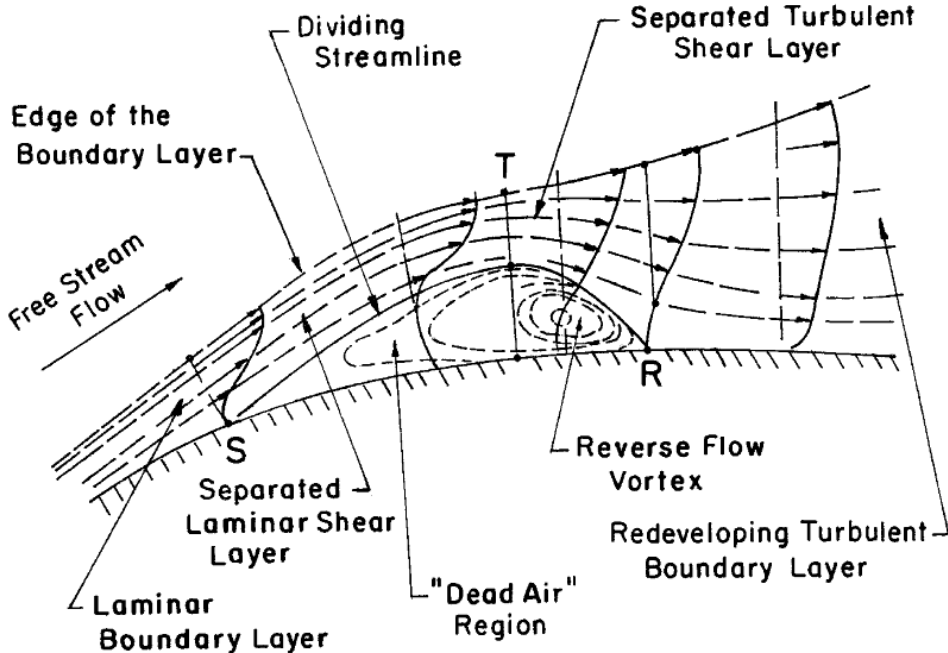


Fig. 2.2: Structure of laminar separation bubble (taken from Ref. 20).

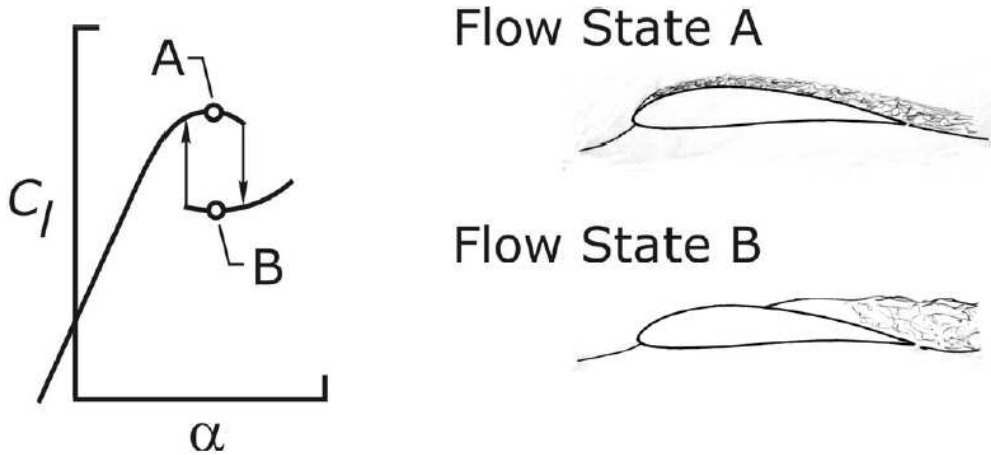


Fig. 2.3: Low Reynolds number airfoil hysteresis effects (taken from Ref. 19).

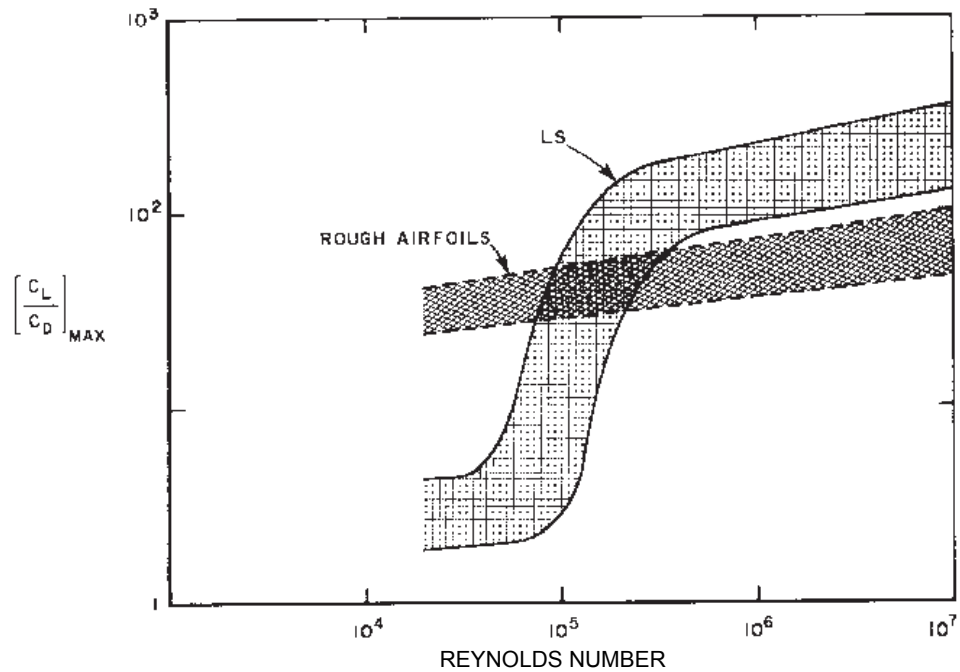


Fig. 2.4: Low Reynolds number airfoil performance (taken from Ref. 18).

the aforementioned critical Reynolds number of $\approx 70,000$. Both McMasters [21] and Lissaman [18] elude to this performance jump. This large change in airfoil performance is primarily due to the boundary layer effects discussed previously at these low Reynolds numbers. A rough or turbulated airfoil does not exhibit this abrupt performance change with Reynolds number as transition to turbulent flow has already occurred. Similarly, the effects of the laminar separation bubble on airfoil performance is clearly illustrated in the airfoil lift-drag polar shown in Fig. 2.5. The well-

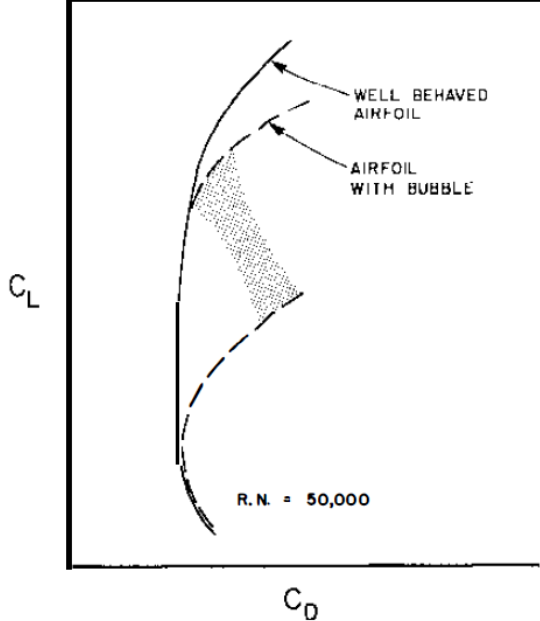


Fig. 2.5: Effect of laminar separation bubble on lift-drag polar (taken from Ref. 18).

behaved polar is similar to that of conventional airfoils at Reynolds numbers above 1,000,000; the other polar represents the gyrations that can occur in the critical Reynolds-number range, in this case at a Reynolds number of 50,000. For these reasons, the design of low Reynolds number airfoils proves to be a very interesting problem.

2.2.2 Boundary Layer Management

As detailed previously, the high sensitivity of transition and separation to Reynolds number, pressure gradient, and the disturbance environment play a critical role in determining the development of the boundary layer which, in turn, affects the overall performance of the airfoil. Therefore, the management of this sensitive boundary layer for a particular Reynolds number airfoil design is critical. To better understand the sensitivity of airfoil performance with respect to Reynolds number, a short summary of a low Reynolds number survey done by Carmichael [22] is shown below for Reynolds numbers between 30,000 and 200,000.

- $30,000 \leq Re \leq 70,000$: In this flow regime the choice of airfoil section is very important since relatively thick airfoils (i.e., 6% and above) can have significant hysteresis effects caused by laminar separation with transition to turbulent flow. In addition, for the range below

50,000, when separation occurs, the flow does not have time to transition to turbulent flow and reattaching.

- $70,000 \leq Re \leq 200,000$: In this range, the laminar separation bubble is ever present. Extensive laminar flow can be obtained and therefore airfoil performance improves albeit taking into account the performance effects of the bubble.
- $Re \geq 200,000$: Airfoils performance improves greatly with increasing Reynolds number as the effect of the LSB is diminished.

The LSB primarily affects low Reynolds number airfoil performance through form drag. Form drag is caused by the displacement effects of the boundary layers and wake modifying the inviscid surface velocity, creating a net aft component of the pressure forces normal to the airfoil surface. A LSB contributes significantly to the form drag via the lower pressure over the bubble acting over the aft-facing airfoil surface. Therefore airfoil design is strongly driven by the minimization of form drag caused by the size of the LSB.

There have been several methods developed in literature with the aim of decreasing the bubble size and hence lessen airfoil drag. These methods include the use of boundary trips [23], blowing or suction [24] over the airfoil, and the most commonly used method, airfoil design (direct and inverse) [18, 19, 21, 22, 25–31]. The goals and challenge of these methods is to force transition to occur at a location close to the laminar separation point over as much of the operating range of the airfoil as possible. The performance of low Reynolds number airfoils is strongly dependent on the location of transition as that sets the length of the LSB and consequently the magnitude of the drag rise attributable to the bubble.

2.3 Three-Dimensional Aerodynamics

2.3.1 High Aspect Ratio Wings

The flow around a wing at low Reynolds number is characterized by complex three-dimensional flow phenomena as shown in Fig. 2.6. Two-dimensional airfoil data plays an essential role in high-aspect ratio wing applications where the local flow behaves approximately two-dimensionally, and this can be seen in the flow around central section of the wing shown in Fig. 2.6.

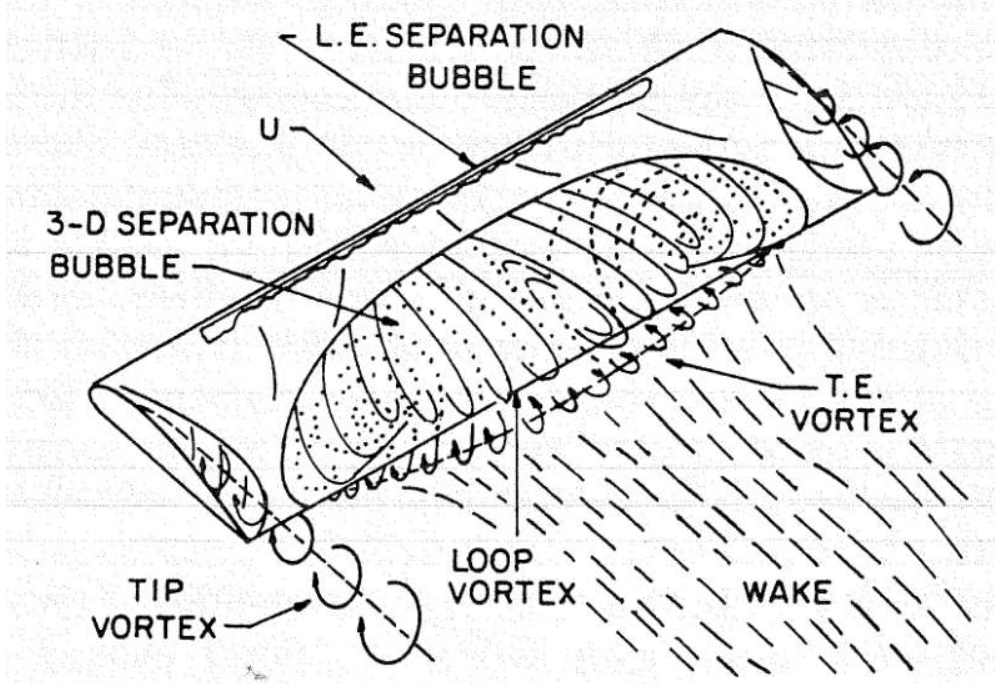


Fig. 2.6: Schematic of flowfield for a rectangular planform wing at low Reynolds numbers (taken from Ref. 32).

The classical lifting-line theory developed by Prandtl [33] provides a local downwash correction to account for finite aspect ratio effects of the wing-tip vortices. Wing-tip vortices result from the pressure difference between the top and bottom surfaces of an airfoil. The flow above the upper surface of an airfoil has a much lower pressure in comparison to the bottom surface. Therefore, as initially expounded by Lancaster [34], the high pressure region of flow beneath the wings would spill out around the wing tips into the lower pressure region above the wings. The spillage around the wing tips forms two main vortices that roll up and stream out behind the wings. These vortices would be of opposite sign and deflected downwards thereby causing the lift vector of the wing to be tipped backwards creating induced drag.

2.3.2 Low Aspect Ratio Wings

For low aspect ratio (LAR) wings ($\mathcal{A} \leq 2$), the lifting-line concept becomes of limited value as the local airfoil section characteristics cannot be separated from the wing as an entirety. LAR wings have two main sources of lift, a linear, and nonlinear source. The linear lift is derived from the bound vortex flow associated with circulation around the wing. The non-linear lift is associated with strong

wing-tip vortices that emanate from LAR wings. These strong vortices induce strong cross-flow velocities on the upper surface of the wing resulting in a decrease in pressure. The resultant increase in lift is the essence of the leading edge suction analogy expounded by Polhamus [35]. The leading edge suction analogy states that the extranormal force produced by LAR wings at moderate-to-high angles of attack is equal to the loss of leading-edge and side-edge suction associated with the separated flow. The effects of leading edge suction can be vividly seen in Fig. 2.7.

In addition to leading edge suction, Torres and Mueller [6] stated that the strong wing-tip vortices of LAR wings inhibit and delay flow separation. This conclusion was also eluded to by Gad-el-Hak [37] who stated that, for LAR wings, the unsteadiness related to low Reynolds number flow over airfoils is attenuated by its strong wing-tip vortices. As the wing reaches the angle $\alpha_{C_{Lmax}}$, the wing-tip vortex induced flow is able to energize the flow on the upper surface of the wing and delay separation. The strength of these wing-tip vortex structures on the upper surface of the wing decreases with increasing aspect ratio, and as a result separation occurs at lower angles of attack and lower corresponding lift coefficients.

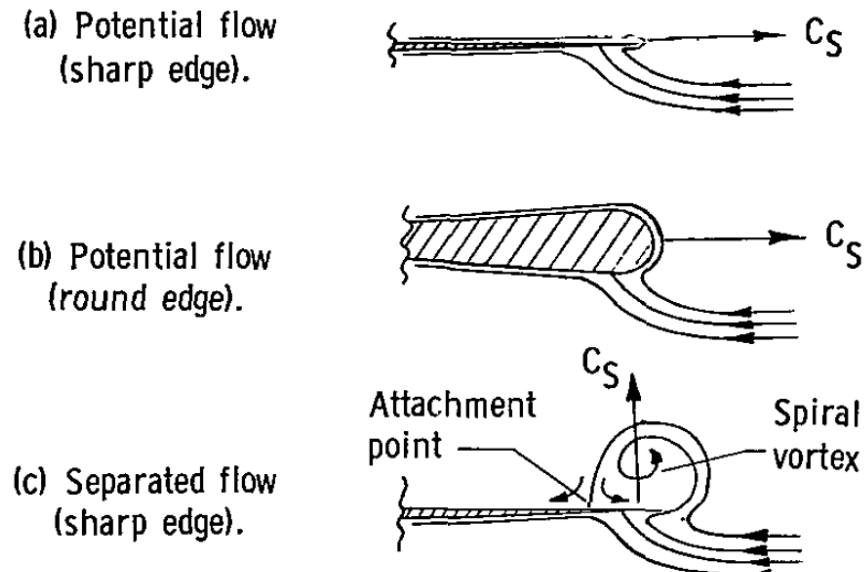
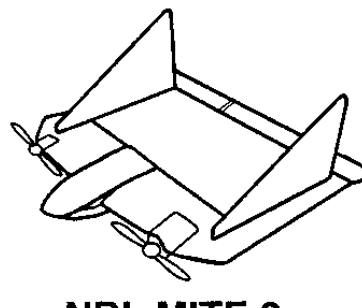


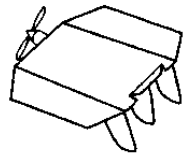
Fig. 2.7: Leading-edge flow conditions (taken from Ref. 36).

2.4 Motivation for Testing

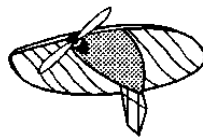
The push for small scaled UAVs over the past 20 years, particularly by the Defense Advanced Research Projects Agency (DARPA) and Naval Research Laboratory (NRL) in their Micro Air Vehicle (MAV) development initiative [38] from 1996–2002, yielded the fruitful and energetic field of MAV research. In context with the DARPA’s initiative, vehicles with wingspans less than 6 in (15 cm) were referred to as MAVs. However, more practically, the less than 12-in wingspan was used to categorize MAVs. In the fixed-wing category, numerous MAV systems have been introduced as shown in Fig. 2.8. The most notable of these are the Black Widow MAV by AeroVironment [39], the University of Florida flexible-wing concept MAV designs [40–43], the University of Arizona fixed-wing and vertical take-off and landing (VTOL) MAV designs [44–46], the Naval Research Laboratory (NRL) MITE MAV concept vehicles [38, 47, 48], and the biplane MAVs developed at Ecole Nationale Supérieure de l’Aéronautique et de l’Espace (SUPAERO) in France [49].



NRL MITE 2



BLACK WIDOW MAV



UF MAV

Fig. 2.8: Micro air vehicle designs (taken from Ref. 1).

In addition to MAV design and flight testing, detailed fundamental experimental work has been carried out in the aerodynamics of low aspect ratio, low Reynolds number wings most notably by Mueller [1, 5, 6, 50], Mohseni [2, 8, 51], Laitone [7], Kaplan [52], and Vierendeels [3]. Although MAVs have been proven from a feasibility standpoint, the practicality of the MAV concept however still leaves much to be desired [53]. Due to the fixed wingspan limitations, MAVs that spawned from these requirements were of low aspect ratios ($0 \leq AR \leq 2$). This was done to minimize wing loading in an effort to expand its payload capabilities. Despite this, the payload capacity and endurance of MAVs have not reached levels that are practical for use [53]. The current level of technology though has produced a plethora of small-UAVs (man-portable UAVs, hand launch UAVs) that are in service both in military and civilian environments. Most of the UAVs in this category fall into the low to moderate aspect ratio category ($2 \leq AR \leq 6$). In this aspect ratio range where finite wing effects still play a large effect for low Reynolds numbers, the reliance on two-dimensional experimental data would be insufficient. Despite this, there seems to be a lack of experimental data in this category as discussed in Chapter 1, and the ongoing work at the UIUC Applied Aerodynamics Group intends to address these needs. This thesis represents the beginnings of the effort.

Chapter 3

Testing Facility and Experimental Techniques

All tests were conducted in the low turbulence subsonic wind tunnel in the Aerodynamics Research Laboratory at UIUC. The small aerodynamic loads of wings tested at low Reynolds numbers made it critical that the measurement and data acquisition systems employed were of high sensitivity, precision, and accuracy. This chapter discusses the experimental apparatus and methodology employed to collect accurate and repeatable lift, drag, and moment measurements for low-to-moderate aspect ratio wings at low Reynolds numbers. Detailed descriptions of the custom-designed and fabricated three-component force balance, data acquisition equipment, calibration methodology, and data correction procedures are presented in this chapter. Uncertainty analysis of the force balance and measurement system is also presented.

3.1 Experimental Facility

The aforementioned low turbulence subsonic wind tunnel shown in Fig. 3.1 is an open-return tunnel. The overall length of the tunnel is 60 ft (18.29 m), and its contraction ratio from the inlet to the test section is 7.5:1. The test section of the tunnel is rectangular and measures 2.8×4.0 ft (0.85×1.22 m) in cross-section and 8 ft (2.44 m) in length. Over the length of the test section, its width increases by approximately 0.5 in (1.27 cm) to account for boundary layer growth along the tunnel side walls. Test section speeds up to 165 mph (73.76 m/s) can be obtained via a 125 hp (93.25 kW) alternating current (AC) electric motor connected to a five bladed fan. The power of the AC motor is regulated by an ABB ACS 600 Low Voltage AC Frequency Drive. Photographs of the tunnel fan and inlet are presented in Figs. 3.2 and 3.3.

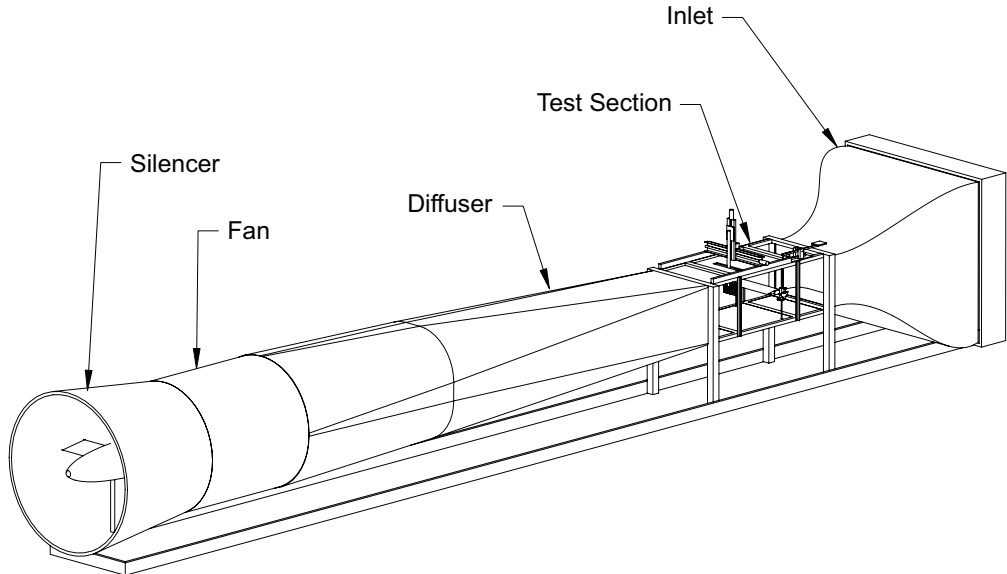


Fig. 3.1: UIUC low-speed subsonic wind tunnel.



Fig. 3.2: Photograph of wind tunnel fan and stators (photograph by Gregory Williamson).

Detailed in Ref. 54, the turbulence intensity of the wind tunnel was measured to be less than 0.1%. These low turbulence levels were achieved by the use of a 4-in (10.16-cm) thick honeycomb and four anti-turbulence screens located in the settling-chamber of the wind tunnel. Low levels of test-section turbulence ensure good flow quality in the test section. Most importantly, low



Fig. 3.3: Photograph of wind tunnel inlet showing the honeycomb (photograph by Gregory Williamson).

turbulence levels allow for accurate measurement of low Reynolds number behavior as laminar flow does not prematurely transition to turbulent flow [22, 51].

3.2 Force Balance

3.2.1 Design

A substantial part of the research work involved in this project was in the design, fabrication, and assembly of a three-component external platform force balance (LRN-FB) that was capable of measuring the small aerodynamic loads of low Reynolds number wings. The experimental setup is depicted in Fig. 3.4.

The LRN-FB was designed to be conceptually similar to the University of Notre Dame's UND-FB2 force/moment balance [50]. The LRN-FB attached to the ceiling of the test section, and the

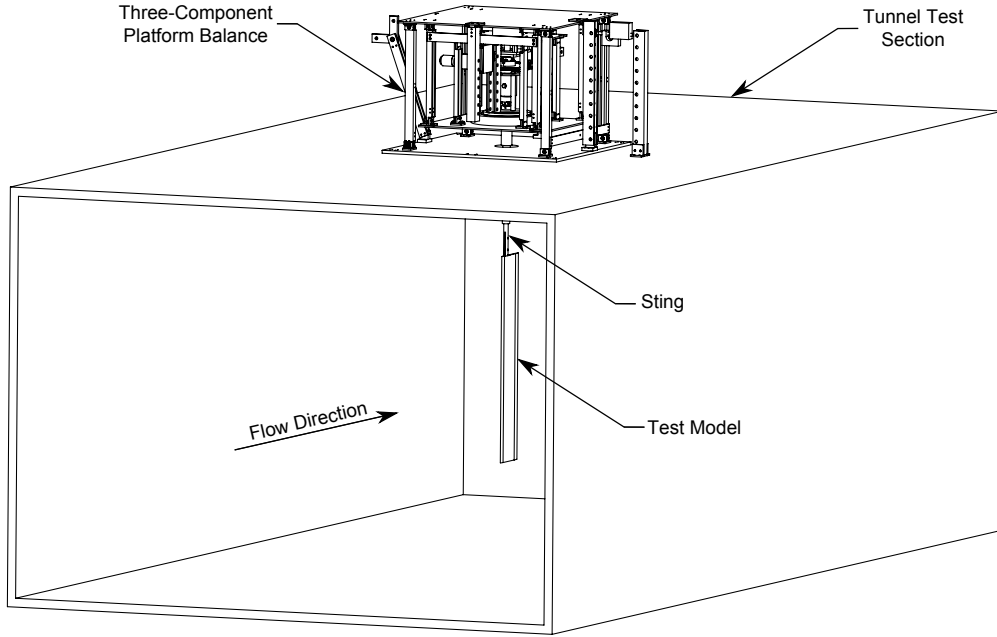


Fig. 3.4: UIUC LRN-FB setup in tunnel test section.

wings were mounted at quarter chord using a wing-tip mounted sting. The spanwise axis of the wing was in the vertical direction. The sting was designed to vary with the type of wing tested (i.e., thickness, camber, planform shape, etc.) and transfer the aerodynamic loads of the wing to the balance.

The balance consisted of two perpendicularly mounted platforms that allowed it to measure principally lift and drag forces from the wing. Each platform used eight Series 6000 double-ended flexural pivot bearings (flex-pivots) manufactured by the Riverhawk Company. As discussed in Ref. 55, flexure's are one of the main components of an external wind tunnel balance. They are designed to ensure that the balance reacts similarly in all principal directions and without hysteresis. Additional benefits of flex-pivots are that they are stiction-free and have, theoretically, infinite cycle life. The diameter of the flex-pivots used on the lift platform was 0.3125 in (0.794 cm) and the diameter of the flex-pivots used on the drag platform was 0.25 in (0.635 cm). The rotational stiffness and strength of the flex-pivots were directly proportional to its diameter. The flex-pivots used for the platforms was set at the minimum possible diameter based on the maximum applied loads projected. The small diameter of the flex-pivots minimized its rotational stiffness thereby ensuring that the sensitivity of the lift and drag measurements to small loads was not sacrificed.

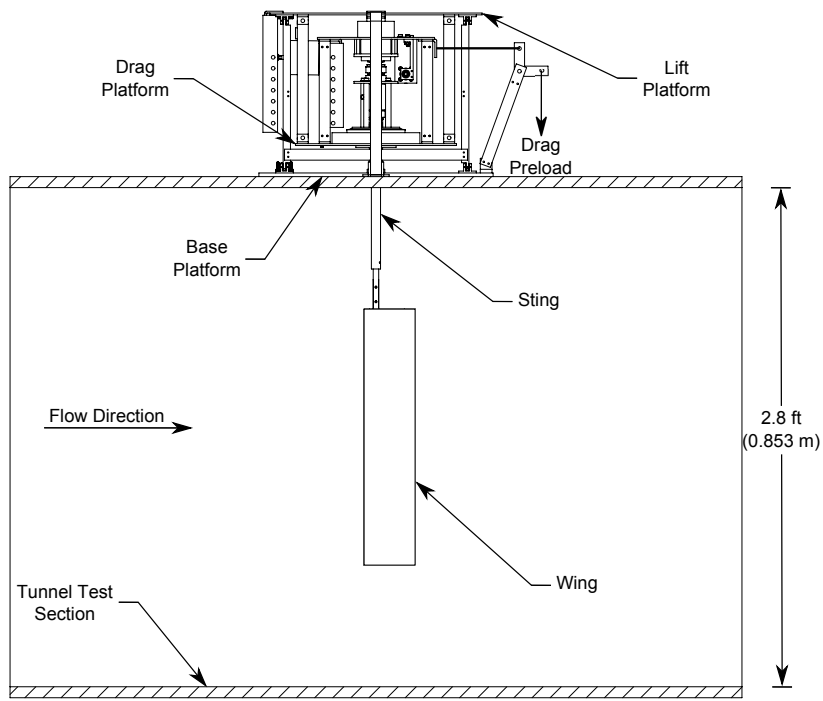


Fig. 3.5: Side view of UIUC LRN-FB experimental setup.

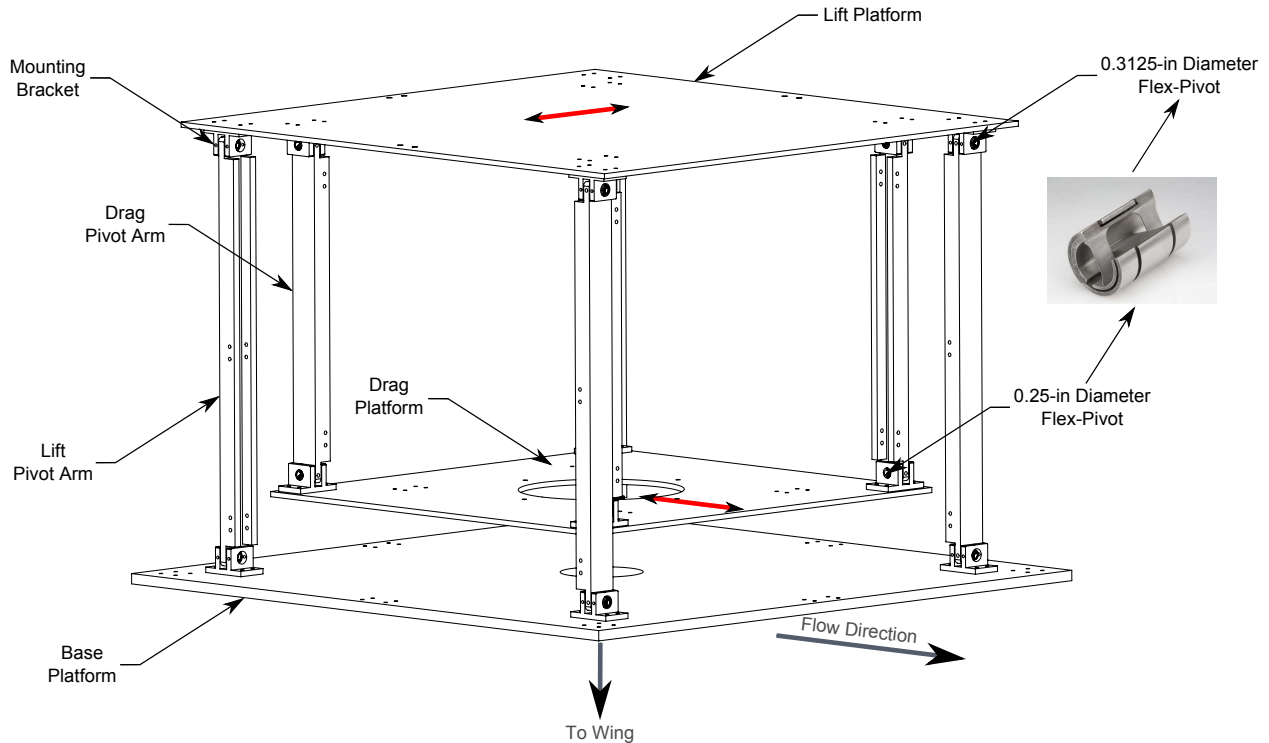


Fig. 3.6: LRN-FB lift and drag force balance platform.

As shown in Fig. 3.6, the lift platform was mounted on the base platform, and the drag platform was suspended within the lift platform. Both platforms were connected to SMT-S load cells [5.6 lb (25 N) for lift, 2.2 lb (10 N) for drag] manufactured by Interface, Inc. via load cell mounting brackets. The mounting brackets accepted different load cell attachment points to allow for variations in the operational range of the lift and drag platforms. The platforms were pre-loaded to ensure that the load cells were always working in tension. This approach allowed the force balance to be able to accurately measure both small and large forces occurring in the Reynolds number range of 40,000 to 160,000. A detailed annotated view of the lift and drag platforms are shown in Figs. 3.7(a–b).

Within the drag platform, a US Digital® absolute optical encoder (Model A2), a Faulhaber® DC gear motor, and a worm gear measured and set the angle of attack of the wing respectively. The optical encoder was an optical rotary position sensor that reported its shaft angle within a 360-deg range. The resolution of the optical encoder was 0.09 deg, and the zero position of its shaft could be reset to any location. The Faulhaber® 308:1 ratio DC gear motor ran a 48-pitch worm shaft via a rotary-flex coupling. The worm shaft drove a 45:1 gear ratio, 180-tooth worm gear aligned in the axis of rotation of the spanwise axis of the wing. The drag platform also housed a Transducer Techniques® 100-oz-in (0.71-N-m) torque sensor (Model RTS-100) that measured the aerodynamic pitching moment of the wing. Given that the torque sensor could not handle axial loads, an intricate setup was designed to house it. This setup included a 0.625-in (15.9-mm) diameter double-ended flexural pivot (Model 6020-800), two large tapered roller bearings and multiple fittings. The goals of the angle-of-attack and torque-sensor setups were two pronged:

- To allow the torque sensor to rotate with change in the angle of attack of the sting/wing.
The non-measuring end of the torque sensor attached directly to the worm gear allowing the torque sensor to measure the pitching moment of the wing at each angle of attack.
- To ensure that only the moment loads of the wing were transmitted to the torque sensor.
A fitting attached the measurement end of the torque sensor to the sting via the 0.625-in (15.9-mm) flex-pivot. The central portion of the flex-pivot was fixed with respect to the angle of attack thereby preventing the axial loads of the wing from reaching the torque sensor.

A detailed annotated and sectional view of the pitching moment and angle-of-attack setup is shown in Fig. 3.8. The finalized drawings of all components of the LRN-FB balance can be found

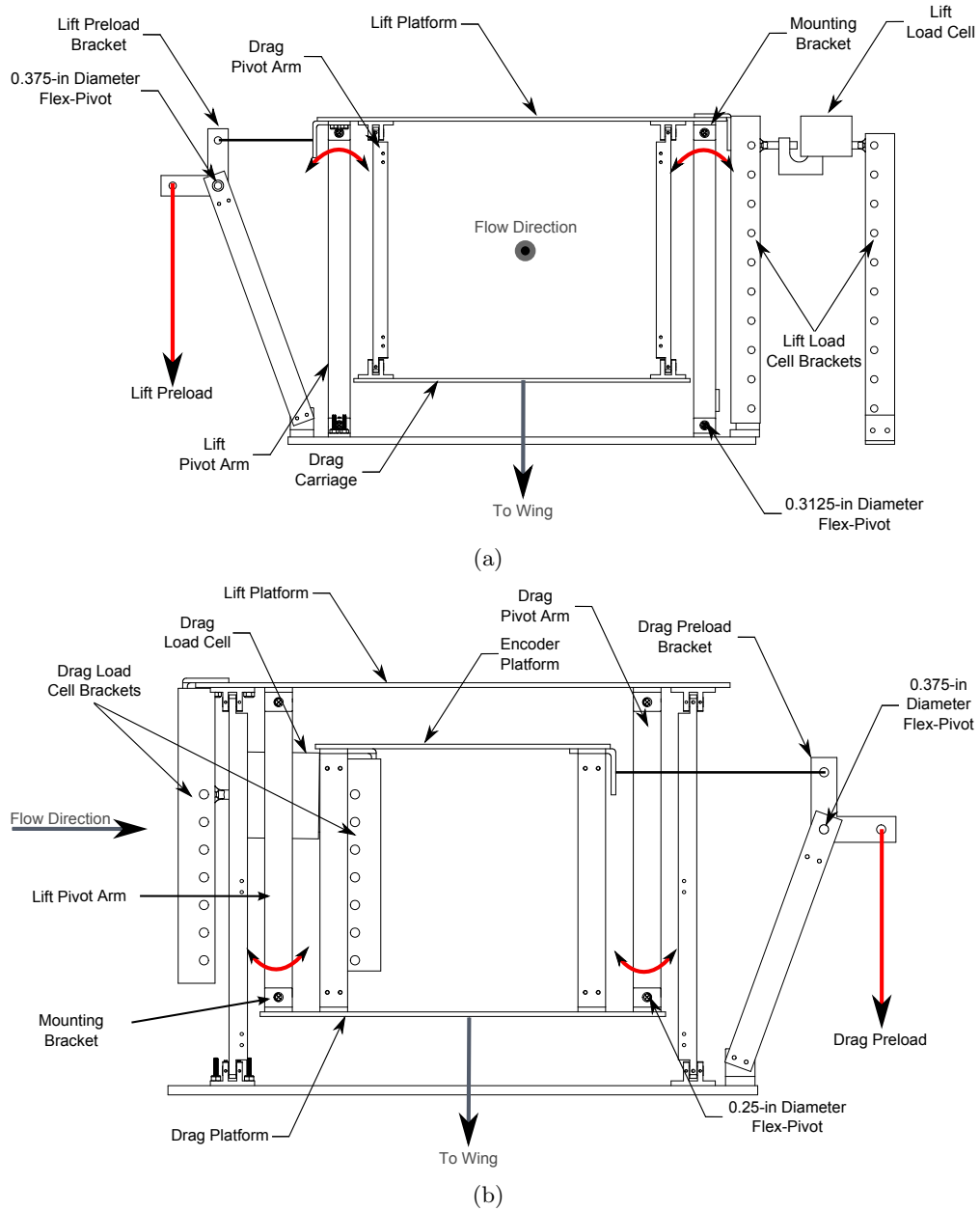


Fig. 3.7: Annotated LRN-FB lift and drag platforms: (a) lift platform (front view) and (b) drag platform (side view).

in Appendix D.

3.2.2 Fabrication and Assembly

Most of the components of the LRN-FB were fabricated and assembled at the Student Machine Shop located at the UIUC Department of Electrical and Computer Engineering (ECE) between

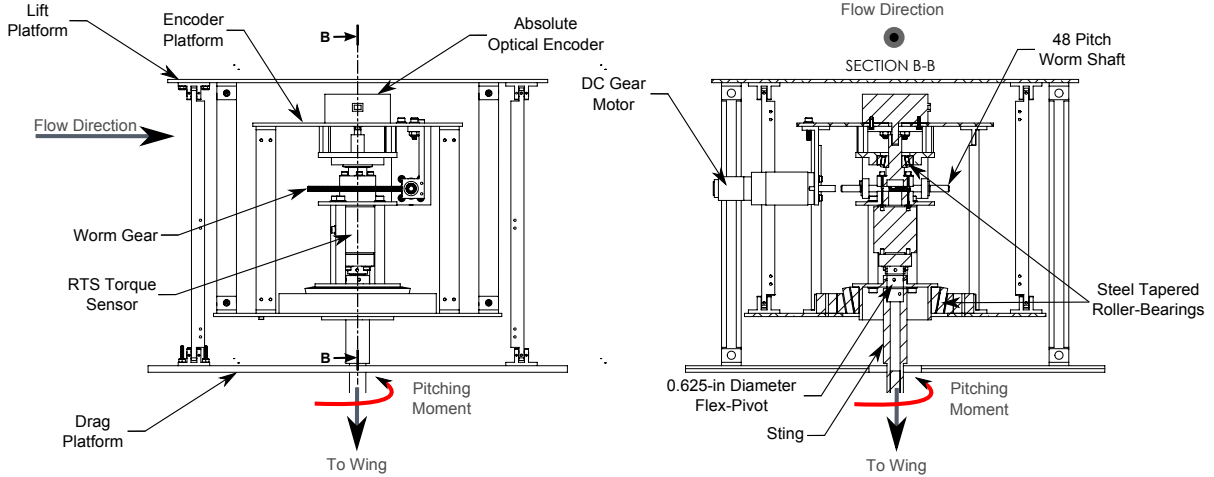


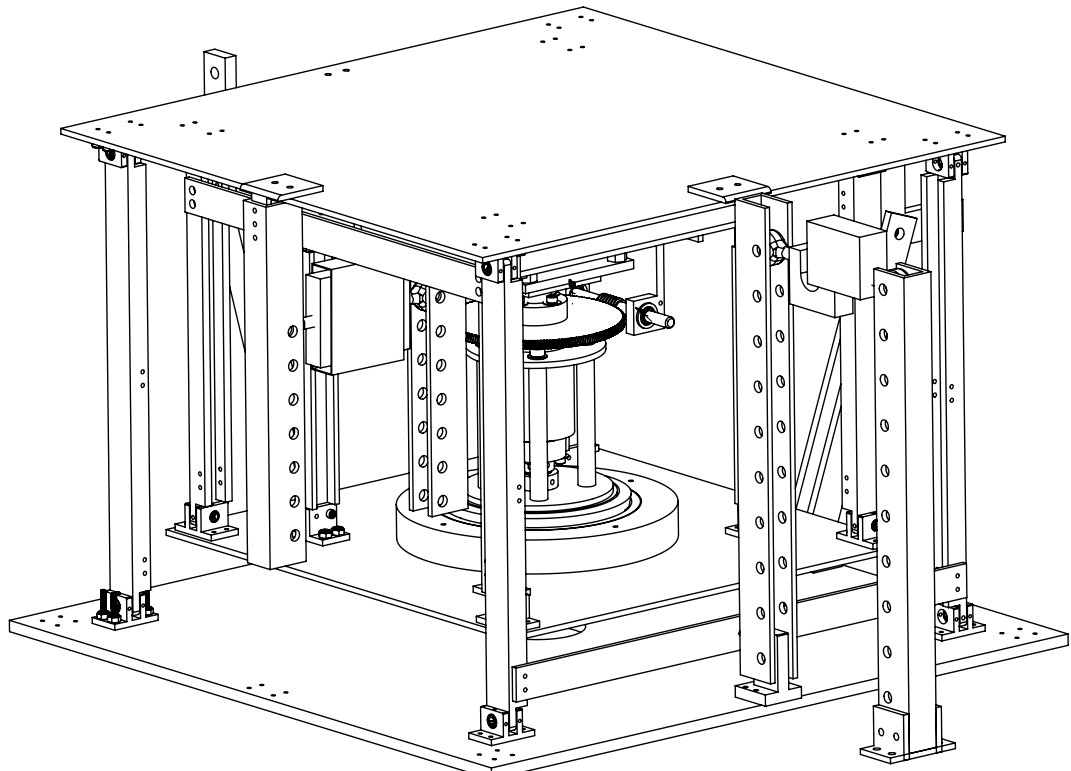
Fig. 3.8: Annotated LRN-FB pitching moment and angle-of-attack setup side and sectional view.

May and August 2011. The LRN-FB balance was specifically designed with ease of machining and assembly in mind. Given that the machines available were a manual-readout mill and lathe, most parts were designed to tolerance levels of ± 0.002 to ± 0.005 in (± 0.05 to ± 0.13 mm). This tolerance level ensured that assembly of the balance was performed with minimal fitting issues. An isometric view of the CAD model and a photograph of the fabricated LRN-FB is shown in Fig. 3.9. Additional photographs of the key components of the LRN-FB are shown in Figs. 3.10(a–c).

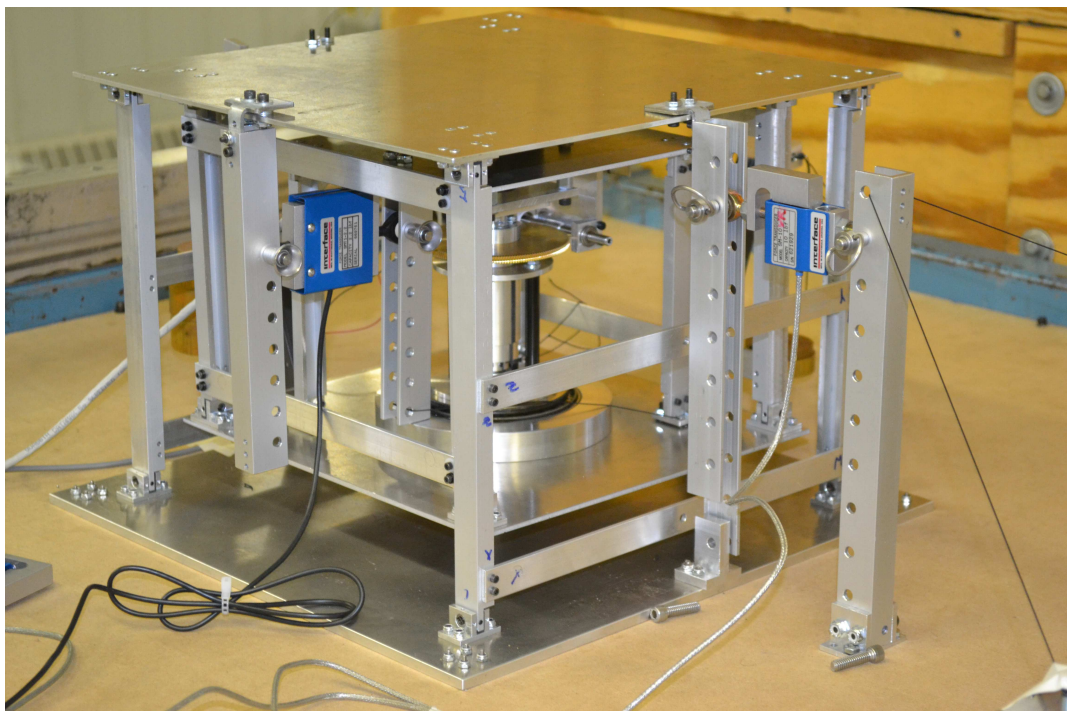
As built, the maximum, minimum, and resolution forces that the LRN-FB was designed to measure are detailed in Table 3.1. The values that are asterisked are limits set solely by the maximum bending moment limit of the flex-pivot that attaches the sting to the torque sensor on the LRN-FB. Currently, a Model 6020-800 double-ended flex-pivot is used. The flex-pivot was chosen as it had the lowest torsional spring rate among the 0.625-in (15.9-mm) diameter flex-pivots provided by Riverhawk®. If higher load measuring capabilities are required for future tests, a simple replacement of the 0.625-in (15.9-mm) diameter flex-pivot to one of a higher torsional spring rate would suffice as its bending moments limits would also increase. The resolutions in Table 3.1 are calculated by methods discussed in Chapter 3.3.2.

3.2.3 Alignment and Installation

A new tunnel section ceiling was built to accommodate the LRN-FB balance during testing. Medium density fiberboard (MDF) was used as the material for construction. MDF was cho-



(a)



(b)

Fig. 3.9: UIUC LRN-FB: (a) CAD model and (b) fabricated rig.

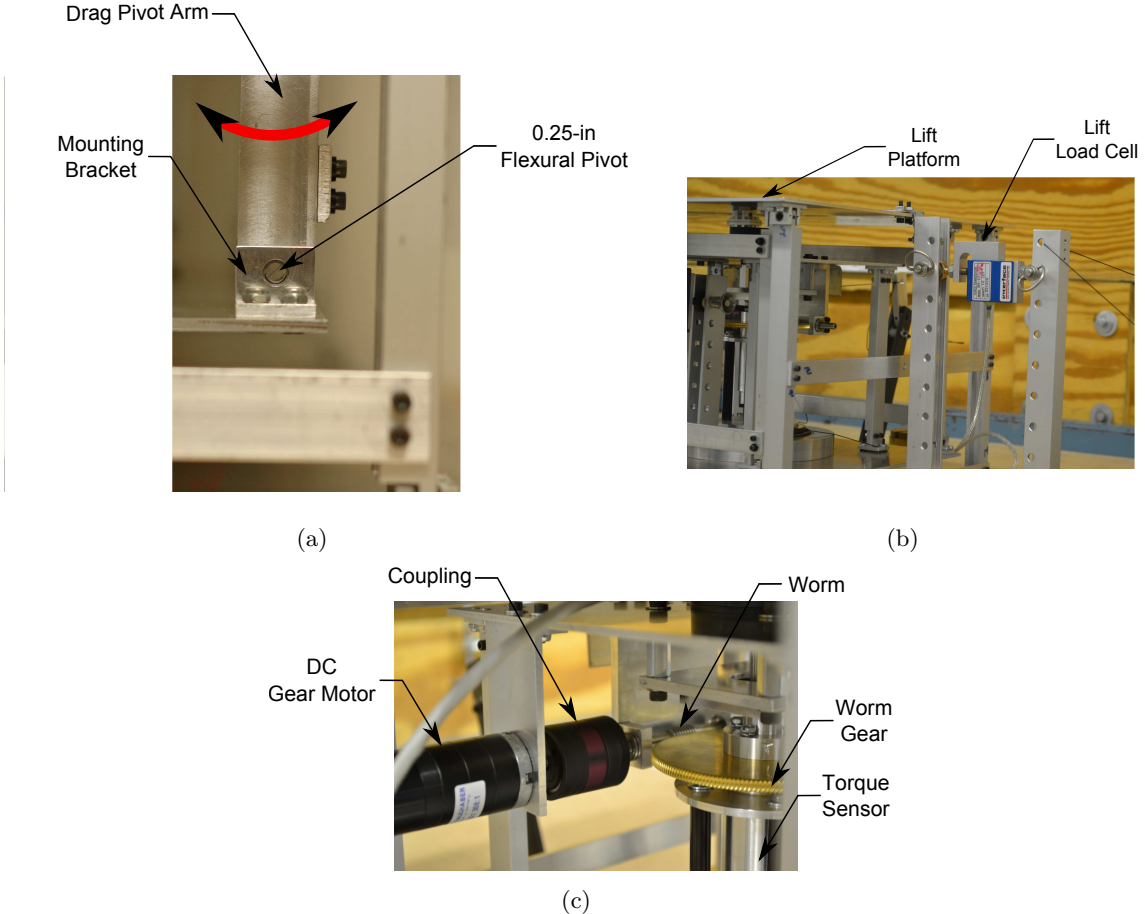


Fig. 3.10: UIUC LRN-FB components: (a) flexural pivot, (b) lift load cell and (c) gear motor to worm gear setup.

Table 3.1: Force balance aerodynamic loads

Property	Units	Maximum	Minimum	Resolution
L	lb (g)	2.50* (1134*)	-2.50* (-1134)	0.0013 (0.6)
D	lb (g)	2.50* (1134*)	0.01 (0.5)	0.0013 (0.6)
$M_{c/4}$	oz-in (N-m)	89.1 (0.63)	-89.1 (-0.63)	0.06 (0.0004)

* Limits set solely by the maximum bending moment limit of the 0.625-in (15.9-mm) flex-pivot that attaches the sting to the torque sensor.

osen as it was low cost, light weight, and did not chip easily in comparison with plywood. Care was taken to ensure that the necessary mounting holes drilled into the ceiling were accurate as they determined the final alignment of the LRN-FB with respect to the tunnel. The alignment of the LRN-FB was also reverified with respect to the tunnel centerline once it was installed onto the tunnel ceiling.

3.3 Measurement Techniques

3.3.1 Data Acquisition System

A PC with a National Instruments (NI) PCI-6052E data acquisition board was used to communicate with the wind tunnel and the force balance. The NI PCI-6052E has a varying resolution of 0.047–0.070 % of the full-scale reading and 16 analog input channels. The sampling rate of the PCI-6052E is 333,000 samples/second and given its resolution, an analog input full-scale range of ± 10 V provides an accuracy of ± 4.747 mV.

The National Instruments Labview[®] 2010 graphical user interface (GUI) software was used for recording and processing the raw force, moment and flow condition data during testing. The easy-to-use GUI also allowed commands and tasks to be sent via the data acquisition board to the different components of the wind tunnel and experimental setup. During a run, the entire data-acquisition process was automated. The Labview[®] interface set and maintained the Reynolds number within the test section and the angle of attack of the wing, acquired raw data (dynamic pressure, lift, drag, pitching moment, angle of attack, ambient temperature and ambient pressure), and finally reduced and plotted the data graphically during a run for realtime inspection. Once a run was complete, the data was corrected using correction methods detailed in Chapter 3.8. Raw, corrected and conditions data at all angles of attack tested were saved to different output files for future data reduction.

3.3.2 Lift, Drag, and Pitching Moment Measurements

Raw lift, drag and moment signals from the load and torque cells were voltages based on its rated output and excitation voltage. The primary load cells used for lift and drag measurements were Interface Inc. SMT S-Type 5.6 lb (25 N) and 2.2 lb (10 N) load cells. These load cells had a nominal rated output of 2.0 mV/V. With a fixed excitation voltage of 10 V, the raw signals from the load cells were signal conditioned using a Vishay Measurement Group Model 2210A signal conditioning amplifier. The signal conditioning amplifier low-pass filtered the raw signals at 10 Hz and amplified it with a gain of X100. The signal-conditioned signals were then read by the NI data acquisition board. As a result, the full-scale range and resolution accuracy of the lift and drag analog input signals were ± 2 V and 1.190 mV respectively. Consequently, given the 2.2-lb (998 g) capacity drag

cell, the drag measurement was accurate to a resolution of 0.0013 lb (0.6 g).

Similarly, the primary torque cell used for pitching moment measurements was the Transducer Techniques RTS-100 low capacity torque sensor. The maximum capacity of the RTS-100 is 100 oz-in (0.71 oz-in) and its rated output is 1.5 mV/V. The same excitation voltage, low-pass filter, gain value, full-scale range and resolution was used, allowing the moment measurement to be accurate down to a resolution of 0.0595 oz-in (0.00042 N-m).

Raw signals for lift, drag and moment were sampled at a rate of 3,000 samples/second. At each angle of attack, 30,000 samples were averaged for each signal to overcome the small time-dependent fluctuations in tunnel speed due to the inertia of both the drive system and air at low speeds. Each run involved taking measurements of the wing at both increasing and decreasing angles of attack to capture any aerodynamic hysteresis.

3.3.3 Freestream Velocity Measurements

Measurement of freestream velocity within the test section was done by taking the pressure difference between the tunnel settling section (inlet), P_{ss} , and test section, P_{ts} , static pressures. The tunnel settling-section static pressure was taken from four static ports located just downstream of the anti-turbulence screens. Four static ports located slightly upstream of the test section were used for the test-section static pressures. The pneumatically averaged static pressures were connected to three separate differential pressure transducers, a Setra[®] Model 239 [56], a 1-Torr Baratron[®] Model 220 [57] and a 10 Torr Baratron[®] Model 221 [58]. The pressure transducer used depended on the speed at which the tests were run. For all runs, differential pressures from the less-accurate Setra and a chosen Baratron transducer were taken. The Setra transducer served as a check for the freestream velocities calculated by the Baratron transducer. Derived from Bernoulli's incompressible equation and conservation of mass, the freestream velocity in the test section was determined by Eq. 3.1.

$$V_\infty = \sqrt{\frac{2(P_{ss} - P_{ts})}{\rho_{amb} \left(1 - \left(\frac{A_{ts}}{A_{ss}}\right)^2\right)}} \quad (3.1)$$

where ρ_{amb} is the ambient air density calculated using Eq. 3.2, and A_{ts} and A_{ss} are the respective

test-section and settling-section (inlet) areas.

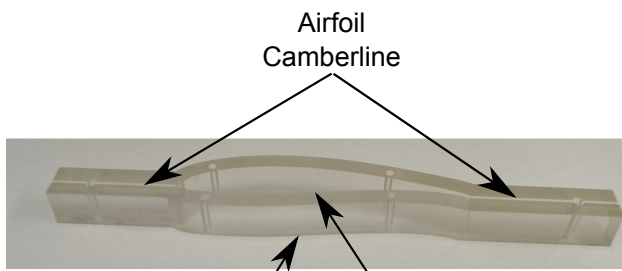
$$\rho_{amb} = \frac{P_{amb}}{RT_{amb}} \quad (3.2)$$

where R is the ideal gas constant, P_{amb} is the ambient atmospheric pressure, and T_{amb} is the ambient temperature. The ambient pressure was measured using a Setra model 270 pressure transducer and the ambient temperature was taken using a ± 1 deg R accurate Omega Model CJ thermocouple that was mounted to the side of the tunnel.

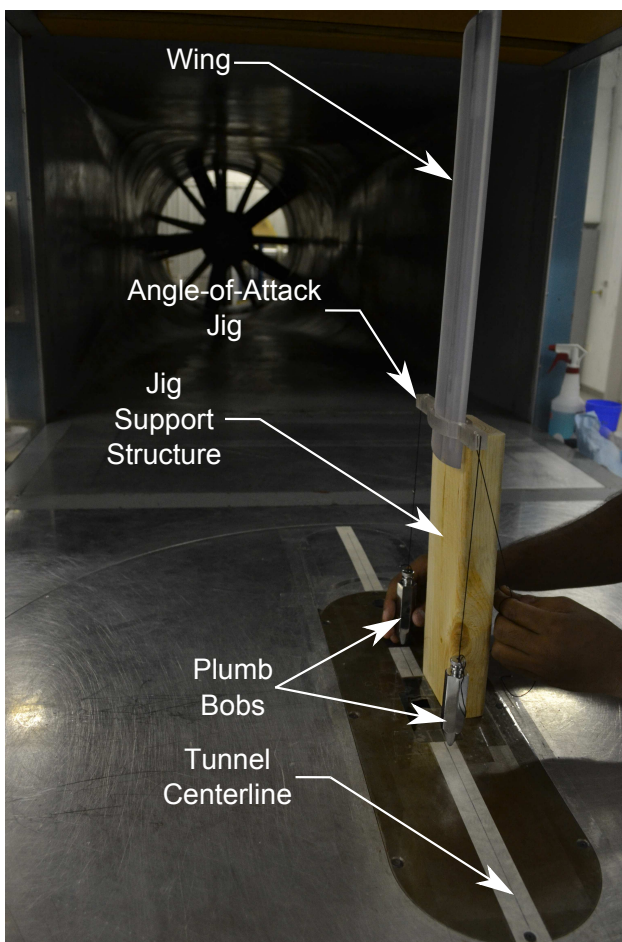
3.3.4 Angle of Attack Measurements

The angle of attack (α) measurements were taken using a US Digital® A2 optical encoder as discussed in Chapter 3.2.1. The A2 used a serial encoder interface (SEI) that communicated with the Labview® tunnel code via a RS-232 serial port.

Prior to testing, it was imperative that the measured α of a wing matched its true α as this directly affected the recorded performance of a wing. Therefore, the zero α of wings tested was set by aligning the wing reference chord line to the tunnel centerline. The angle-of-attack alignment of a wing became complicated when a wing with a cambered airfoil was tested. An angle-of-attack jig shown in Fig. 3.11(a) was designed to conform with a 0.02-in (0.51-mm) offset to the outline of the wing airfoil. An indented camber line of the airfoil extends from both ends of the jig. The angle-of-attack jig was created by the stereolithography (SLA®) rapid prototyping method (further discussed in Chapter 3.5) to ensure part accuracy. The alignment method used was purely manual and somewhat reliant on the eyes of the person testing. It was however found to be accurate to 0.2 deg, approximately double the resolution of the optical encoder. As shown in Fig. 3.11(b), alignment was performed with the help of two plumb bobs that extended from the camber line of the angle-of-attack jig to the tunnel floor. The plumb bobs had sharp tips that allowed the user to easily check the alignment of the wing with respect to the tunnel centerline.



(a)



(b)

Fig. 3.11: Angle-of-attack alignment method: (a) angle-of-attack jig and (b) alignment method.

3.4 Force and Moment Calibration

Although the LRN-FB was designed so that the lift L , drag D , and moment M measured were pure and with minimal interactions, there always exists some first- or second-order interactions (e.g. lift and drag platforms not exactly perpendicular) between the different parts of the balance under loading. A calibration matrix was created for the LRN-FB to account for these effects. The calibration matrix took the signal-conditioned lift, drag, and moment voltages and determined the true lift, drag, and moment loads that a wing faced.

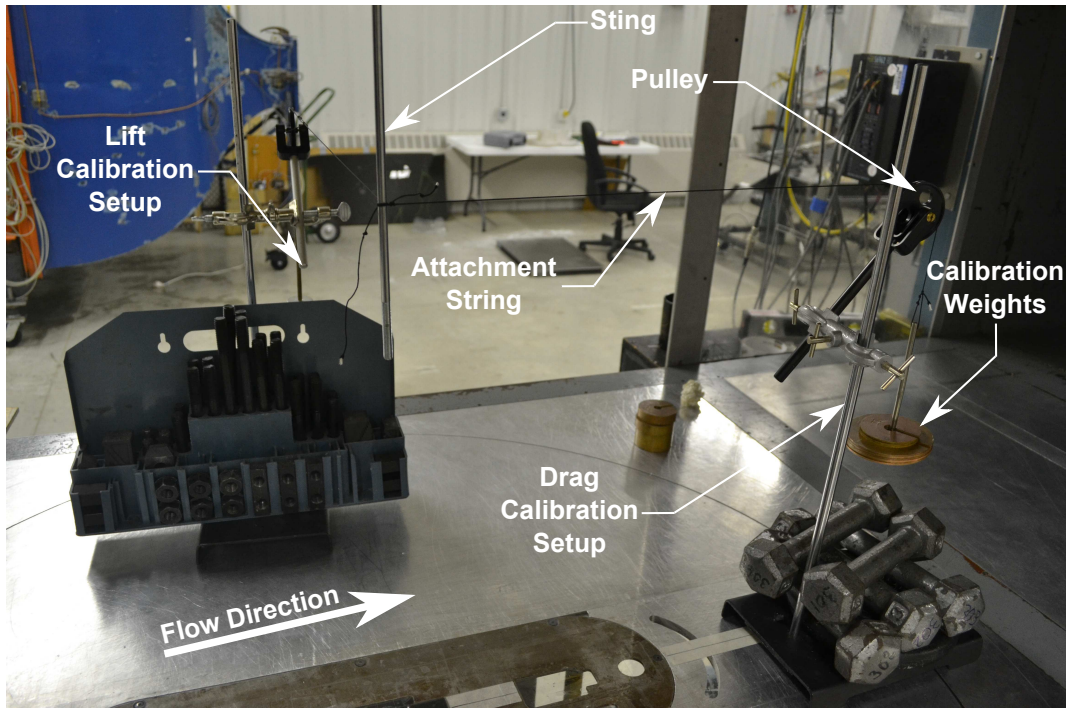
As discussed in Ref. 55, a calibration matrix can be determined by loading and recording the outputs of all three component output devices for each load applied. A calibration setup was created to perform lift, drag, and moment calibration as shown in Figs. 3.12(a–b). The calibration setup consisted of pulleys, attachment strings, calibration weight holders, alignment bobs, and test weights of known magnitude.

The lift and drag calibration setup shown in Fig. 3.12(a) involved aligning the pulleys perpendicular and parallel to the tunnel centerline respectively. The sting of the force balance was extended to the vertical spanwise center of the tunnel. Strings attached to the calibration weight holders were connected to the sting at this point. The vertical spanwise center of the tunnel was chosen as it was the center span location of all wings tested. Care was taken to ensure that the strings were level and properly aligned.

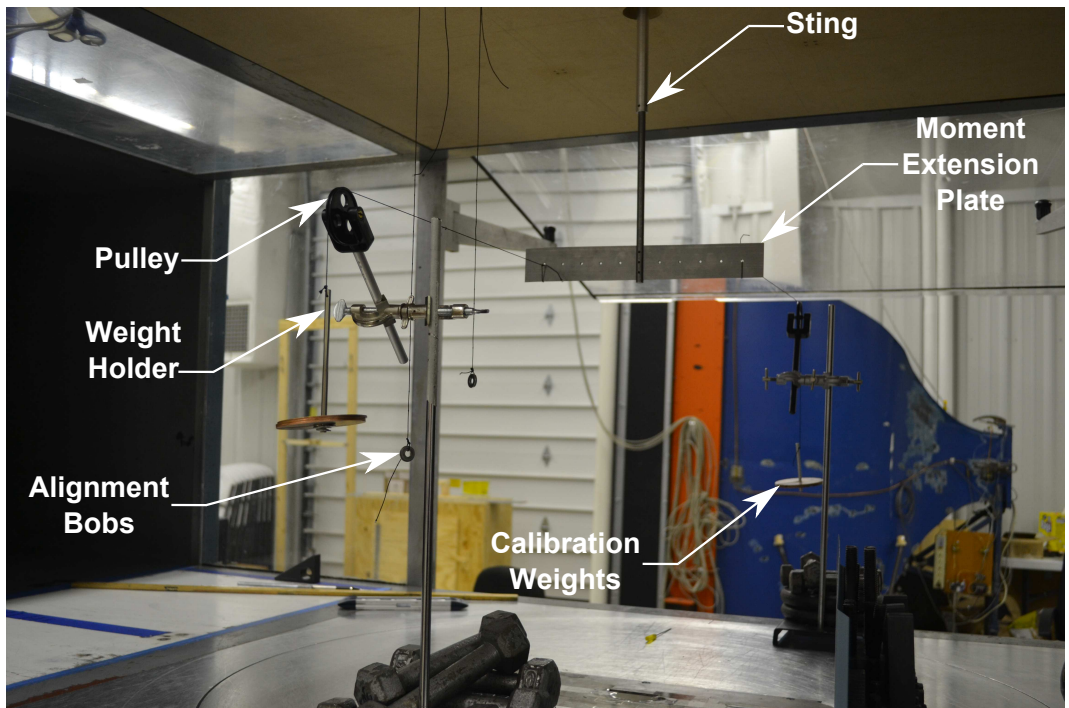
The moment calibration setup used an additional extension plate that had perforated holes spaced at known locations with respect to the centerline of the sting. The extension plate was aligned with the tunnel centerline and created a moment arm to which the loads could be applied. Pulley systems similar to that used for lift and drag calibration were also used. Equal and opposite loads were applied to equally spaced ends of the extension plate to ensure that no lift forces were inadvertently applied.

3.4.1 Linear Calibration (Lift and Drag)

Lift and drag calibration was performed linearly. Linear calibration was performed by loading the three components, L , D , and M up to its full capacity. Each loading was done individually up until



(a)



(b)

Fig. 3.12: LRN-FB calibration setup: (a) lift and drag calibration and, (b) moment calibration.

its maximum value and back down to zero to ensure linearity of load readings in both directions. With each loading, all three force and moment measurements were taken. Once all measurements for a particular loading were taken, linear fits for the three measurements were performed and recorded. The linear fits yielded a total of nine coefficients, $K_{L,L}$, $K_{L,D}$, $K_{L,M}$; $K_{D,L}$, $K_{D,D}$, $K_{D,M}$; and $K_{M,L}$, $K_{M,D}$, $K_{M,M}$, where the first letter in the subscript refers to the readings of the output device and the second letter in the subscript refers to the type of applied load. For example, $K_{L,D}$ refers to the linear fit coefficient of a lift reading due to a drag applied load. The nine coefficients created matrix K that related the load applied to the balance reading by Eq. 3.3. The calibration matrix, K^{-1} , was obtained by inverting the K matrix. The true load (H) equation shown in Eq. 3.4 is given by

$$\begin{bmatrix} Rdg \end{bmatrix} = \begin{bmatrix} K_{i,j} \end{bmatrix} \begin{bmatrix} H \end{bmatrix} = \begin{bmatrix} K_{L,L} & K_{L,D} & K_{L,M} \\ K_{D,L} & K_{D,D} & K_{D,M} \\ K_{M,L} & K_{M,D} & K_{M,M} \end{bmatrix} \begin{bmatrix} H \end{bmatrix} \quad (3.3)$$

$$\begin{bmatrix} H \end{bmatrix} = \begin{bmatrix} K_{i,j} \end{bmatrix}^{-1} \begin{bmatrix} Rdg \end{bmatrix} \quad (3.4)$$

When a calibration matrix is created, its coefficients correspond to the conditions and settings of the force balance at the time of calibration. This means that the coefficients of a calibration matrix are different if changes are made to the force balance that include different load cells, load cell mounting locations, and sting replacements. Slight differences in the calibration coefficients are also seen due to drift and different tunnel ambient conditions. All measurements taken for this thesis were with the force balance in the following configuration.

1. Lift: 5.6-lb (25-N) Model SMT-S load cell located at the topmost hole of the lift load cell mounting bracket.
2. Drag: 2.2-lb (10-N) Model SMT-S load cell located at the topmost hole of the drag load cell mounting bracket.
3. Moment: 100-oz.in (0.71-N-m) Model RTS-100 torque cell attached to a Model 6020-800 flex-pivot.

A Labview[®] sub-code was created to help in the creation of the calibration matrix and aid the process of calibration detailed above. The final calibration matrix, K^{-1} and balance output equation obtained from repeated calibrations is shown in Eqs. 3.5 and 3.6:

$$K^{-1} = \begin{bmatrix} 2.7341063 & 0.0185891 & 0.0137825 \\ -0.0115399 & 1.1303588 & -0.0000320 \\ -0.1303852 & -0.0008865 & 5.1350323 \end{bmatrix} \quad (3.5)$$

$$\begin{bmatrix} H_L \\ H_D \\ H_M \end{bmatrix} = \begin{bmatrix} 2.7341063Rdg_L - 0.0185891Rdg_D + 0.0137825Rdg_M \\ -0.0115399Rdg_L + 1.1303588Rdg_D - 0.0000320Rdg_M \\ -0.1303852Rdg_L - 0.0008865Rdg_D + 5.1350323Rdg_M \end{bmatrix} \quad (3.6)$$

3.4.2 Non-linear Calibration (Moment)

Although linear calibration was found to be accurate for lift and drag, moment was calibrated non-linearly in an effort to improve its accuracy. Non-linear calibration accounts for both first- and second-order effects of the forces measured. In addition, the non-linear method also accounts for interactions from combination forces (i.e. lift and drag, drag and moment, and lift and moment). A second-degree (quadratic) polynomial fit was applied for the pure lift, drag, and moment loadings previously performed. The second-degree polynomial fit created 18 constants. With an applied moment load, the constants obtained were, $C_{M,L}$, $C_{M,LL}$, $C_{M,D}$, $C_{M,DD}$, $C_{M,M}$, $C_{M,MM}$. When only a moment load is applied,

$$Rdg_M = C_{M,M}H_M + C_{M,MM}H_M^2 \quad (3.7)$$

where Rdg_M is the moment load cell reading and H_M is the true moment load. Lift and drag constants were also similarly found to create the linear ($C1$) and quadratic ($C2$) coefficient matrices shown in Eqs. 3.8–3.9.

$$\begin{bmatrix} C1 \\ C2 \end{bmatrix} = \begin{bmatrix} C_{L,L} & C_{L,D} & C_{L,M} \\ C_{D,L} & C_{D,D} & C_{D,M} \\ C_{M,L} & C_{M,D} & C_{M,M} \end{bmatrix} \quad (3.8)$$

$$\begin{bmatrix} C2 \end{bmatrix} = \begin{bmatrix} C_{L,LL} & C_{L,DD} & C_{L,MM} \\ C_{D,LL} & C_{D,DD} & C_{D,MM} \\ C_{M,LL} & C_{M,DD} & C_{M,MM} \end{bmatrix} \quad (3.9)$$

Once pure load calibration was performed, lift-drag, drag-moment, and lift-moment load interaction calibration was performed. Lift-drag load interaction calibration was performed by adding incremental known loadings in the lift and drag directions and taking lift, drag, and moment measurements. Loadings are done in both directions to ensure linearity of load readings. Once all measurements for a particular loading were taken, linear fits for the three measurements were performed and recorded. These steps were also performed for drag-moment and lift-moment calibration. An interaction coefficient matrix ($C3$) was then created using the nine coefficients obtained.

$$\begin{bmatrix} C3 \end{bmatrix} = \begin{bmatrix} C_{L,LD} & C_{L,DM} & C_{L,LM} \\ C_{D,LD} & C_{D,DM} & C_{D,LM} \\ C_{M,LD} & C_{M,DM} & C_{M,LM} \end{bmatrix} \quad (3.10)$$

Using the linear, quadratic and interaction coefficient matrices, an iterative reverse calibration method detailed in Refs. 59–61 was implemented in Labview to obtain true moment loads realtime from measured readings. The iterative method is introduced below in Eqs. 3.11–3.19.

$$\begin{bmatrix} Rdg \end{bmatrix} = \begin{bmatrix} C1 \end{bmatrix} \begin{bmatrix} H1 \end{bmatrix} + \begin{bmatrix} C2 \end{bmatrix} \begin{bmatrix} H2 \end{bmatrix} + \begin{bmatrix} C3 \end{bmatrix} \begin{bmatrix} H3 \end{bmatrix} \quad (3.11)$$

$$\begin{bmatrix} H1 \end{bmatrix} = \begin{bmatrix} H_L \\ H_D \\ H_M \end{bmatrix} \quad (3.12)$$

$$\begin{bmatrix} H2 \end{bmatrix} = \begin{bmatrix} H_L^2 \\ H_D^2 \\ H_M^2 \end{bmatrix} \quad (3.13)$$

$$\begin{bmatrix} H3 \end{bmatrix} = \begin{bmatrix} H_L H_D \\ H_D H_M \\ H_L H_M \end{bmatrix} \quad (3.14)$$

Given that Rdg , $C1$, $C2$, and $C3$ are known, H is obtained by the following iterative method.

In the first iteration,

$$\begin{bmatrix} H1_1 \end{bmatrix} = \begin{bmatrix} C1 \end{bmatrix}^{-1} \begin{bmatrix} Rdg \end{bmatrix} \quad (3.15)$$

In the second iteration,

$$\begin{bmatrix} H1_2 \end{bmatrix} = \begin{bmatrix} H1_1 \end{bmatrix} + \begin{bmatrix} D \end{bmatrix} \begin{bmatrix} H2_1 \end{bmatrix} + \begin{bmatrix} E \end{bmatrix} \begin{bmatrix} H3_1 \end{bmatrix} \quad (3.16)$$

where D and E are calculated by Eqs. 3.17 & 3.18. $H2_1$ and $H3_1$ are calculated using $H1_1$.

$$\begin{bmatrix} D \end{bmatrix} = -\begin{bmatrix} C1 \end{bmatrix}^{-1} \begin{bmatrix} C2 \end{bmatrix} \quad (3.17)$$

$$\begin{bmatrix} E \end{bmatrix} = -\begin{bmatrix} C1 \end{bmatrix}^{-1} \begin{bmatrix} C3 \end{bmatrix} \quad (3.18)$$

For further iterations, the second iteration is repeated until the $H1$ converges.

$$\begin{bmatrix} H1_n \end{bmatrix} = \begin{bmatrix} H1_1 \end{bmatrix} + \begin{bmatrix} D \end{bmatrix} \begin{bmatrix} H2_n \end{bmatrix} + \begin{bmatrix} E \end{bmatrix} \begin{bmatrix} H3_n \end{bmatrix} \quad (3.19)$$

According to Ref. 60, solutions should converge between 2 to 10 iterations to provide the final calculated applied loads. To re-iterate, only moment loads were calculated by the non-linear method. Lift and drag were calculated using the linear method.

3.5 Wind Tunnel Models

All models tested in this thesis were rapid prototyped using stereolithography (SLA[®]) technology. SLA allows three-dimensional models to be created with the use of a computer-controlled process that involves layering successions of curable material based on the cross section of the model. The

wings created with this process conformed to tolerances of about ± 0.005 in (0.127 mm) [62] ensuring model accuracy and surface quality. Curing materials used for the wings were chosen based on the final rigidity of the material. High rigidity was required as the wings were to be placed under high loading conditions.

A Wortmann FX 63-137 rectangular ($\lambda=1$) wing with an aspect ratio (\mathcal{R}) of 4 was chosen as a test validation case. The availability of experimental data in literature [4, 63] made it a good choice for validation. An aspect ratio of 4 was chosen as it represented the mean aspect ratio of wings intended to be tested with the balance. To aid in validation, an additional rectangular flat-plate wing with an \mathcal{R} of 3 was chosen as a benchmark for low aspect ratio flat plate measurements. The \mathcal{R} -3 flat-plate wing was designed to emulate that tested by Pelletier and Mueller,[5] and Shields and Mohseni [8]. The key differences though was that the thickness-to-chord ratio of the flat-plate model was 4.3% in comparison with 2.6% in Refs. 5 and 8. In addition, the flat-plate model was designed to have a 10-to-1 elliptical trailing edge thickness ratio instead of the 5-to-1 ratio used by Refs. 5 and 8.

The airfoils used for the Wortmann and \mathcal{R} -3 flat-plate wings are shown in Fig. 3.13. The Wortmann FX 63-137 airfoil was a modification of a smooth version obtained from the UIUC Airfoil Database [64]. The subsonic airfoil development system, XFOIL [65], was used to modify the thickness of the trailing edge of the airfoil to 0.02 in (0.51 mm) while ensuring that the airfoil pressure distribution was not substantially affected. A finite thickness was set to ensure that the trailing edge of the completed wing would not easily break under loading. The coordinates for the modified FX 63-137 airfoil are listed in Appendix A. The airfoil used for the \mathcal{R} -3 flat-plate model was easily created in SolidWorks[®] using two straight lines and two half-ellipses.

Once both validation cases were completed, nine additional flat-plate wings were tested as shown in Table 3.2. The flat-plate models were manufactured to the same airfoil configuration as that of the \mathcal{R} -3 validation wing. A flat-plate airfoil was chosen for testing as it serves as a good baseline to observe and decipher the effects of Reynolds number, aspect ratio, and taper ratio on low-to-moderate aspect ratio wings. In addition, the geometries and Reynolds numbers tested were those typically used for small-scale UAV wings and stabilizers.

Variations in taper ratios for the all wings were done about the quarter chord. This ensured that the the quarter chord line of all the wings were fixed. A mean aerodynamic chord (\bar{c}) of

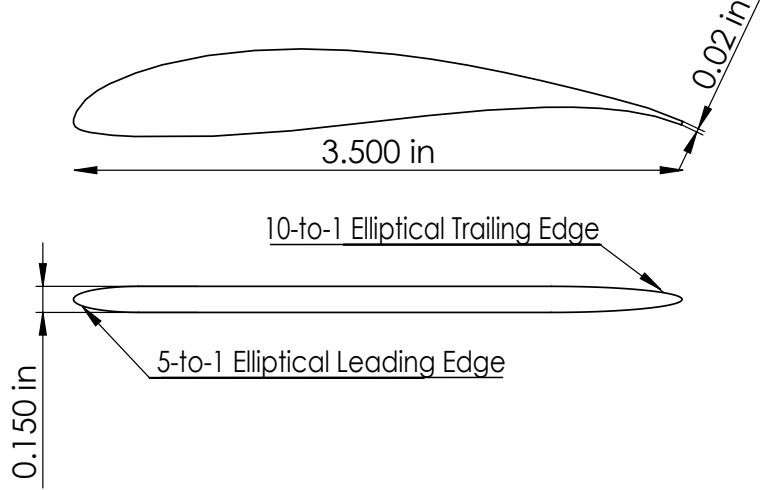
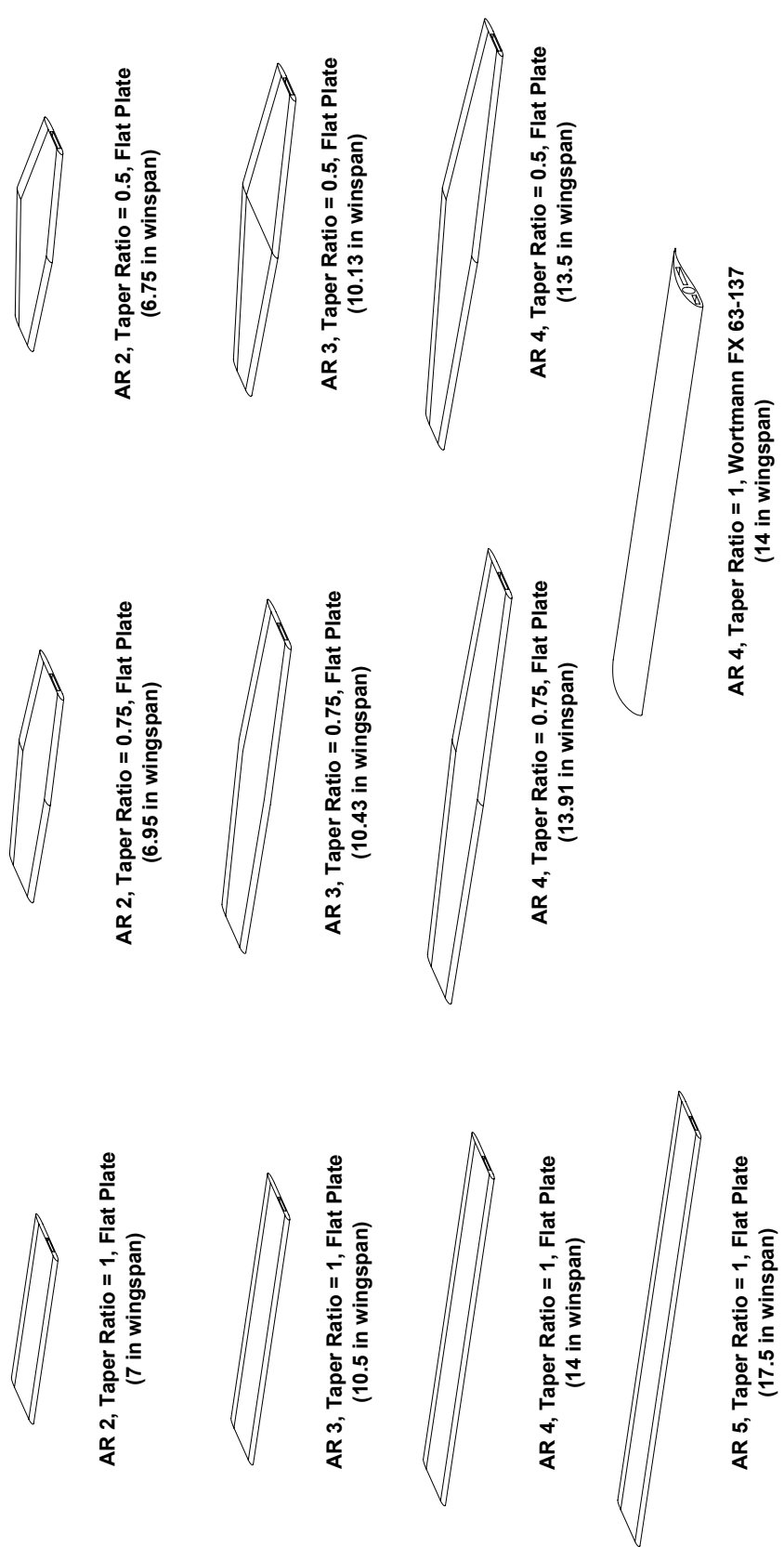


Fig. 3.13: Airfoils of wings tested: Wortmann FX 63-137 airfoil (smooth) and 5-to-1 elliptical leading edge, 10-to-1 elliptical trailing edge flat plate.

Table 3.2: Flat-plate model test matrix.

		\mathcal{R}			
		2	3	4	5
λ	0.5	0.5	0.5	-	
	0.75	0.75	0.75	-	
	1	1	1	1	

3.5 in was chosen for all wings tested. The 3.5-in mean aerodynamic chord minimized the Reynolds numbers that could be tested in the wind tunnel before flow speed unsteadiness became an issue. In addition, the model span fraction (MSF) of all the wings tested was to be kept under 0.8. The MSF is the ratio of the wingspan (b) to the spanwise width (H) of the test section. According to Refs. 55 and 66, a MSF value that is less than 0.8 is desirable in order for standard wind tunnel corrections to apply. All wings tested fall under this limitation with the maximum MSF being 0.52. The final designs of all the wings tested are shown in Fig. 3.14.



All models drawn to scale

Fig. 3.14: Isometric view of all wings tested.

3.6 Flow Visualization Technique

Flow visualization techniques provide an important tool for aerodynamicists to understand or identify issues on the performance characteristics of a test model. Fluorescent surface oil flow visualization was employed on three wings tested. The primary goal of using flow visualization was to ensure that the surface flow quality over the wings tested weren't hindered by the effects of the sting. The three models and their corresponding Reynolds number tested are as follows.

- Wortmann FX 63-137 wing: $\mathcal{R} = 4, \lambda = 1, Re = 90,000$
- Flat-plate wing: $\mathcal{R} = 2, \lambda = 1, Re = 140,000$
- Flat-plate wing: $\mathcal{R} = 2, \lambda = 0.5, Re = 120,000$

The process of performing surface oil flow visualization involved the initial application of a uniform, smooth layer of matte black Ultracote Plus[®] on the upper and lower surface of the wing. The Ultracote Plus layer was necessary since the models were made using SLA curing materials that skewed photographs taken of the fluorescent oil on the surface of the wing. All flow visualization was performed on the upper surface as it was deemed to be of most interest given the time constraints. Also, since flat-plate wings had symmetric airfoils, upper surface flow visualization was sufficient.

After cleaning the wing of impurities (i.e. dust particles, etc.), 10W-30 motor oil was applied using a lint-free shop rag to the upper surface of the wing. Excess oil was removed to leave a smooth finish. An airbrush run by regulated Nitrogen gas at 30 psi was then used to apply a thin layer of a fluorescent leak detector dye-mineral oil mixture onto the upper surface of the airfoil. The mix contained four drops of Tracer TP34000601 UV fluorescent leak detection die and approximately 250 mL of standard mineral oil. Application of the dye-mineral oil mixture was done with the wind tunnel running at 20 RPM to allow extra fumes from the airbrush to advect downstream and not clutter the test section. A check was performed to ensure that the whole upper surface of the wing was covered with the dye-mineral oil layer by using fluorescent tube black lights. Once the dye-mineral oil mix was applied, the tunnel was set to the desired test RPM. Given that the speeds tested were low, it was critical that sufficient time was provided to allow the dye-mineral oil layer to sufficiently flow under the shear stress from the air stream. The mineral oil ensured that the dye mix had enough viscosity to not succumb to the influences of gravity too fast. At the low

Reynolds numbers tested, tests were run for approximately 15 minutes to allow the oil to reveal the surface patterns required. Photographs were taken immediately after tunnel runs were complete to minimize movement of the dye-oil layer due to gravity. This process was then repeated for the different settings required.

Fig. 3.17 shows a photograph of a fluorescent oil flow over the upper surface of the Wortmann wing at $\alpha = 9$ deg and $Re = 90,000$. Several important features of low Reynolds number flow over wings were discernible such as the laminar flow, laminar separation bubble, and turbulent flow regions. Wing vortex induced separation was also observed in the regions of the wing tips.

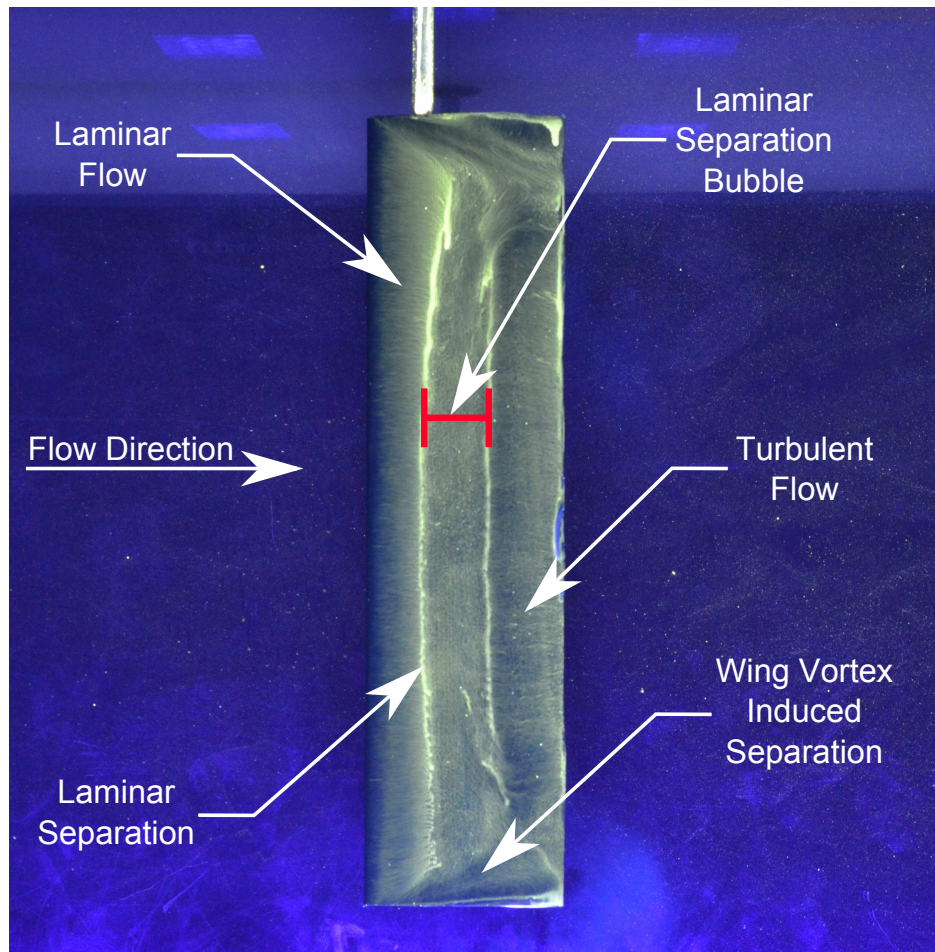


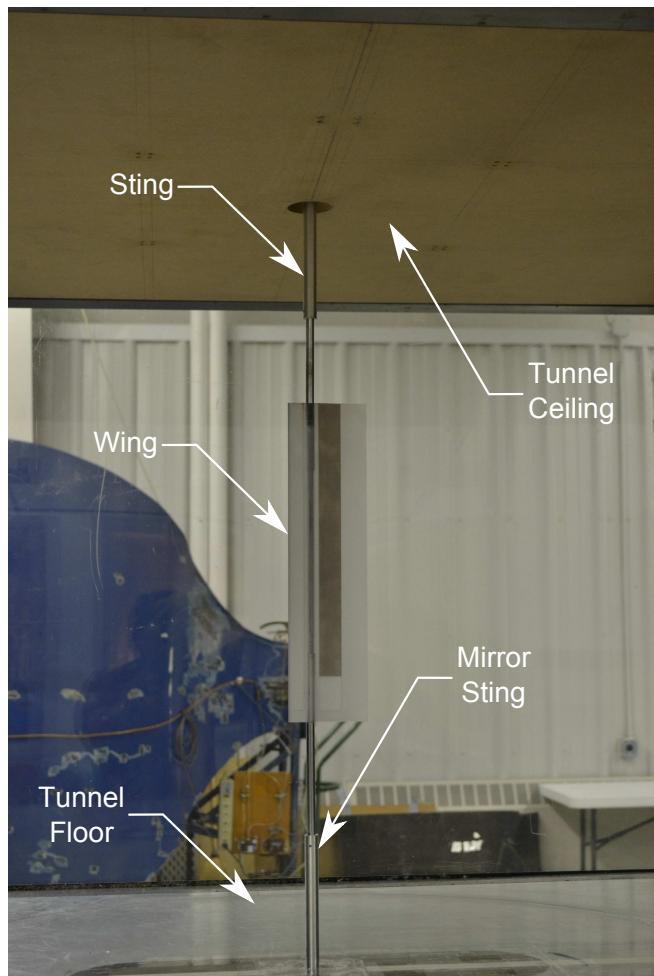
Fig. 3.15: Upper surface oil flow visualization of major flow features on the Wortmann FX 63-137 AR - 4 rectangular wing ($\alpha = 9$ deg, $Re = 90,000$).

3.7 Tare and Interference Determination

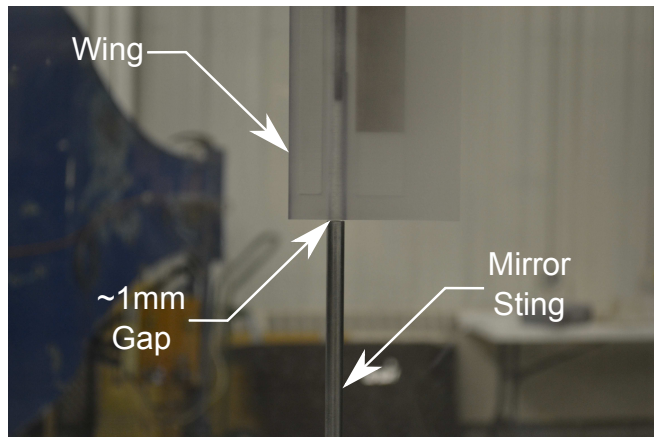
The cantilever beam mounting setup for all wings tested made it necessary to account for the interference and tare effects of the sting. As discussed in Ref. 55, the tare of the sting is its direct drag effects and the interference are its effect on the free air flow over the wing.

Prior to performing wing tests, sting tares were taken at the different test Reynolds numbers. Lift, drag and moment voltage measurements of the sting were recorded and stored. The Labview tunnel code then accounted for the sting effects during wing tests by subtracting the corresponding sting voltage measurements from the measurements read. Aerodynamics loads were then calculated from the tare subtracted measurements using the calibration matrix described in Chapter 3.4.

Interference effects of the sting on the wing was tested by mounting a mirror sting to the tunnel floor as shown in Fig. 3.16(a). Interference tests were performed using the Wortmann FX 63-137 \mathcal{A} -4 rectangular wing. The mirror sting was not attached to the wing and a gap of approximately 1 mm was maintained as shown in Fig. 3.16(b). Tests performed at Reynolds numbers of 30,000 and 60,000 showed that the mirror sting had negligible interference effects on the lift, drag and moment measurements of the wing. This conclusion was further supported by flow visualization photographs of the Wortmann wing at a Re of 90,000, and a \mathcal{A} -2 rectangular flat-plate wing at a Re of 140,000 as shown in Figs. 3.17(a–b).

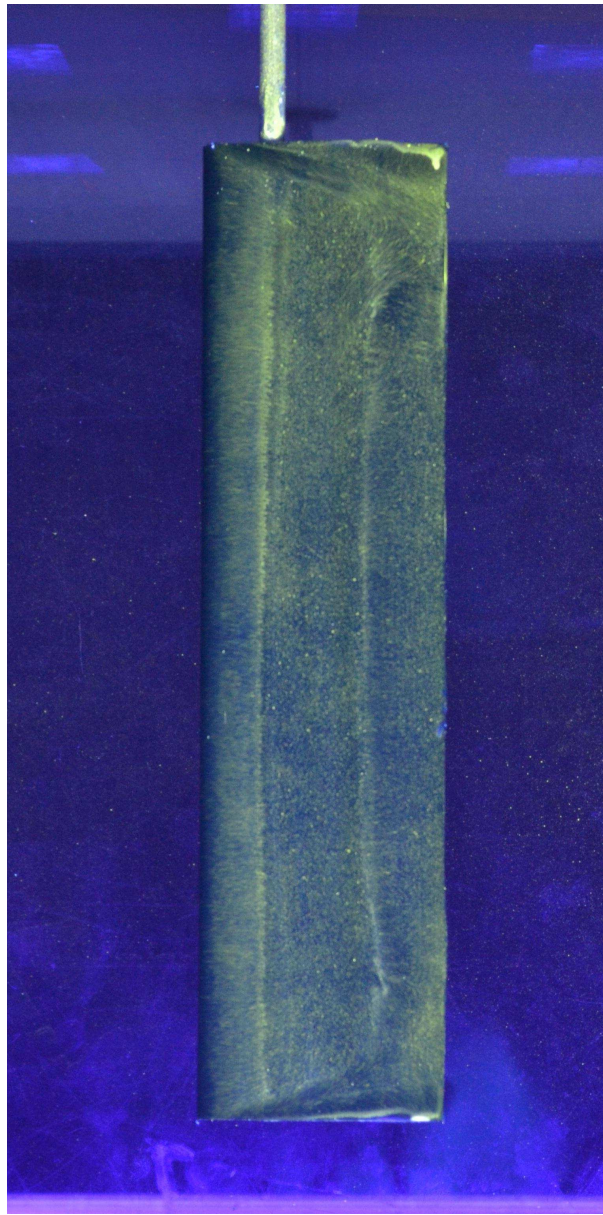


(a)

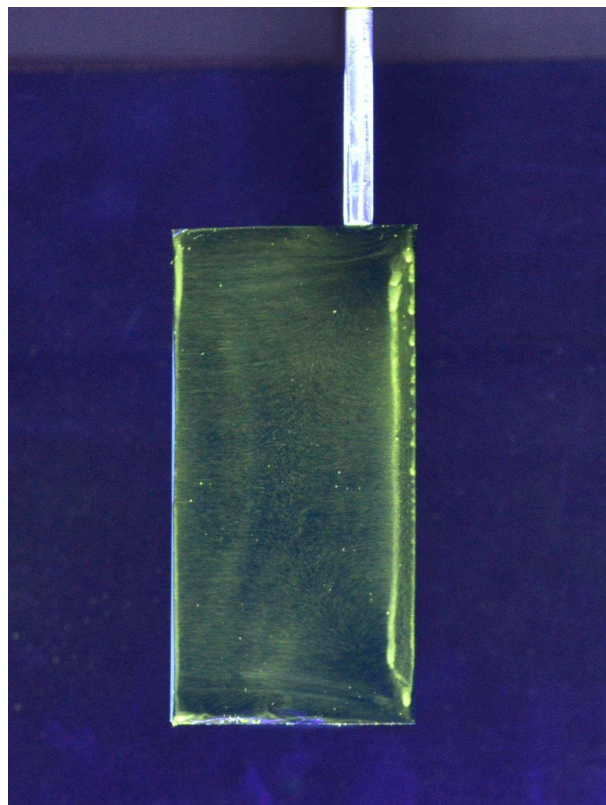


(b)

Fig. 3.16: Experimental setup for mirror sting interference tests: (a) Wortmann FX 63-137 \mathcal{A} R-4 rectangular wing shown with sting and mirror sting and (b) Mirror sting to wing gap.



(a)



(b)

Fig. 3.17: Upper surface oil flow visualization photographs: (a) Wortmann FX 63-137 \mathcal{R} -4 rectangular wing ($\alpha = 7$ deg, $Re = 90,000$) and (b) \mathcal{R} -2 rectangular flat-plate wing ($\alpha = 10$ deg, $Re = 140,000$).

3.8 Data Correction

Given the bounded nature of free stream flow in a wind tunnel, model performance characteristics measured experimentally may not always match the actual aerodynamic performance of the model in ‘free air’. There exists a number of effects that cause these experimental discrepancies to exist. As detailed in Ref. 55, various correction methods have been devised to account for these effects. This section details the various tunnel corrections that were implemented for the three-dimensional wings tested. The implementations were made in the LRN-FB Labview tunnel code and data corrections were performed upon completion of a tunnel run. The four most important effects on the flow-field of a wing in a test section were its buoyancy effects, solid blockage, wake blockage and its streamline curvature effects.

3.8.1 Buoyancy Effects

Buoyancy effects were assumed to be neglected as the slight increase in tunnel test-section width discussed in Chapter 3.1 minimizes the thickening effect of the boundary layer. The expanding test section therefore decreases the static pressure gradient across the tunnel test section thereby making buoyancy effects negligible. In addition, Ref. 55 state that the ‘horizontal buoyancy’ is usually insignificant for wings.

3.8.2 Solid Blockage

Solid blockage is the constraining effect of the tunnel walls on the flow around a wing. The wing causes an effective shrink in test-section area for flow to pass through. As a result, there is an increase in dynamic pressure and has to be corrected using

$$\varepsilon_{sb} = \frac{K_1 \tau_1 (\text{wing volume})}{C^{3/2}} \quad (3.20)$$

where K_1 is the body shape factor, τ_1 is related to the tunnel test-section and the MSF, K_1 and τ_1 are determined from figures in Ref. 55, and C is the tunnel test-section area.

3.8.3 Wake Blockage

The wake blockage effects derived by Maskell [67] includes the effects of separated flow and is given by

$$\varepsilon_{wb} = \frac{S}{4C} C_{D_0} + \frac{5S}{4C} (C_{D_u} - C_{D_i} - C_{D_0}) \quad (3.21)$$

where S is the wing surface area, C_{D_u} is the uncorrected drag coefficient, C_{D_i} is the uncorrected induced drag component and C_{D_0} is the uncorrected minimum drag coefficient. When a run is complete, C_{D_0} and C_{D_i} are determined by plotting $C_{L_u}^2$ versus C_{D_u} . The minimum value of C_{D_u} is picked as C_{D_0} and for wings with no flaps, the slope of the linear portion of the curve is used to calculate C_{D_i} using

$$C_{D_i} = C_{L_u}^2 \left[\frac{dC_{D_u}}{dC_{L_u}^2} \right] - C_{D_0} \quad (3.22)$$

As alluded to in Ref. 55, the Maskell approach works well for wings that yield a separation bubble across the whole span and wings of aspect ratios less than five. Given that the wings tested were of low-to-moderate aspect ratio, the Maskell approach was deemed to be an acceptable method of wake blockage correction.

3.8.4 Final Blockage Corrections

Using the calculated solid and wake blockages, the final blockage correction and resultant dynamic pressure and velocity corrections are given by

$$\varepsilon_T = \varepsilon_{sb} + \varepsilon_{wb} \quad (3.23)$$

$$q_{\infty_c} = q_{\infty_u} (1 + \varepsilon_T)^2 \quad (3.24)$$

$$V_{\infty_c} = V_{\infty_u} (1 + \varepsilon_T) \quad (3.25)$$

3.8.5 Streamline Curvature

Streamline curvature effects arise from the distortion of the natural streamlines due to the presence of wind tunnel walls. Discussed in more detail in Ref. 55, for three dimensional wings, the streamline curvature correction is related to the variation of boundary-induced upwash along the chord and accounts for the induced flow of the doubly infinite image system at the lifting line of a real wing.

Given that the dynamic pressure and lift are corrected for blockage, the angle of attack, drag, and pitching moment are corrected for boundary induced upwash and streamline curvature by

$$\alpha_c = \alpha_u + \frac{\delta S}{C} (1 + \tau_2) C_{Lc} \quad (3.26)$$

$$C_{Dc} = \frac{D_u}{q_{\infty c} S} + \frac{\delta S}{C} C_{Lc}^2 \quad (3.27)$$

$$C_{M_c} = \frac{M_u}{q_{\infty c} S \bar{c}} + 0.125 \tau_2 \frac{\delta S}{C} \left(\frac{dC_{Lc}}{d\alpha_c} \right) \quad (3.28)$$

3.9 Uncertainty Analysis

Uncertainty analysis was carried out on the newly designed LRN-FB force balance and measurement system by a methodology similar to that discussed in Noe [68]. The methodology involved using the second-power equation introduced by Kline and McClintock [69] and further discussed by Coleman and Steel [70].

The total error given by an instrument is a combination of its precision and bias error. Precision error is a non-repeatable error due to unknown sources affecting measurement. Reduction of precision error is done by averaging multiple sample sets. Bias error however is a repeatable error that does not vary with more measurement sample sets from the true value. Experimental uncertainties calculated using the Kline and McClintock method mainly address bias uncertainties. Uncertainties due to precision or wind tunnel corrections are not accounted for.

Given an output R that is represented as a function of several measured values, x_1, x_2, \dots, x_n in the form of Eq. 3.29, the experimental uncertainty associated with output R is found with

$$R = R(x_1, x_2, \dots, x_n) \quad (3.29)$$

$$U_R = \sqrt{\left(\frac{\partial R}{x_1} U_{x_1}\right)^2 + \left(\frac{\partial R}{x_2} U_{x_2}\right)^2 + \left(\frac{\partial R}{x_3} U_{x_3}\right)^2 + \dots + \left(\frac{\partial R}{x_n} U_{x_n}\right)^2} \quad (3.30)$$

The root-sum-square (RSS) method is employed when multiple uncertainties need to be combined as shown in

$$U_{x_{RSS}} = \sqrt{(x_1^2 + x_2^2 + x_3^2 + \dots + x_n^2)} \quad (3.31)$$

3.9.1 Uncertainty Equations

Using the methods described above, the flow conditions and force balance uncertainties are calculated using the equations shown in Tables 3.3 and 3.4.

Table 3.3: Uncertainty equation table

Property	Symbol	Uncertainty Equation	Partial Derivatives
Dynamic Pressure	q_∞	$U_{q_\infty} = \sqrt{\left(\frac{\partial q_\infty}{\partial(P_{ss}-P_{ts})} U_{P_{ss}-P_{ts}}\right)^2}$	$\frac{\partial q_\infty}{\partial(P_{ss}-P_{ts})} = \frac{1}{1-\left(\frac{A_{ts}}{A_{ss}}\right)}$
Ambient Density	ρ_{amb}	$U_{\rho_{amb}} = \sqrt{\left(\frac{\partial \rho_{amb}}{\partial P_{amb}} U_{P_{amb}}\right)^2 + \left(\frac{\partial \rho_{amb}}{\partial T_{amb}} U_{T_{amb}}\right)^2}$	$\frac{\partial \rho_{amb}}{\partial P_{amb}} = \frac{1}{RT_{amb}}$ $\frac{\partial \rho_{amb}}{\partial T_{amb}} = \frac{1}{RT_{amb}^2}$
Dynamic Viscosity	μ	$U_\mu = \sqrt{\left(\frac{\partial \mu}{\partial q_\infty} U_{T_{amb}}\right)^2}$	$\frac{\partial \mu}{\partial T_{amb}} = \frac{3}{2}\mu_0 \sqrt{\frac{T_{amb}}{T_0}} \frac{T_0+Su}{T_0(T_{amb}+Su)} \dots$ $-\mu_0 \left(\frac{T_{amb}}{T_0}\right)^{\frac{3}{2}} \frac{T_0+Su}{(T_{amb}+Su)^2}$
Freestream Velocity	V_∞	$U_{V_\infty} = \sqrt{\left(\frac{\partial V_\infty}{\partial q_\infty} U_{q_\infty}\right)^2 + \left(\frac{\partial V_\infty}{\partial \rho_{amb}} U_{\rho_{amb}}\right)^2}$	$\frac{\partial V_\infty}{\partial q_\infty} = \frac{1}{\sqrt{2q_\infty \rho_{amb}}}$ $\frac{\partial V_\infty}{\partial \rho_{amb}} = -\frac{1}{\rho_{amb}} \sqrt{\frac{q_\infty}{2\rho_{amb}}}$
Reynolds Number	Re	$U_{Re} = \sqrt{\left(\frac{\partial Re}{\partial \rho} U_\rho\right)^2 + \left(\frac{\partial Re}{\partial V_\infty} U_{V_\infty}\right)^2 + \left(\frac{\partial Re}{\partial \bar{c}} U_{\bar{c}}\right)^2 + \left(\frac{\partial Re}{\partial \mu} U_\mu\right)^2}$	$\frac{\partial Re}{\partial \rho} = \frac{V_\infty \bar{c}}{\mu}$ $\frac{\partial Re}{\partial V_\infty} = \frac{\rho \bar{c}}{\mu}$ $\frac{\partial Re}{\partial \bar{c}} = \frac{\rho V_\infty}{\mu}$ $\frac{\partial Re}{\partial \mu} = \frac{\rho V_\infty \bar{c}}{\mu^2}$

Table 3.4: Force uncertainty equation table

Property	Symbol	Uncertainty Equation	Partial Derivatives
Lift Coefficient	C_L	$U_{C_L} = \sqrt{\left(\frac{\partial C_L}{\partial L} U_L\right)^2 + \left(\frac{\partial C_L}{\partial q_\infty} U_{q_\infty}\right)^2 + \left(\frac{\partial C_L}{\partial b} U_b\right)^2 + \left(\frac{\partial C_L}{\partial \bar{c}} U_{\bar{c}}\right)^2}$	$\frac{\partial C_L}{\partial L} = \frac{1}{q_\infty b \bar{c}}$ $\frac{\partial C_L}{\partial q_\infty} = \frac{L}{q_\infty^2 b \bar{c}}$ $\frac{\partial C_L}{\partial b} = \frac{L}{q_\infty b^2 \bar{c}}$ $\frac{\partial C_L}{\partial \bar{c}} = \frac{L}{q_\infty b \bar{c}^2}$
Drag Coefficient	C_D	$U_{C_D} = \sqrt{\left(\frac{\partial C_D}{\partial D} U_D\right)^2 + \left(\frac{\partial C_D}{\partial q_\infty} U_{q_\infty}\right)^2 + \left(\frac{\partial C_D}{\partial b} U_b\right)^2 + \left(\frac{\partial C_D}{\partial \bar{c}} U_{\bar{c}}\right)^2}$	$\frac{\partial C_D}{\partial D} = \frac{1}{q_\infty b \bar{c}}$ $\frac{\partial C_D}{\partial q_\infty} = \frac{D}{q_\infty^2 b \bar{c}}$ $\frac{\partial C_D}{\partial b} = \frac{D}{q_\infty b^2 \bar{c}}$ $\frac{\partial C_D}{\partial \bar{c}} = \frac{D}{q_\infty b \bar{c}^2}$
Moment Coefficient	C_M	$U_{C_M} = \sqrt{\left(\frac{\partial C_M}{\partial M} U_M\right)^2 + \left(\frac{\partial C_M}{\partial q_\infty} U_{q_\infty}\right)^2 + \left(\frac{\partial C_M}{\partial b} U_b\right)^2 + \left(\frac{\partial C_M}{\partial \bar{c}} U_{\bar{c}}\right)^2}$	$\frac{\partial C_M}{\partial M} = \frac{1}{q_\infty b \bar{c}^2}$ $\frac{\partial C_M}{\partial q_\infty} = \frac{M}{q_\infty^2 b \bar{c}^2}$ $\frac{\partial C_M}{\partial b} = \frac{M}{q_\infty b^2 \bar{c}^2}$ $\frac{\partial C_M}{\partial \bar{c}} = \frac{2M}{q_\infty b \bar{c}^3}$

3.9.2 Example Test Case Uncertainty Calculation

An example test case was used for uncertainty analysis. The test case used was the Wortmann FX 63-137 \mathcal{A} -4 rectangular wing tested at a Reynolds number of 90,000 and angle of attack of 5 deg. Tables 3.5 and 3.6 show the uncertainties of the pressure and temperature measurement devices used. Table 3.7 shows the constants that were used for the uncertainty calculations. Table 3.8 presents variables where uncertainties were obtained from known sources (i.e. datasheets, tests, etc.).

All the flow condition uncertainties calculated for the example test case using equations in Table 3.3 are shown in Table 3.9. Force/moment coefficient uncertainties calculated for the example test case using equations in Table 3.4 are shown in Table 3.10. The force/moment uncertainties were

Table 3.5: Pressure transducer characteristics

Setra Model 239		
Property	Units	Values
$P_{fullscale}$	psi	5
Non-linearity	% Full Scale (psi)	0.20 (0.01)
Hysteresis	% Full Scale (psi)	0.10 (0.005)
Non-repeatability	% Full Scale (psi)	0.02 (0.001)
Accuracy RSS at const. temp	% Full Scale (psi)	0.28 (0.014)

MKS Type 221 10 Torr Baratron General Purpose Pressure Transducer		
Property	Units	Values
$P_{fullscale}$	Torr (psi)	10 (0.19337)
Resolution	% Full Scale (psi)	0.01 (0.000019337)
Accuracy	% Reading. (psi)	0.5 (0.00096685)

Setra Model 239		
Property	Units	Values
$P_{fullscale}$	psi	20
Non-linearity	% Full Scale (psi)	0.05 (0.010)
Hysteresis	% Full Scale (psi)	0.03 (0.006)
Non-repeatability	% Full Scale (psi)	0.01 (0.002)
Accuracy RSS at const. temp	% Full Scale (psi)	0.05 (0.010)

Table 3.6: Temperature sensor characteristics

Omega Model CJ Thermocouple		
Property	Units	Values
Compensation Accuracy (25 deg C)	deg C (deg R)	0.25 (0.45)
Compensation Accuracy (15 to 35 deg C)	deg C (deg R)	0.5 (0.9)
Compensation Accuracy (10 to 50 deg C)	deg C (deg R)	0.75 (1.35)

calculated from the bias error of load tests that were carried out during testing. In load tests, the LRN-FB was loaded with multiple loads of known actual weights. The bias error between the load readings and the actual weights were averaged. The averages obtained for lift, drag and moment were calculated to be 3.28%, 2.66% and 4.56% respectively. The main source of the force/moment uncertainty was from calibration errors.

Table 3.7: Given constants

Property	Units	Values
Contraction Ratio (A_{ts}/A_{ss})	-	1/7.5
Gas Constant (R)	ft-lb/(slug-deg R)	1716
Reference Temperature (T_0)	deg R	491.6
Sutherland Temperature (S)	deg R	199.8
Reference Dynamic Viscosity (μ_0)	lb-s/ft ²	3.58E-7

Table 3.8: Known uncertainties

Property	Units	Reference Value	Absolute Uncertainty	Relative Uncertainty (%)
Angle of Attack (α)	deg	5	0.02	4
Mean Aerodynamic Chord (\bar{c})	in (ft)	3.5 (0.292)	0.01 (0.000833)	0.29
Wingspan (b)	in (ft)	14 (1.167)	0.01 (0.000833)	0.07
Ambient Pressure (P_{amb})	lb/in ² (lb/ft ²)	14.57 (2097.36)	0.01 (1.44)	0.07
Ambient Temperature (T_{amb})	deg F (deg R)	67.3 (526.9)	0.9 (0.9)	0.17

Table 3.9: Flow condition uncertainties

Property	Units	Reference Value	Absolute Uncertainty	Relative Uncertainty (%)
Dynamic Pressure ($q_{\infty,10 \text{ Torr}}$)	lb/in ² (lb/ft ²)	0.0204 (2.94)	0.000104 (0.0150)	0.51
Ambient Density (ρ_{amb})	slug/ft ³	0.00232	1.122E-08	0.17
Dynamic Viscosity (μ)	lb-s/ft ²	3.78E-07	5.01E-10	0.13
Freestream Velocity (V_{∞})	ft/s	50.3	0.129	0.26
Reynolds Number (Re)	-	9000	370.9	0.41

Table 3.10: Force balance uncertainties

Property	Units	Reference Value	Absolute Uncertainty	Relative Uncertainty (%)
Lift (L)	lb	0.3082	0.0101	3.28
Drag (D)	lb	0.0393	0.00104	2.66
Moment (M)	ft-lb	0.00149	6.79E-05	4.56
Lift Coefficient (C_L)	-	0.308	0.0103	3.33
Drag Coefficient (C_D)	-	0.0393	0.00107	2.72
Moment Coefficient (C_M)	-	0.0051	0.00024	4.62

Chapter 4

Data Validation

Data validation serves as a method of reinforcing and rechecking the quality of the experimental results acquired using a specific wind tunnel balance. Since the LRN-FB was newly designed, data validation was performed to ensure that future testing with the LRN-FB was possible. As discussed in Chapter 3.5, data validation was performed on two main test cases for lift, drag, and moment data.

4.1 Wortmann FX 63-137 Wing (Check Standard) Validation

The first and primary data validation case was the Wortmann FX 63-137 \mathcal{R} -4 rectangular wing. The Wortmann wing is also the check standard for future testing with the LRN-FB. Lift, drag, and moment validation for the Wortmann wing was performed to compare with historical data from Refs. 4, 14, and 63. Aerodynamic performance results obtained for the test validation case using the LRN-FB are shown in Figs. 4.1–4.3. Data was taken from -15 to 25 deg at increasing and decreasing angles of attack to capture possible hysteresis effects known to exist in the low Reynolds number regime.

Lift data at Reynolds numbers of 80,000 and 100,000 from Bastedo and Mueller [4] and Marchman [63] are co-plotted together with the ideal theoretical lift curve for an \mathcal{R} -4 wing in Figs. 4.1(a–b). Figure 4.1(a) shows that the results obtained using the LRN-FB matches the data from Ref. 4 at low angles of attack. A higher $C_{L_{max}}$ and a post-stall hysteresis loop is observed though in the data from Ref. 4 indicative of the formation of a short laminar separation bubble (lower critical Reynolds number). The lower critical Reynolds number may be due to different wind tunnel turbulence characteristics [51, 63], wing mounting differences, or a combination of both. Figure 4.1(b) shows that the data lies between the historical data [4, 63]. The large lift curve slope difference seen in the

data from Bastedo and Mueller [4] in Fig. 4.1(b) may be attributed to their use of semi-span wings. The same slope differences was seen when comparing two-dimensional airfoil data from Ref. 4 with Ref. 14 taken at the current UIUC subsonic wind tunnel as shown in Fig. 4.1(c). Figure 4.1(a–b) also shows that the data obtained using the LRN-FB agrees closely with the theoretical lift curve for an aspect ratio of 4 wing over the angle of attack range for which the drag is low due to a relatively small laminar separation bubble effect. The theoretical lifting line slope for a finite wing of elliptical wing loading is given by

$$C_{L\alpha} = C_{l\alpha} \frac{AR}{AR + 2} \quad (4.1)$$

Drag comparisons with Bastedo and Mueller [4] at a Reynolds number of 80,000 and 100,000 are shown in Fig. 4.2. Drag data from Ref. 63 was unavailable for the Reynolds number tested. The general trends and $C_{D_{min}}$ values from the figure shows good correlation with the data from Ref. 4. Both Ref. 4 and 63 did not have pitching-moment data, so only two dimensional data was available for comparison. Quarter-chord pitching moment comparisons between the LRN-FB data and two-dimensional data from Selig, et al. [14] are presented in Fig. 4.3. The moment curves from the LRN-FB data in Fig. 4.3(b) show good correlation with Fig. 4.3(a) in the characteristics observed. There only difference exists in the post-stall moment characteristics as would be expected because of finite span effects.

Finally, as an added validation, the data from the LRN-FB and the historical data at a Reynolds number of 100,000 showed post-stall hysteresis in lift, drag, and moment. Post-stall hysteresis will be further discussed in Chapter 5.

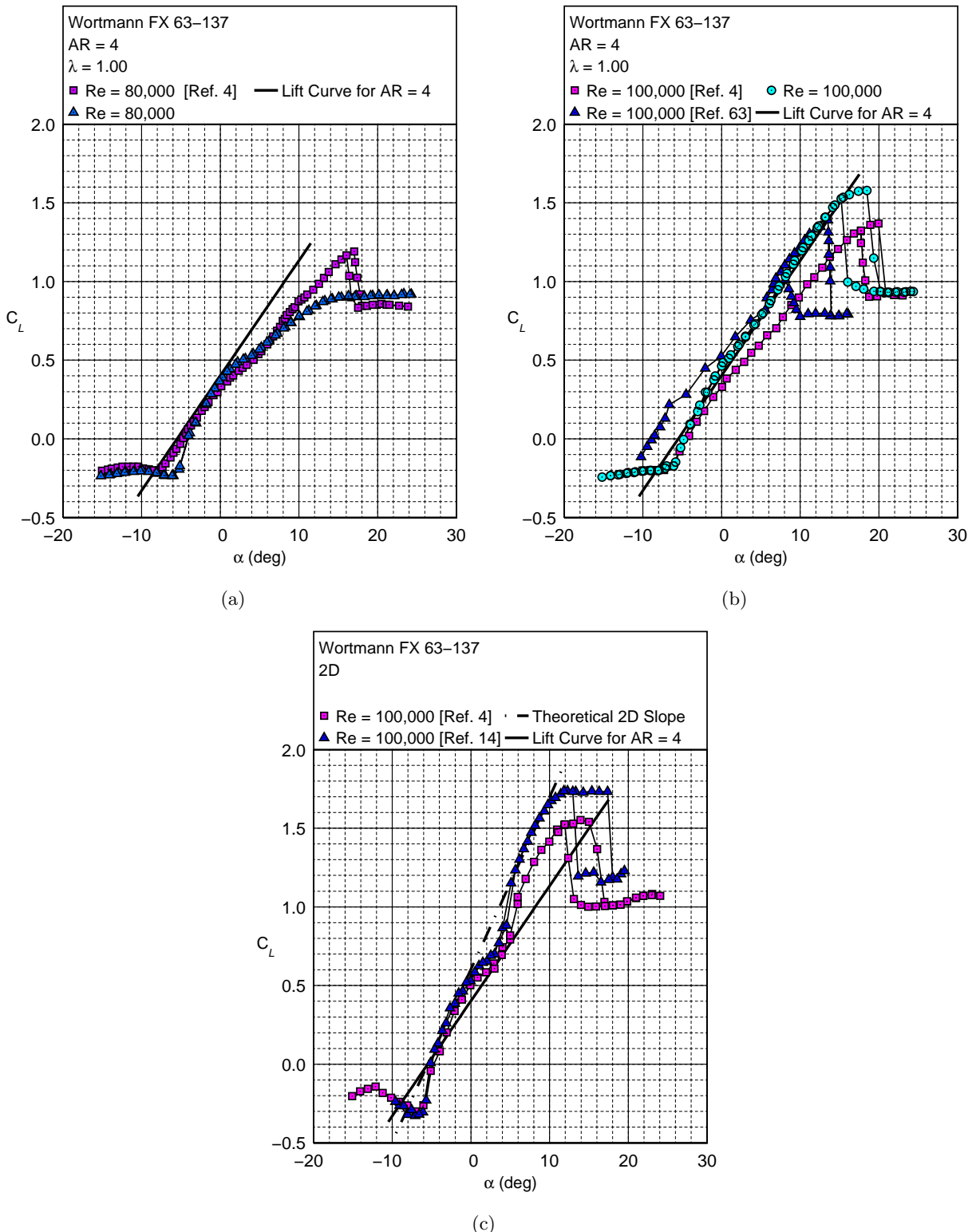


Fig. 4.1: Lift comparison results for the Wortmann FX 63-137 airfoil and $AR=4$ rectangular wing: (a) $Re = 80,000$ wing data, (b) $Re = 100,000$ wing data, and (c) $Re = 100,000$ two-dimensional data.

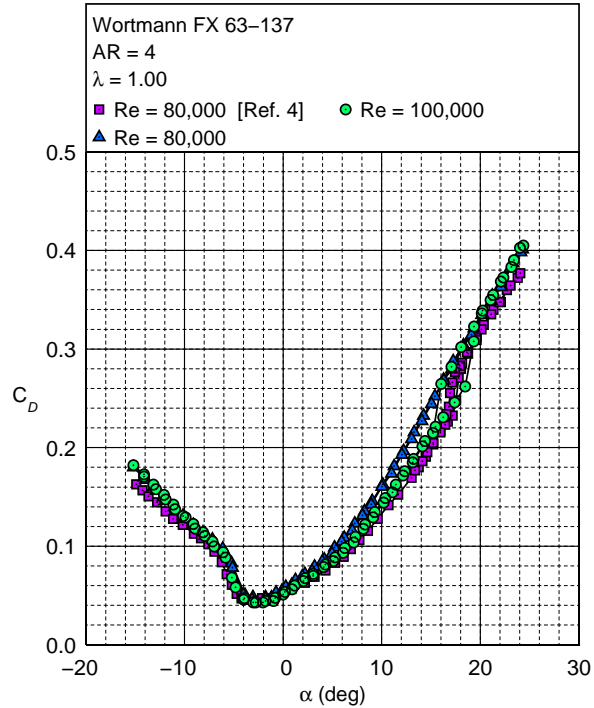


Fig. 4.2: Drag comparison results for the Wortmann FX 63-137 *R*-4 rectangular wing.

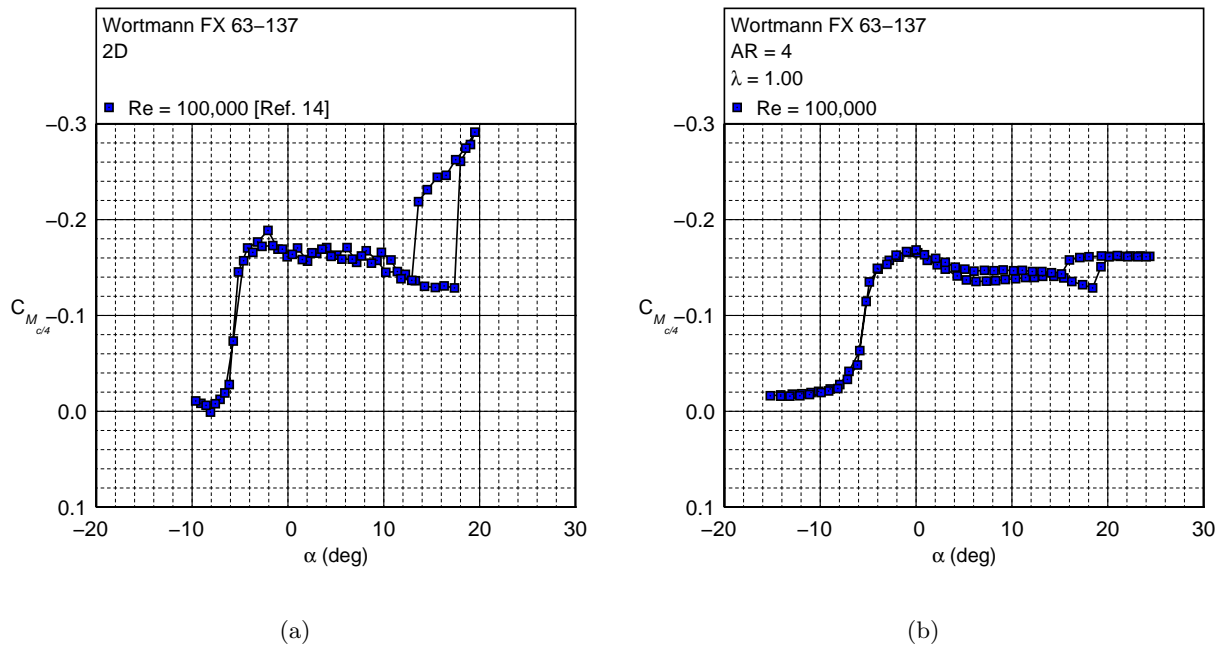


Fig. 4.3: Moment comparisons for the Wortmann FX 63-137 airfoil and \mathcal{R} -4 rectangular wing: (a) $Re = 100,000$ two-dimensional data and (b) $Re = 100,000$ wing data.

4.2 \mathcal{R} -3 Rectangular Flat-Plate Wing Validation

An additional validation case was performed on an \mathcal{R} -3 rectangular ($\lambda = 1$) flat-plate wing. Validation was performed by comparing with data from Pelletier and Mueller [5] and Shields and Mohseni [8]. The differences between the \mathcal{R} -3 wing tested with the LRN-FB and that tested by Refs. 5 and 8 were discussed in detail in Chapter 3.5. Lift, drag, moment, and drag polar comparison results are shown in Figs. 4.4–4.7.

Lift comparison results show close agreement with the theoretical lift curve for an aspect ratio 3 wing and data from Ref. 5. The only difference is the stall angle of attack and maximum lift coefficient which can be explained by the differences in the models tested as discussed prior. Similarly, drag data shows good agreement with Ref. 5. An attempt was made to assess whether the measured and Ref. 5 minimum drag coefficient value of approximately 0.0175 or the Ref. 8 minimum drag coefficient value of approximately 0.04 was more accurate. XFOIL [29] was used to find the C_{d_0} for an airfoil similar to the flat plate profile tested. At a Reynolds number of 80,000, the C_{d_0} of the airfoil was calculated to be approximately 0.0122. Given that the XFOIL approximation

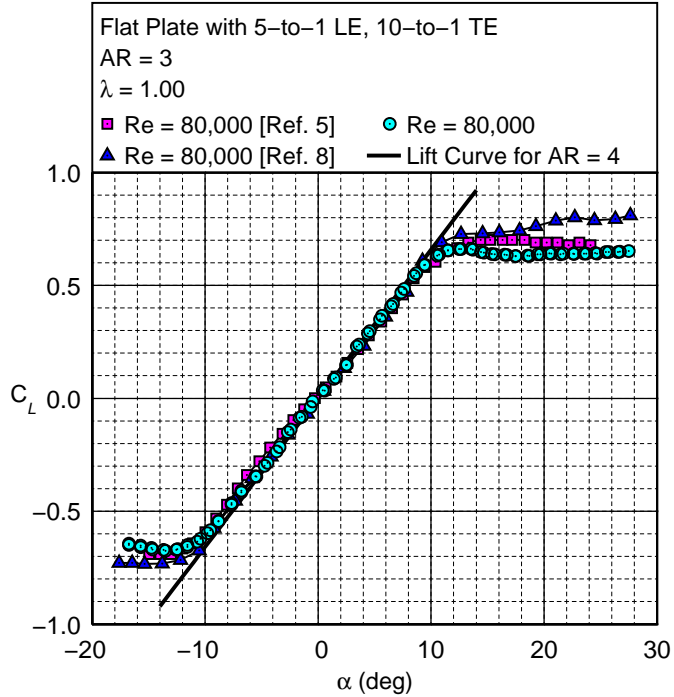


Fig. 4.4: Lift comparison results for the \mathcal{R} -3 rectangular flat-plate wing at a Reynolds number of 80,000.

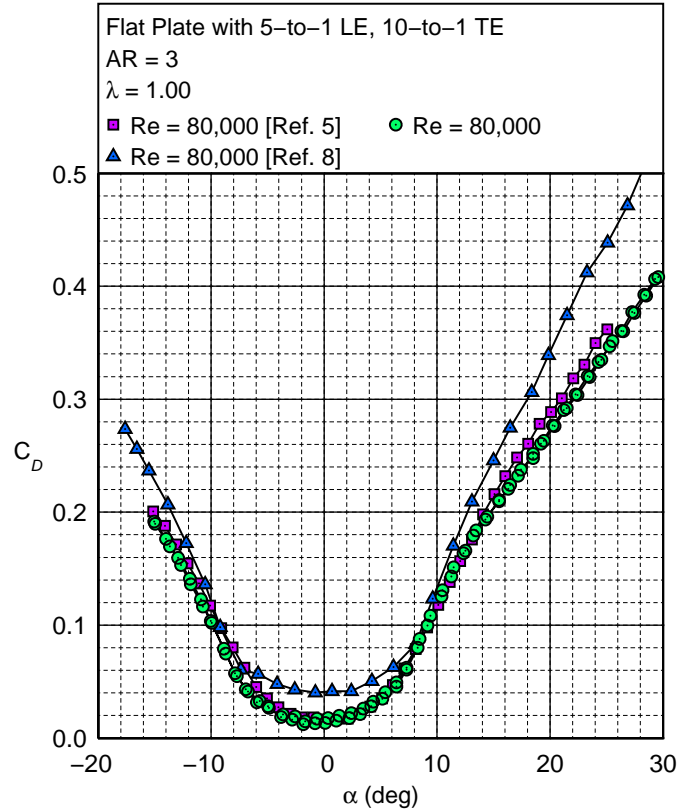


Fig. 4.5: Drag comparison results for the *A*R-3 rectangular flat-plate wing at a Reynolds number of 80,000.

did not account for wing tip or surface roughness effects, it can be concluded that the measured and Ref. 5 minimum drag coefficient is of higher accuracy. Finally, moment comparison results with data from Refs. 5 and 8 show small differences that can be attributed as Ref. 8 suggests to experimental setup variations between the three tunnels and test model differences.

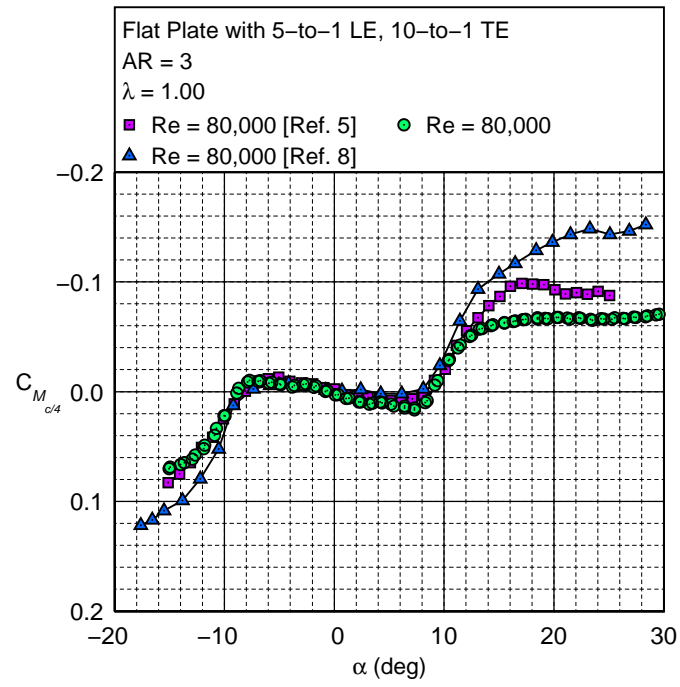


Fig. 4.6: Moment comparison results for the \mathcal{R} -3 rectangular flat-plate wing at a Reynolds number of 80,000.

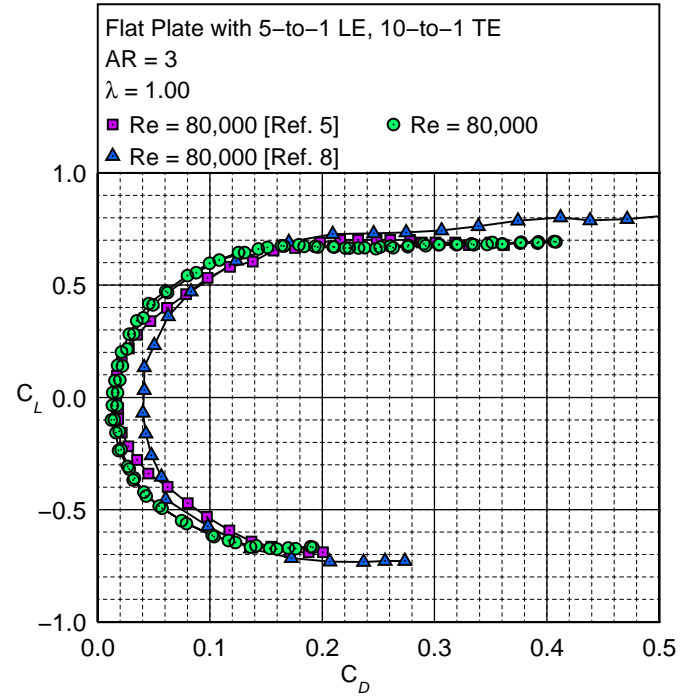


Fig. 4.7: Drag polar comparison results for the \mathcal{R} -3 rectangular flat-plate wing at a Reynolds number of 80,000.

4.3 Repeatability of Measurements

The inherently unsteady nature of low Reynolds number aerodynamics made it necessary to ensure the repeatability of measurements. Therefore, during testing, wing polars are repeated at least twice to ensure repeatability of data acquired. Figures. 4.8 and 4.9 show repeatability results of the Wortmann wing and \mathcal{R} -3 flat-plate wing. It is to be noted that, the scatter in the data decreases with increasing loads measured. The slight variation in the drag values close to $\alpha=0$ seen in Fig. 4.9 are discussed in more detail in Chapter 6.2.1.

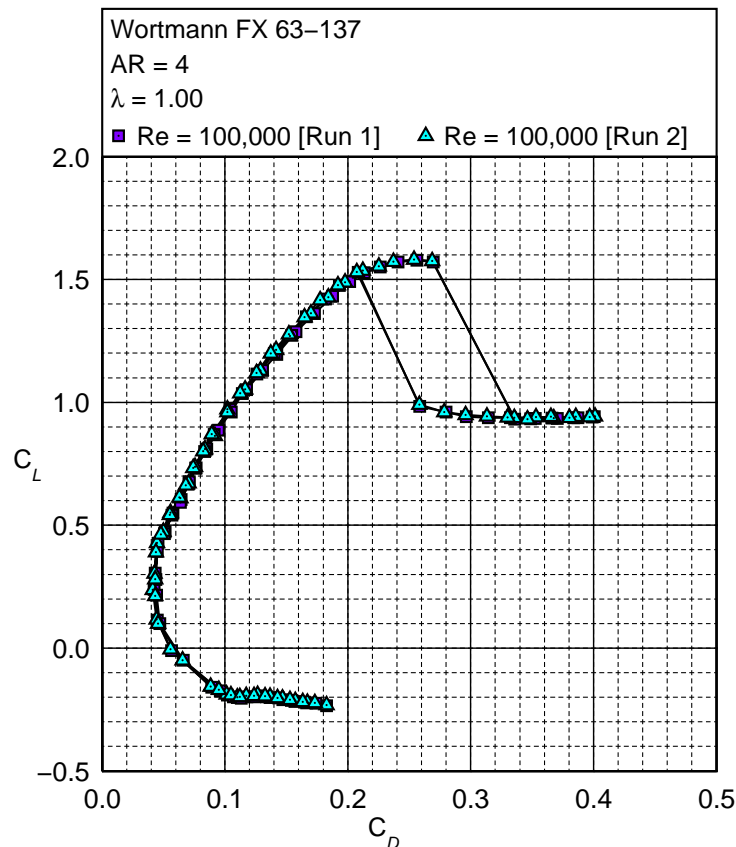


Fig. 4.8: Repeatability of the Wortmann FX 63-137 \mathcal{R} -4 rectangular wing at a Reynolds number of 100,000.

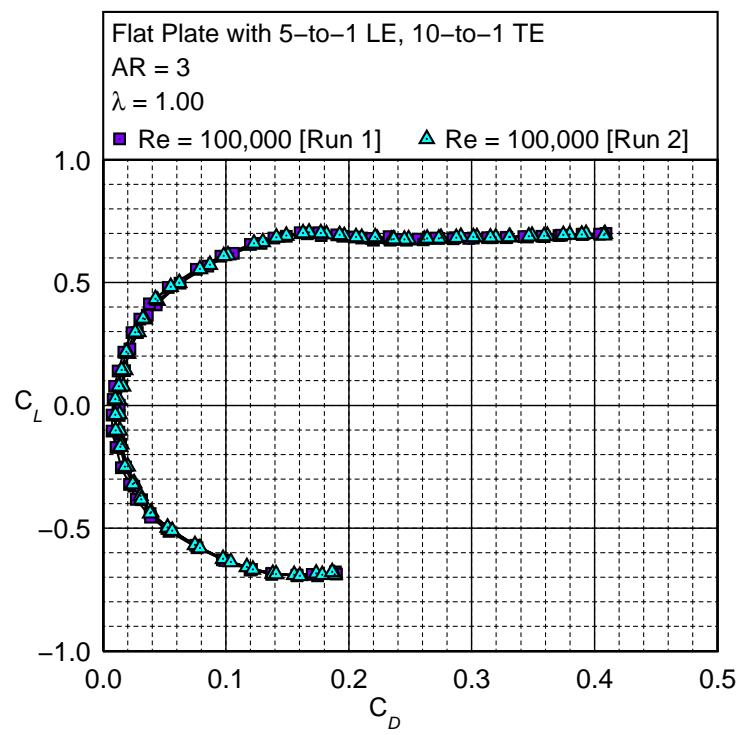


Fig. 4.9: Repeatability for the \mathcal{R} -3 rectangular flat-plate wing at a Reynolds number of 100,000.

Chapter 5

Experimental Results

The data presented in this chapter are performance data for the Wortmann FX 63-137 \mathcal{A} -4 rectangular ($\lambda = 1$) wing and 10 flat-plate wings that were tested as discussed in Chapter 3.5. A detailed table of all the wings tested is presented in Table 5.1. Model configuration, test configuration, figure and page numbers, run numbers, and other test details are listed in Table 5.1. Sting numbers listed in Table 5.1 represent file names of recorded sting tare voltage measurements used for each corresponding run.

Drag polars, and lift and moment curves at varying Re for the Wortmann FX 63-137 wing are shown in Fig. 5.1. For the flat-plate wing tests, three key characteristics were varied, Reynolds number Re , aspect ratio \mathcal{A} , and taper ratio λ . Drag polars and lift and moment curves at varying Re for all 10 flat-plate wings are presented in Figs. 5.2–5.11. Figure and page numbers for these plots can be obtained from Table 5.1. In addition, performance comparison results are presented where \mathcal{A} is varied with respect to λ and Re (Figs. 5.12–5.25), and λ is varied with respect to \mathcal{A} and Re (Figs. 5.26–5.40).

Table 5.1: Test matrix and run number index.

Model		Model & Testing Details				Lift, Drag, & Moment Data						
Airfoil	Configuration	c _{mac} (ft)	b (ft)	Pressure Transducer	α Range	Drag	Lift & Moment		Re	Sting #	Run #	
		Fig.	p.	Fig.	p.							
Wortmann FX 63-137	Clean Aspect Ratio=4 $\lambda=1$	0.29167	1.16667	10 Torr Setra 10 Torr Setra	-15° to 25°	5.1	61	5.1	61	40,000 60,000 80,000 90,000 100,000	0186sga 0187sga 0188sga 0192sga 0192sga 0098sga 0098sga 0098sga 0190sga 0100sga 0100sga	0431aj 0432aj 0433aj 0436aj 0430aj 0209ga 0206ga 0207ga 0208ga 0434aj 0210ga 0211ga
5-to-1 Leading Edge 10-to-1 Trailing Edge Flat Plate	Clean Aspect Ratio =2 $\lambda = 0.5$	0.29167	0.56250	10 Torr	-15° to 30°	5.2	62	5.2	62	80,000 90,000 100,000 120,000	0114saj 0115saj 0116saj 0117saj	0227ga 0228ga 0229ga 0230ga
5-to-1 Leading Edge 10-to-1 Trailing Edge Flat Plate	Clean Aspect Ratio = 2 $\lambda = 0.75$	0.29167	0.57939	10 Torr	-15° to 30°	5.3	63	5.3	63	80,000 100,000 120,000 140,000	0195sga 0196sga 0196sga 0197sga 0198sga	0448aj 0446ga 0452cs 0449aj 0450cs
5-to-1 Leading Edge 10-to-1 Trailing Edge Flat Plate	Clean Aspect Ratio = 2 $\lambda = 1$	0.29167	0.58333	10 Torr	-15° to 30°	5.4	64	5.4	64	80,000 100,000 120,000 140,000 160,000	0195sga 0196sga 0197sga 0198sga 0199sga	0441ga 0439ga 0442ga 0443ga 0444ga
5-to-1 Leading Edge 10-to-1 Trailing Edge Flat Plate	Clean Aspect Ratio = 3 $\lambda = 0.5$	0.29167	0.84375	10 Torr	-15° to 30°	5.5	65	5.5	65	60,000 80,000 100,000 120,000	0164sga 0165sga 0166sga 0166sga 0167sga	0377ar 0376ar 0380ga 0375ga 0379ga

Table 5.1: Continued.

5-to-1 Leading Edge 10-to-1 Trailing Edge Flat Plate	Clean Aspect Ratio = 3 $\lambda = 0.75$	0.29167	0.86909	10 Torr	-15° to 30°	5.6	66	5.6	66	60,000 80,000 100,000 120,000	0164sga 0165sga 0166sga 0166sga 0167sga	0371ga 0372ga 0369ga 0374ga 0373ga
5-to-1 Leading Edge 10-to-1 Trailing Edge Flat Plate	Clean Aspect Ratio = 3 $\lambda = 1$	0.29167	0.87500	10 Torr	-15° to 30°	5.7	67	5.7	67	60,000 80,000 100,000 120,000	0164sga 0165sga 0166sga 0166sga 0167sga	0383ar 0384ar 0386ar 0381ga 0385ar
5-to-1 Leading Edge 10-to-1 Trailing Edge Flat Plate	Clean Aspect Ratio = 4 $\lambda = 0.5$	0.29167	1.12500	10 Torr	-15° to 30°	5.8	68	5.8	68	60,000 80,000 100,000 120,000	0170sga 0171sga 0172sga 0173sga	0403ga 0404ga 0405ga 0406ga
5-to-1 Leading Edge 10-to-1 Trailing Edge Flat Plate	Clean Aspect Ratio = 4 $\lambda = 0.75$	0.29167	1.15878	10 Torr	-15° to 30°	5.9	69	5.9	69	60,000 80,000 100,000 120,000	0176sga 0177sga 0177sga 0178sga 0178sga 0179sga	0412ar 0413ar 0416ar 0415ar 0409ga 0414ar
5-to-1 Leading Edge 10-to-1 Trailing Edge Flat Plate	Clean Aspect Ratio = 4 $\lambda = 1$	0.29167	1.16667	10 Torr	-15° to 30°	5.10	70	5.10	70	60,000 80,000 100,000 120,000	0170sga 0171sga 0172sga 0173sga	0396cs 0395cs 0394cs 0399cs
5-to-1 Leading Edge 10-to-1 Trailing Edge Flat Plate	Clean Aspect Ratio = 5 $\lambda = 1$	0.29167	1.45833	10 Torr	-15° to 30°	5.11	71	5.11	71	60,000 80,000 100,000	0182sar 0183sar 0185sar	0420ga 0421ga 0423ga

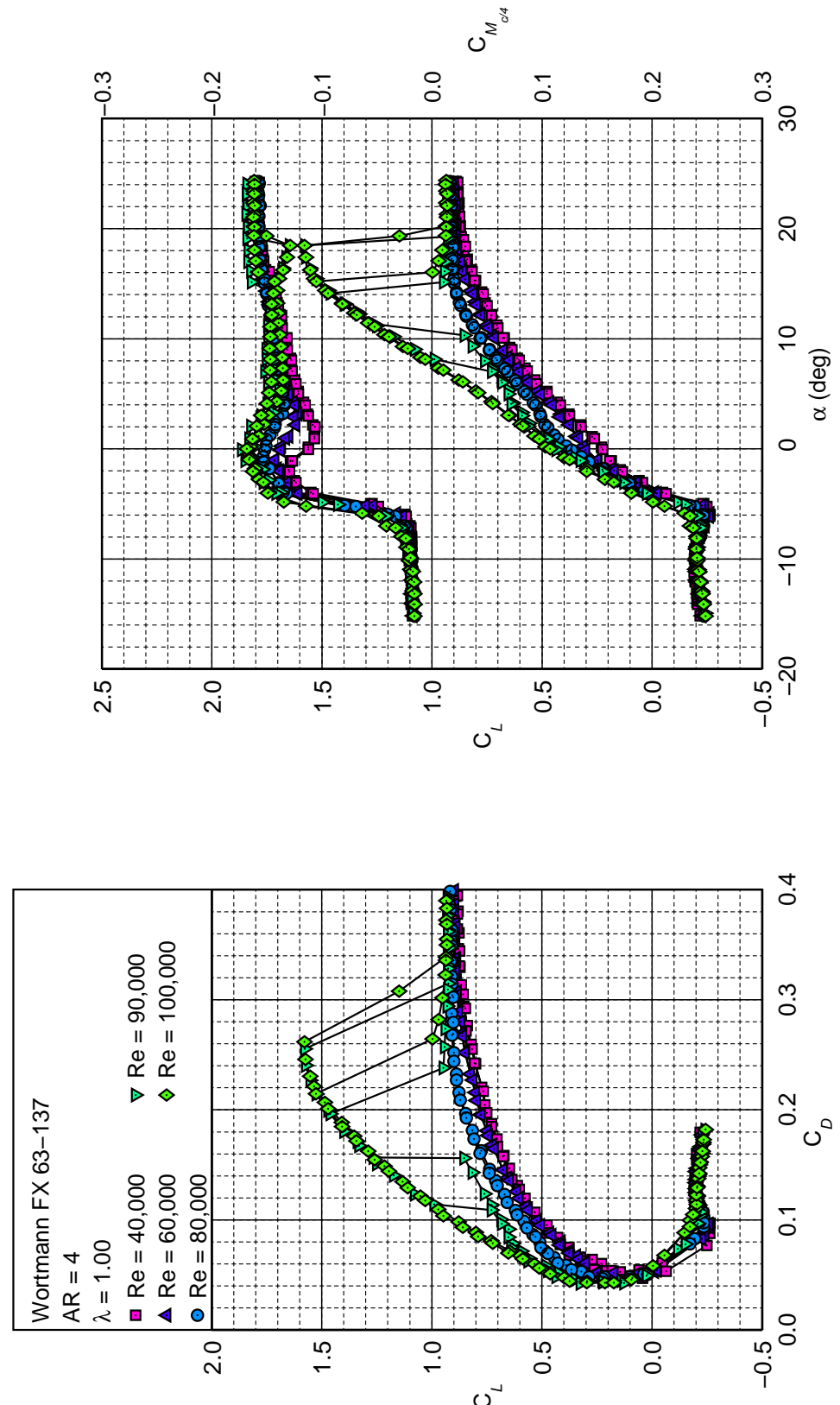


Fig. 5.1: Drag polar for the Wortmann FX 63-137 wing with an \mathcal{R} of 4 and λ of 1.00.

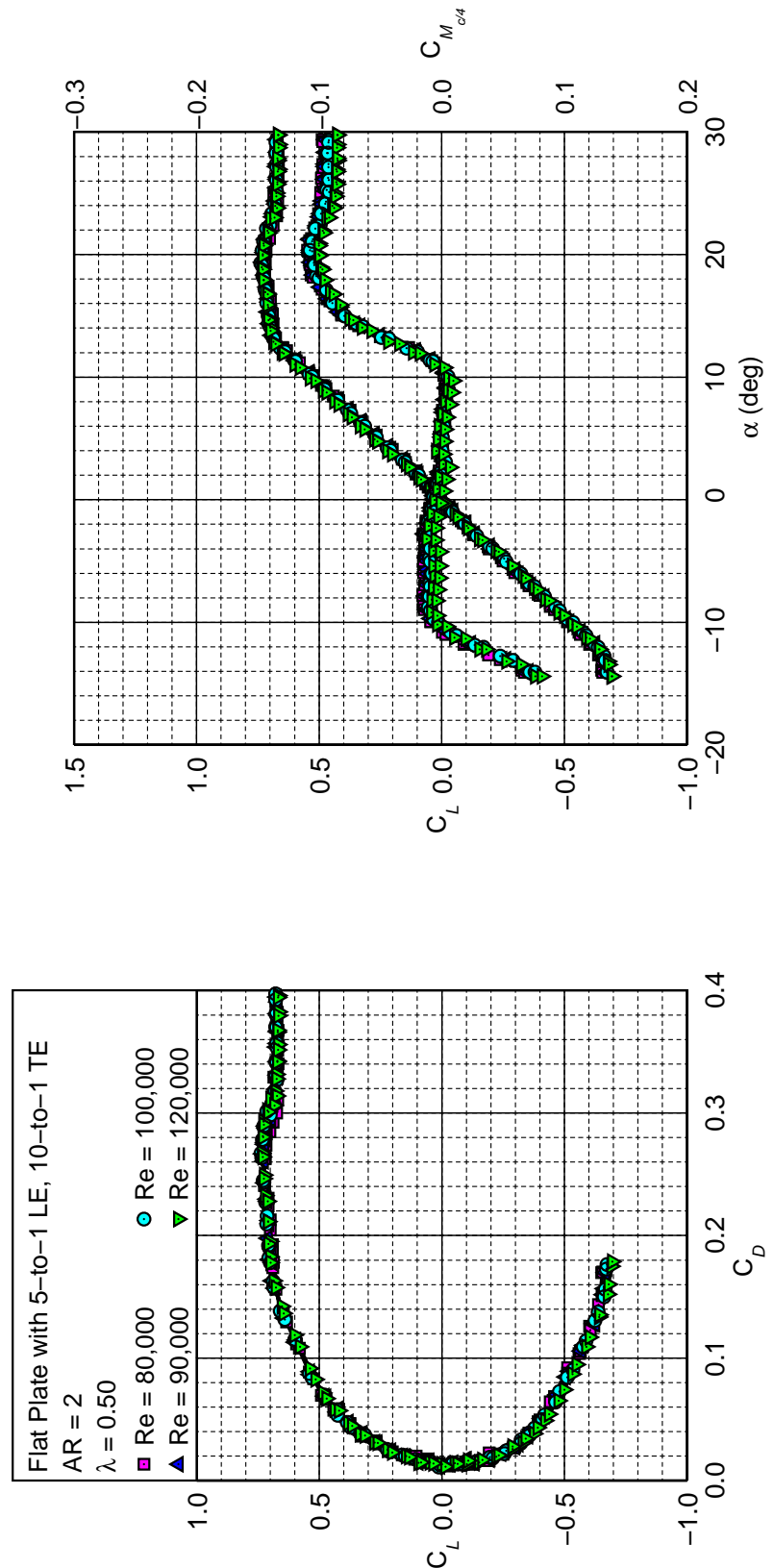


Fig. 5.2: Drag polar for the 5-to-1 LE, 10-to-1 TE flat-plate wing with an AR of 2 and λ of 0.50.

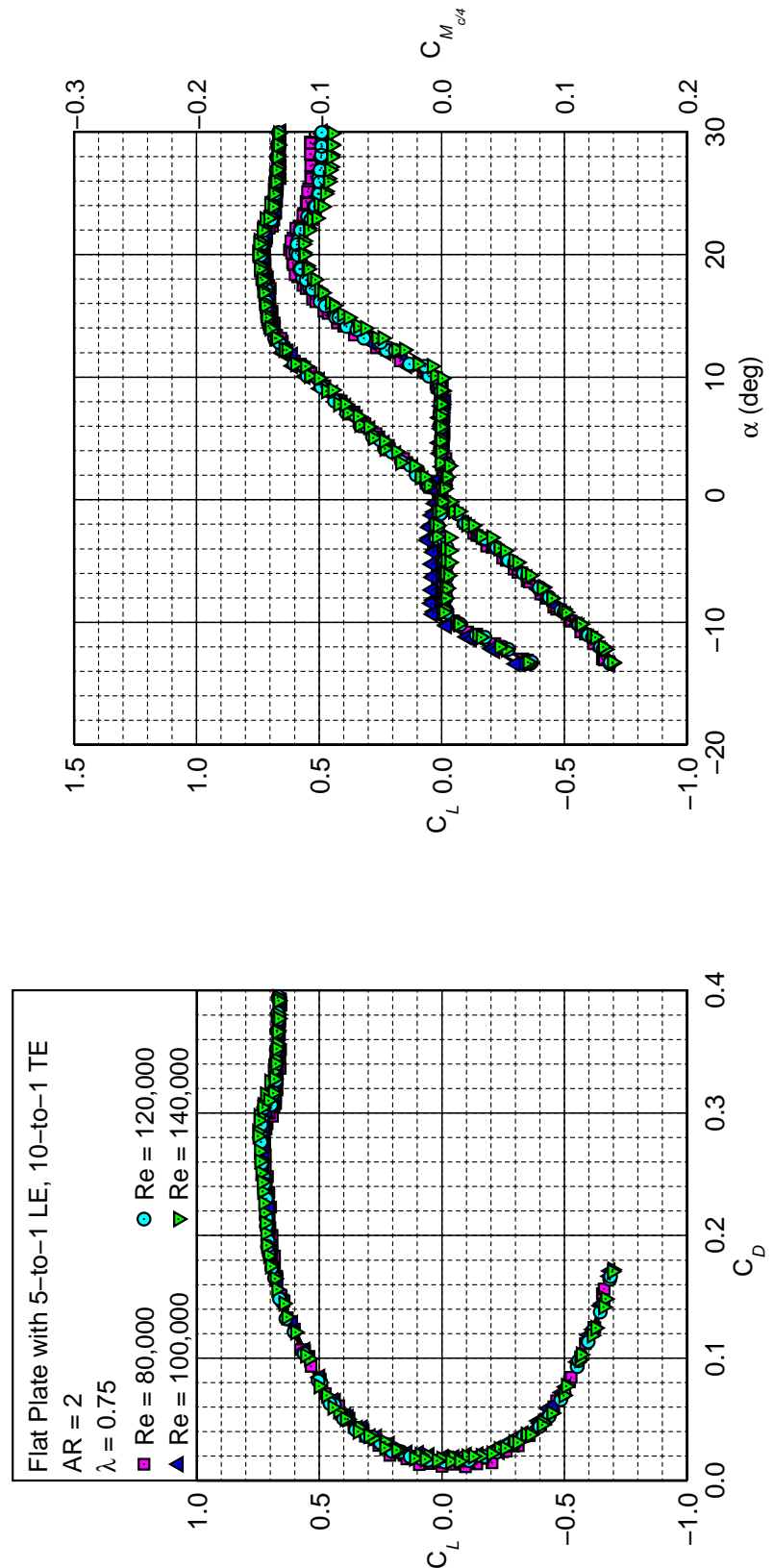


Fig. 5.3: Drag polar for the 5-to-1 LE, 10-to-1 TE flat-plate wing with an AR of 2 and λ of 0.75.

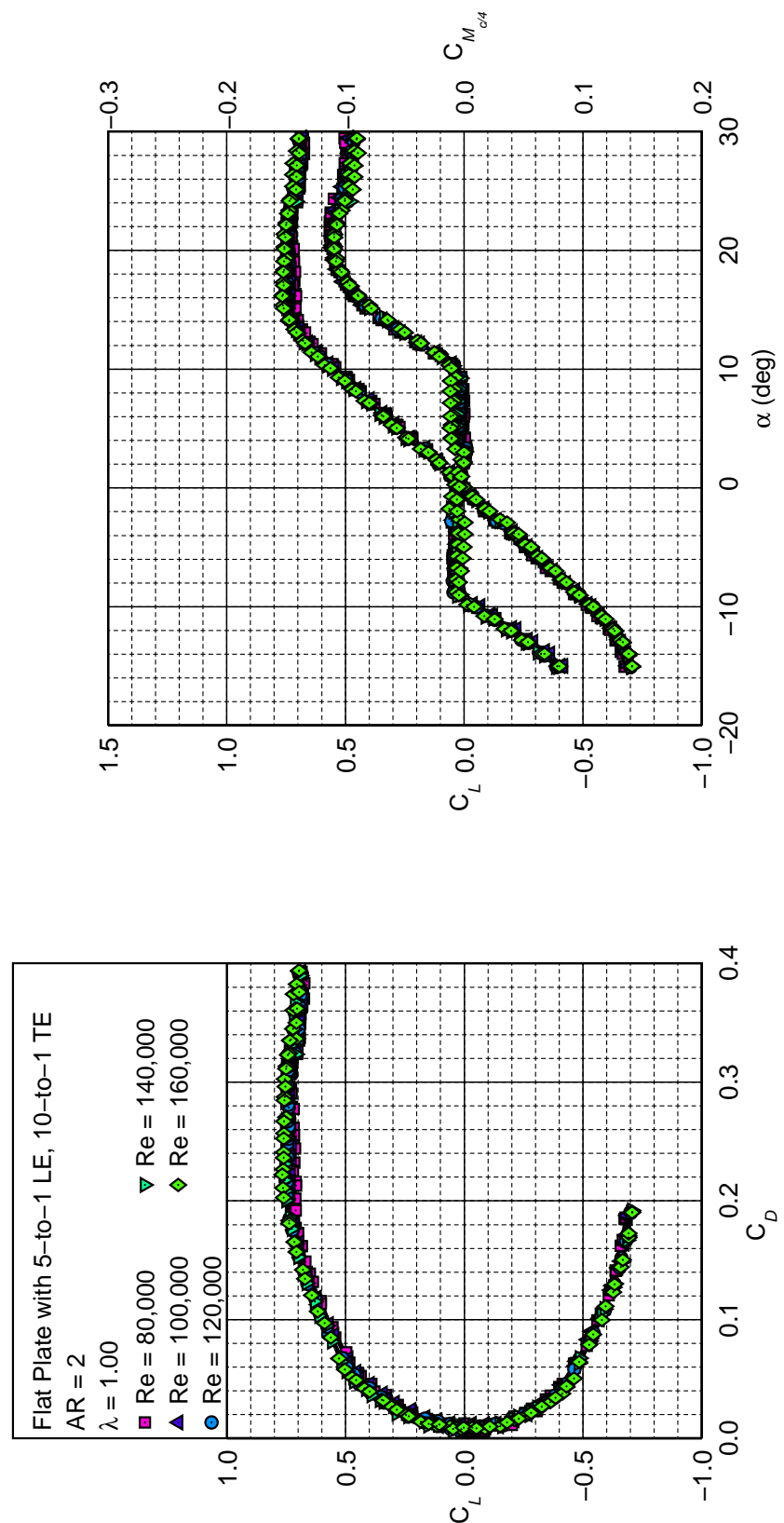


Fig. 5.4: Drag polar for the 5-to-1 LE, 10-to-1 TE flat-plate wing with an AR of 2 and λ of 1.00.

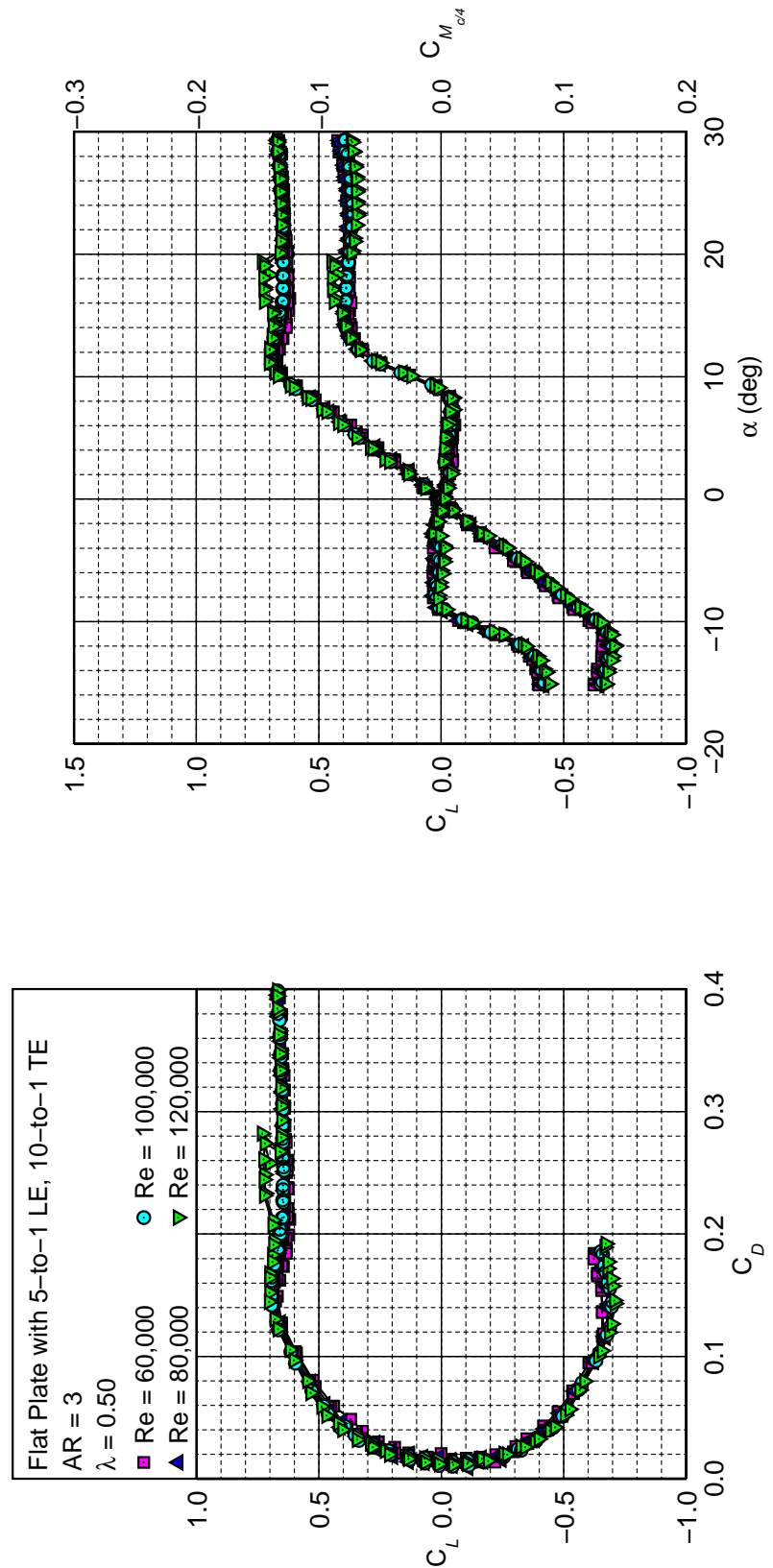


Fig. 5.5: Drag polar for the 5-to-1 LE, 10-to-1 TE flat-plate wing with an AR of 3 and λ of 0.50.

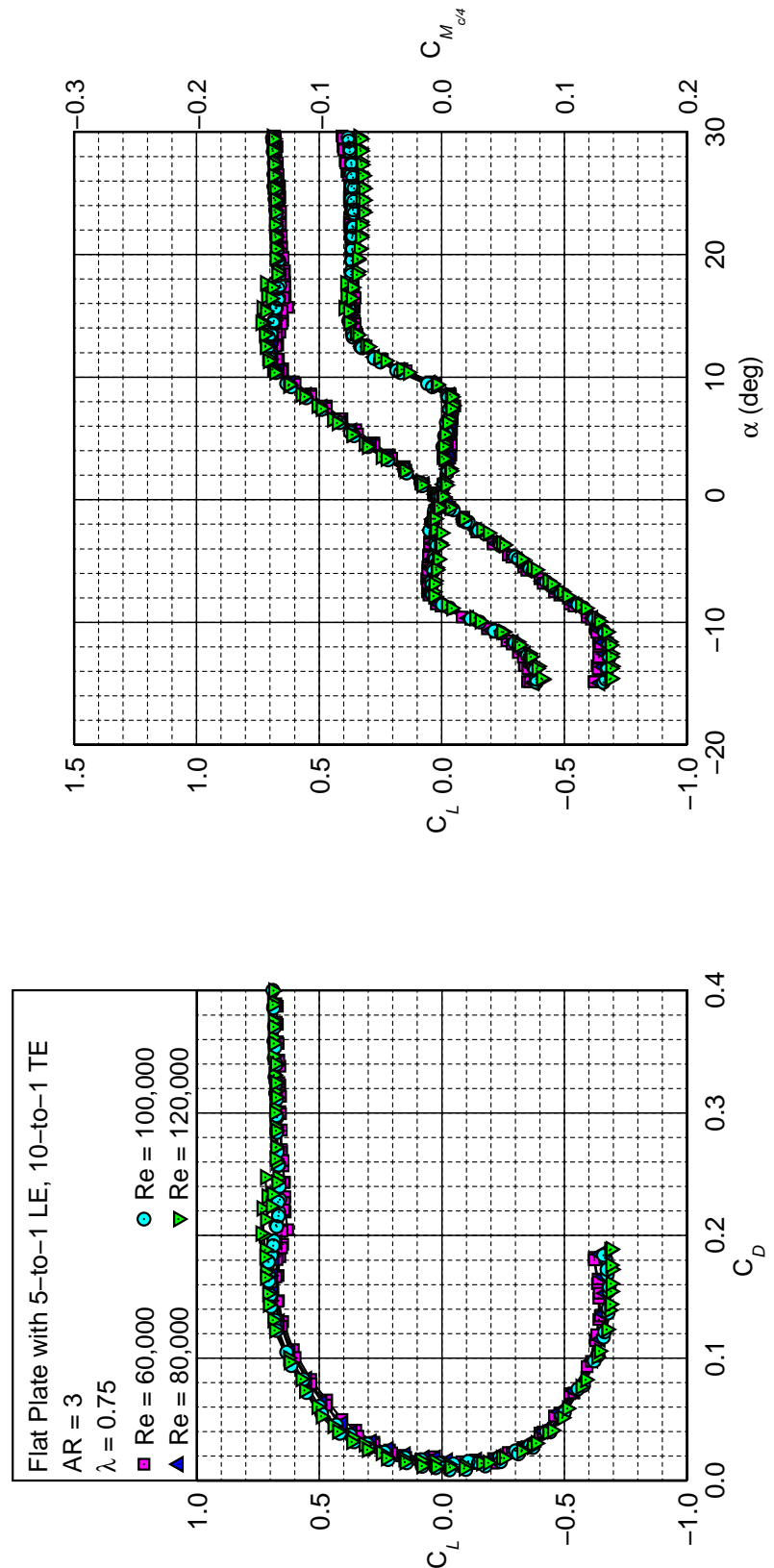


Fig. 5.6: Drag polar for the 5-to-1 LE, 10-to-1 TE flat-plate wing with an AR of 3 and λ of 0.75.

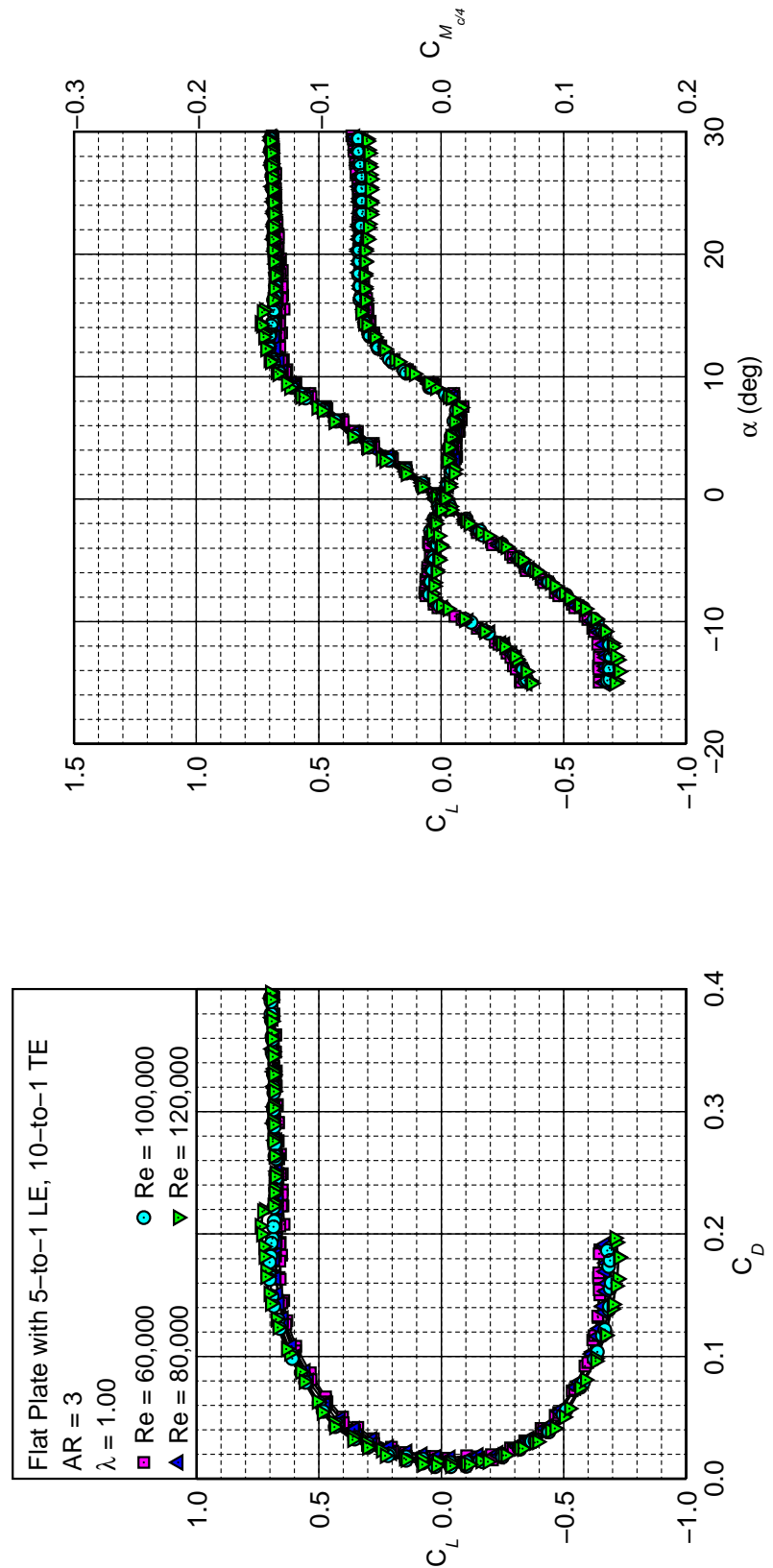


Fig. 5.7: Drag polar for the 5-to-1 LE, 10-to-1 TE flat-plate wing with an AR of 3 and λ of 1.00.

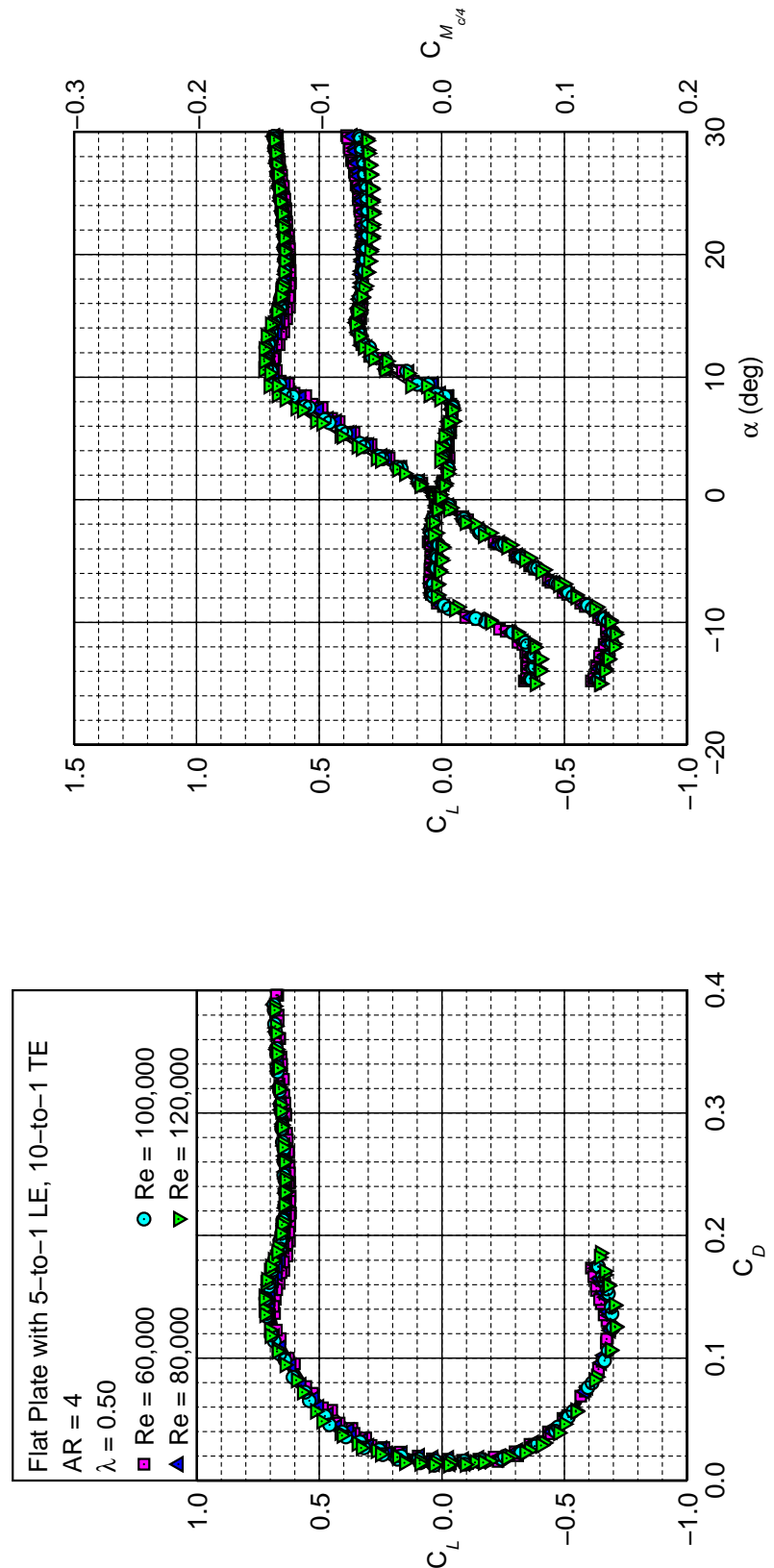


Fig. 5.8: Drag polar for the 5-to-1 LE, 10-to-1 TE flat-plate wing with an AR of 4 and λ of 0.50.

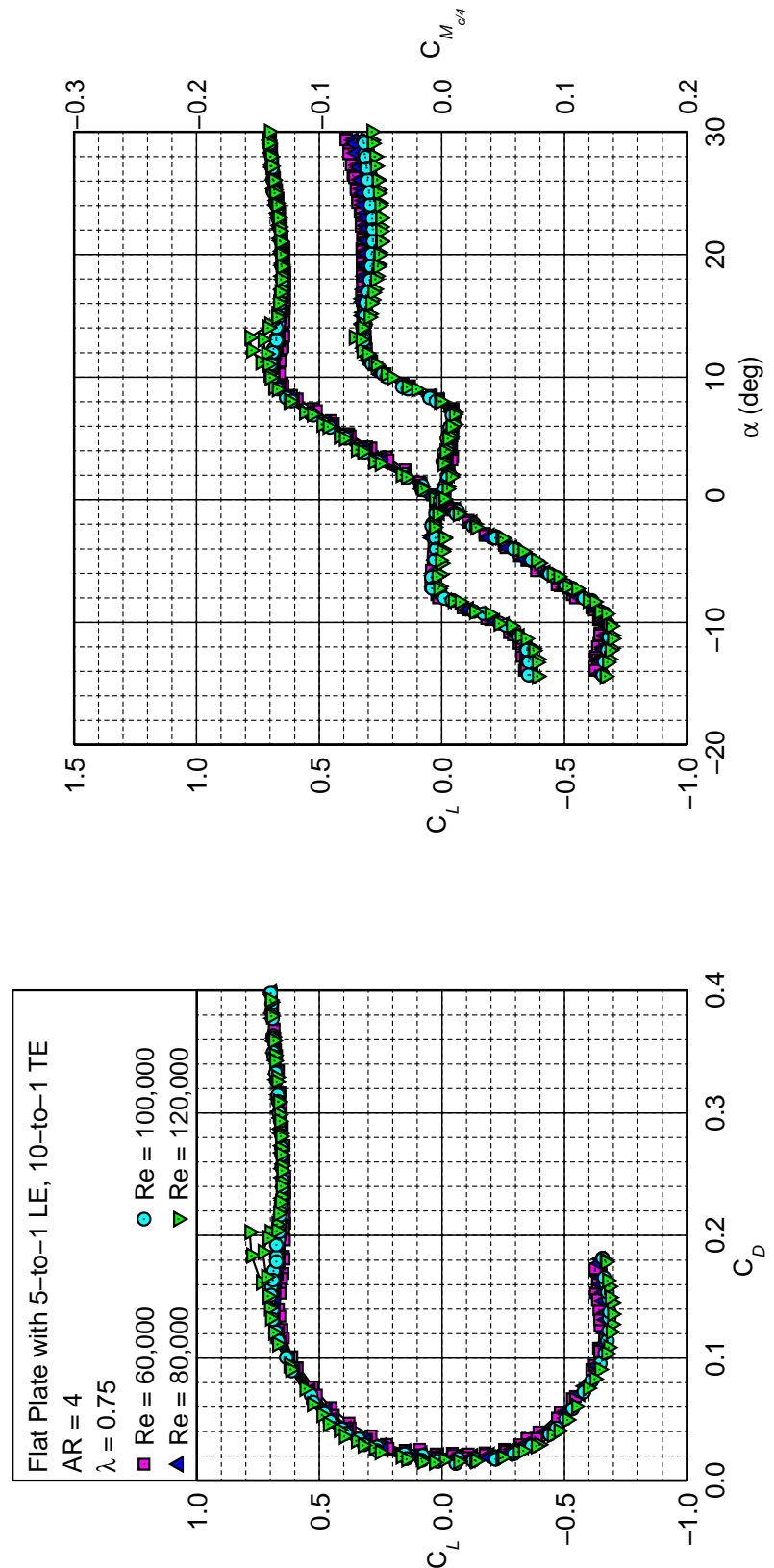


Fig. 5.9: Drag polar for the 5-to-1 LE, 10-to-1 TE flat-plate wing with an AR of 4 and λ of 0.75.

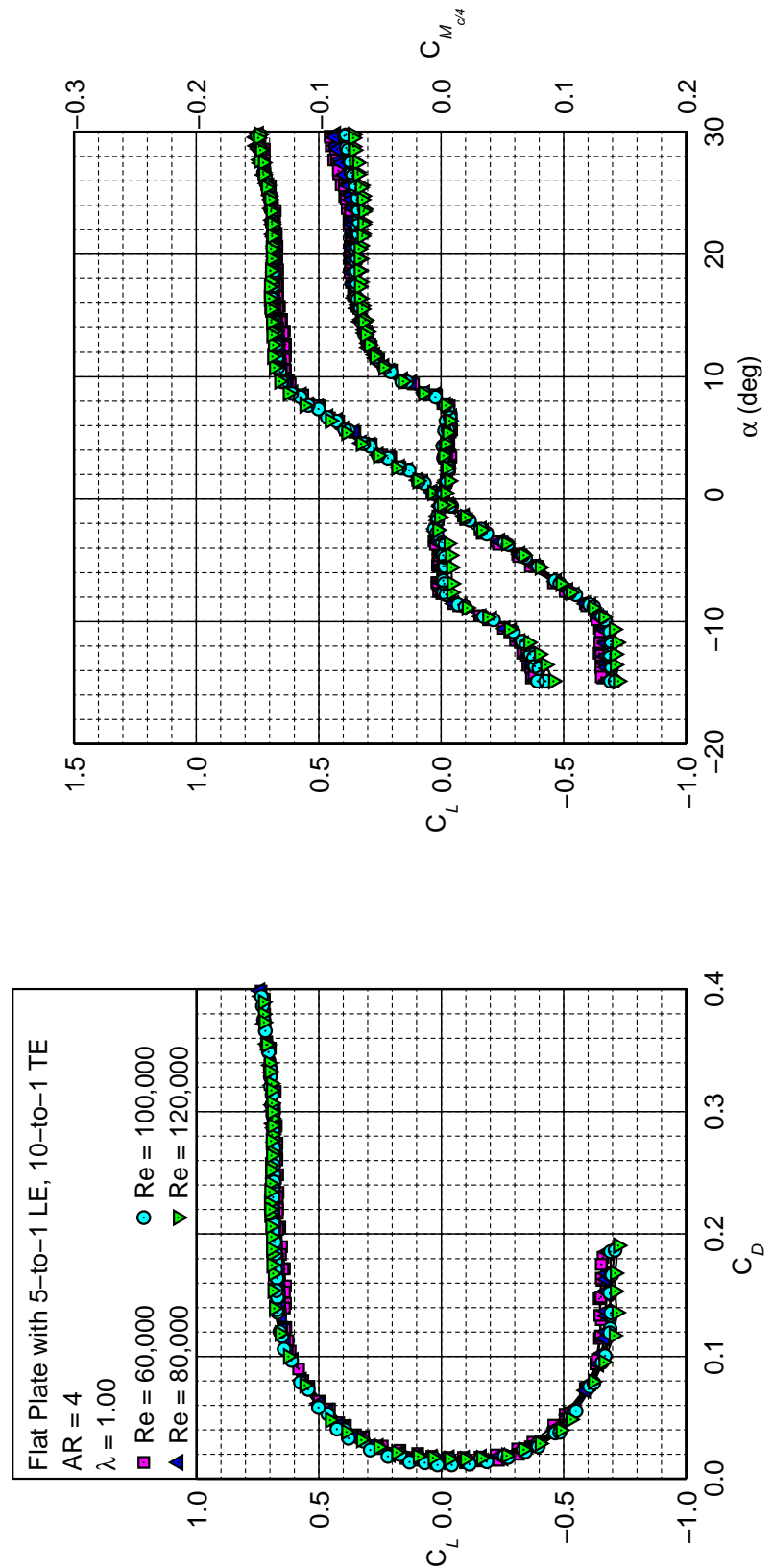


Fig. 5.10: Drag polar for the 5-to-1 LE, 10-to-1 TE flat-plate wing with an AR of 4 and λ of 1.00.

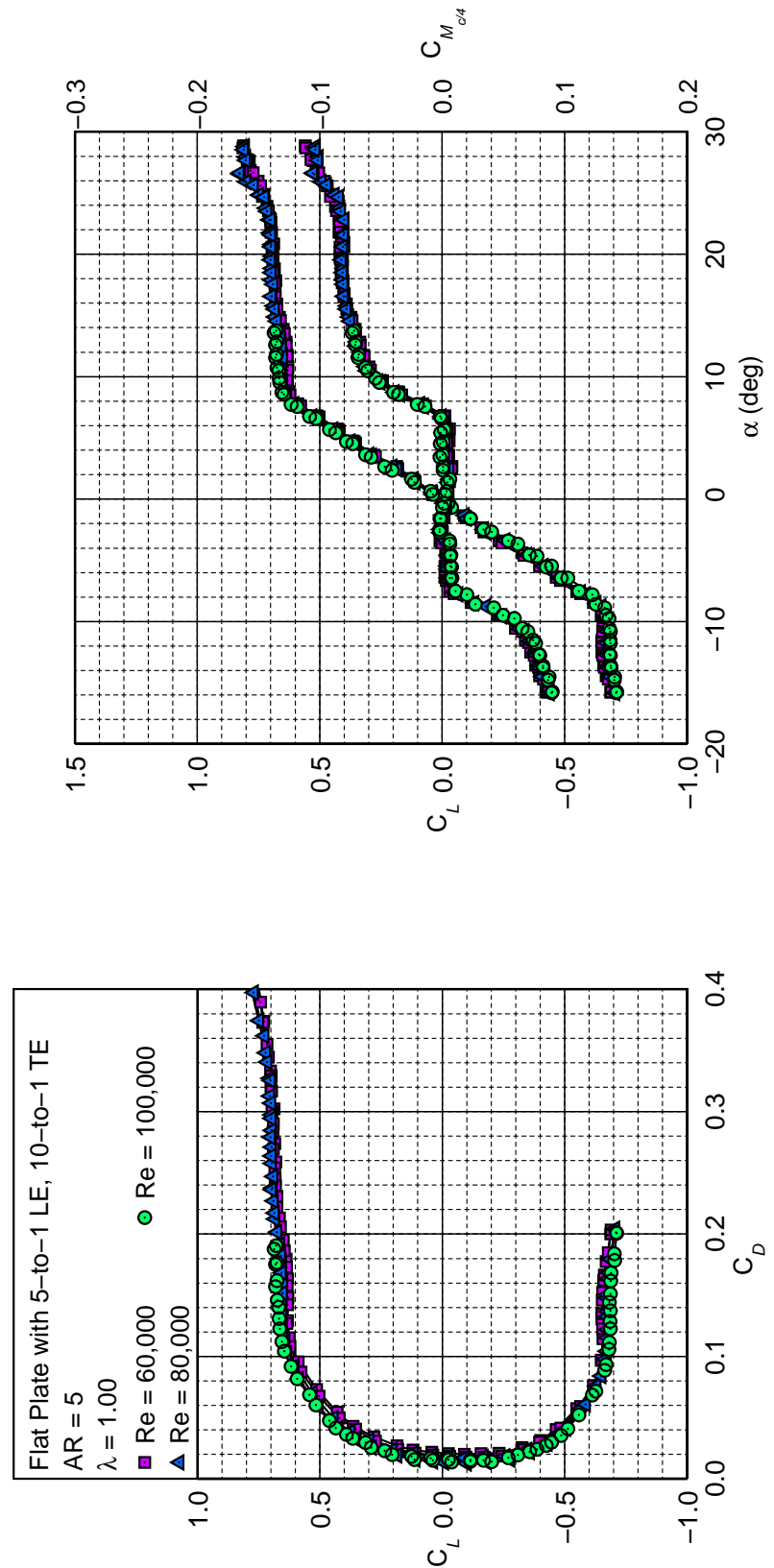


Fig. 5.11: Drag polar for the 5-to-1 LE, 10-to-1 TE flat-plate wing with an AR of 5 and λ of 1.00.

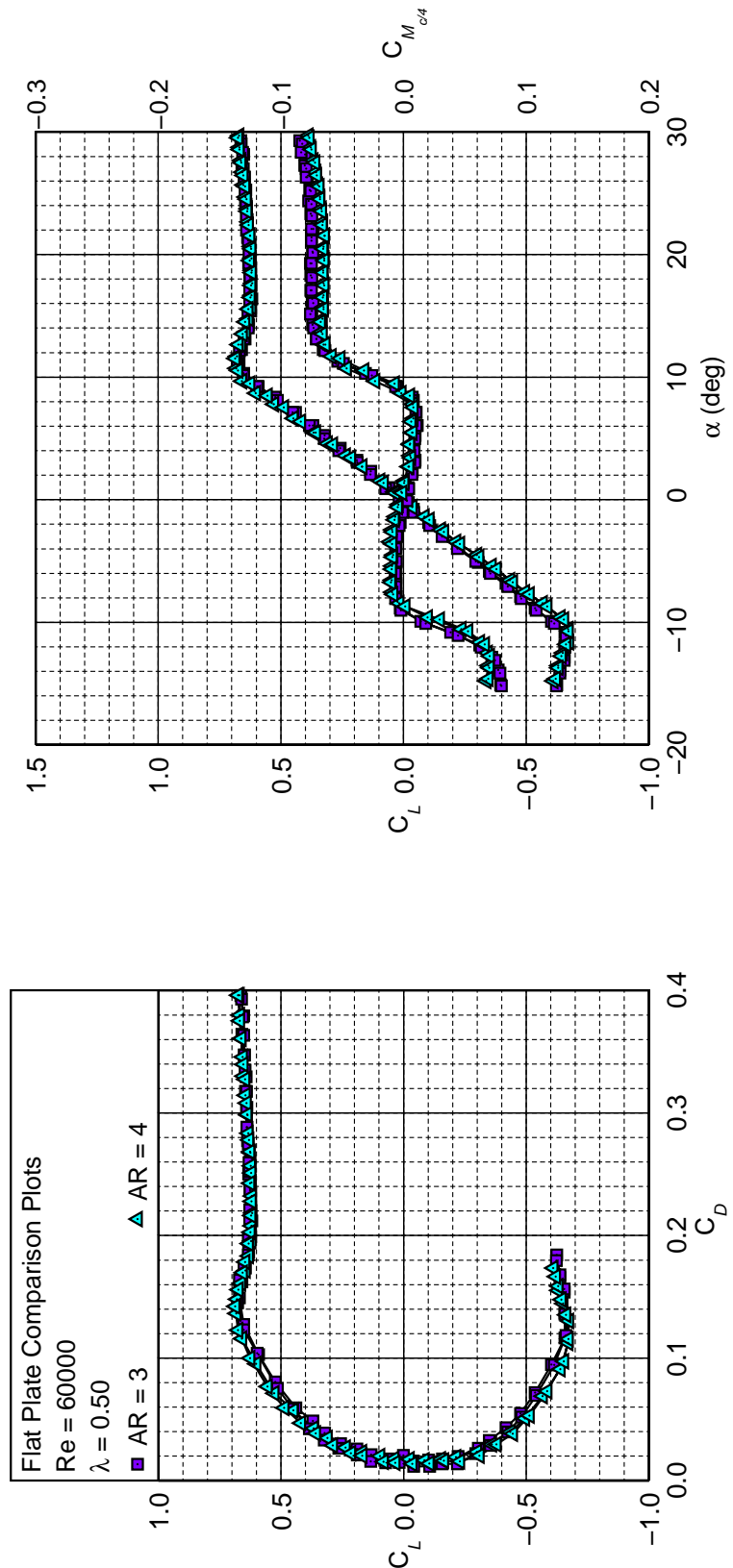


Fig. 5.12: Flat plate comparison results for a fixed Re of 60,000 and λ of 0.50.

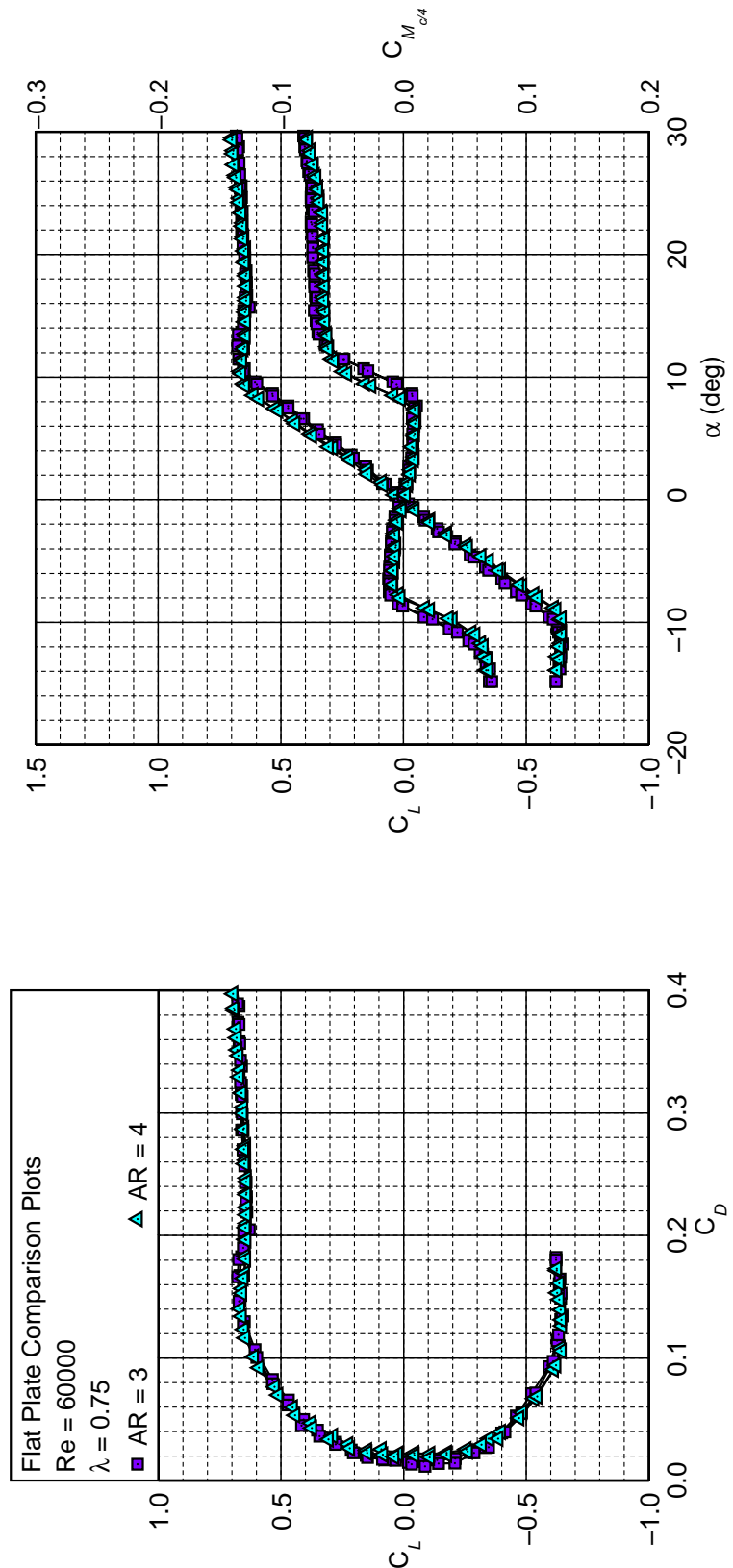


Fig. 5.13: Flat plate comparison results for a fixed Re of 60,000 and λ of 0.75.

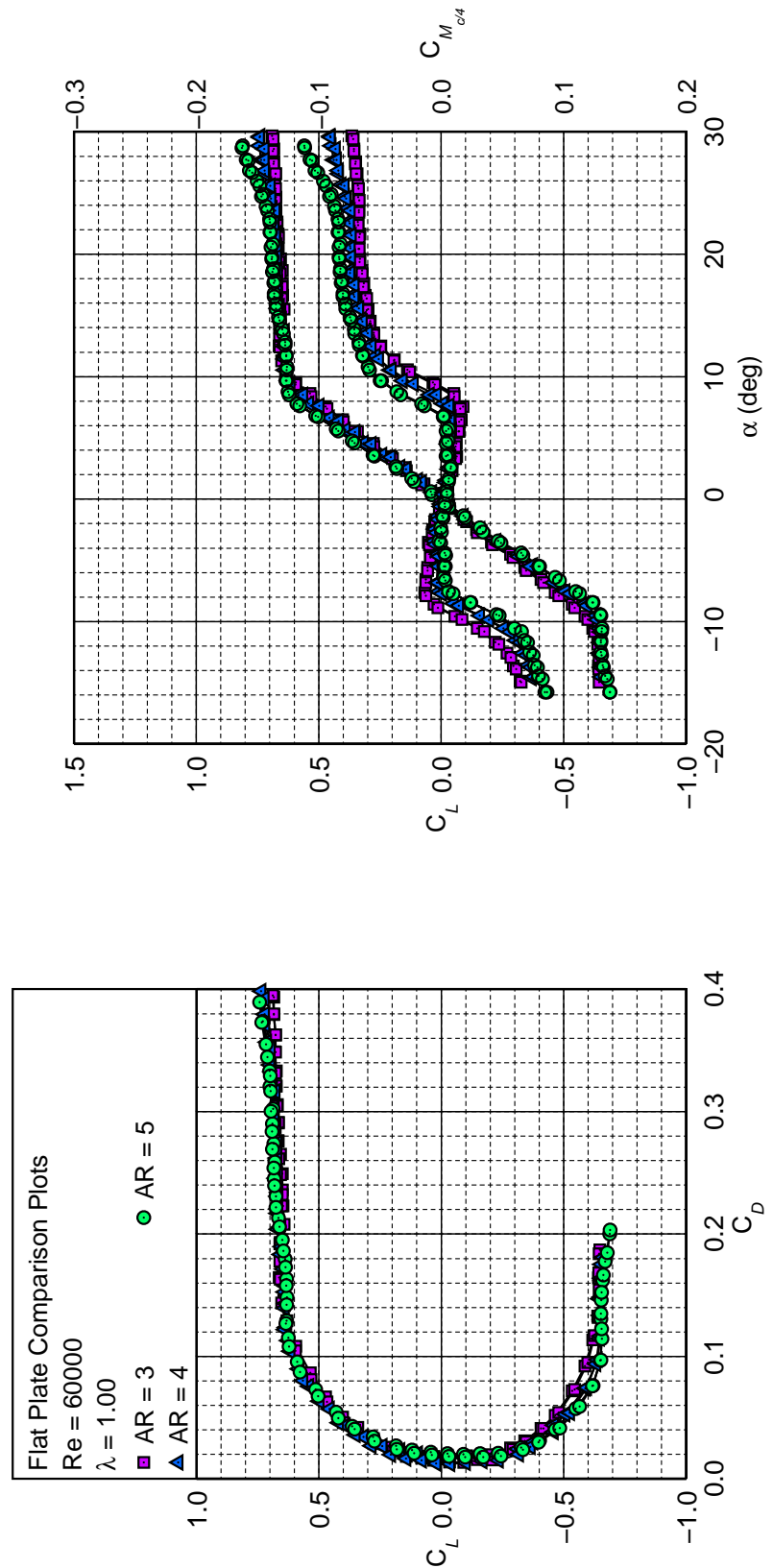


Fig. 5.14: Flat plate comparison results for a fixed Re of 60,000 and λ of 1.00.

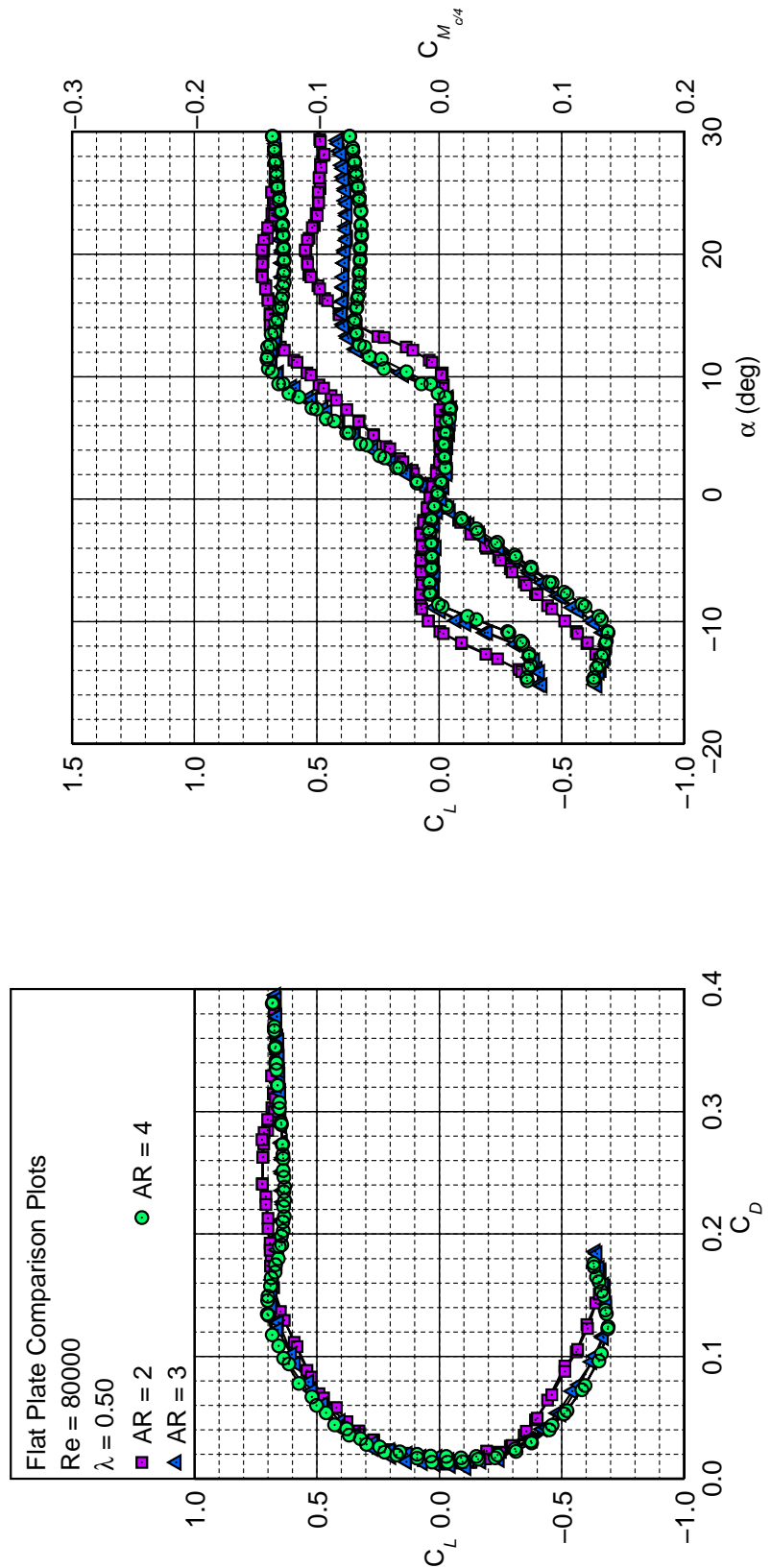


Fig. 5.15: Flat plate comparison results for a fixed Re of 80,000 and λ of 0.50.

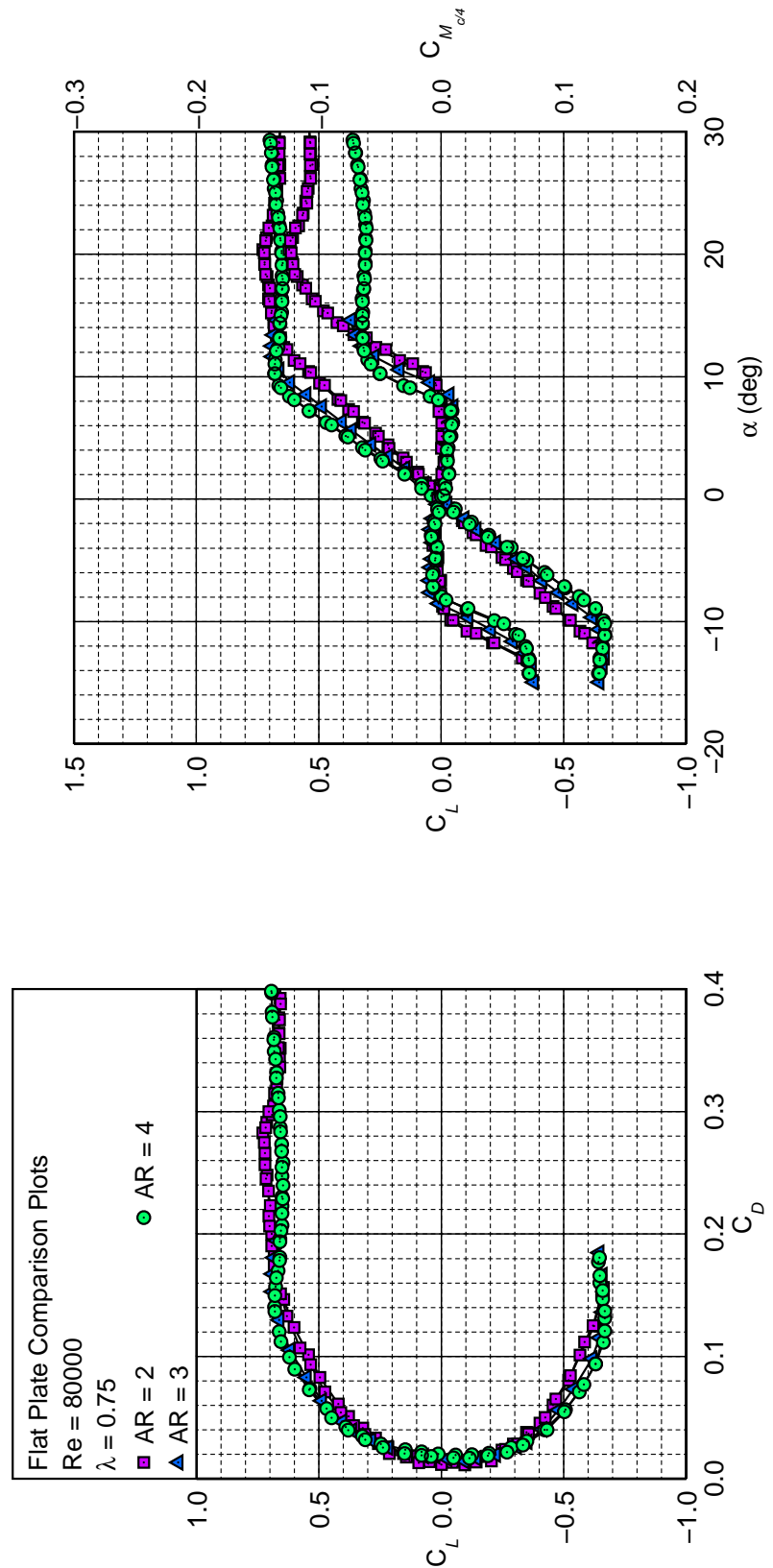


Fig. 5.16: Flat plate comparison results for a fixed Re of 80,000 and λ of 0.75.

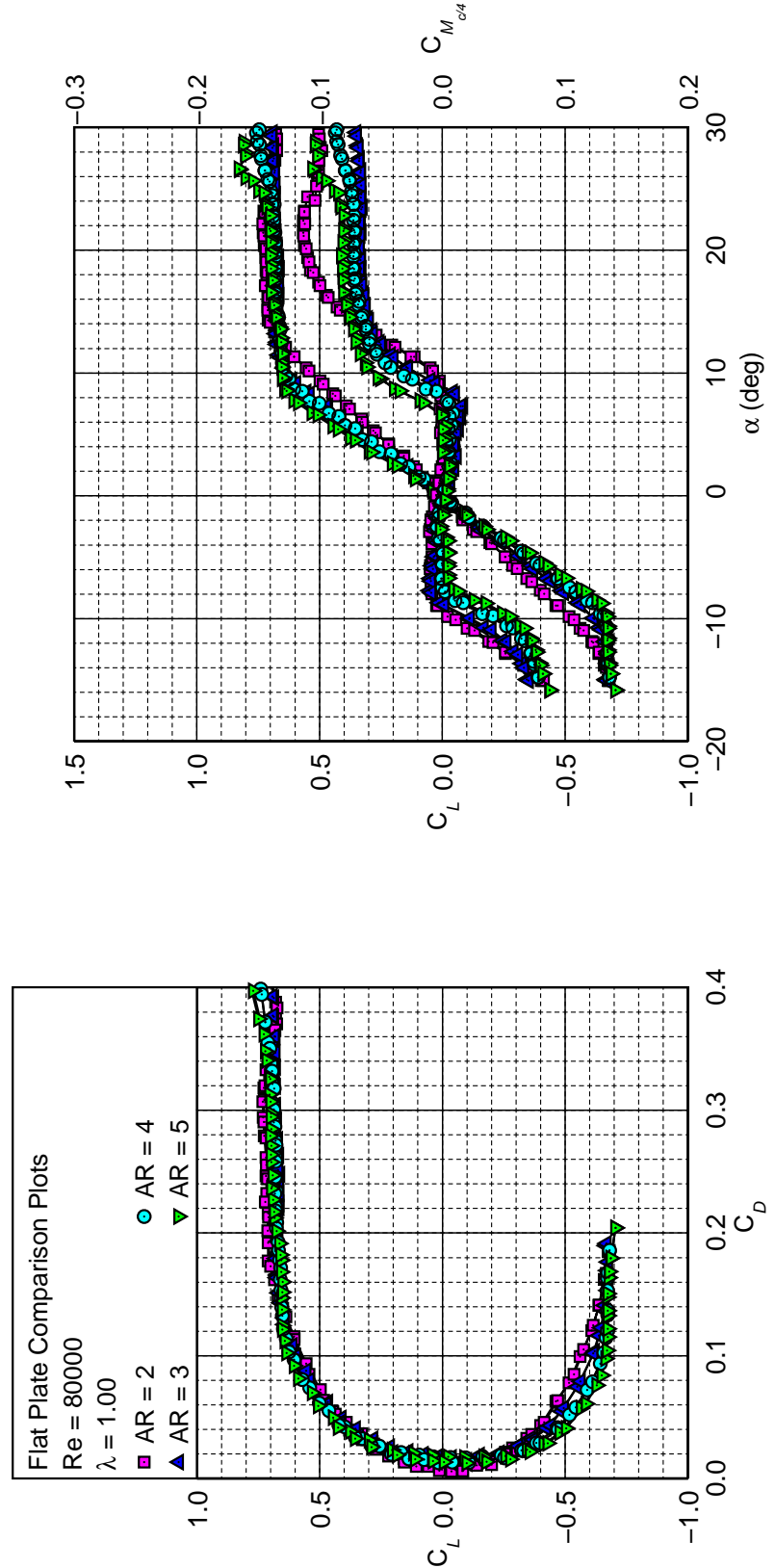


Fig. 5.17: Flat plate comparison results for a fixed Re of 80,000 and λ of 1.00.

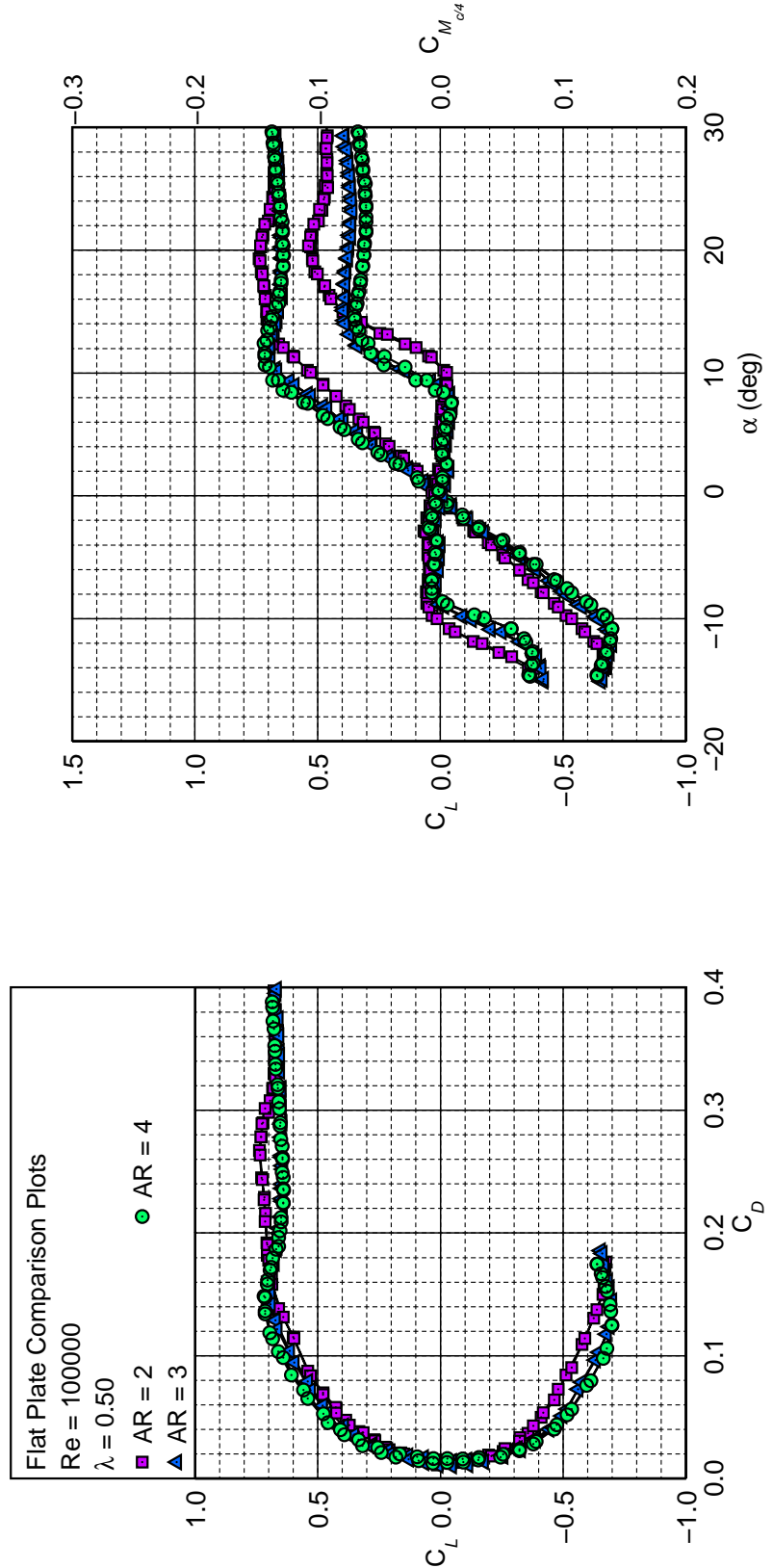


Fig. 5.18: Flat plate comparison results for a fixed Re of 100,000 and λ of 0.50.

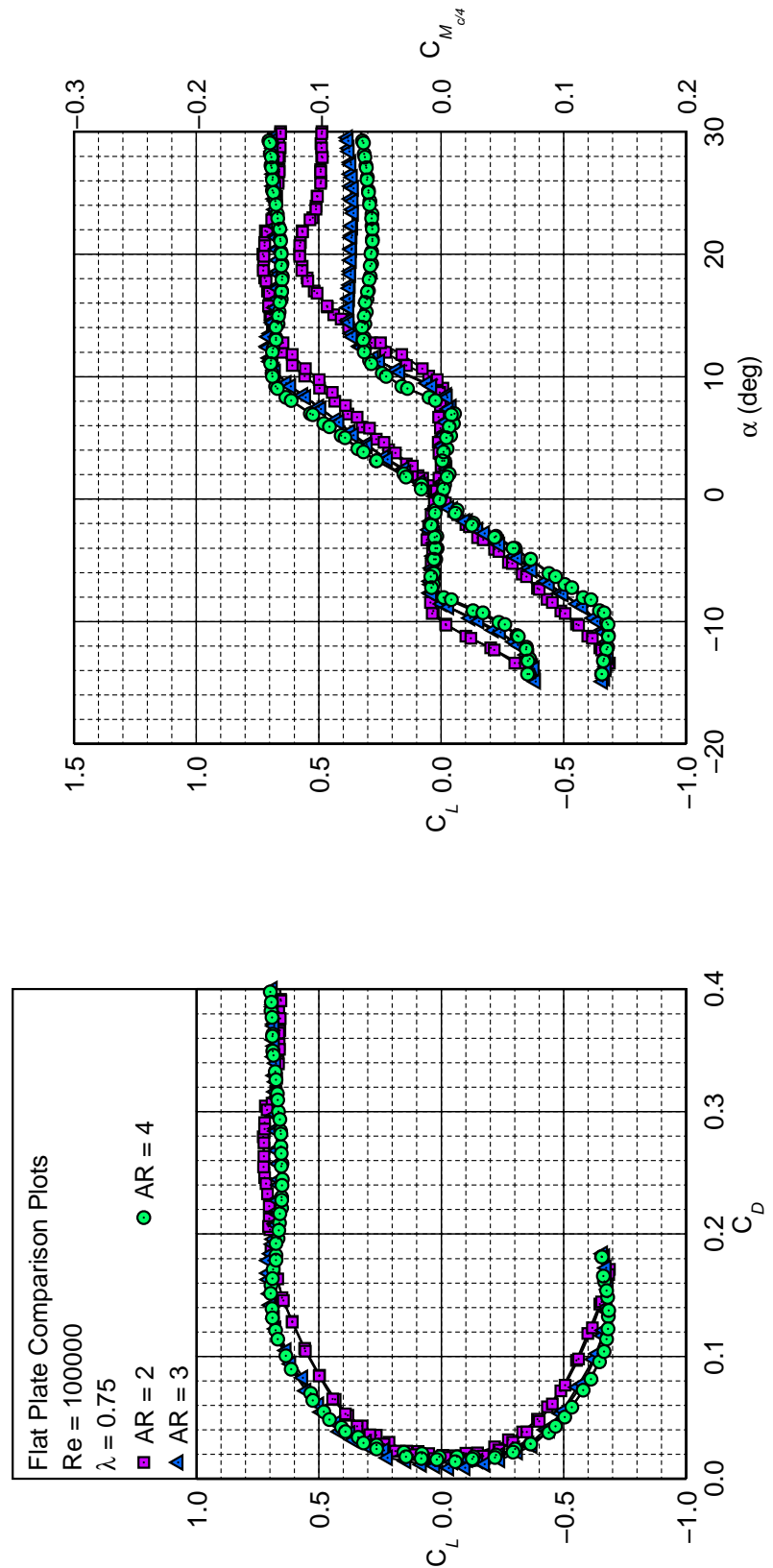


Fig. 5.19: Flat plate comparison results for a fixed Re of 100,000 and λ of 0.75.

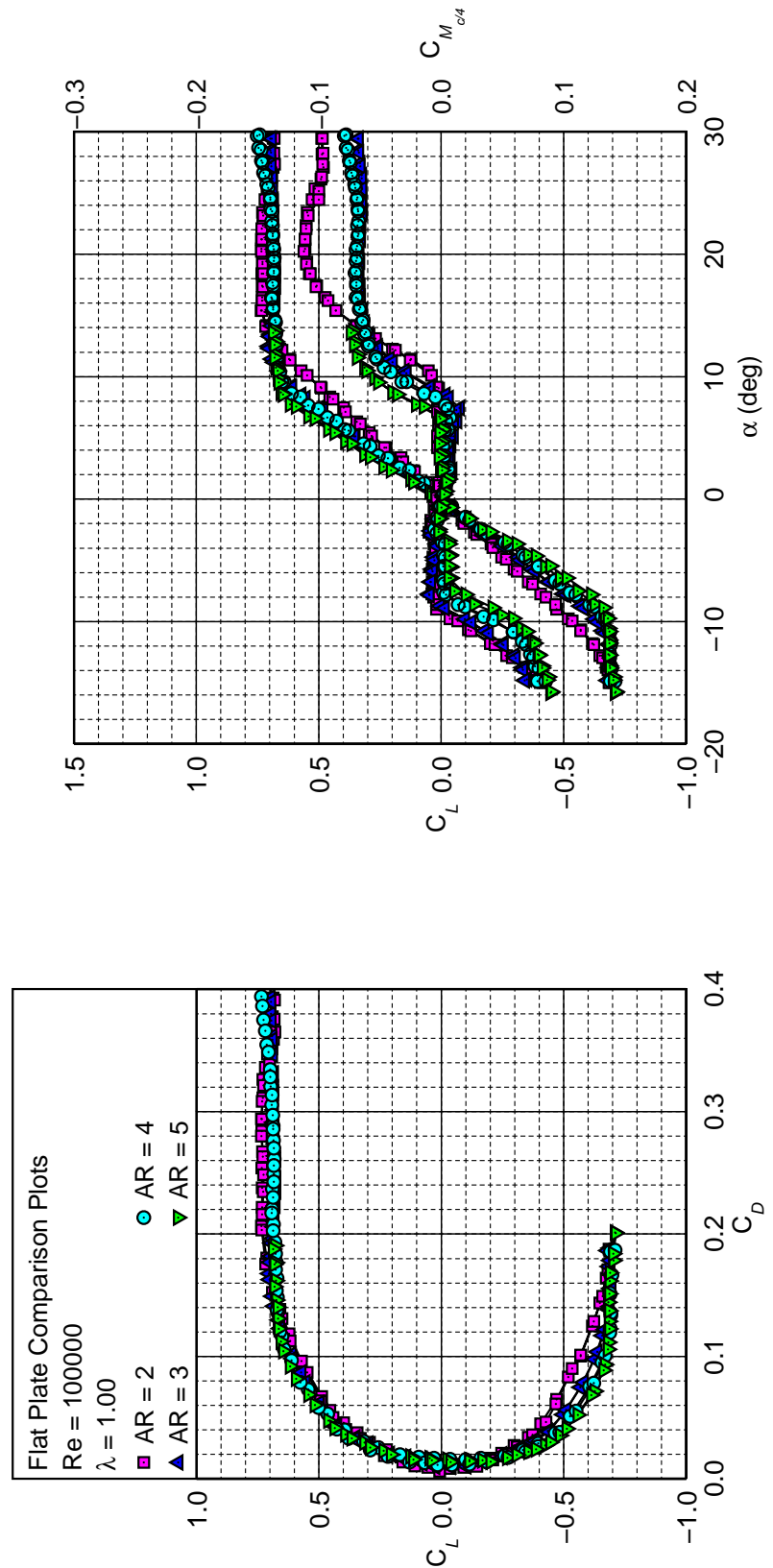


Fig. 5.20: Flat plate comparison results for a fixed Re of 100,000 and λ of 1.00.

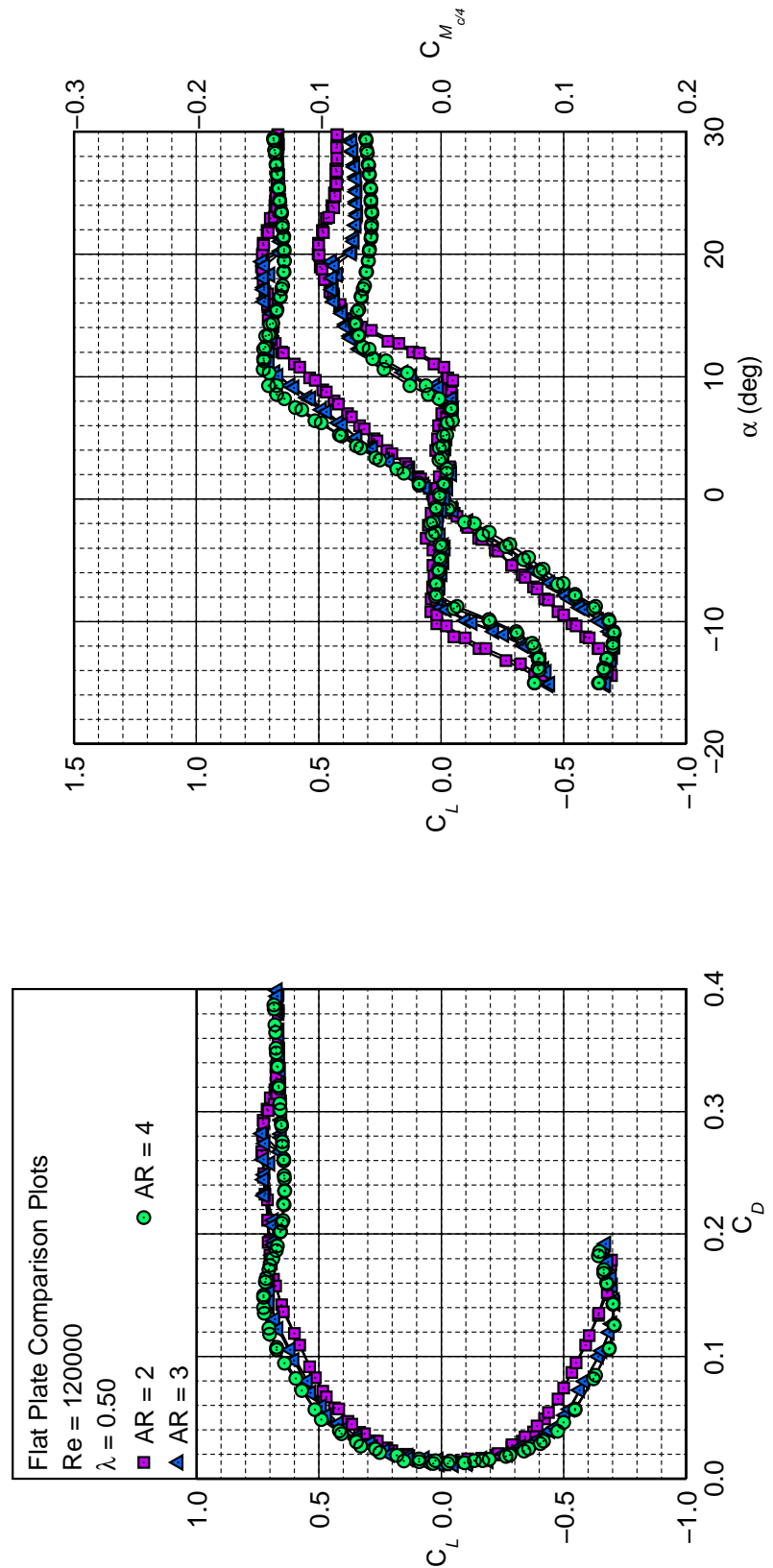


Fig. 5.21: Flat plate comparison results for a fixed Re of 120,000 and λ of 0.50.

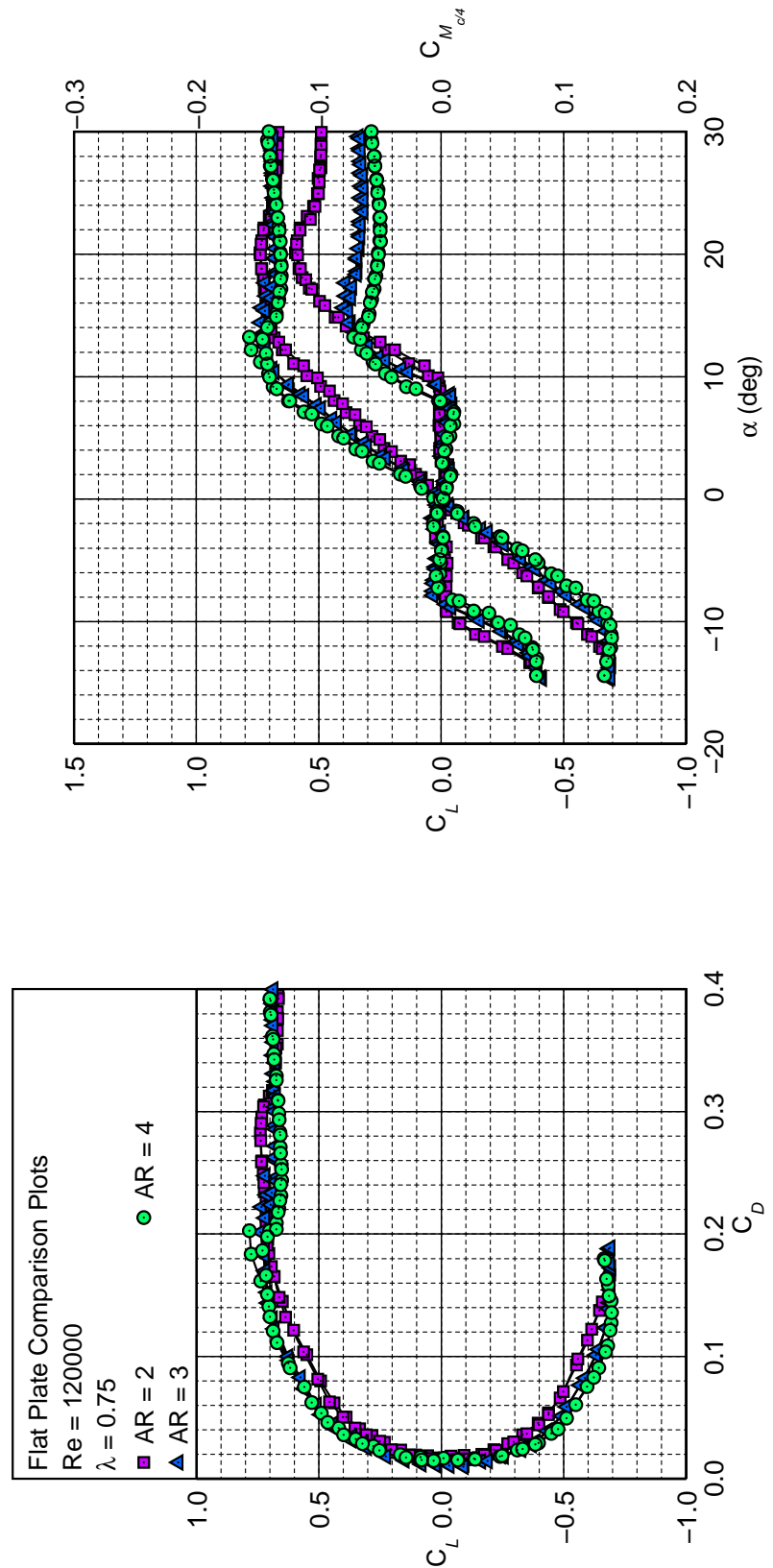


Fig. 5.22: Flat plate comparison results for a fixed Re of 120,000 and λ of 0.75.

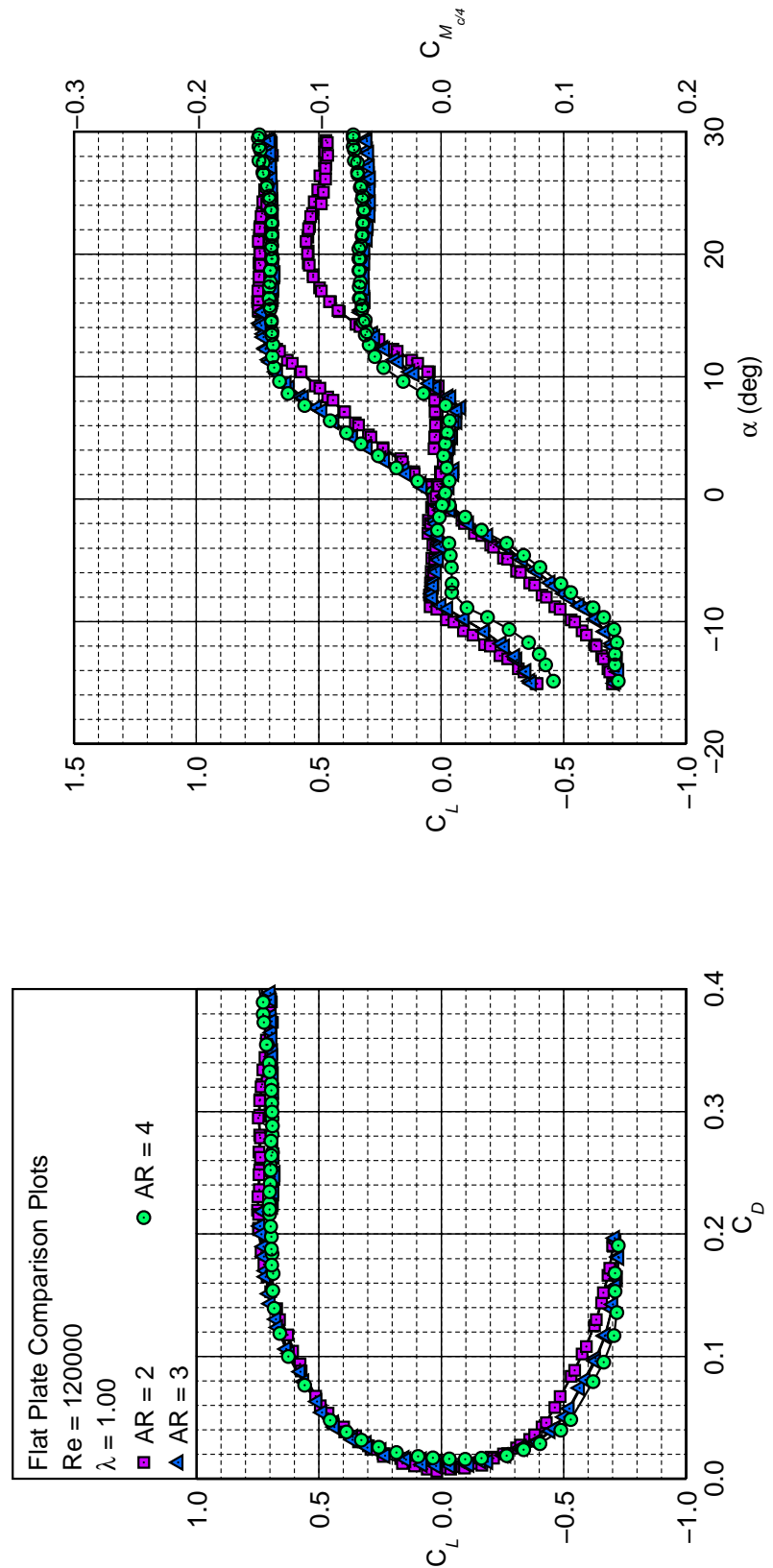


Fig. 5.23: Flat plate comparison results for a fixed Re of 120,000 and λ of 1.00.

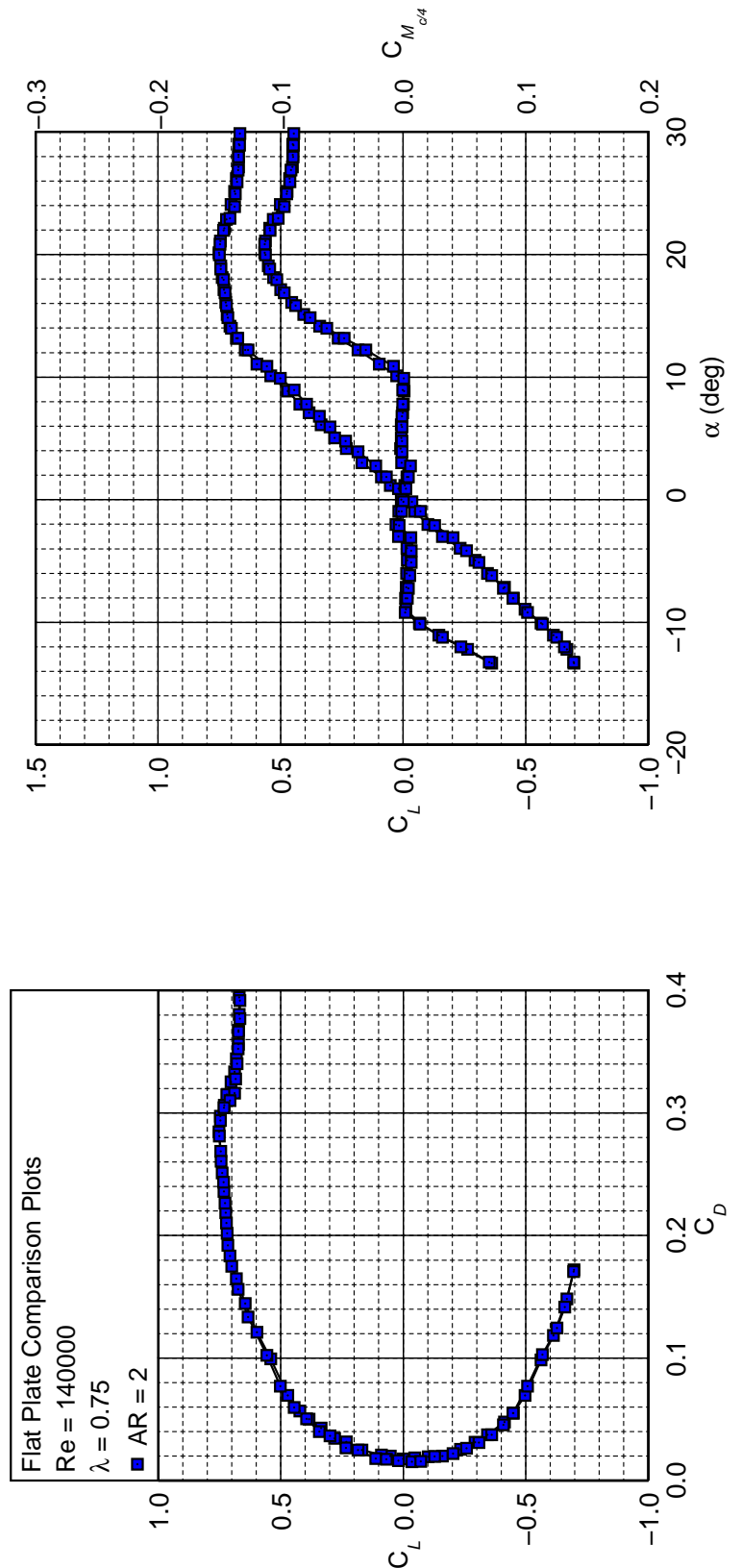


Fig. 5.24: Flat plate comparison results for a fixed Re of 140,000 and λ of 0.75.

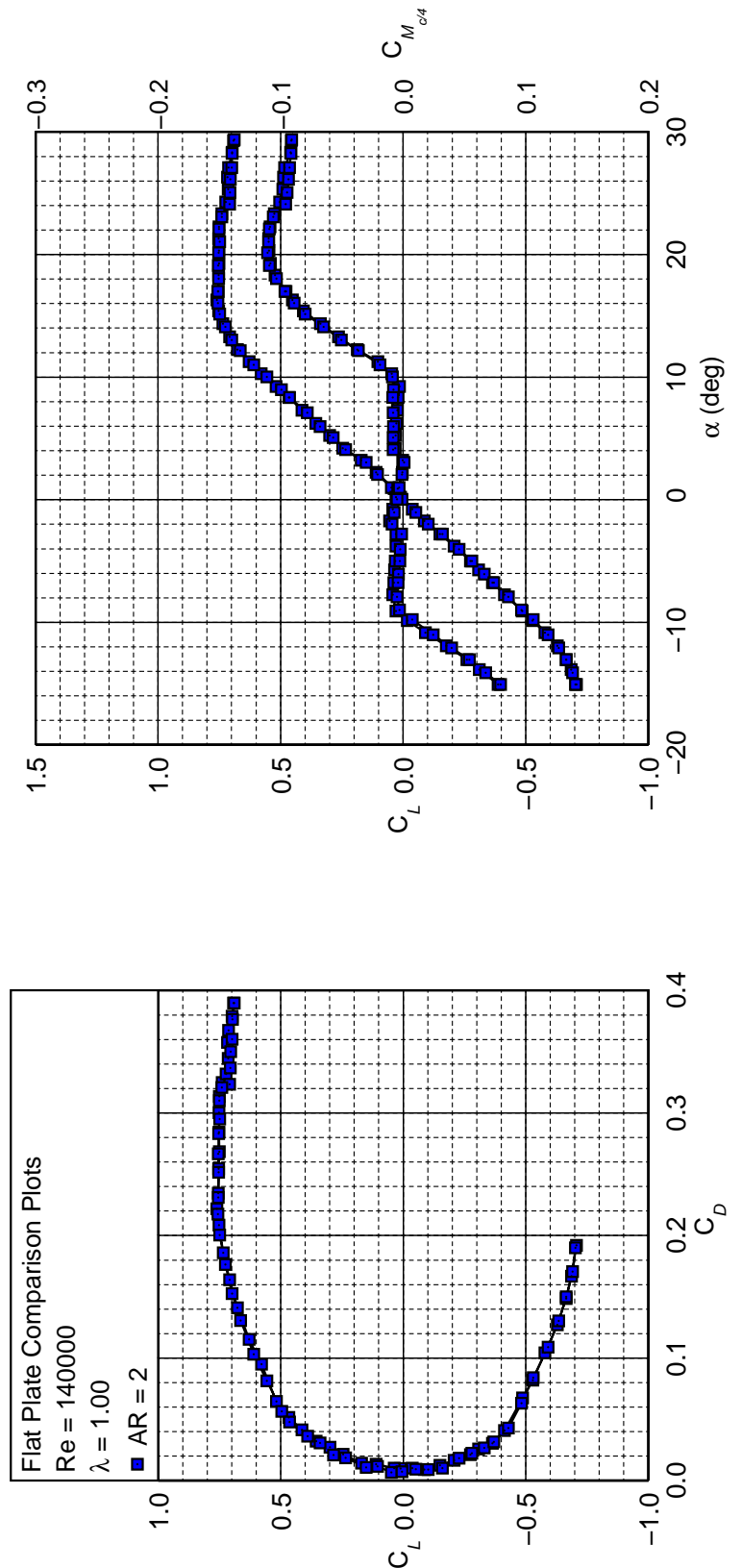


Fig. 5.25: Flat plate comparison results for a fixed Re of 140,000 and λ of 1.00.

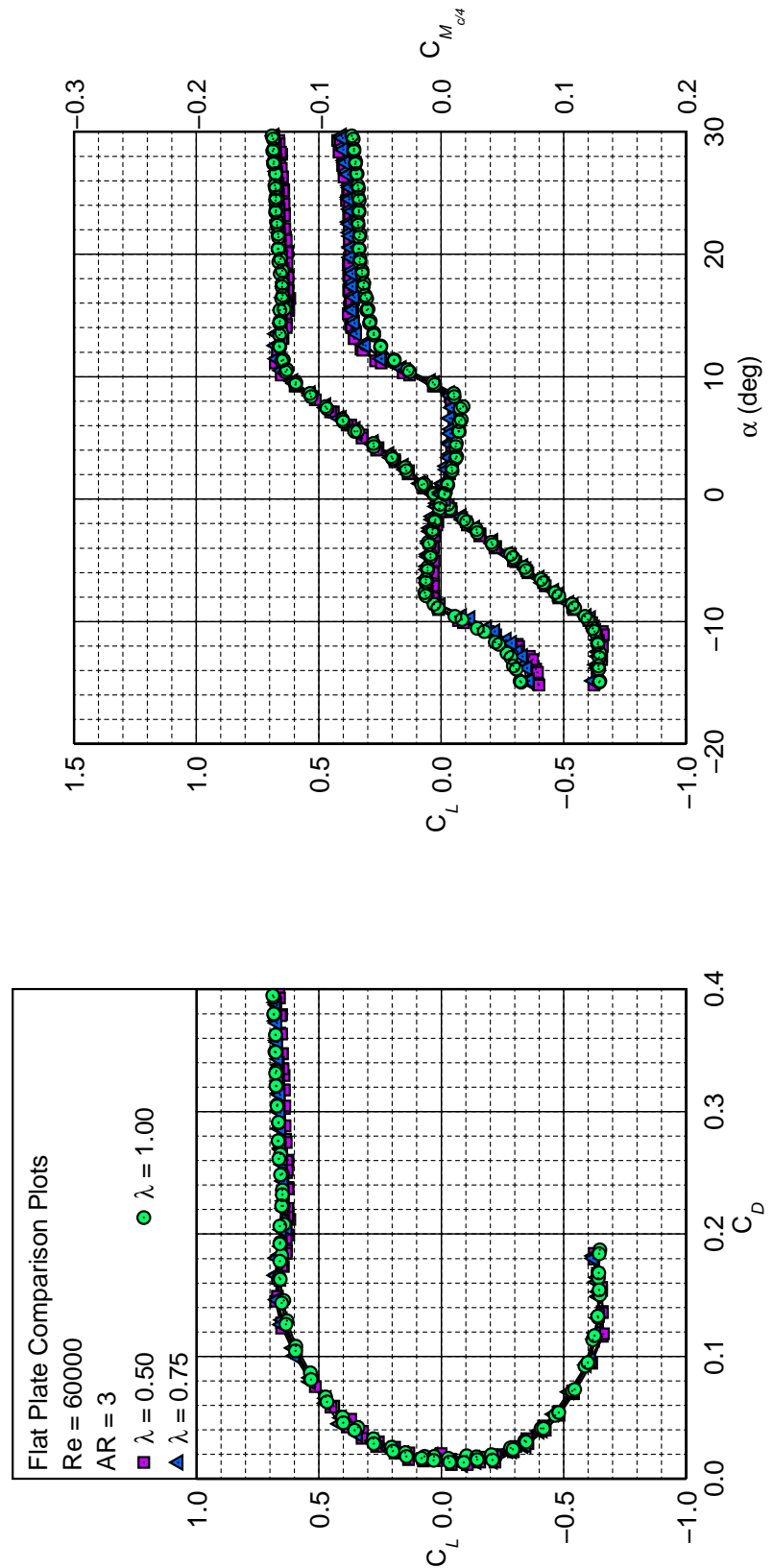


Fig. 5.26: Flat plate comparison results for a fixed Re of 60,000 and AR of 3.

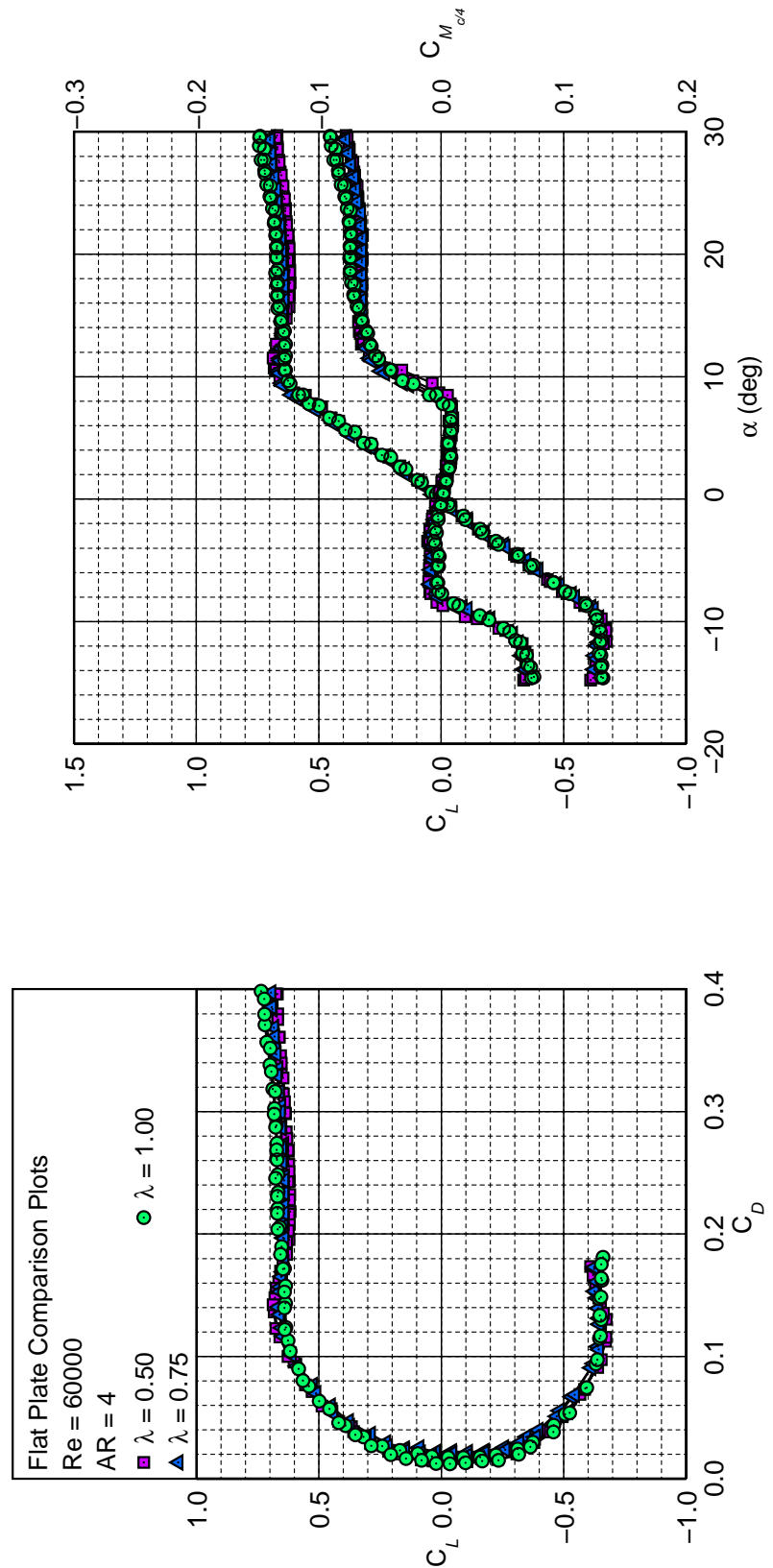


Fig. 5.27: Flat plate comparison results for a fixed Re of 60,000 and AR of 4.

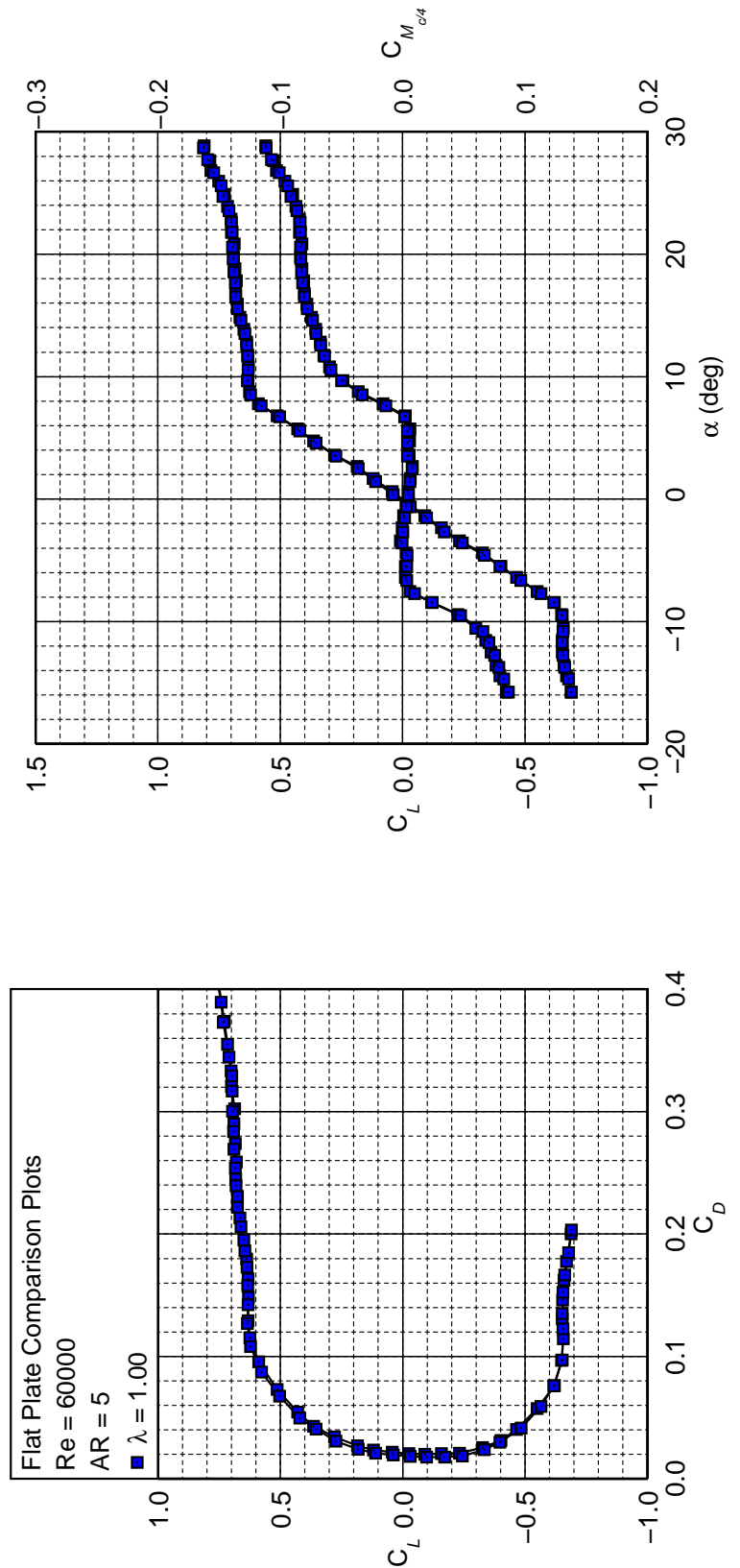


Fig. 5.28: Flat plate comparison results for a fixed Re of 60,000 and AR of 5.

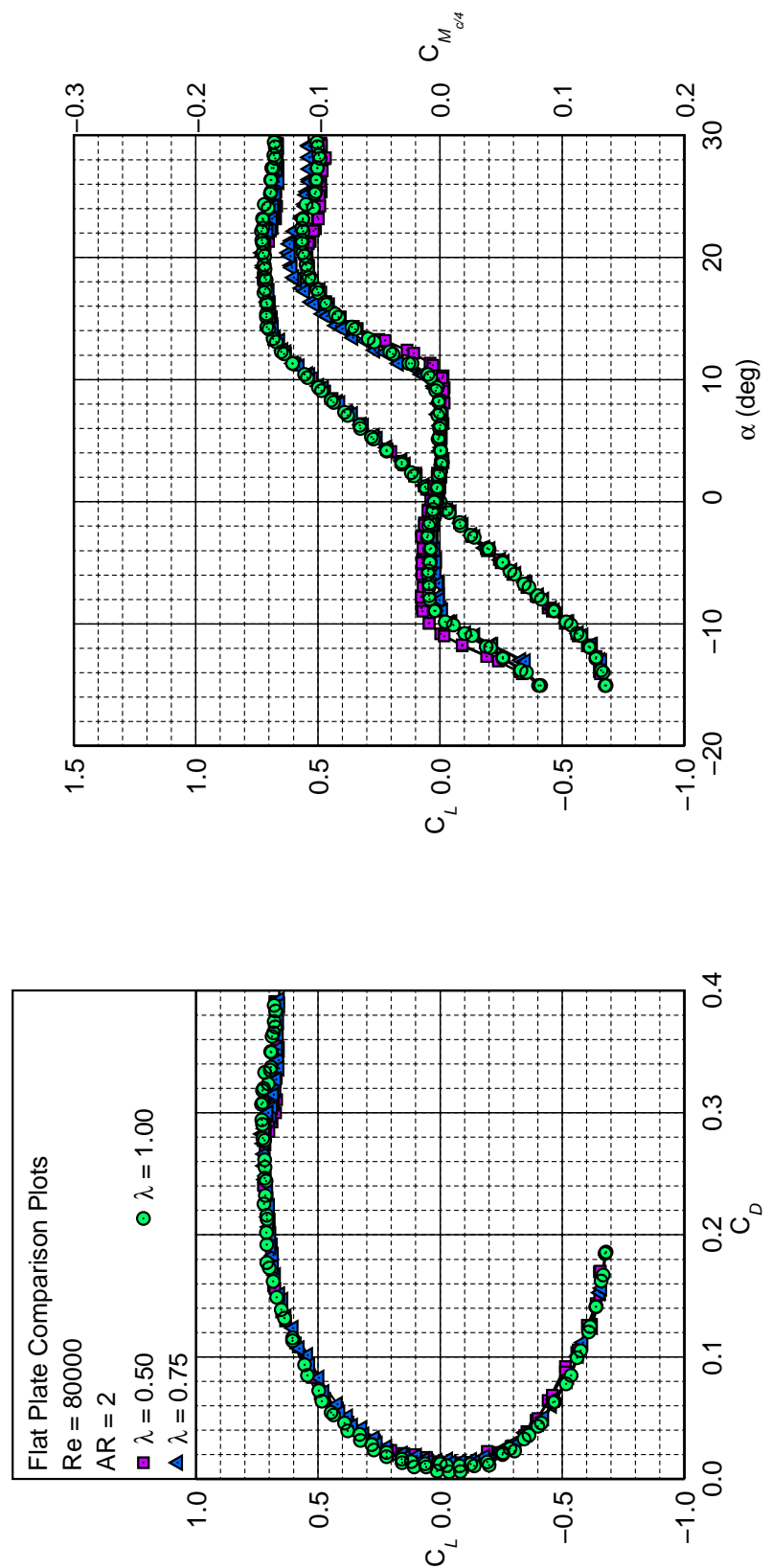


Fig. 5.29: Flat plate comparison results for a fixed Re of 80,000 and AR of 2.

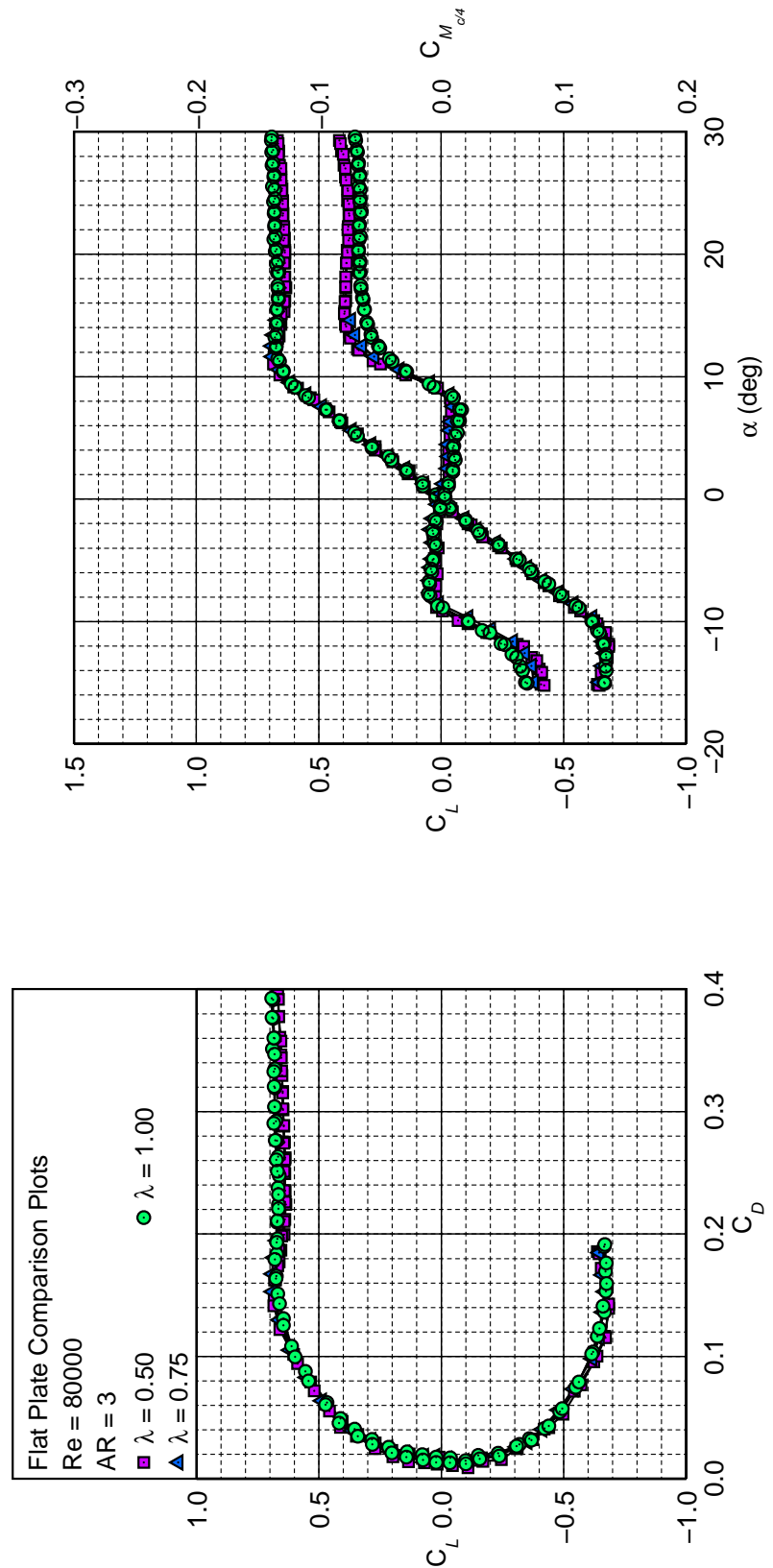


Fig. 5.30: Flat plate comparison results for a fixed Re of 80,000 and AR of 3.

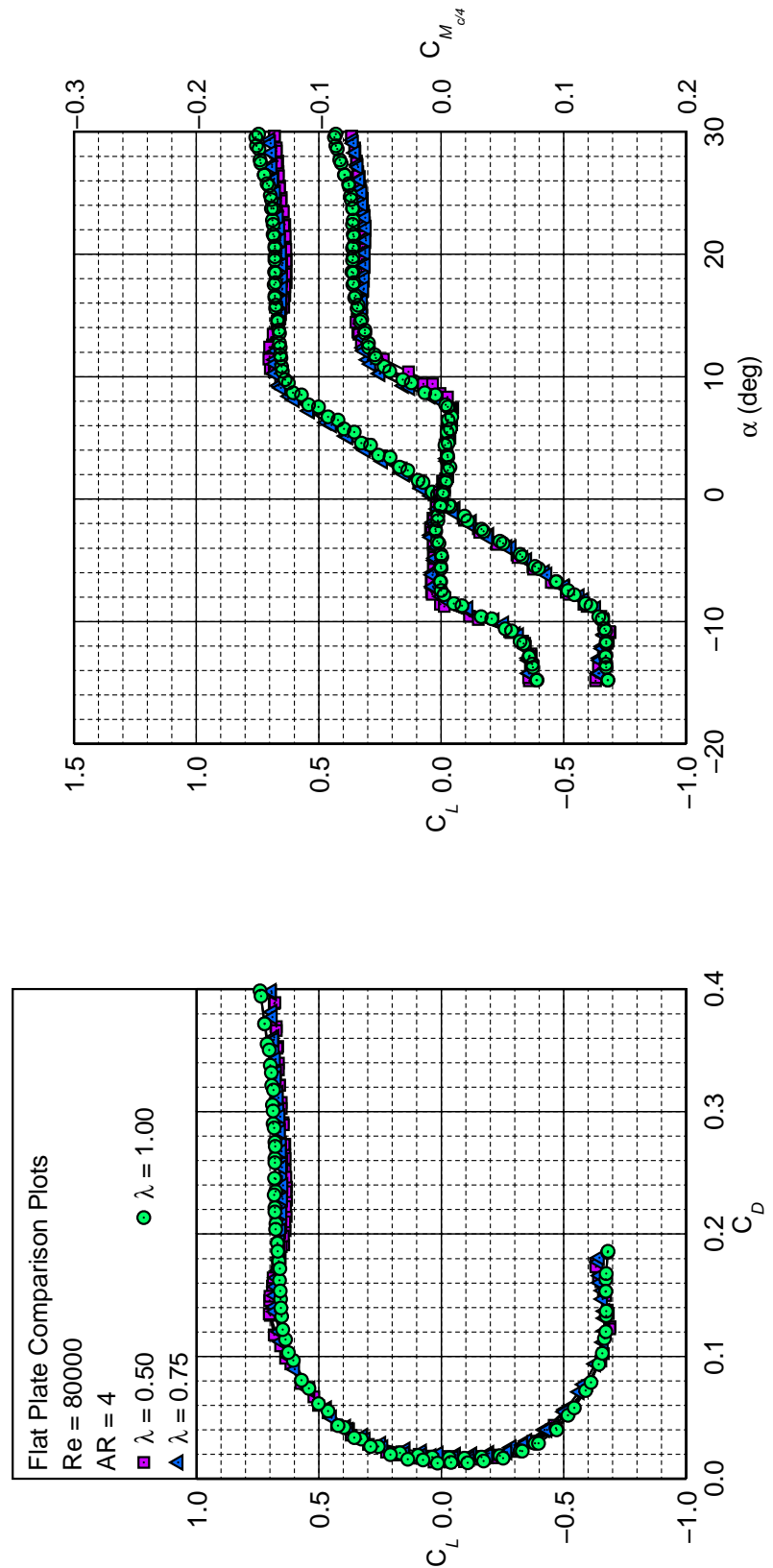


Fig. 5.31: Flat plate comparison results for a fixed Re of 80,000 and \mathcal{R} of 4.

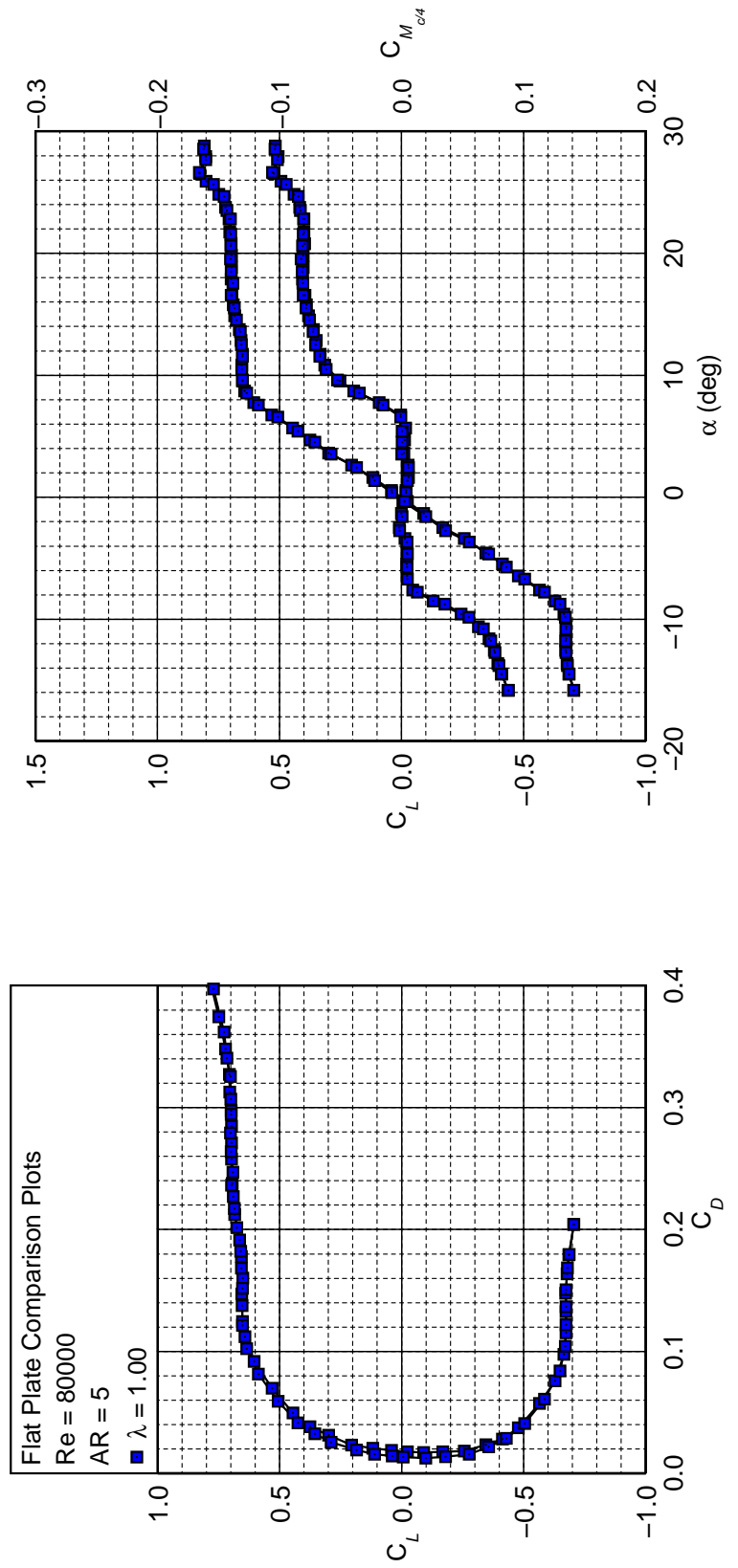


Fig. 5.32: Flat plate comparison results for a fixed Re of 80,000 and \mathcal{R} of 5.

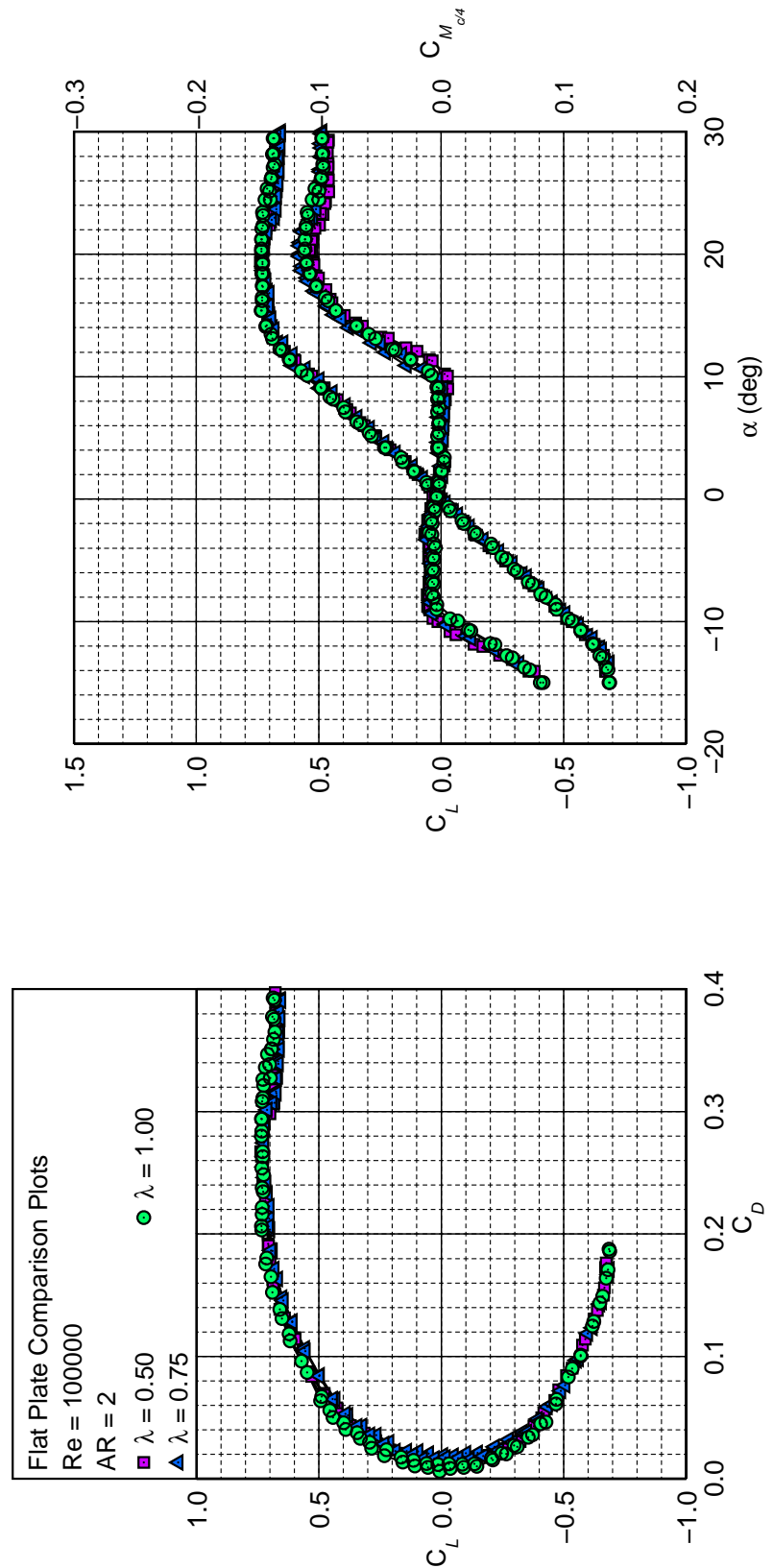


Fig. 5.33: Flat plate comparison results for a fixed Re of 100,000 and \mathcal{R} of 2.

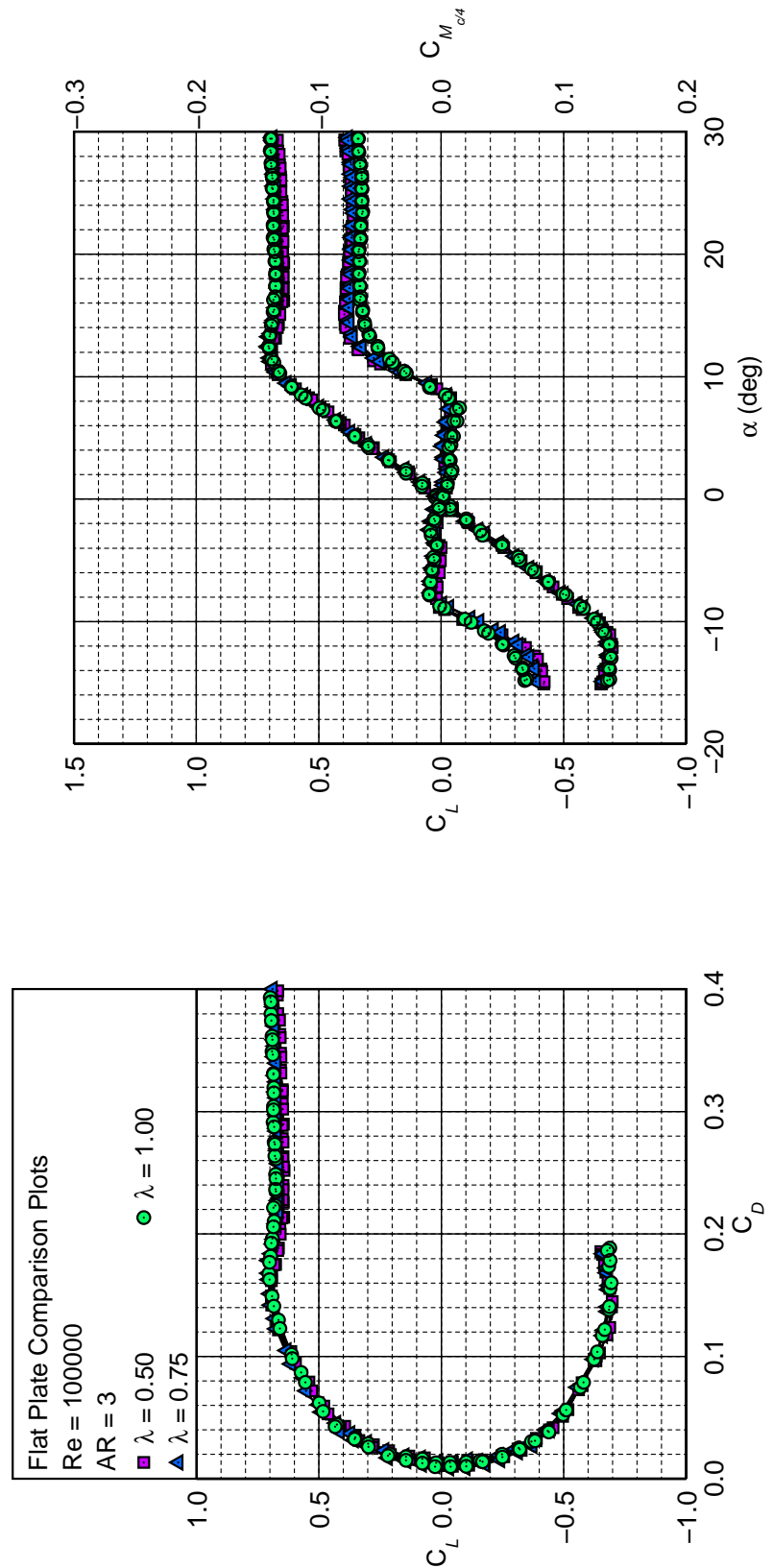


Fig. 5.34: Flat plate comparison results for a fixed Re of 100,000 and AR of 3.

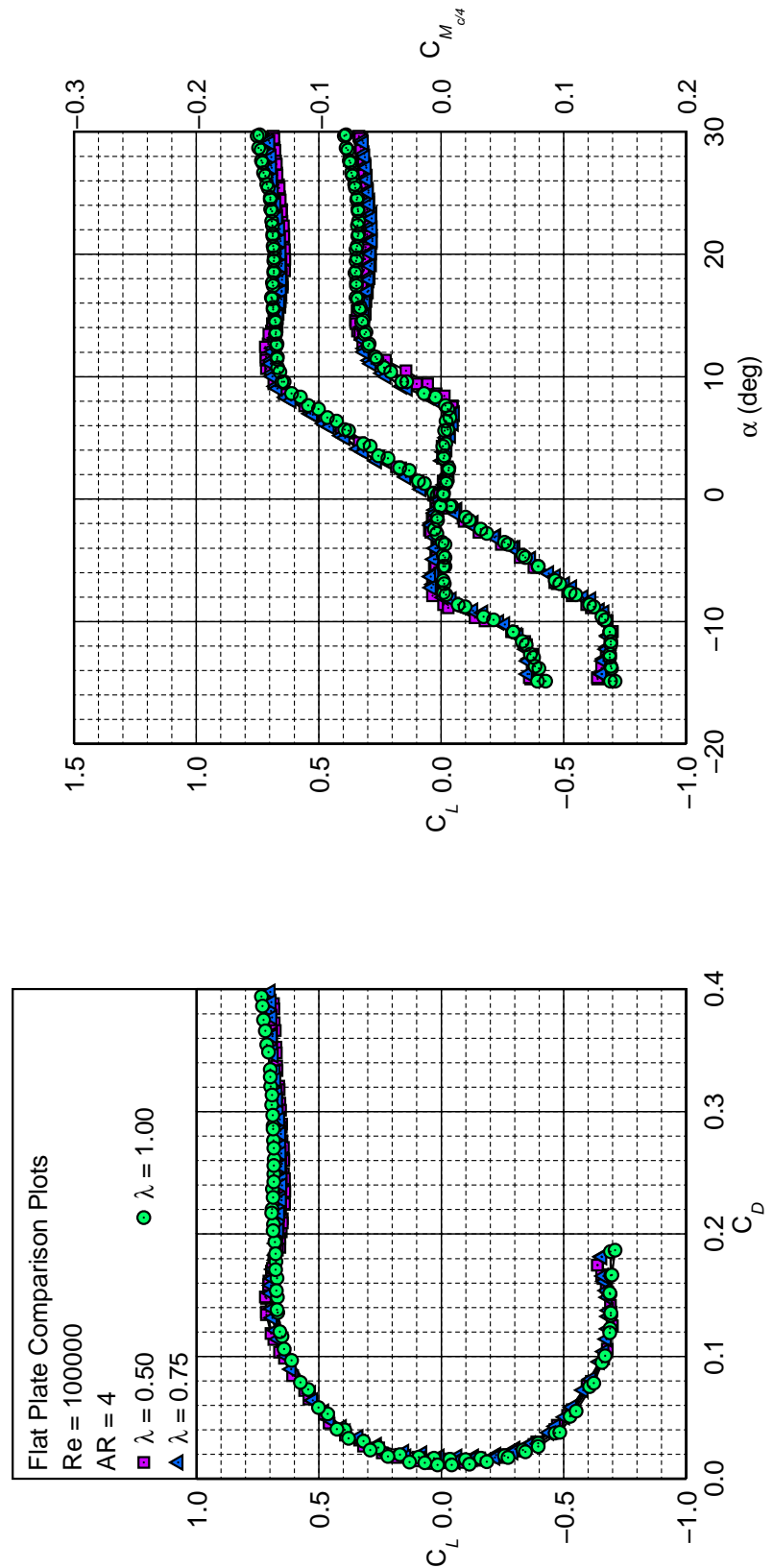


Fig. 5.35: Flat plate comparison results for a fixed Re of 100,000 and \mathcal{R} of 4.

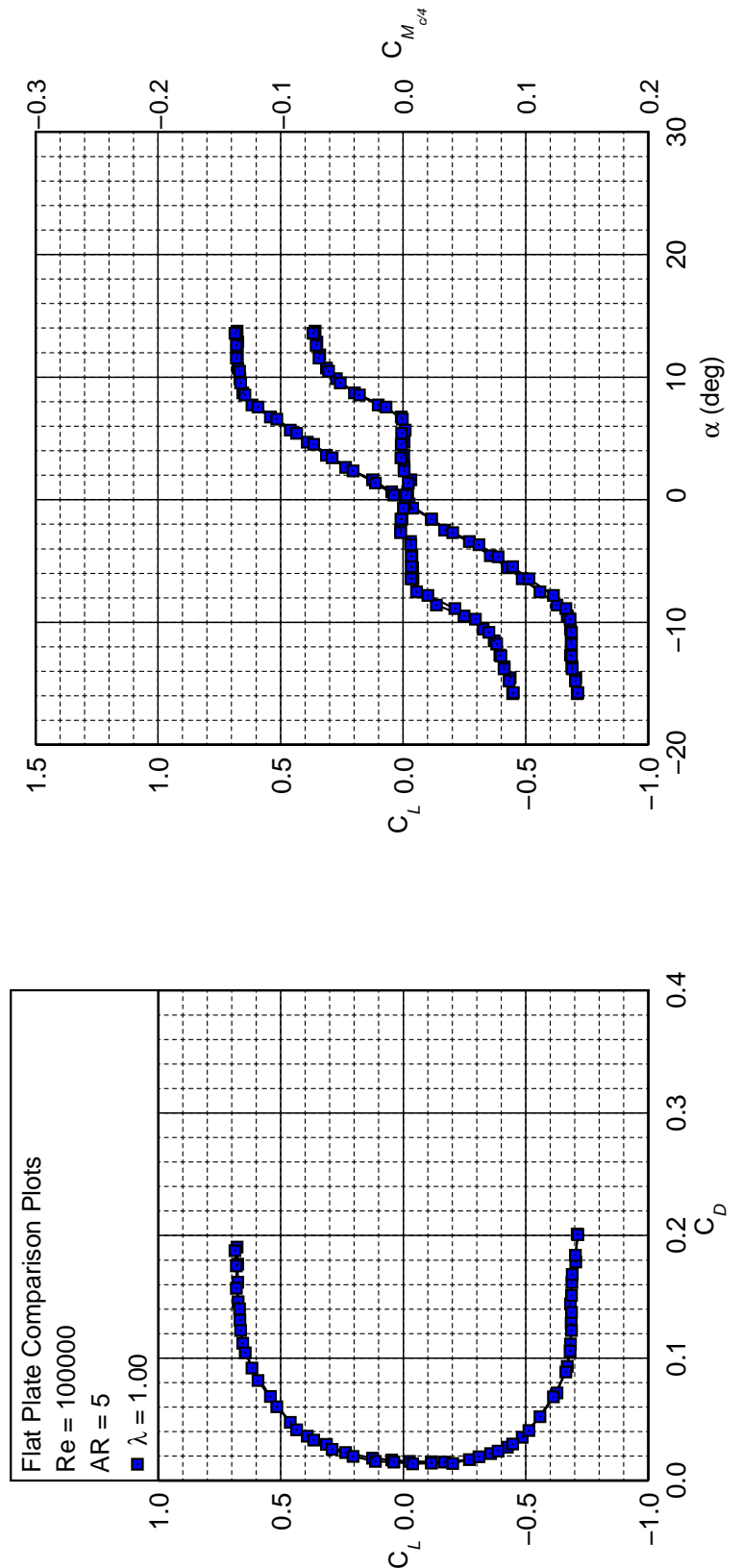


Fig. 5.36: Flat plate comparison results for a fixed Re of 100,000 and AR of 5.

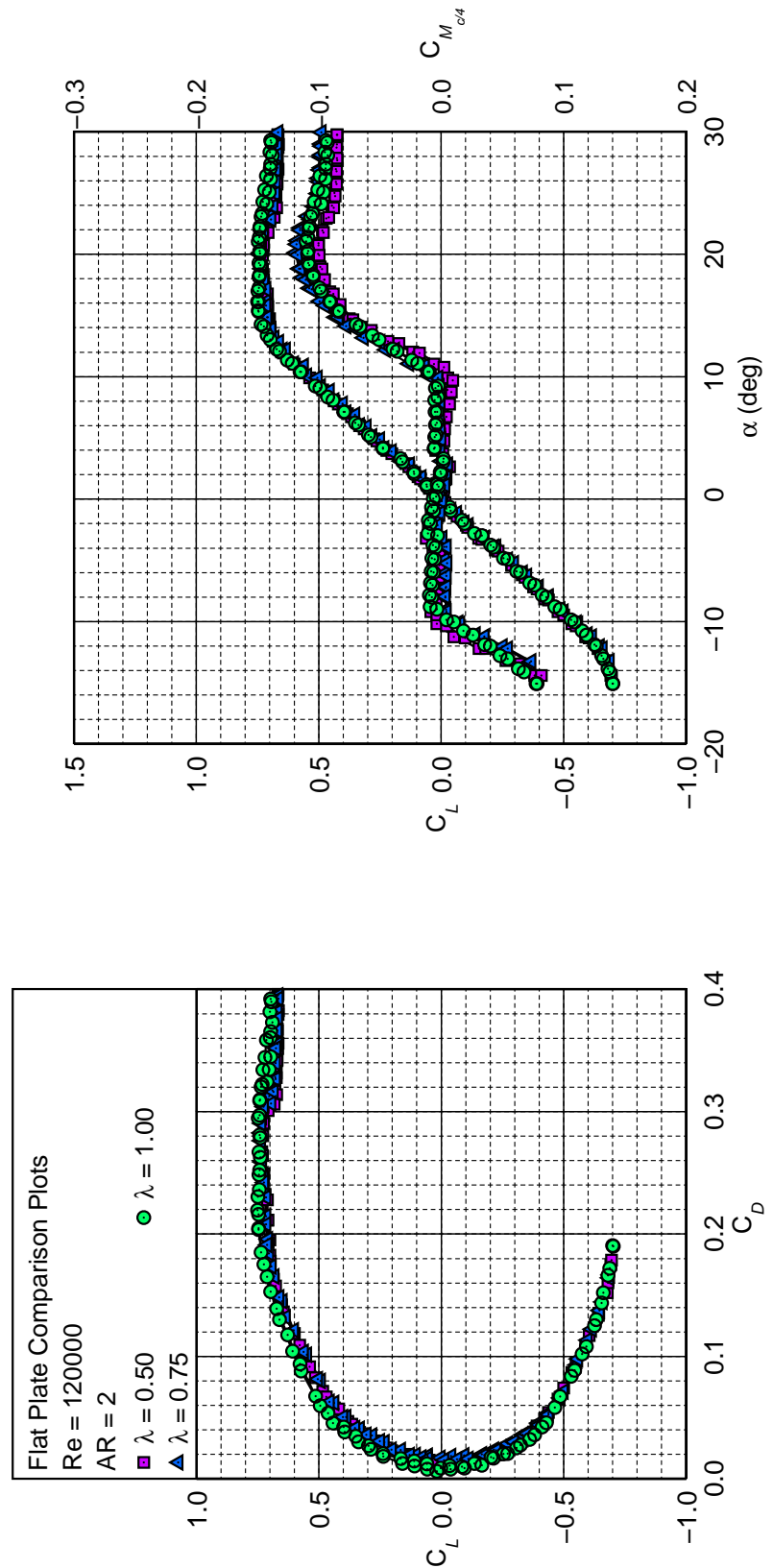


Fig. 5.37: Flat plate comparison results for a fixed Re of 120,000 and \mathcal{R} of 2.

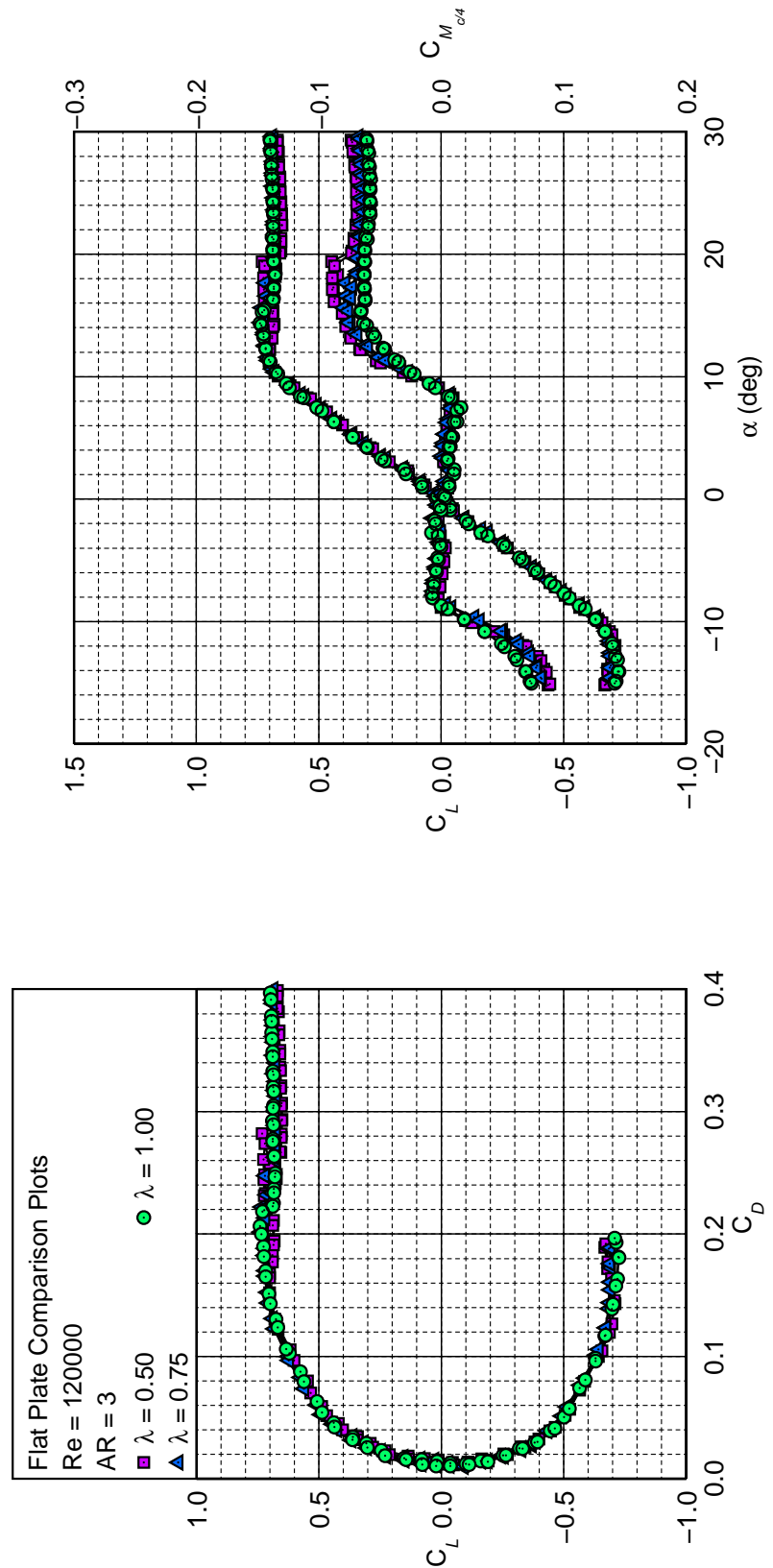


Fig. 5.38: Flat plate comparison results for a fixed Re of 120,000 and \mathcal{R} of 3.

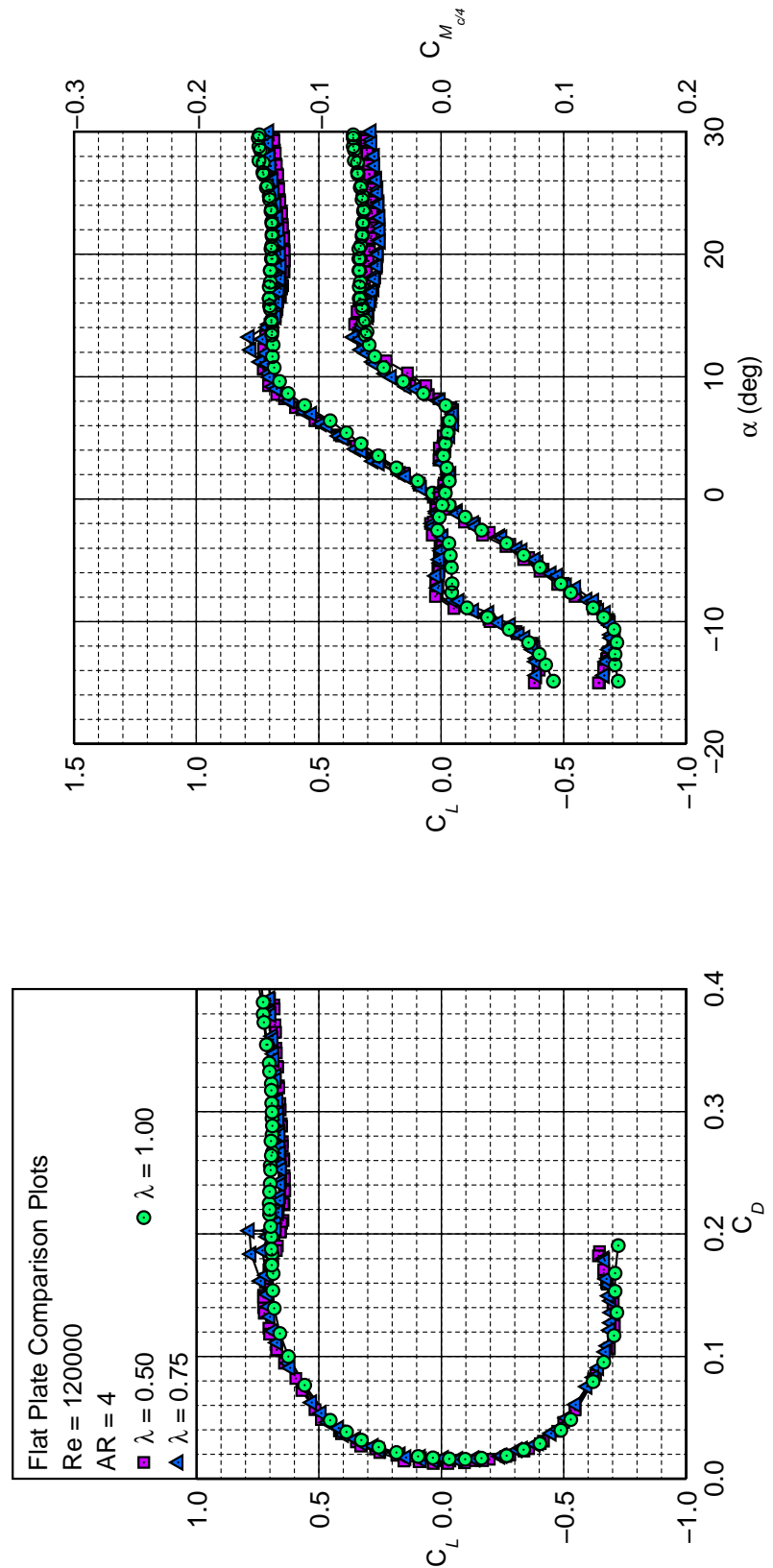


Fig. 5.39: Flat plate comparison results for a fixed Re of 120,000 and \mathcal{R} of 4.

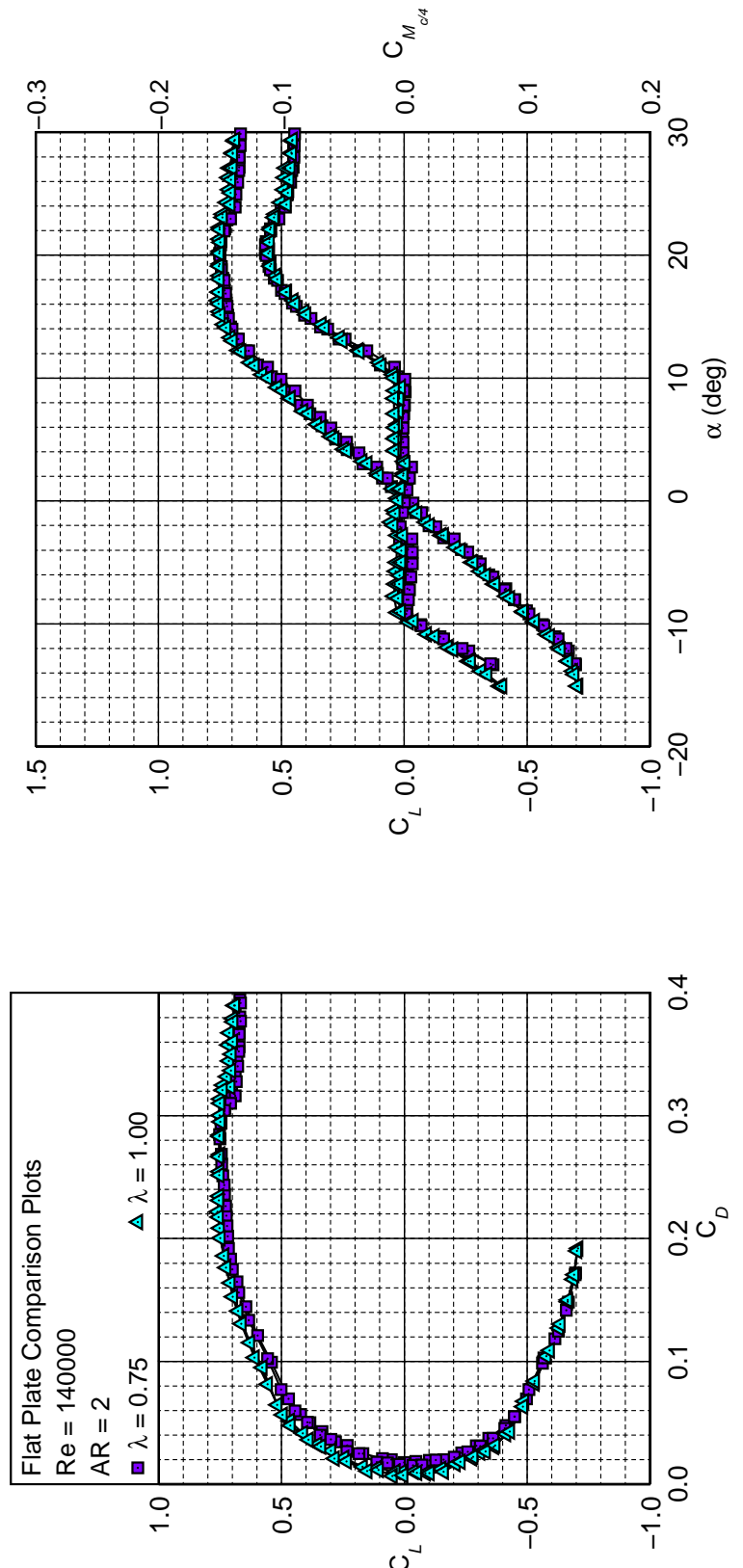


Fig. 5.40: Flat plate comparison results for a fixed Re of 140,000 and AR of 2.

Chapter 6

Discussion of Results

This chapter discusses the aerodynamic performance measurements presented in Chapter 5. Aerodynamic trends emanating from the tests performed are also analyzed and presented.

6.1 Wortmann FX 63-137 Wing Results

The Wortmann FX 63-137 *A*-4 rectangular wing was chosen because it has been used extensively in small aircraft and RC models owing primarily to its high-lift capabilities at low Reynolds numbers. As a result, the FX 63-137 airfoil and wing have been widely tested in many wind tunnel facilities. Drag polars, lift curves, and moment curves at varying Reynolds numbers for the Wortmann wing are shown in Fig. 5.1. Data were taken from an angle of attack of -15 to 25 deg for increasing and then decreasing angles of attack to capture possible aerodynamic hysteresis.

Figure 5.1 shows that the critical Reynolds number for the Wortmann wing is 90,000. A jump in lift-to-drag ratio occurs at this Reynolds number. For Reynolds numbers less than 90,000, stall occurs via a long laminar separation bubble that does not reattach, thereby resulting in a shallow lift curve. Laminar separation occurs when the laminar boundary layer encounters an adverse pressure gradient that is strong enough to cause it to separate from the wing surface. At Reynolds numbers less than 90,000, the separated laminar boundary or shear layer has insufficient energy to form a short laminar separation bubble by transitioning to turbulent flow and reattaching to the wing.

At the critical Reynolds number of 90,000, both pre-stall and post-stall hysteresis phenomena are observed on the Wortmann wing. Pre-stall hysteresis, as discussed in Ref. 71, is a type of lift hysteresis that is caused initially by laminar stall with increasing angle of attack. As the angle of attack increases further, the separated laminar shear layer suddenly forms a short laminar

separation bubble over the wing. The laminar separation bubble formation yields a large jump in the lift of the wing and corresponding increase in the lift-to-drag ratio. The effect of bubble formation is also captured in the drag and moment data. With decreasing angles of attack, however, the drop in lift occurs at a lower angle of attack compared with the prior jump. This delay happens because there is a delay in the disintegration ('bursting') of the short bubble caused by the instabilities inherent in the turbulent flow over the surface of the wing. To date, as far as the author is aware, pre-stall hysteresis has not been captured in literature for Wortmann FX 63-137 airfoils or wings and has been rarely observed on other airfoils [72]. Although repeatably reproduced, pre-stall hysteresis for the Wortmann wing only occurred at a Reynolds number of 90,000 for the Wortmann wing. Any slight deviations from the 90,000 Reynolds number resulted in no pre-stall hysteresis.

Post-stall hysteresis is observed and repeatably reproduced at Reynolds numbers of 90,000 and 100,000. Post-stall hysteresis occurs when the laminar separation bubble on the wing upper surface bursts, and flow separation occurs, resulting in a large loss of lift. As angle of attack then decreases, the laminar separation bubble reattaches at an angle of attack lower than that for which the burst occurred, thereby creating the post-stall hysteresis loop.

Another conclusion that was obtained from the performance results was that the stall angle of attack is observed to increase with an increase in Reynolds number. Also, it is important to note the increase in the zero-lift angle of attack with decreasing Reynolds number. This trend is similar to that discussed in Bastedo and Mueller [4].

Surface oil-flow visualization tests were performed at a number of angles of attack to further understand the interesting flow phenomena on the Wortmann wing at a Reynolds number of 90,000. Figures 6.1(a–h) show photographs of the upper surface of the Wortmann wing at these different angles of attack. Laminar flow accompanied by flow separation or a long separation bubble is seen at an α of -2 and 7 deg. The bubble moves toward the leading edge of the wing with increasing angle of attack. For both these angles of attack, it can be also observed that turbulent flow has not fully developed over the trailing-edge section of the wing. At an α of 9 deg, the long bubble 'collapses' into a short separation bubble. Fully developed turbulent flow is also seen at the trailing edge of the wing. It can be concluded that because the short separation bubble formed, the jump in the lift for the wing has prematurely occurred and the pre-stall hysteresis stage was bypassed. The premature tripping of the wing boundary layer may have been caused by the slight surface

roughness produced by the texture of the flow visualization oil.

The short separation bubble is seen to further move toward the leading edge and reduce in length at an angle of attack of 12 deg. A small laminar flow region is seen at an α of 14 deg

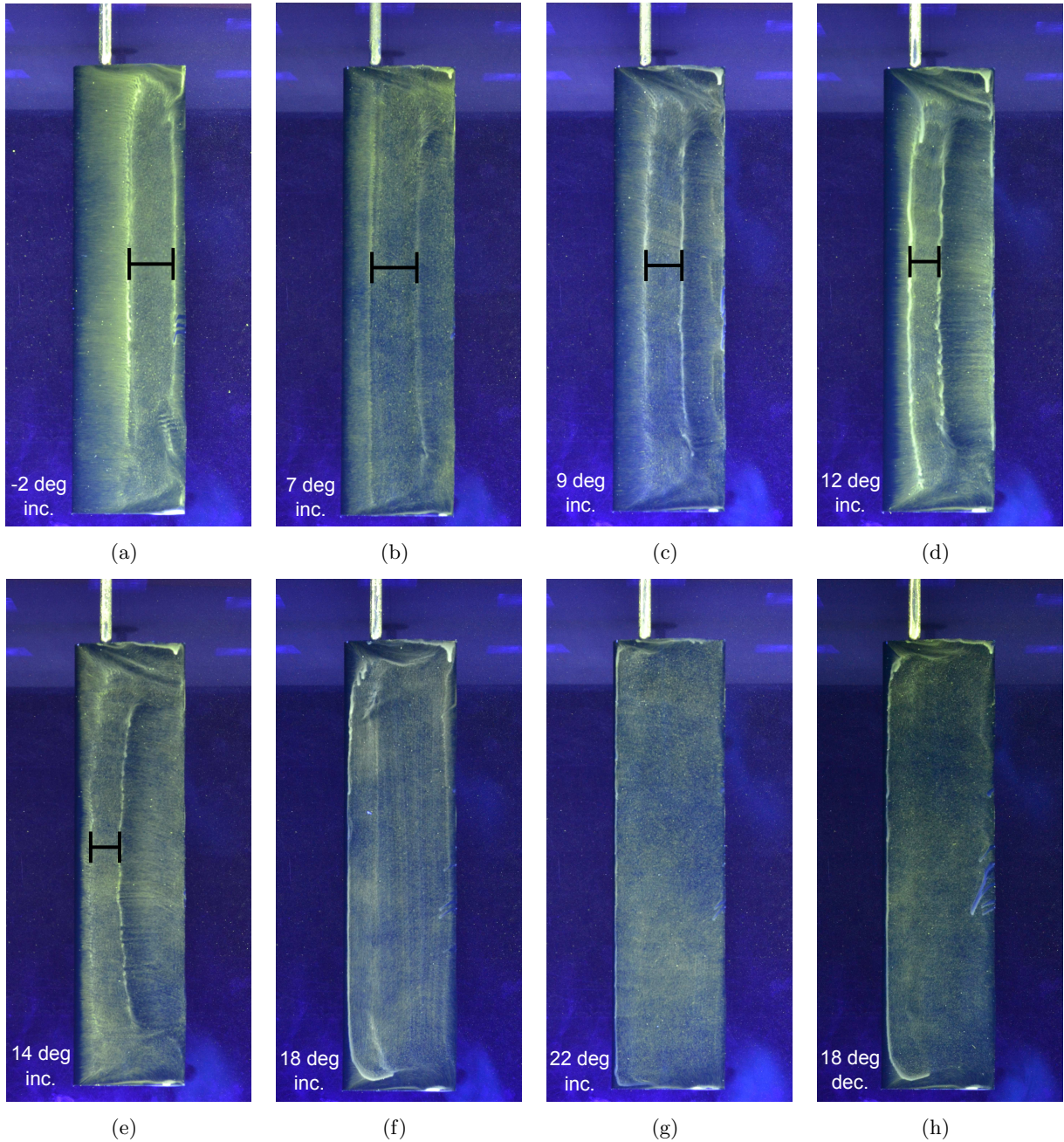


Fig. 6.1: Upper surface oil flow visualization of major flow features on the Wortmann FX 63-137 A-4 rectangular wing at a Re of 90,000: (a) $\alpha = -2$ deg (increasing α), (b) $\alpha = 7$ deg (increasing α), (c) $\alpha = 9$ deg (increasing α), (d) $\alpha = 12$ deg (increasing α), (e) $\alpha = 14$ deg (increasing α), (f) $\alpha = 18$ deg (increasing α), (g) $\alpha = 22$ deg (increasing α), and (h) $\alpha = 18$ deg (decreasing α).

with the separation bubble and turbulent regions covering most of the upper surface of the wing. From an α of -2 to 14 deg, a steady growth is observed in the disturbance caused by the wing tip vortices. The steady growth is most likely caused by the strength of wing tip vortices that increase with lift. At an α of 18 deg, the bubble is not present, and the steady bands of oil on the upper surface of the wing represent the fully turbulent region of the flow over the wing. Finally, at an α of 22 deg, the unaltered oil flow indicates complete flow separation from the upper surface of the wing. Post-stall hysteresis was captured when the angle of attack of the wing was initially set to 22 deg and then reduced to 18 deg during a flow visualization test run. Figure 6.1(h) shows that the flow was still fully separated in comparison with the fully turbulent flow in Fig. 6.1(f).

6.2 Flat-Plate Wing Results

For the flat-plate wing tests, drag polars, and lift and moment curves are shown for all ten flat-plate wings described in Chapter 3.5. Data was taken from -20 to 30 deg for increasing and decreasing angles of attack. A large angle-of-attack range was chosen to capture post-stall effects of the flat-plate wing. The flat-plate wing results are presented in terms of Reynolds number effects, aspect ratio effects, and taper ratio effects as shown below.

6.2.1 Reynolds Number Effects

The drag polars, and lift and moment curves from Figs. 5.2–5.11 shows a number of interesting observations related to an increase in Reynolds number. Firstly, there is a widening of the drag bucket with increasing Reynolds number. The widening of the drag bucket suggests a reduction in the degree of separated flow over the flat-plate wings when the Reynolds number increases.

A decreasing minimum drag coefficient $C_{D_{min}}$ is generally seen for wings of aspect ratio 3 to 5. Aspect ratio 2 wings however show scatter in the $C_{D_{min}}$ values. To further understand the scatter in $C_{D_{min}}$, the minimum drag coefficient for all flat-plate wings as a function of Reynolds number are presented in Fig. 6.2. Theoretically, the minimum drag coefficient of a flat plate should decrease with increasing Reynolds number. The results shown in Figure 6.2 though does not fully satisfy this prediction. Part of the reason, as noted in Pelletier and Mueller [5], is that the forces being measured were very low. The low forces meant that the scatter in the $C_{D_{min}}$ values were within uncertainty levels of each other. In addition, since sting measurements had to be taken prior to wing tests, there could have been small setup differences with and without the wing that was not accounted for. As a result, any minimal offset in the C_D vs α curve of a particular wing would create the differences observed and therefore skew results.

The issues created by the scatter in $C_{D_{min}}$ values are also observed in Figs. 6.8 and 6.9 where the trends of $(C_L/C_D)_{max}$ and $(C_L^{3/2}/C_D)_{max}$ as a function of Reynolds number are presented for flat-plate wings. Figures 6.8 and 6.9 are presented as they relate to the maximum range and endurance of propeller-driven aircraft respectively. The general trends observed for both figures were that both maximum range and endurance increased with Reynolds number.

For the lift curves, an increase in $C_{L_{max}}$ and lift curve slope $C_{L\alpha}$ is seen from Figs. 5.2–5.11.

The $C_{L_{max}}$ increase with Reynolds number is further verified in Fig. 6.5. The general increasing $C_{L\alpha}$ trends with respect to Reynolds number seen is observed in Fig. 6.6 where lift curve slopes for all flat-plate wings as a function of Reynolds number are co-plotted. The trends witnessed are smooth (low scatter) as the slopes were calculated by fitting the data to a linear trendline thereby reducing its variance. Figure 6.6 also shows the difference in slopes with respect to aspect ratios tested. Apart from the aspect ratio 4 wings, there also seems to be very little difference between the slopes of different taper ratio wings.

Stall for the flat-plate wings occurs as a result of laminar separation as it is not accompanied by

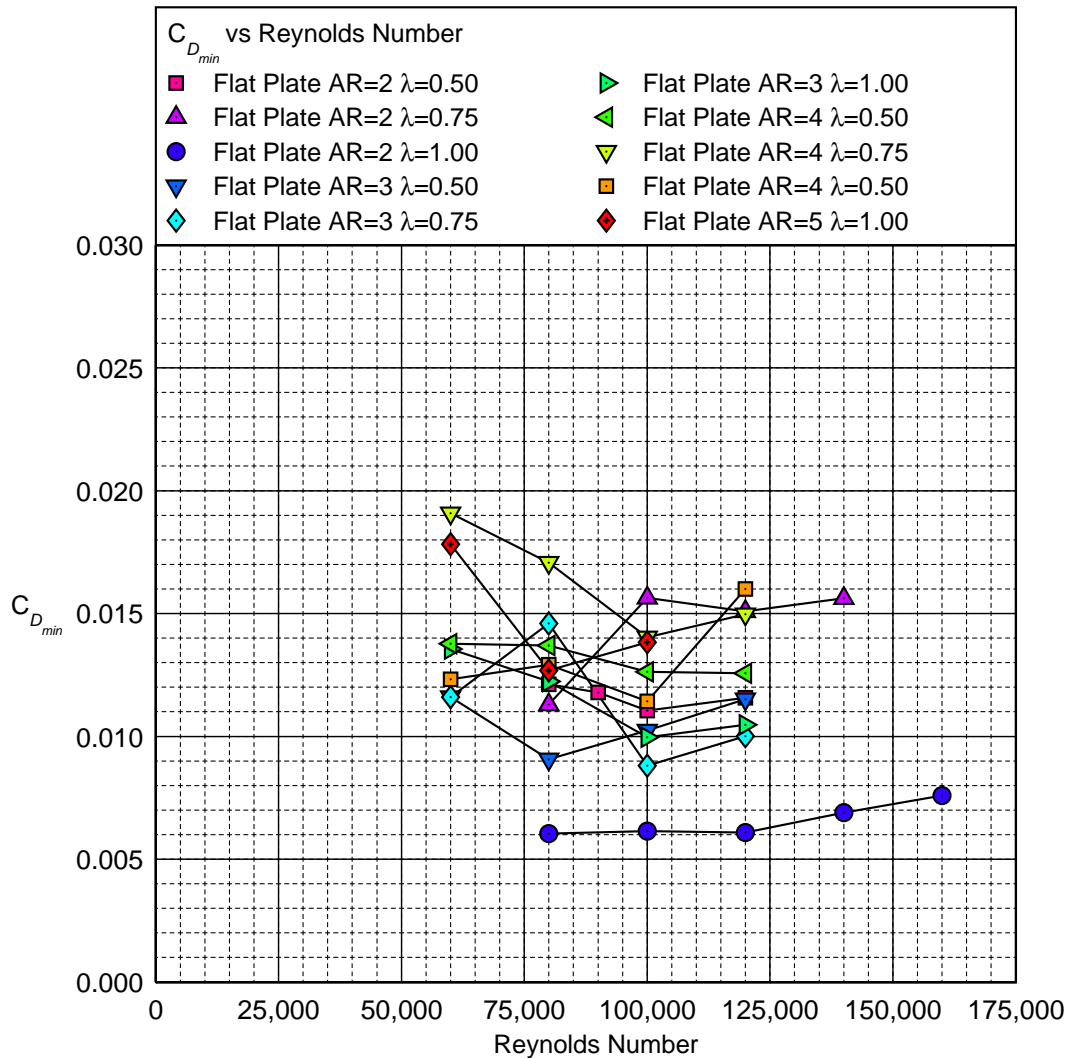


Fig. 6.2: $C_{D_{min}}$ as a function of Reynolds number for flat-plate wings.

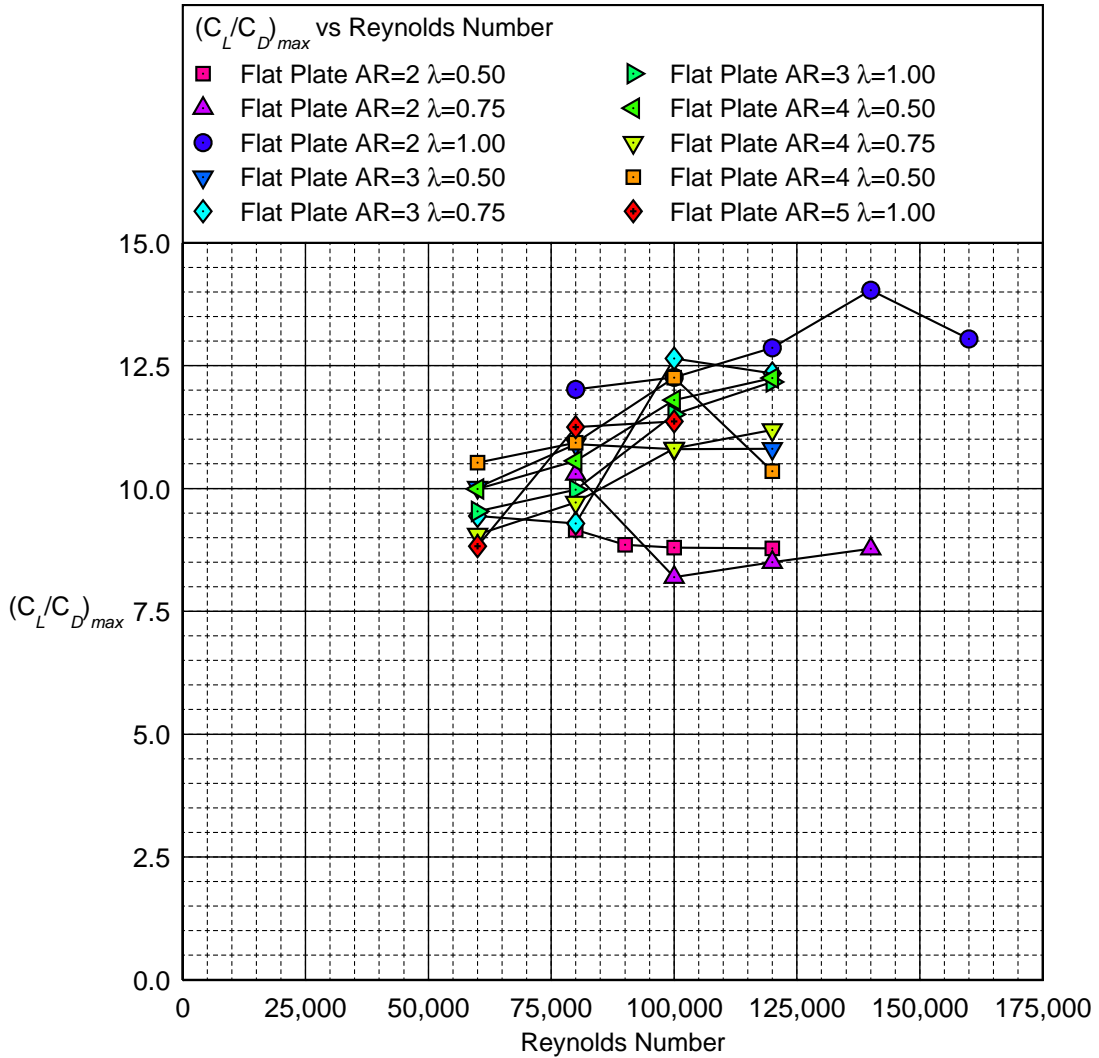


Fig. 6.3: $(C_L/C_D)_{max}$ as a function of Reynolds number for flat-plate wings.

a large drop in lift, and a critical Reynolds number is not observed. The lack of a critical Reynolds number suggests that the laminar boundary (shear) layer that separates from the central region of the flat-plate wing was unable to reattach resulting in no laminar separation bubble formation. For post-stall angles of attack, the lift and moment of the wing stays roughly the same. However, there is a corresponding decrease in the lift-to-drag ratio of the wing that results from an increase in the wake drag with angle of attack. Finally, no flow hysteresis was observed.

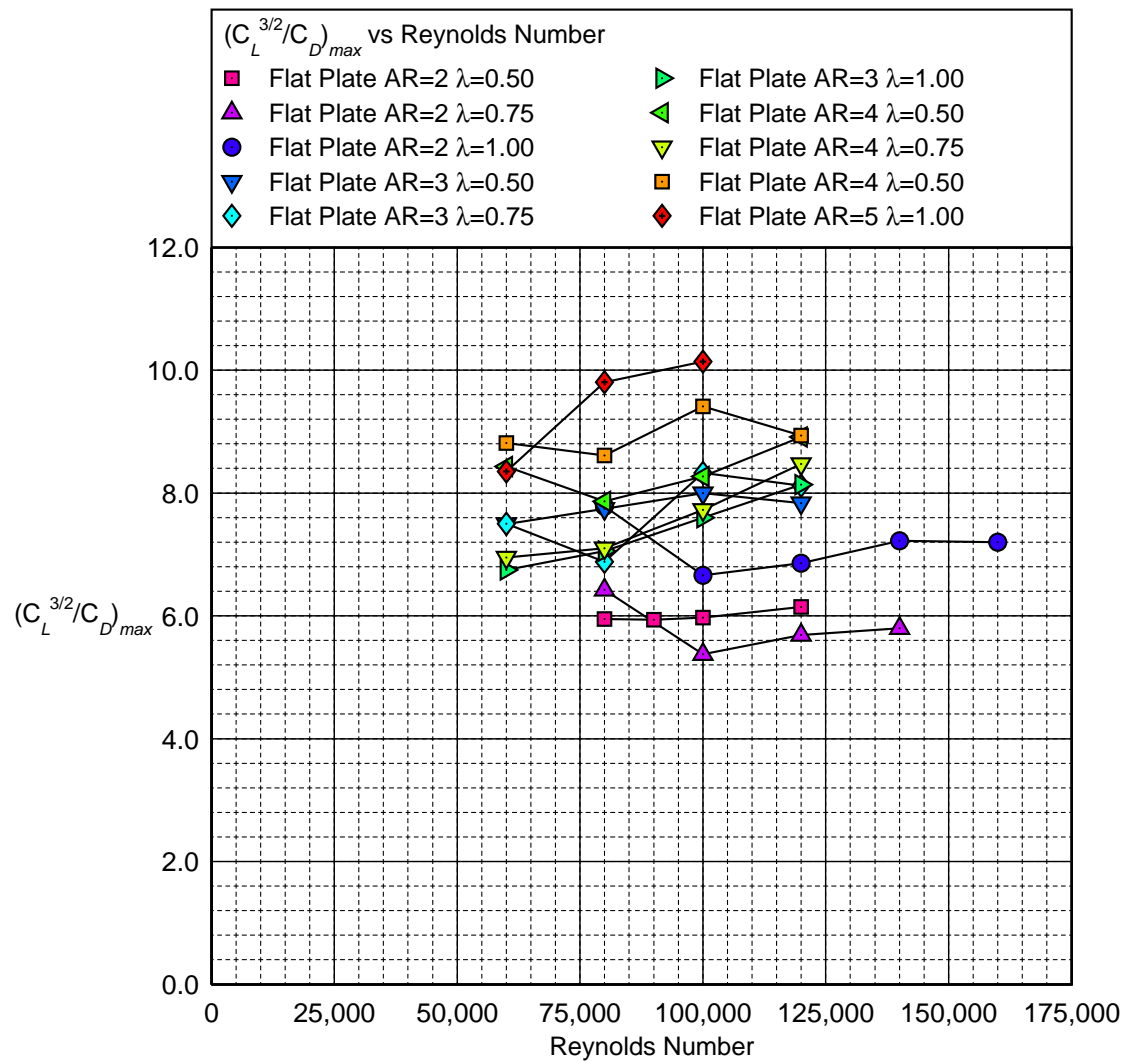


Fig. 6.4: $(C_L^{3/2}/C_D)_{max}$ as a function of Reynolds number for flat-plate wings.

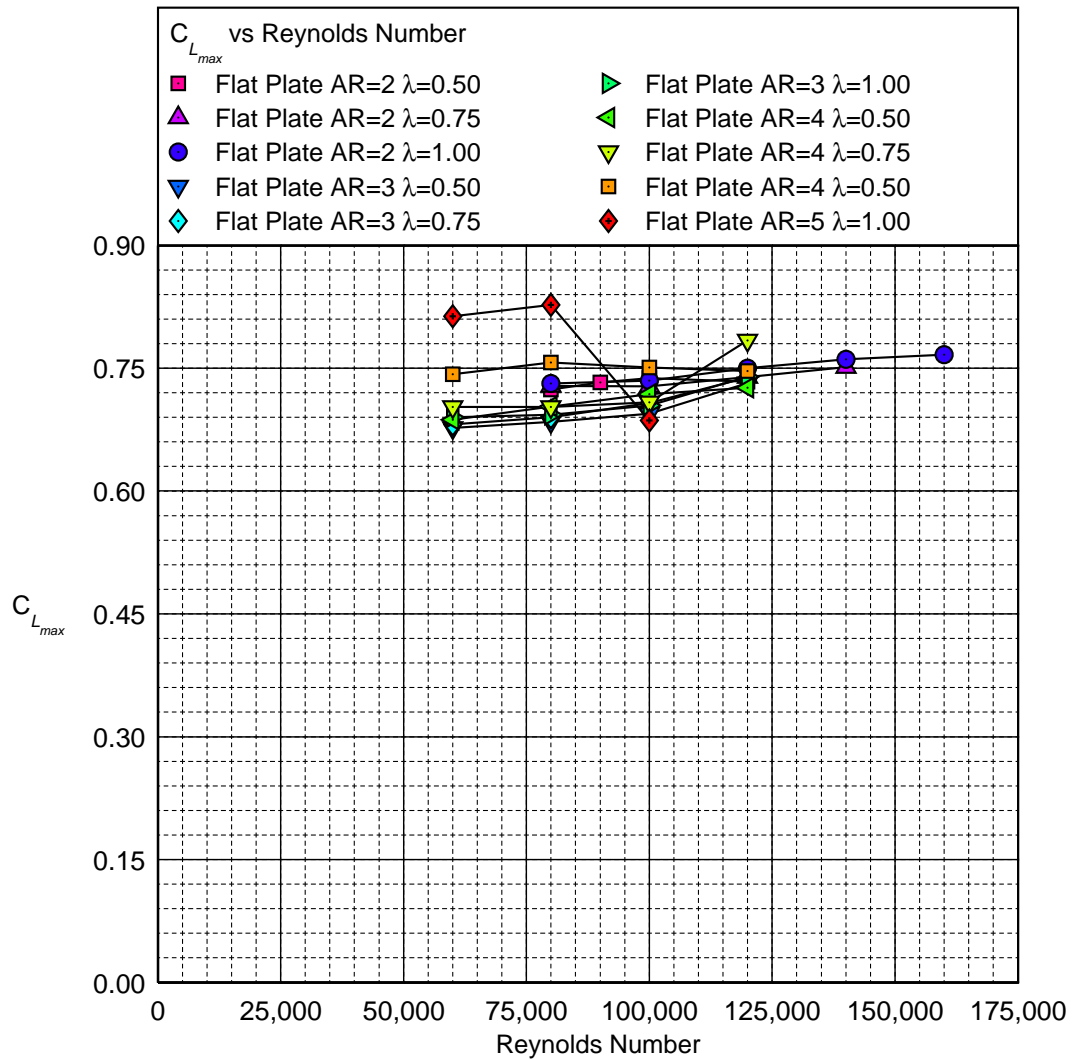


Fig. 6.5: $C_{L_{max}}$ as a function of Reynolds number for flat-plate wings.

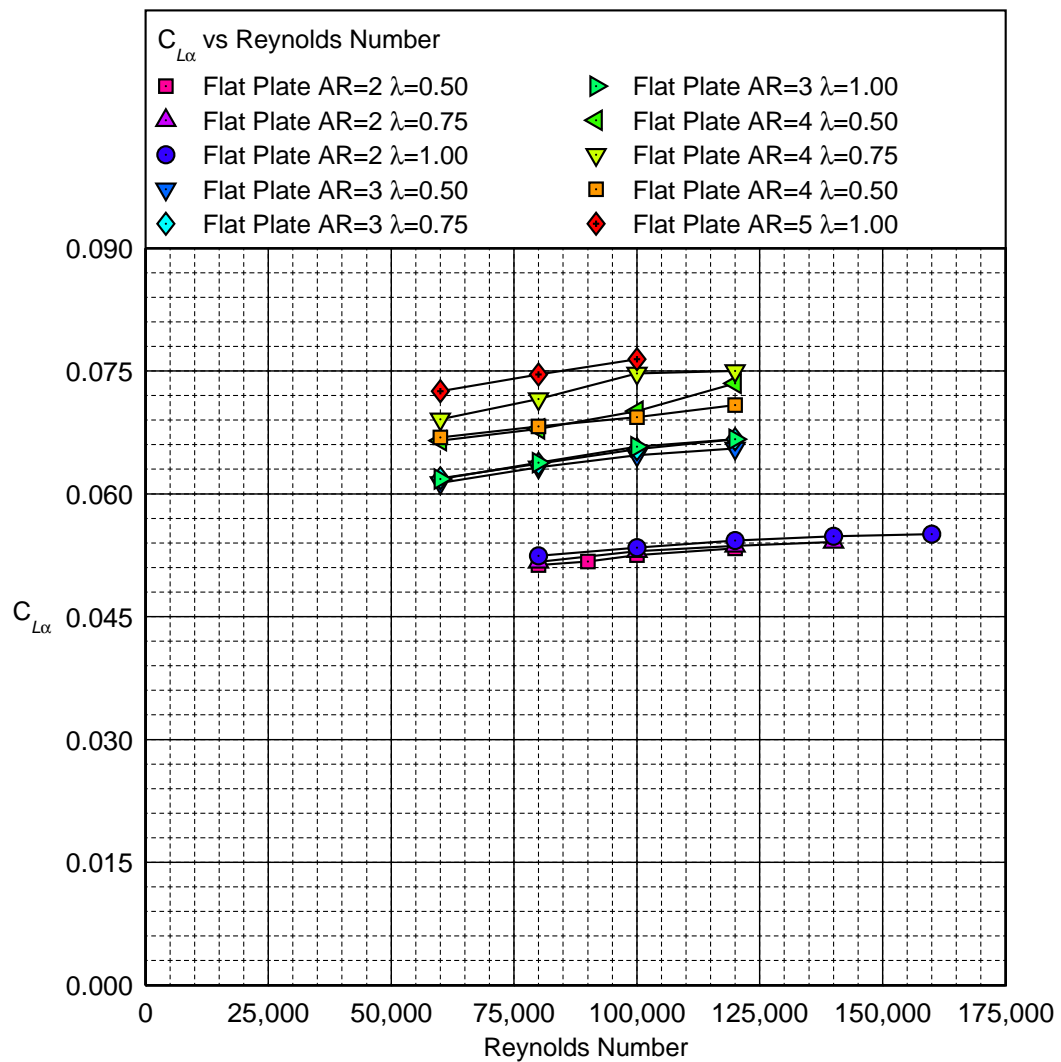


Fig. 6.6: $C_{L\alpha}$ as a function of Reynolds number for flat-plate wings.

6.2.2 Aspect Ratio Effects

Flat-plate wing comparison results where \mathcal{R} is varied for a fixed λ and Re (Figs 5.12–5.25) shows an increase in drag bucket size with aspect ratio especially from an aspect ratio of 2. At low aspect ratios, the drag due to the wing tip vortices reduces the drag bucket size. Correspondingly the stall angle of attack also increases resulting in a smaller lift curve slope in comparison with higher aspect ratio wings. Finally, in terms of moment, moments of larger magnitude are induced in the stall and post-stall regions of the wing for lower aspect ratio wings.

Lift curve slopes ($C_{L\alpha}$) for different flat-plate wings are presented as a function of aspect ratio in Fig. 6.7(a–c). Each subfigure in Fig. 6.7 represents results for different taper ratios. In addition, both the theoretical lifting line slope and Helmbold's low aspect ratio straight wing equation slopes are co-plotted against the flat-plate wing slopes. The theoretical lifting line slope is given from Eq. 4.1 and Helmbold's equation, taken from Ref. 73, is calculated from

$$C_{L\alpha} = \frac{C_{l\alpha}}{\sqrt{1 + (\frac{C_{l\alpha}}{\pi\mathcal{R}})^2 + \frac{C_{l\alpha}}{\pi\mathcal{R}}}} \quad (6.1)$$

Figure 6.7 shows that the flat-plate wing slopes follow the general trends given by the theoretical lifting line and Helmbold's equation. It is interesting to note that with increasing Reynolds number the flat-plate wing lift curve slopes tend to converge towards the theoretical lifting line slope (Eq. 4.1).

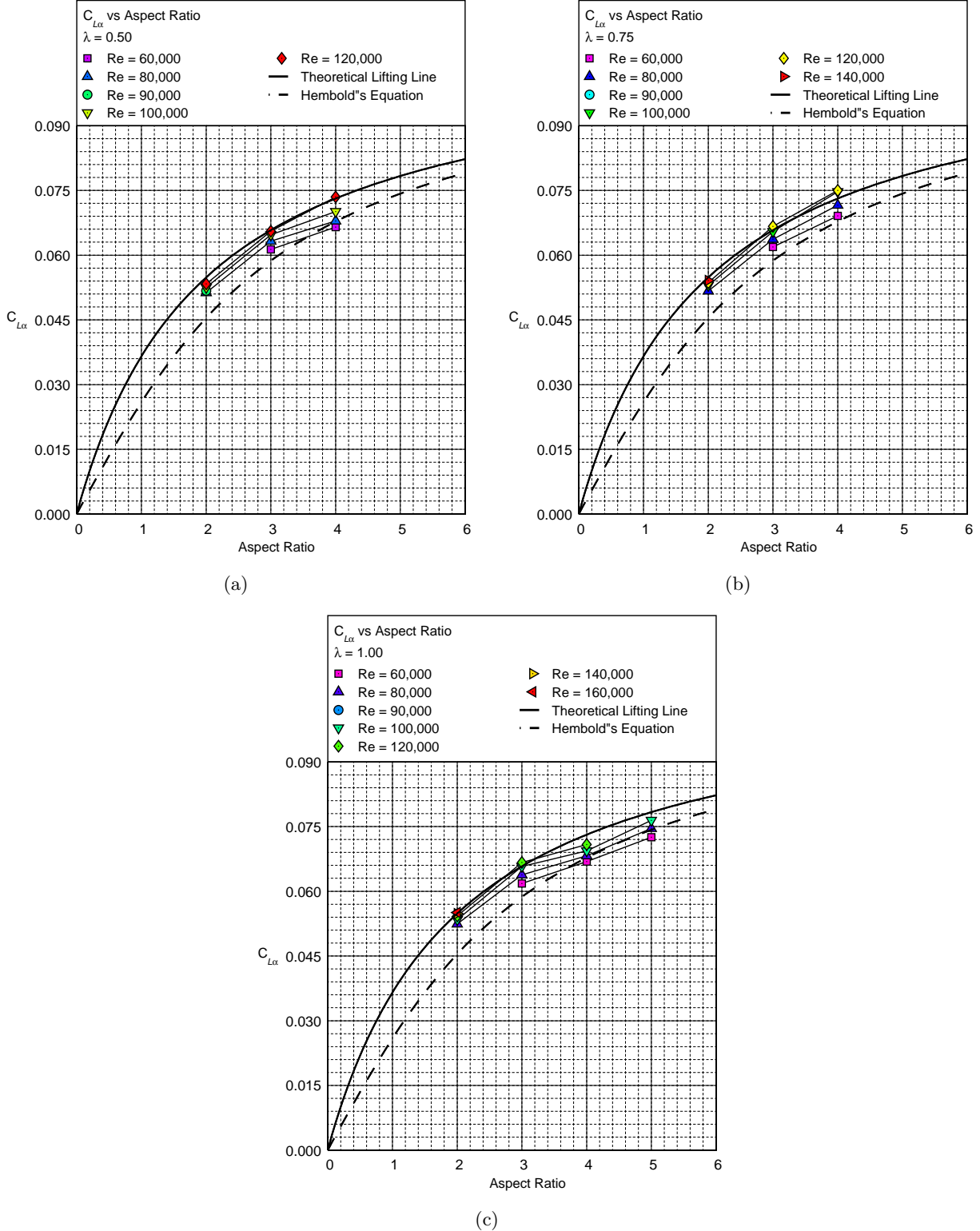


Fig. 6.7: $C_{L\alpha}$ as a function of $\mathcal{A}R$ for flat-plate wings: (a) $\lambda = 0.5$, (b) $\lambda = 0.75$, and (c) $\lambda = 1$.

6.2.3 Taper Ratio Effects

Flat-plate wing comparison results where λ is varied for a fixed AR and Re (Figs. 5.26–5.40) showed minimal taper ratio effects at low Reynolds numbers.

Figure 6.6 shows that taper ratio seems to have a negligible effect on the lift curve slope of the wing at aspect ratios of 2 and 3 which suggests that the effects of taper ratio are attenuated at low aspect ratios owing to the dominance of vortex lift. However, the lift curves and drag polars from Figs. 5.26–5.40 show that with increasing taper ratio, a more flattened stall occurs. Lift curves for rectangular wings ($\lambda=1$) show constant post-stall lift whereas tapered wings exhibit a small drop in lift initially during stall. In addition, $C_{L_{max}}$ is observed to increase with taper ratio. The post-stall lift and $C_{L_{max}}$ effects are both seen to be more pronounced with increasing aspect ratio as shown in Fig 6.5 which is understandable because for low aspect ratio wings, vortex lift dominates regardless of the taper ratio.

Taper ratio effects are seen in the moment curves where lower moments are observed in the post-stall region with increasing taper ratio. The differences observed become more pronounced at lower aspect ratios.

6.3 Performance Comparison of \mathcal{R} -4 Rectangular Wings

Although of the same aspect ratio and planform, both the Wortmann FX 63-137 \mathcal{R} -4 rectangular wing and the \mathcal{R} -4 rectangular flat-plate wing have very different aerodynamic characteristics. This fact is vividly visualized in Figs. 5.1 and 5.10. To gain a better understanding of the performance characteristics of each wing, the maximum range ($(C_L/C_D)_{max}$) and maximum endurance ($(C_L^{3/2}/C_D)_{max}$) of each wing are presented as a function of Reynolds number in Figs. 6.8 and 6.9.

Figures 6.8 and 6.9 show that the formation of the short laminar separation bubble on the Wortmann wing has a large effect on its performance. A large performance jump is seen at Reynolds

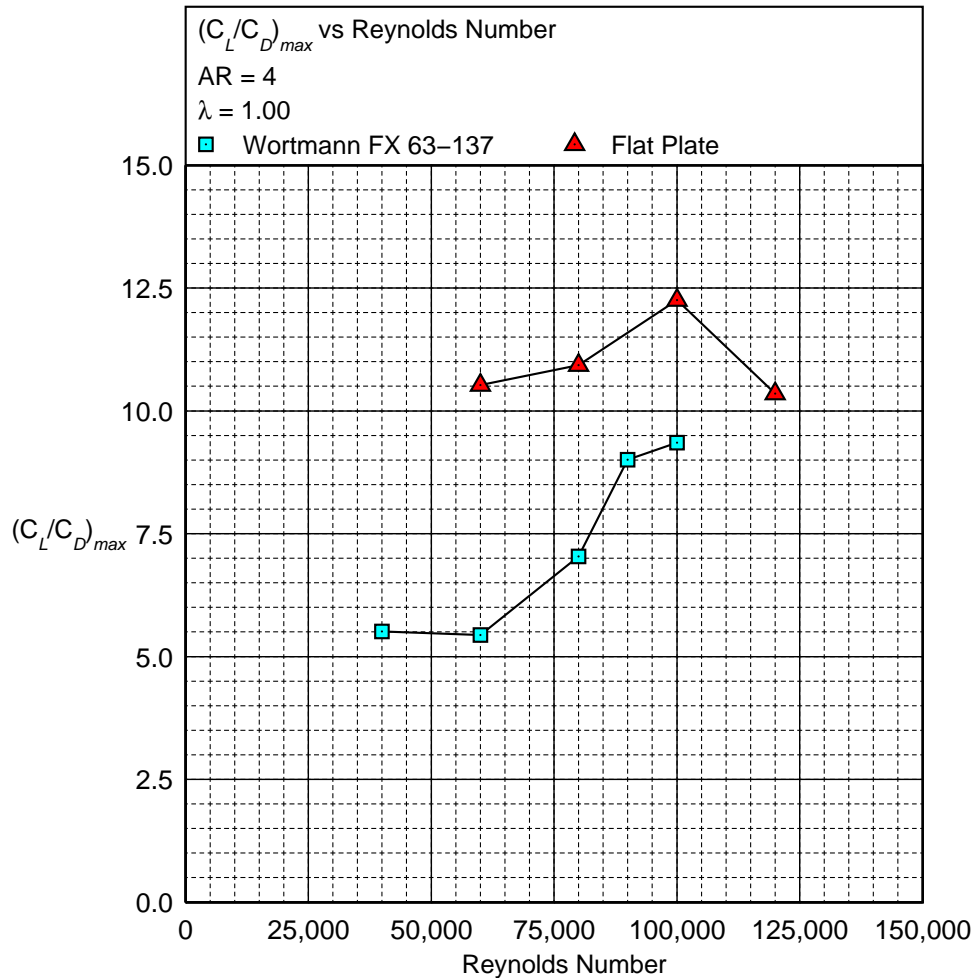


Fig. 6.8: Maximum range ($(C_L/C_D)_{max}$) as a function of Reynolds number for the \mathcal{R} -4, $\lambda = 1$ wings.

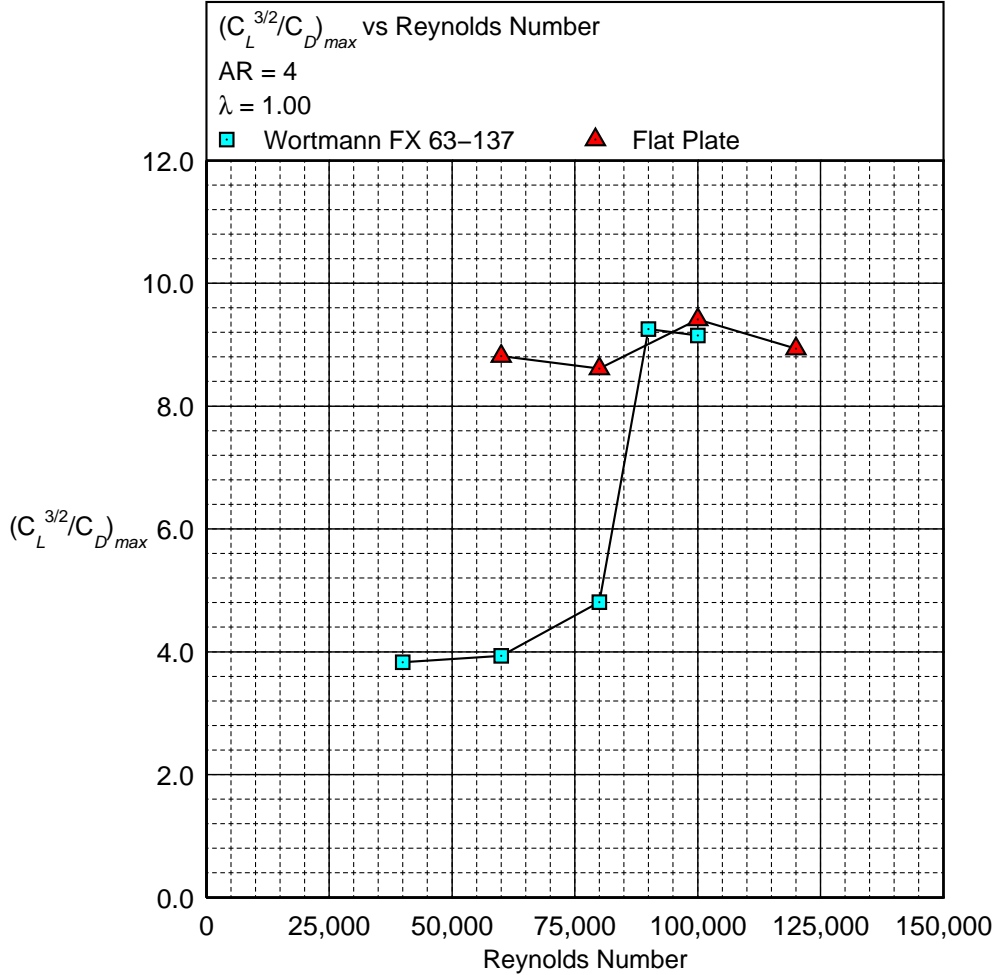


Fig. 6.9: Maximum endurance ($(C_L^{3/2}/C_D)_{max}$) as a function of Reynolds number for the $\mathcal{A}R\text{-}4$, $\lambda = 1$ wings.

numbers more than 90,000. In comparison, the performance characteristics of the $\mathcal{A}R\text{-}4$ flat-plate wing generally increases with Reynolds number and exceeds that of the Wortmann wing for most Reynolds numbers tested. An important resultant conclusion of these observations is that for low Reynolds number, low-to-moderate aspect ratio wings, the maximum lift of an airfoil plays a less significant role in comparison with its drag characteristics on the performance of the wing. An improvement in the lift performance of a wing does not necessarily justify the high drag penalties that would be incurred in the low Reynolds number flight regime.

Chapter 7

Summary, Conclusions, and Future Work

7.1 Summary and Conclusions

In summary, it was realized that there was an area of experimental research need in the low-to-moderate aspect ratio, low Reynolds number regime. In response to this need, a new external platform force balance, the LRN-FB, was designed, fabricated, and assembled to carry out low Reynolds number wing testing at the UIUC subsonic wind tunnel.

The LRN-FB was validated with the use of a mirror sting test, flow visualization techniques, and data comparisons with historical data. Experimental mirror sting and surface oil-flow visualization results showed that the sting mounting setup used had minimal interference effects on the flow over a wing. Historical data comparisons for two different wings also showed good agreement in lift, drag, and moment data.

As a check standard test and to further understand flow phenomena over low-to-moderate aspect ratio wings, aerodynamic performance results and surface oil-flow visualization results were taken for the Wortmann FX 63-137 \mathcal{R} -4 rectangular wing. The results suggested that there exists a critical Reynolds number ($Re = 90,000$) for which a jump in lift and lift-to-drag ratio occurs. In addition, both pre-stall and post-stall hysteresis were captured at this Reynolds number. Surface oil-flow visualization was used to chart and discuss the progress of the laminar flow, separation-bubble, turbulent flow, and wing-tip region with change in angle of attack at a Reynolds number of 90,000. With flow visualization, pre-stall hysteresis was not captured, but post-stall hysteresis was captured successfully.

Ten rectangular and tapered, flat-plate, low-to-moderate aspect ratio ($2 \leq \mathcal{R} \leq 5$) wings were also tested at Reynolds numbers of 60,000 to 160,000. The results obtained suggested that for flat plates, there is either no critical Reynolds number or that the critical Reynolds number does not

seem to lie between the Reynolds numbers of 60,000 and 160,000. Aerodynamic hysteresis was also not found for the flat-plate wings at the tested conditions.

Given that the Reynolds number, aspect ratio, and taper ratio were the three main parameters varied for the flat-plate wings tested, a number of conclusions were observed. With increasing Reynolds number an increase in lift curve slope ($C_{L\alpha}$), $C_{L_{max}}$ and a widening of the drag bucket was observed. A generally decreasing $C_{D_{min}}$ with increasing Reynolds number was also observed despite the scatter seen in the data due to the low forces measured. With an increase in aspect ratio, an increase in the lift curve slope and widening of the drag bucket was observed. The lift curve slopes were seen to conform between the slopes calculated from Hembold's equation and lifting line theory. Minimal effects were observed with changes in taper ratio. Also, the post-stall data for the flat-plate wings showed that lift and moment were relatively constant with increasing angles of attack up to 30 deg.

Finally, when the performance of the Wortmann FX 63-137 \mathcal{R} -4 rectangular wing and the \mathcal{R} -4 rectangular flat-plate wing were compared in terms of $(C_L/C_D)_{max}$ and $(C_L^{3/2}/C_D)_{max}$ as a function of Reynolds number, better range and endurance performance characteristics were observed for the flat-place wing. The results suggested that although the proliferation of small-scaled UAVs both in military and commercial environments has created an increasing need for higher payload capacities and increased endurance times, a conflicting tradeoff remains, whereby an improvement in the lift performance of a wing does not necessarily justify the high drag penalties incurred in the low Reynolds number flight regime.

7.2 Future Work

The LRN-FB serves as a platform to expand the low Reynolds number experimental work performed by the UIUC Applied Aerodynamics Group. Given that a multitude of airfoils and propellers have already been tested, further wing testing may be done where parameters such as wing-tip geometry, wing twist and spanwise airfoil geometry can be varied to help provide a better understanding of the performance of wings in the low Reynolds number regime.

In addition, a possible next step in research would be to perform propeller-wing combination experiments. For low-to-moderate aspect ratio wings, a large portion of the flow over the wing can

come from the slipstream of a propeller. Experiments can be performed where a propeller setup is mounted separately but changes with the angle-of-attack of the wing. In this way the LRN-FB will be able to measure wing aerodynamic performance data under varying propeller slipstream conditions.

Appendix A

Tabulated Airfoil Coordinates

Appendix A contains the modified airfoil coordinates used for the Wortmann FX 63-137 \mathcal{R} -4 rectangular wing.

Wortmann			0.038063	0.052642	0	0.749545	0.025333	0
FX 63-137			0.026532	0.044306	0	0.803805	0.026372	0
modified			0.017041	0.035486	0	0.852843	0.025120	0
<i>x</i>	<i>y</i>	<i>z</i>	0.009611	0.026363	0	0.895835	0.021650	0
1.001285	0.002706	0	0.004280	0.017422	0	0.932030	0.016343	0
0.996983	0.004921	0	0.001070	0.009265	0	0.960837	0.009964	0
0.984160	0.010749	0	0	0.002411	0	0.981760	0.003703	0
0.963042	0.018743	0	0.001070	-0.002958	0	0.994457	-0.000964	0
0.933990	0.027879	0	0.004280	-0.007022	0	0.998715	-0.002706	0
0.897525	0.037932	0	0.009609	-0.010157	0			
0.854256	0.049056	0	0.017039	-0.012753	0			
0.804954	0.061216	0	0.026528	-0.015038	0			
0.750455	0.074005	0	0.038057	-0.017070	0			
0.691692	0.086699	0	0.051556	-0.018799	0			
0.629676	0.098439	0	0.066985	-0.020189	0			
0.565457	0.108405	0	0.084263	-0.021245	0			
0.500143	0.115925	0	0.103311	-0.022006	0			
0.434842	0.120529	0	0.124068	-0.022506	0			
0.370662	0.121949	0	0.146435	-0.022749	0			
0.339340	0.121429	0	0.170312	-0.022706	0			
0.308710	0.120088	0	0.195597	-0.022344	0			
0.278901	0.117936	0	0.222182	-0.021625	0			
0.250034	0.114990	0	0.249966	-0.020502	0			
0.222238	0.111282	0	0.278819	-0.018925	0			
0.195642	0.106848	0	0.308610	-0.016857	0			
0.170348	0.101723	0	0.339220	-0.014306	0			
0.146464	0.095943	0	0.370518	-0.011328	0			
0.124091	0.089571	0	0.434638	-0.004426	0			
0.103329	0.082719	0	0.499857	0.003107	0			
0.084277	0.075533	0	0.565063	0.010504	0			
0.066995	0.068127	0	0.629144	0.017045	0			
0.051564	0.060528	0	0.690988	0.022130	0			

Appendix B

Tabulated Drag Polar Data

Appendix B contains all of the polar data seen in Chapter 5. The data presented in this appendix is identified by airfoil name, figure number, and run number. The airfoil name is an identification given during testing. For example, the ‘CHK-STD-1’ refers to the Wortmann FX 63-137 $\mathcal{A}\mathcal{R}$ -4 rectangular wing. For a flat-plate wing example, in ‘AR2-l050-FP1’, ‘AR2’ refers to an aspect ratio 2 wing, ‘l050’ refers to a taper ratio of 0.5, and FP1 refers to the specific model number.

CHK-STD-1								
Fig. 5.1			23.14	0.884	0.3779	-8.83	-0.204	0.1163
Run: 0431aj			22.26	0.884	0.3642	-7.96	-0.218	0.1101
$Re = 39998.3$			21.11	0.874	0.3443	-7.00	-0.240	0.1025
α	C_L	C_D	20.15	0.876	0.3308	-5.86	-0.262	0.0935
-15.17	-0.219	0.1797	19.00	0.857	0.3050	-5.15	-0.238	0.0864
-13.93	-0.203	0.1605	18.38	0.848	0.2922	-3.96	-0.011	0.0530
-13.14	-0.203	0.1551	17.06	0.844	0.2717	-3.06	0.066	0.0506
-12.00	-0.195	0.1424	16.09	0.817	0.2552	-1.80	0.184	0.0497
-10.94	-0.195	0.1339	15.30	0.805	0.2425	-1.09	0.246	0.0529
-9.97	-0.193	0.1261	14.06	0.767	0.2170	0.25	0.313	0.0602
-8.83	-0.199	0.1177	13.00	0.750	0.1973	1.13	0.344	0.0673
-7.96	-0.212	0.1120	12.12	0.730	0.1848	2.19	0.375	0.0718
-7.00	-0.233	0.1059	10.97	0.701	0.1667	3.17	0.414	0.0799
-5.95	-0.263	0.0971	10.08	0.677	0.1575	4.23	0.466	0.0881
-4.97	-0.230	0.0841	9.02	0.637	0.1367	5.21	0.523	0.0995
-3.96	-0.047	0.0611	8.04	0.603	0.1278	6.28	0.575	0.1122
-2.89	0.059	0.0545	7.07	0.567	0.1118	7.34	0.617	0.1258
-1.90	0.145	0.0527	5.92	0.525	0.0993	8.32	0.656	0.1381
-1.10	0.185	0.0540	5.03	0.478	0.0882	8.94	0.676	0.1456
0.14	0.230	0.0603	3.96	0.417	0.0776	10.27	0.726	0.1679
1.12	0.271	0.0642	2.98	0.375	0.0680	11.24	0.750	0.1809
2.18	0.325	0.0661	2.00	0.322	0.0628	12.21	0.779	0.1954
3.16	0.377	0.0752	0.94	0.262	0.0549	13.36	0.803	0.2157
4.23	0.430	0.0841	-0.04	0.224	0.0536	14.33	0.825	0.2326
5.20	0.478	0.0953	-1.10	0.192	0.0474	15.39	0.848	0.2521
6.27	0.533	0.1069	-2.08	0.135	0.0459	16.27	0.861	0.2696
7.34	0.577	0.1198	-3.07	0.044	0.0469	17.25	0.879	0.2889
8.22	0.612	0.1313	-4.06	-0.064	0.0535	18.30	0.886	0.3072
9.20	0.647	0.1468	-5.24	-0.249	0.0768	19.36	0.891	0.3248
10.08	0.672	0.1586	-6.12	-0.262	0.0877	20.32	0.888	0.3370
11.23	0.705	0.1736	-7.17	-0.228	0.0969	21.38	0.893	0.3559
12.20	0.729	0.1874	-8.22	-0.208	0.1029	22.26	0.895	0.3693
13.26	0.759	0.2045	-9.10	-0.195	0.1099	23.31	0.896	0.3867
14.23	0.774	0.2205	-10.15	-0.197	0.1185	24.11	0.905	0.4021
15.30	0.801	0.2420	-11.21	-0.192	0.1271	24.11	0.898	0.3992
16.27	0.821	0.2593	-12.09	-0.197	0.1358	23.05	0.898	0.3812
17.24	0.839	0.2765	-13.14	-0.205	0.1452	22.08	0.891	0.3662
18.03	0.855	0.2938	-14.11	-0.207	0.1547	21.12	0.899	0.3526
19.26	0.866	0.3137	Run: 0432aj			20.06	0.896	0.3373
20.23	0.872	0.3296	$Re = 60000.2$			19.36	0.892	0.3257
21.38	0.879	0.3462	α	C_L	C_D	18.13	0.885	0.3042
22.34	0.877	0.3607	-15.17	-0.226	0.1773	16.98	0.869	0.2801
23.31	0.882	0.3804	-14.02	-0.216	0.1635	16.10	0.862	0.2670
24.28	0.890	0.3940	-13.14	-0.212	0.1558	15.39	0.850	0.2519
24.19	0.883	0.3946	-11.91	-0.198	0.1439	14.07	0.814	0.2270
			-10.94	-0.196	0.1339	13.10	0.799	0.2086
			-9.98	-0.198	0.1248	12.13	0.777	0.1956
						10.98	0.744	0.1766

10.09	0.717	0.1644	4.16	0.540	0.0867	-3.14	0.104	0.0461
8.94	0.678	0.1454	5.23	0.582	0.0988	-4.04	0.020	0.0506
8.05	0.648	0.1358	6.20	0.621	0.1088	-5.14	-0.172	0.0782
6.99	0.605	0.1198	7.27	0.670	0.1231	-6.12	-0.235	0.0975
6.01	0.564	0.1089	8.24	0.710	0.1357	-7.17	-0.231	0.1069
4.95	0.508	0.0949	9.04	0.738	0.1461	-8.13	-0.216	0.1142
3.97	0.455	0.0860	10.10	0.776	0.1627	-9.10	-0.208	0.1213
2.90	0.420	0.0772	11.26	0.816	0.1812	-10.15	-0.205	0.1312
2.19	0.376	0.0698	12.23	0.846	0.1966	-11.03	-0.208	0.1396
0.95	0.334	0.0643	13.29	0.876	0.2159	-12.18	-0.214	0.1496
-0.11	0.303	0.0608	14.26	0.889	0.2325	-13.15	-0.221	0.1601
-1.00	0.250	0.0519	15.40	0.900	0.2520	-14.11	-0.229	0.1701
-1.98	0.174	0.0520	16.28	0.903	0.2691			
-3.06	0.074	0.0504	17.25	0.910	0.2877	Run: 0436aj		
-4.05	-0.021	0.0541	18.31	0.907	0.3039	$Re = 90001.3$		
-5.15	-0.226	0.0830	19.36	0.910	0.3211	α	C_L	C_D
-6.12	-0.258	0.0963	20.24	0.910	0.3356	-14.91	-0.241	0.1817
-7.17	-0.228	0.1051	21.21	0.915	0.3543	-13.94	-0.231	0.1699
-8.13	-0.209	0.1118	22.09	0.912	0.3647	-12.97	-0.227	0.1607
-9.10	-0.201	0.1180	23.32	0.921	0.3871	-12.00	-0.215	0.1500
-10.15	-0.198	0.1282	24.29	0.919	0.4012	-10.94	-0.209	0.1396
-11.12	-0.198	0.1368	24.11	0.917	0.3984	-9.89	-0.204	0.1306
-12.09	-0.203	0.1469	23.06	0.915	0.3820	-8.92	-0.206	0.1218
-13.23	-0.215	0.1570	22.09	0.908	0.3631	-7.87	-0.214	0.1134
-14.11	-0.220	0.1666	21.12	0.910	0.3489	-6.90	-0.219	0.1042
			20.15	0.914	0.3347	-5.93	-0.204	0.0954
Run: 0433aj			19.10	0.909	0.3142	-4.86	-0.118	0.0738
$Re = 80001.7$			18.31	0.902	0.3024	-3.95	0.021	0.0512
	α	C_L	C_D					
-15.17	-0.235	0.1800	17.07	0.903	0.2795	-2.87	0.139	0.0451
-13.94	-0.226	0.1673	16.29	0.908	0.2679	-1.88	0.226	0.0448
-12.88	-0.218	0.1563	15.05	0.899	0.2442	-0.80	0.349	0.0458
-12.00	-0.210	0.1459	14.08	0.888	0.2271	0.18	0.424	0.0517
-10.86	-0.205	0.1357	13.03	0.870	0.2089	1.16	0.484	0.0584
-9.89	-0.202	0.1279	12.05	0.844	0.1927	2.32	0.558	0.0649
-9.10	-0.206	0.1218	10.99	0.808	0.1736	3.29	0.593	0.0716
-7.96	-0.221	0.1103	10.02	0.782	0.1604	4.18	0.632	0.0787
-7.00	-0.235	0.1031	8.95	0.739	0.1425	5.33	0.651	0.0915
-5.94	-0.235	0.0941	8.07	0.703	0.1311	6.22	0.685	0.1004
-5.23	-0.195	0.0830	7.00	0.658	0.1159	7.28	0.729	0.1137
-3.86	0.037	0.0509	5.94	0.613	0.1045	7.99	0.760	0.1238
-3.05	0.099	0.0484	4.96	0.568	0.0927	9.32	0.816	0.1430
-1.80	0.217	0.0484	3.98	0.529	0.0848	10.30	0.853	0.1563
-0.72	0.321	0.0532	2.92	0.505	0.0748	11.36	1.265	0.1568
0.26	0.390	0.0589	1.95	0.473	0.0695	12.43	1.338	0.1711
1.24	0.444	0.0660	0.89	0.427	0.0608	13.14	1.393	0.1810
2.22	0.488	0.0718	-0.10	0.365	0.0550	14.39	1.471	0.1997
3.19	0.510	0.0795	-1.17	0.287	0.0481	15.46	1.525	0.2144
			-1.80	0.225	0.0469	16.43	1.552	0.2269

17.40	1.573	0.2403	Run: 0434aj	19.37	0.937	0.3227		
18.45	1.577	0.2554	$Re = 100001.3$	18.05	0.952	0.3019		
19.28	0.924	0.3147	α	C_L	C_D	17.09	0.969	0.2820
20.25	0.927	0.3312	-15.17	-0.243	0.1821	16.04	0.997	0.2645
21.30	0.920	0.3471	-14.11	-0.233	0.1705	15.19	1.526	0.2147
22.27	0.927	0.3633	-12.88	-0.226	0.1577	14.13	1.472	0.2012
23.15	0.932	0.3779	-11.91	-0.214	0.1475	13.14	1.407	0.1849
24.02	0.929	0.3937	-10.95	-0.210	0.1375	12.16	1.342	0.1717
24.02	0.928	0.3919	-10.15	-0.205	0.1306	11.09	1.261	0.1546
23.15	0.928	0.3760	-8.92	-0.201	0.1180	10.20	1.195	0.1443
22.09	0.927	0.3620	-7.95	-0.200	0.1104	9.12	1.110	0.1291
21.30	0.928	0.3501	-6.98	-0.172	0.0996	8.14	1.030	0.1176
20.16	0.925	0.3283	-5.83	-0.148	0.0885	7.15	0.948	0.1037
19.10	0.928	0.3092	-4.84	-0.004	0.0584	6.08	0.860	0.0933
18.05	0.931	0.2943	-3.94	0.089	0.0472	5.10	0.790	0.0851
17.00	0.939	0.2735	-2.77	0.214	0.0430	4.12	0.723	0.0788
16.12	0.941	0.2572	-1.78	0.295	0.0444	3.04	0.653	0.0698
15.15	0.947	0.2381	-0.79	0.399	0.0477	2.06	0.588	0.0647
14.12	1.461	0.1964	0.20	0.484	0.0536	0.91	0.513	0.0562
13.14	1.398	0.1803	1.17	0.534	0.0600	0.01	0.463	0.0511
12.25	1.331	0.1673	2.24	0.598	0.0676	-0.97	0.375	0.0445
11.18	1.250	0.1511	3.04	0.647	0.0719	-2.04	0.296	0.0429
10.19	1.173	0.1405	4.29	0.730	0.0813	-3.04	0.173	0.0429
9.03	1.078	0.1235	5.28	0.800	0.0887	-4.02	0.095	0.0457
8.13	0.989	0.1143	6.26	0.879	0.0982	-5.20	-0.056	0.0680
7.02	0.728	0.1090	7.33	0.971	0.1094	-6.10	-0.173	0.0940
6.04	0.682	0.0966	8.32	1.051	0.1218	-7.16	-0.187	0.1049
4.98	0.652	0.0844	9.30	1.132	0.1348	-8.13	-0.202	0.1142
4.10	0.640	0.0751	10.38	1.215	0.1489	-9.10	-0.202	0.1225
3.03	0.590	0.0680	11.45	1.289	0.1626	-9.89	-0.204	0.1293
2.06	0.563	0.0627	12.34	1.353	0.1762	-11.12	-0.214	0.1422
0.90	0.473	0.0540	13.23	1.409	0.1885	-12.09	-0.220	0.1521
-0.08	0.436	0.0484	14.39	1.486	0.2067	-13.15	-0.228	0.1624
-1.07	0.326	0.0425	15.46	1.535	0.2212	-14.11	-0.235	0.1728
-2.06	0.223	0.0434	16.25	1.552	0.2306			
-3.05	0.127	0.0428	17.40	1.573	0.2459			
-4.04	0.025	0.0494	18.45	1.579	0.2619			
-5.04	-0.152	0.0780	19.33	1.148	0.3078			
-6.11	-0.208	0.0968	20.25	0.936	0.3389			
-7.17	-0.221	0.1072	21.30	0.931	0.3550			
-8.13	-0.209	0.1146	22.36	0.935	0.3725			
-9.19	-0.204	0.1225	23.41	0.935	0.3901			
-9.98	-0.204	0.1301	24.38	0.935	0.4050			
-11.21	-0.212	0.1407	24.03	0.938	0.4026			
-12.18	-0.218	0.1530	23.15	0.931	0.3832			
-13.15	-0.227	0.1622	22.09	0.931	0.3686			
-13.85	-0.230	0.1685	21.04	0.931	0.3498			
			20.16	0.935	0.3360			

AR2-1050-FP1

Fig. 5.2

Run: 0227ga

 $Re = 79997.8$

α	C_L	C_D
-13.91	-0.652	0.1699
-12.67	-0.638	0.1437
-11.79	-0.603	0.1261
-10.82	-0.560	0.1037
-9.94	-0.513	0.0922
-8.70	-0.442	0.0644

-7.73	-0.393	0.0483	21.13	0.716	0.2830	-5.69	-0.299	0.0275
-6.75	-0.347	0.0357	20.34	0.724	0.2770	-4.72	-0.241	0.0221
-5.69	-0.291	0.0268	19.20	0.722	0.2626	-3.75	-0.195	0.0172
-4.72	-0.243	0.0218	18.14	0.722	0.2407	-2.78	-0.133	0.0144
-4.01	-0.193	0.0227	17.17	0.709	0.2241	-1.89	-0.100	0.0174
-2.78	-0.128	0.0134	16.21	0.699	0.2046	-0.66	-0.034	0.0133
-1.72	-0.079	0.0128	15.06	0.691	0.1867	0.32	0.016	0.0124
-0.66	-0.029	0.0121	14.18	0.690	0.1737	1.29	0.057	0.0152
0.31	0.014	0.0131	13.22	0.677	0.1563	2.26	0.100	0.0154
1.29	0.066	0.0150	12.16	0.633	0.1296	3.32	0.160	0.0202
2.35	0.110	0.0176	11.18	0.581	0.1081	4.38	0.219	0.0248
3.32	0.162	0.0210	10.12	0.524	0.0831	5.35	0.273	0.0315
4.29	0.218	0.0237	9.06	0.473	0.0661	6.33	0.325	0.0386
5.26	0.268	0.0310	8.09	0.421	0.0584	7.38	0.381	0.0478
6.41	0.327	0.0391	7.29	0.377	0.0469	8.18	0.420	0.0588
7.29	0.378	0.0460	6.32	0.329	0.0365	9.06	0.472	0.0684
8.45	0.441	0.0574	5.17	0.268	0.0320	10.39	0.540	0.0891
9.33	0.491	0.0696	4.11	0.201	0.0237	11.45	0.595	0.1147
10.30	0.541	0.0886	3.05	0.148	0.0210	12.16	0.642	0.1347
11.36	0.593	0.1116	2.08	0.105	0.0202	13.39	0.694	0.1632
12.42	0.649	0.1368	1.02	0.056	0.0179	14.36	0.705	0.1806
13.30	0.682	0.1582	0.14	0.011	0.0144	15.33	0.711	0.1978
14.36	0.687	0.1782	-0.75	-0.033	0.0129	16.38	0.707	0.2123
15.15	0.691	0.1927	-1.89	-0.088	0.0135	17.18	0.712	0.2278
16.38	0.700	0.2128	-2.87	-0.129	0.0137	18.32	0.719	0.2441
17.44	0.708	0.2305	-3.84	-0.189	0.0164	19.37	0.733	0.2668
18.32	0.723	0.2413	-4.99	-0.250	0.0216	20.34	0.724	0.2761
19.37	0.719	0.2629	-5.96	-0.298	0.0273	21.31	0.719	0.2876
20.25	0.717	0.2738	-7.02	-0.355	0.0389	22.36	0.703	0.2964
21.30	0.702	0.2846	-7.82	-0.401	0.0496	23.33	0.689	0.3069
22.36	0.688	0.2925	-8.96	-0.460	0.0688	24.38	0.680	0.3194
23.32	0.683	0.3033	-9.94	-0.514	0.0878	25.43	0.674	0.3311
24.38	0.678	0.3145	-11.00	-0.565	0.1058	26.31	0.671	0.3414
25.34	0.671	0.3280	-11.70	-0.605	0.1228	27.37	0.674	0.3567
26.31	0.668	0.3402	-13.03	-0.653	0.1508	28.33	0.672	0.3663
27.36	0.666	0.3547	-14.08	-0.657	0.1703	29.39	0.674	0.3809
28.07	0.669	0.3642				30.18	0.675	0.3945
29.39	0.671	0.3821	Run: 0228ga			30.09	0.670	0.3906
30.35	0.676	0.3912	$Re = 89996.9$			29.39	0.668	0.3795
30.09	0.675	0.3893	α	C_L	C_D	28.33	0.670	0.3670
29.21	0.673	0.3800	-14.08	-0.664	0.1699	27.19	0.676	0.3538
28.16	0.668	0.3675	-13.03	-0.657	0.1519	26.14	0.674	0.3418
27.10	0.670	0.3513	-11.79	-0.617	0.1280	25.17	0.671	0.3289
26.22	0.670	0.3388	-10.73	-0.566	0.1058	24.12	0.680	0.3174
25.08	0.685	0.3293	-9.67	-0.504	0.0846	23.06	0.692	0.3054
24.20	0.669	0.3108	-8.96	-0.465	0.0691	22.18	0.699	0.2950
23.15	0.674	0.3000	-7.82	-0.404	0.0509	21.22	0.721	0.2892
22.18	0.701	0.2937	-6.75	-0.351	0.0362	20.16	0.726	0.2746

19.11	0.727	0.2605	-3.82	-0.195	0.0192	17.11	0.719	0.2271
18.32	0.724	0.2431	-2.85	-0.135	0.0153	16.05	0.714	0.2095
17.35	0.716	0.2296	-1.79	-0.090	0.0133	15.00	0.705	0.1905
16.12	0.706	0.2097	-0.81	-0.039	0.0145	14.12	0.700	0.1779
15.07	0.695	0.1893	0.25	0.012	0.0110	13.15	0.687	0.1581
14.19	0.693	0.1781	1.22	0.055	0.0163	12.09	0.640	0.1314
13.22	0.683	0.1569	2.19	0.106	0.0176	11.29	0.597	0.1140
12.16	0.645	0.1326	3.25	0.161	0.0211	10.06	0.529	0.0839
11.36	0.599	0.1130	4.22	0.223	0.0255	8.99	0.478	0.0685
10.30	0.539	0.0867	5.19	0.270	0.0317	8.11	0.425	0.0535
9.15	0.479	0.0690	6.26	0.332	0.0384	7.05	0.371	0.0437
8.18	0.429	0.0559	7.32	0.386	0.0477	5.99	0.314	0.0374
7.12	0.370	0.0447	8.11	0.426	0.0580	5.11	0.267	0.0309
6.41	0.329	0.0375	9.08	0.478	0.0700	4.04	0.209	0.0237
5.09	0.264	0.0310	10.23	0.541	0.0875	3.07	0.150	0.0200
4.11	0.208	0.0244	11.38	0.600	0.1153	2.01	0.094	0.0164
3.14	0.150	0.0198	12.35	0.659	0.1384	0.95	0.047	0.0155
2.08	0.096	0.0149	13.24	0.688	0.1627	0.07	0.006	0.0128
1.11	0.052	0.0160	14.38	0.706	0.1820	-0.99	-0.044	0.0139
0.05	0.008	0.0118	15.00	0.707	0.1921	-1.96	-0.093	0.0151
-0.92	-0.045	0.0146	16.31	0.713	0.2161	-2.94	-0.143	0.0157
-1.89	-0.095	0.0173	17.02	0.718	0.2292	-4.00	-0.208	0.0183
-2.86	-0.134	0.0160	18.25	0.729	0.2450	-5.06	-0.263	0.0244
-4.01	-0.197	0.0180	19.31	0.738	0.2672	-6.03	-0.322	0.0306
-4.99	-0.257	0.0254	20.27	0.731	0.2784	-7.09	-0.378	0.0431
-6.05	-0.311	0.0296	21.24	0.722	0.2899	-7.89	-0.419	0.0536
-6.93	-0.363	0.0418	22.38	0.700	0.2981	-9.03	-0.480	0.0728
-7.90	-0.417	0.0524	23.25	0.684	0.3069	-10.01	-0.535	0.0906
-8.96	-0.468	0.0701	24.31	0.684	0.3175	-11.07	-0.588	0.1142
-9.94	-0.519	0.0894	25.28	0.678	0.3297	-12.04	-0.638	0.1378
-11.00	-0.577	0.1103	26.24	0.677	0.3425	-13.10	-0.666	0.1563
-11.71	-0.625	0.1279	27.38	0.674	0.3574	-14.07	-0.674	0.1764
-13.03	-0.661	0.1567	28.26	0.678	0.3705			
-13.99	-0.674	0.1734	29.32	0.675	0.3821			
			30.37	0.677	0.3971			

Run: 0229ga

$Re = 100000.4$

α	C_L	C_D
-14.06	-0.671	0.1727
-12.75	-0.662	0.1501
-11.86	-0.625	0.1305
-10.80	-0.576	0.1094
-9.74	-0.511	0.0845
-8.77	-0.464	0.0642
-7.80	-0.410	0.0501
-6.83	-0.357	0.0370
-6.03	-0.323	0.0335
-4.79	-0.255	0.0221

α	C_L	C_D
30.11	0.678	0.3923
29.14	0.676	0.3805
28.26	0.676	0.3701
27.12	0.673	0.3533
26.07	0.675	0.3407
25.10	0.673	0.3272
24.13	0.681	0.3178
23.34	0.693	0.3077
22.12	0.714	0.3014
21.06	0.727	0.2889
20.36	0.732	0.2783
19.13	0.734	0.2636
18.07	0.725	0.2435

Run: 0230ga

$Re = 119995.0$

-2.13	-0.103	0.0135	14.65	0.706	0.1931	-2.73	-0.130	0.0156
-1.16	-0.053	0.0143	13.78	0.698	0.1778	-1.76	-0.086	0.0142
-0.01	-0.001	0.0136	12.72	0.677	0.1576	-0.70	-0.031	0.0157
0.88	0.049	0.0148	11.92	0.644	0.1366	0.27	0.012	0.0146
1.85	0.095	0.0145	10.77	0.578	0.1091	1.33	0.064	0.0161
2.91	0.145	0.0200	9.71	0.515	0.0827	2.21	0.097	0.0189
3.97	0.222	0.0253	8.74	0.469	0.0669	3.36	0.155	0.0208
4.94	0.274	0.0312	7.77	0.420	0.0572	4.42	0.218	0.0261
6.00	0.334	0.0382	6.71	0.366	0.0448	5.40	0.268	0.0334
6.97	0.382	0.0469	5.74	0.314	0.0368	6.28	0.321	0.0415
8.03	0.437	0.0580	4.76	0.262	0.0309	7.34	0.378	0.0510
8.92	0.484	0.0715	3.70	0.202	0.0230	8.14	0.421	0.0612
9.89	0.538	0.0917	2.64	0.132	0.0193	9.46	0.496	0.0830
11.04	0.600	0.1187	1.67	0.084	0.0150	10.44	0.542	0.1014
12.01	0.651	0.1422	0.70	0.034	0.0139	11.32	0.601	0.1236
12.89	0.686	0.1630	-0.28	-0.015	0.0116	12.38	0.643	0.1467
14.04	0.699	0.1829	-1.42	-0.065	0.0139	13.44	0.673	0.1669
14.74	0.700	0.1953	-2.31	-0.109	0.0164	14.41	0.683	0.1834
15.71	0.708	0.2115	-3.28	-0.166	0.0170	15.38	0.693	0.2001
16.94	0.719	0.2326	-4.25	-0.232	0.0206	16.34	0.704	0.2146
17.91	0.725	0.2494	-5.40	-0.288	0.0279	17.49	0.705	0.2351
18.96	0.734	0.2674	-6.37	-0.342	0.0343	18.19	0.711	0.2482
20.02	0.730	0.2811	-7.35	-0.392	0.0434	19.33	0.721	0.2661
20.90	0.727	0.2931	-8.23	-0.438	0.0543	20.39	0.728	0.2827
21.95	0.711	0.3020	-9.47	-0.500	0.0741	21.35	0.713	0.2914
22.92	0.698	0.3112	-10.35	-0.551	0.0947	22.32	0.691	0.2975
23.97	0.680	0.3181	-11.32	-0.605	0.1170	23.37	0.677	0.3079
25.02	0.674	0.3314	-12.21	-0.643	0.1354	24.34	0.673	0.3187
25.90	0.670	0.3426	-13.44	-0.681	0.1603	25.39	0.672	0.3314
26.95	0.666	0.3558	-14.41	-0.695	0.1789	26.36	0.661	0.3430
27.66	0.669	0.3661				27.32	0.658	0.3519
28.98	0.665	0.3824	AR2-l075-FP1			28.20	0.663	0.3643
29.77	0.666	0.3959	Fig. 5.3			29.17	0.663	0.3767
29.77	0.667	0.3944				30.40	0.657	0.3926
28.71	0.666	0.3794	Run: 0448aj			31.37	0.658	0.4086
27.83	0.670	0.3673	Re = 79998.1			31.10	0.660	0.4052
26.78	0.668	0.3516	α	C_L	C_D	30.23	0.656	0.3881
25.73	0.670	0.3415	-12.99	-0.655	0.1528	29.08	0.661	0.3750
24.76	0.674	0.3279	-11.75	-0.624	0.1248	28.20	0.662	0.3637
23.79	0.672	0.3140	-10.78	-0.566	0.1011	27.24	0.666	0.3525
23.00	0.682	0.3059	-9.90	-0.521	0.0805	26.18	0.659	0.3364
21.77	0.707	0.3009	-8.75	-0.457	0.0604	25.13	0.671	0.3271
20.72	0.725	0.2905	-7.69	-0.403	0.0457	24.16	0.680	0.3146
19.93	0.729	0.2802	-6.63	-0.348	0.0379	23.20	0.686	0.3048
18.79	0.729	0.2641	-5.65	-0.295	0.0285	22.14	0.704	0.3000
17.91	0.726	0.2464	-4.77	-0.248	0.0235	21.09	0.717	0.2870
16.76	0.709	0.2280	-3.79	-0.183	0.0185	20.13	0.723	0.2747
15.89	0.709	0.2115				19.16	0.721	0.2567

18.37	0.716	0.2452	-1.01	-0.050	0.0190	15.77	0.705	0.2062	
17.22	0.699	0.2233	-0.13	-0.006	0.0193	14.72	0.695	0.1866	
16.17	0.701	0.2065	1.11	0.051	0.0207	13.84	0.682	0.1714	
15.20	0.693	0.1902	1.91	0.094	0.0226	12.78	0.645	0.1459	
14.14	0.683	0.1739	2.88	0.142	0.0228	11.81	0.608	0.1281	
13.17	0.656	0.1511	4.03	0.214	0.0298	10.66	0.555	0.1042	
12.21	0.630	0.1330	4.91	0.266	0.0357	9.77	0.498	0.0840	
11.06	0.576	0.1070	5.88	0.323	0.0432	8.71	0.444	0.0652	
10.35	0.533	0.0935	6.95	0.381	0.0518	7.65	0.391	0.0531	
9.29	0.476	0.0711	8.01	0.434	0.0650	6.68	0.344	0.0430	
8.05	0.410	0.0542	9.07	0.497	0.0847	5.79	0.292	0.0362	
7.17	0.358	0.0437	10.04	0.557	0.1066	4.64	0.233	0.0285	
6.19	0.313	0.0363	10.93	0.608	0.1287	3.76	0.187	0.0228	
5.13	0.257	0.0289	11.99	0.651	0.1480	2.70	0.117	0.0197	
4.16	0.212	0.0206	12.78	0.668	0.1635	1.73	0.075	0.0163	
3.01	0.142	0.0177	14.01	0.689	0.1862	0.67	0.028	0.0167	
2.04	0.093	0.0131	15.07	0.700	0.2036	-0.30	-0.017	0.0174	
1.06	0.048	0.0140	15.68	0.703	0.2126	-1.28	-0.068	0.0170	
0.09	-0.000	0.0116	17.00	0.709	0.2329	-2.25	-0.115	0.0156	
-0.88	-0.046	0.0135	18.06	0.721	0.2462	-3.31	-0.171	0.0186	
-1.94	-0.096	0.0113	19.03	0.725	0.2634	-4.28	-0.235	0.0236	
-2.91	-0.143	0.0138	19.99	0.728	0.2794	-5.26	-0.291	0.0300	
-3.88	-0.205	0.0145	20.96	0.721	0.2911	-6.32	-0.349	0.0383	
-4.95	-0.263	0.0241	21.93	0.718	0.3047	-7.38	-0.400	0.0471	
-5.92	-0.311	0.0286	22.98	0.681	0.3074	-8.44	-0.454	0.0612	
-6.71	-0.356	0.0370	23.94	0.675	0.3164	-9.32	-0.506	0.0765	
-8.04	-0.425	0.0504	24.73	0.677	0.3277	-10.30	-0.561	0.0980	
-8.92	-0.469	0.0654	25.96	0.666	0.3411	-11.36	-0.617	0.1234	
-9.90	-0.528	0.0844	26.93	0.661	0.3552	-12.33	-0.655	0.1447	
-10.96	-0.586	0.1120	27.98	0.659	0.3662	-13.39	-0.683	0.1669	
-11.75	-0.619	0.1251	29.04	0.663	0.3817				
-13.08	-0.663	0.1566	30.00	0.656	0.3918	Run: 0449aj			
			30.97	0.661	0.4079		Re = 119996.7		
Run: 0452cs									
$Re = 100001.4$									
	α	C_L	C_D	30.71	0.658	0.4029	α	C_L	C_D
	-13.39	-0.686	0.1713	29.83	0.655	0.3905	-13.35	-0.686	0.1643
	-12.15	-0.648	0.1427	28.69	0.658	0.3760	-12.02	-0.647	0.1376
	-11.18	-0.599	0.1189	27.90	0.664	0.3641	-11.05	-0.598	0.1132
	-10.21	-0.552	0.0968	26.75	0.661	0.3510	-10.08	-0.552	0.0931
	-9.15	-0.489	0.0720	25.79	0.665	0.3389	-9.02	-0.486	0.0662
	-8.17	-0.433	0.0589	24.73	0.672	0.3271	-8.04	-0.438	0.0541
	-7.29	-0.393	0.0488	23.68	0.673	0.3151	-7.25	-0.396	0.0457
	-6.14	-0.331	0.0384	22.80	0.691	0.3068	-6.01	-0.332	0.0360
	-5.17	-0.275	0.0320	21.84	0.711	0.3013	-4.95	-0.272	0.0289
	-4.11	-0.218	0.0263	20.70	0.721	0.2859	-3.89	-0.215	0.0237
	-3.13	-0.148	0.0214	19.82	0.724	0.2746	-3.18	-0.165	0.0202
	-2.07	-0.100	0.0211	18.67	0.726	0.2550	-1.94	-0.093	0.0192
			17.79	0.716	0.2411	-0.88	-0.040	0.0185	
			16.82	0.702	0.2227	0.09	0.004	0.0171	

1.06	0.055	0.0190	13.88	0.694	0.1734	3.02	0.168	0.0250
2.04	0.105	0.0195	12.82	0.662	0.1484	4.17	0.232	0.0316
3.10	0.165	0.0235	12.20	0.636	0.1321	5.06	0.280	0.0345
4.16	0.233	0.0299	10.88	0.562	0.1038	6.12	0.335	0.0430
5.13	0.283	0.0356	9.90	0.505	0.0815	7.09	0.384	0.0501
6.02	0.333	0.0409	8.84	0.456	0.0629	7.80	0.422	0.0569
7.08	0.389	0.0505	7.78	0.402	0.0506	8.86	0.471	0.0695
8.05	0.437	0.0620	6.90	0.353	0.0415	10.09	0.540	0.0994
9.20	0.493	0.0800	5.92	0.306	0.0360	11.07	0.597	0.1211
10.08	0.549	0.1013	4.86	0.251	0.0309	12.22	0.644	0.1447
11.06	0.602	0.1216	3.89	0.204	0.0240	13.19	0.681	0.1649
12.20	0.649	0.1451	2.83	0.130	0.0196	14.16	0.707	0.1835
13.17	0.682	0.1654	1.77	0.082	0.0176	15.12	0.719	0.2020
14.14	0.703	0.1843	1.15	0.055	0.0166	16.09	0.724	0.2186
14.85	0.708	0.1959	-0.17	-0.010	0.0151	17.15	0.731	0.2359
16.16	0.716	0.2146	-1.15	-0.064	0.0161	18.11	0.739	0.2512
17.22	0.723	0.2345	-2.12	-0.110	0.0164	19.08	0.744	0.2687
18.10	0.727	0.2489	-3.18	-0.177	0.0196	20.14	0.751	0.2846
18.80	0.733	0.2597	-3.89	-0.224	0.0232	21.10	0.746	0.2973
20.12	0.739	0.2826	-5.22	-0.296	0.0303	22.16	0.730	0.3063
21.09	0.733	0.2955	-6.28	-0.349	0.0369	22.86	0.720	0.3152
22.14	0.723	0.3056	-7.16	-0.398	0.0441	24.09	0.702	0.3256
23.11	0.702	0.3126	-7.96	-0.438	0.0526	25.14	0.688	0.3335
23.90	0.689	0.3173	-9.19	-0.498	0.0712	26.19	0.680	0.3441
24.95	0.677	0.3279	-10.17	-0.558	0.0979	27.16	0.672	0.3561
26.18	0.678	0.3425	-11.23	-0.614	0.1224	28.13	0.672	0.3675
27.06	0.669	0.3552	-12.20	-0.658	0.1446	29.00	0.670	0.3805
27.94	0.673	0.3671	-13.26	-0.687	0.1666	30.15	0.669	0.3945
28.99	0.669	0.3815				31.11	0.667	0.4080
30.14	0.666	0.3951	Run: 0450cs			30.94	0.666	0.4075
31.19	0.662	0.4087	$Re = 139997.0$			29.88	0.667	0.3918
30.84	0.667	0.4070	α	C_L	C_D	28.92	0.667	0.3770
29.96	0.665	0.3922	-13.33	-0.697	0.1719	27.95	0.672	0.3663
28.82	0.668	0.3761	-12.19	-0.668	0.1482	26.90	0.673	0.3524
28.11	0.669	0.3664	-11.04	-0.613	0.1184	25.93	0.678	0.3403
26.88	0.675	0.3519	-10.07	-0.562	0.0986	24.96	0.684	0.3279
25.92	0.676	0.3397	-8.92	-0.497	0.0696	23.91	0.688	0.3163
24.95	0.677	0.3266	-8.03	-0.450	0.0551	22.95	0.706	0.3102
23.90	0.686	0.3163	-7.15	-0.413	0.0478	21.98	0.732	0.3044
22.84	0.695	0.3068	-6.00	-0.344	0.0374	20.84	0.746	0.2938
21.97	0.726	0.3041	-4.94	-0.293	0.0314	19.96	0.750	0.2810
20.83	0.735	0.2905	-3.97	-0.233	0.0257	18.82	0.743	0.2607
19.95	0.738	0.2762	-2.99	-0.160	0.0200	17.94	0.733	0.2435
18.80	0.734	0.2588	-2.02	-0.101	0.0196	16.88	0.727	0.2266
17.92	0.724	0.2421	-0.96	-0.047	0.0188	15.83	0.722	0.2104
17.13	0.716	0.2301	0.01	0.001	0.0178	14.86	0.715	0.1921
15.81	0.715	0.2080	1.16	0.052	0.0201	13.98	0.700	0.1751
14.85	0.711	0.1913	1.87	0.089	0.0209	13.19	0.674	0.1561

12.21	0.633	0.1336	-0.63	-0.026	0.0113	12.10	0.638	0.1319
10.89	0.556	0.1024	-0.01	-0.000	0.0125	11.31	0.604	0.1133
9.91	0.501	0.0772	1.23	0.061	0.0125	10.16	0.544	0.0851
8.94	0.445	0.0598	2.38	0.118	0.0145	9.10	0.485	0.0639
7.79	0.395	0.0505	3.26	0.157	0.0164	8.13	0.437	0.0526
6.82	0.342	0.0401	4.23	0.219	0.0219	7.06	0.378	0.0396
5.94	0.299	0.0366	5.30	0.281	0.0281	6.00	0.326	0.0318
4.79	0.234	0.0267	6.27	0.329	0.0366	5.12	0.272	0.0238
3.90	0.184	0.0249	7.33	0.391	0.0460	4.15	0.219	0.0183
2.75	0.112	0.0182	8.30	0.446	0.0547	3.08	0.156	0.0136
1.87	0.068	0.0175	9.36	0.498	0.0726	2.11	0.107	0.0100
0.90	0.019	0.0162	10.42	0.555	0.0936	1.05	0.057	0.0100
-0.16	-0.035	0.0156	11.31	0.604	0.1156	0.08	0.012	0.0065
-0.96	-0.071	0.0158	12.28	0.651	0.1387	-0.89	-0.037	0.0060
-2.11	-0.129	0.0198	13.34	0.684	0.1618	-1.95	-0.083	0.0062
-3.08	-0.204	0.0220	14.31	0.709	0.1774	-2.92	-0.140	0.0109
-4.14	-0.259	0.0265	15.36	0.711	0.2018	-3.90	-0.200	0.0115
-5.12	-0.310	0.0312	16.33	0.710	0.2160	-4.96	-0.255	0.0202
-6.18	-0.361	0.0374	17.39	0.716	0.2322	-5.93	-0.304	0.0231
-7.24	-0.409	0.0456	18.35	0.719	0.2464	-6.99	-0.363	0.0359
-8.03	-0.448	0.0551	19.41	0.719	0.2616	-7.97	-0.415	0.0459
-9.18	-0.508	0.0771	20.38	0.726	0.2791	-8.94	-0.470	0.0635
-10.16	-0.568	0.1028	21.43	0.730	0.2943	-10.09	-0.537	0.0851
-11.22	-0.627	0.1246	22.40	0.726	0.3083	-10.97	-0.575	0.1053
-12.01	-0.659	0.1418	23.19	0.727	0.3181	-11.94	-0.614	0.1250
-13.25	-0.696	0.1708	24.33	0.719	0.3331	-12.74	-0.639	0.1414
			25.38	0.692	0.3374	-13.97	-0.669	0.1672
			26.35	0.693	0.3499	-15.03	-0.680	0.1858
			27.31	0.689	0.3627			
			28.37	0.680	0.3746			
			29.42	0.679	0.3879			

AR2-I100-FP1

Fig. 5.4

Run: 0441ga

$Re = 79999.8$

α	C_L	C_D
-15.03	-0.675	0.1847
-13.80	-0.659	0.1624
-12.82	-0.637	0.1411
-11.86	-0.609	0.1206
-10.80	-0.560	0.0993
-9.82	-0.516	0.0781
-8.94	-0.463	0.0629
-7.70	-0.400	0.0432
-6.73	-0.344	0.0330
-5.67	-0.286	0.0251
-4.96	-0.257	0.0216
-3.81	-0.194	0.0142
-2.75	-0.126	0.0124
-1.69	-0.081	0.0107

α	C_L	C_D
-14.98	-0.688	0.1860
-13.75	-0.674	0.1640
-12.78	-0.648	0.1436
-11.81	-0.617	0.1249
-10.66	-0.570	0.1003
-9.78	-0.519	0.0831
-8.98	-0.471	0.0649
-7.74	-0.407	0.0449
-6.77	-0.355	0.0339
-5.71	-0.297	0.0275
-4.74	-0.247	0.0210
-3.68	-0.204	0.0170
-2.70	-0.135	0.0123
-1.73	-0.085	0.0121
-0.67	-0.031	0.0122
0.30	0.014	0.0117

1.36	0.060	0.0125	10.12	0.548	0.0869	3.31	0.166	0.0166
2.34	0.113	0.0152	9.15	0.493	0.0637	4.20	0.238	0.0207
3.40	0.164	0.0179	8.17	0.442	0.0501	5.26	0.297	0.0272
4.19	0.224	0.0239	7.11	0.391	0.0403	6.23	0.350	0.0350
5.43	0.293	0.0300	6.14	0.331	0.0330	7.12	0.399	0.0424
6.32	0.344	0.0378	5.17	0.284	0.0251	8.35	0.463	0.0536
7.46	0.398	0.0460	4.20	0.232	0.0189	9.24	0.513	0.0677
8.35	0.455	0.0559	3.04	0.157	0.0139	10.39	0.576	0.0939
9.06	0.489	0.0673	2.25	0.108	0.0107	11.36	0.628	0.1177
10.47	0.572	0.0963	1.10	0.054	0.0095	12.24	0.672	0.1391
11.45	0.621	0.1185	0.13	0.007	0.0061	13.39	0.711	0.1651
12.24	0.659	0.1385	-0.93	-0.037	0.0085	14.27	0.735	0.1850
13.48	0.695	0.1652	-1.99	-0.091	0.0093	15.33	0.746	0.2047
14.18	0.712	0.1805	-2.88	-0.145	0.0102	16.12	0.750	0.2195
15.41	0.735	0.2066	-3.94	-0.211	0.0155	17.26	0.744	0.2363
16.47	0.732	0.2218	-4.91	-0.265	0.0205	18.32	0.741	0.2521
17.43	0.731	0.2378	-5.88	-0.311	0.0261	19.28	0.744	0.2670
18.40	0.733	0.2540	-6.95	-0.373	0.0360	20.25	0.741	0.2810
19.37	0.730	0.2674	-8.01	-0.427	0.0465	21.39	0.742	0.2972
20.42	0.733	0.2841	-8.63	-0.467	0.0613	22.27	0.740	0.3097
21.21	0.734	0.2943	-9.95	-0.535	0.0901	23.32	0.732	0.3222
22.36	0.728	0.3114	-10.75	-0.570	0.1011	24.29	0.729	0.3342
23.41	0.729	0.3262	-11.90	-0.623	0.1287	25.26	0.720	0.3444
24.47	0.719	0.3361	-12.96	-0.659	0.1491	26.40	0.714	0.3584
25.34	0.710	0.3469	-13.93	-0.680	0.1708	27.36	0.697	0.3655
26.13	0.694	0.3511	-14.98	-0.686	0.1878	28.33	0.700	0.3816
27.10	0.686	0.3591				29.30	0.696	0.3922
28.15	0.689	0.3777	Run: 0442ga			29.12	0.693	0.3896
29.47	0.686	0.3928	$Re = 119998.1$			28.07	0.689	0.3730
29.47	0.681	0.3912	α	C_L	C_D	27.01	0.698	0.3604
28.24	0.683	0.3755	-15.07	-0.702	0.1901	26.13	0.696	0.3449
27.36	0.680	0.3651	-13.84	-0.681	0.1664	25.08	0.703	0.3344
26.31	0.693	0.3511	-12.78	-0.655	0.1436	24.11	0.712	0.3244
25.16	0.701	0.3385	-11.90	-0.626	0.1252	23.06	0.736	0.3204
24.46	0.698	0.3275	-10.75	-0.576	0.1019	22.09	0.741	0.3090
23.15	0.726	0.3213	-9.87	-0.531	0.0839	21.04	0.748	0.2949
22.09	0.732	0.3083	-8.80	-0.463	0.0582	20.07	0.739	0.2785
21.21	0.733	0.2940	-7.83	-0.412	0.0425	19.11	0.738	0.2626
20.25	0.734	0.2802	-6.86	-0.361	0.0324	18.14	0.744	0.2484
19.19	0.729	0.2631	-5.88	-0.307	0.0253	17.00	0.749	0.2307
18.40	0.726	0.2485	-4.82	-0.254	0.0204	16.12	0.746	0.2161
17.35	0.728	0.2345	-3.76	-0.203	0.0177	15.42	0.746	0.2037
16.20	0.732	0.2162	-2.79	-0.135	0.0126	14.10	0.724	0.1753
15.41	0.733	0.2033	-1.73	-0.085	0.0101	13.04	0.697	0.1531
14.09	0.717	0.1755	-0.67	-0.034	0.0110	12.07	0.660	0.1302
13.12	0.689	0.1524	0.04	0.002	0.0087	11.09	0.608	0.1044
12.15	0.650	0.1309	1.19	0.059	0.0122	10.39	0.572	0.0882
11.36	0.617	0.1128	2.25	0.111	0.0145	9.06	0.495	0.0597

8.09	0.442	0.0456	5.25	0.299	0.0273	5.96	0.339	0.0309
7.11	0.394	0.0383	6.23	0.356	0.0323	5.08	0.285	0.0210
6.05	0.338	0.0302	7.29	0.413	0.0415	4.10	0.235	0.0188
5.08	0.288	0.0243	8.35	0.466	0.0516	3.04	0.151	0.0108
4.11	0.237	0.0184	9.23	0.518	0.0648	2.07	0.105	0.0116
3.04	0.158	0.0127	10.29	0.579	0.0951	1.01	0.048	0.0069
2.07	0.110	0.0105	11.27	0.628	0.1153	0.03	0.005	0.0073
1.01	0.058	0.0079	12.24	0.676	0.1410	-1.03	-0.051	0.0094
0.22	0.018	0.0061	13.30	0.708	0.1640	-2.00	-0.102	0.0092
-0.93	-0.038	0.0080	14.35	0.735	0.1860	-2.80	-0.160	0.0102
-1.99	-0.095	0.0089	15.41	0.752	0.2087	-4.04	-0.228	0.0184
-2.97	-0.165	0.0113	16.29	0.761	0.2220	-5.01	-0.281	0.0224
-3.94	-0.214	0.0171	16.99	0.755	0.2347	-6.07	-0.331	0.0268
-4.91	-0.271	0.0206	18.31	0.753	0.2547	-6.78	-0.369	0.0316
-5.97	-0.323	0.0277	19.28	0.751	0.2683	-7.92	-0.429	0.0428
-7.04	-0.381	0.0360	20.33	0.751	0.2844	-8.99	-0.483	0.0631
-8.01	-0.429	0.0458	21.30	0.752	0.3002	-9.78	-0.531	0.0840
-8.98	-0.485	0.0672	22.27	0.751	0.3135	-11.02	-0.591	0.1090
-10.04	-0.545	0.0887	23.32	0.739	0.3249	-12.08	-0.635	0.1304
-11.10	-0.593	0.1081	24.29	0.723	0.3318	-13.05	-0.665	0.1501
-11.98	-0.633	0.1301	25.34	0.714	0.3444	-14.11	-0.691	0.1707
-13.04	-0.662	0.1522	26.31	0.717	0.3575	-15.07	-0.703	0.1899
-14.10	-0.688	0.1721	27.10	0.713	0.3675			
-15.07	-0.699	0.1905	28.32	0.698	0.3789	Run: 0444ga		
			29.29	0.692	0.3897	Re = 159991.6		
Run: 0443ga			29.38	0.689	0.3898			
Re = 139994.6			28.24	0.697	0.3764			
	α	C_L	C_D			α	C_L	C_D
-15.07	-0.707	0.1922	27.09	0.699	0.3601	-15.02	-0.708	0.1907
-13.84	-0.686	0.1668	26.13	0.704	0.3501	-13.97	-0.693	0.1691
-13.05	-0.665	0.1486	25.07	0.706	0.3366	-12.82	-0.658	0.1443
-11.90	-0.629	0.1273	24.11	0.708	0.3234	-11.85	-0.627	0.1232
-10.84	-0.578	0.1043	23.06	0.740	0.3208	-10.79	-0.579	0.0996
-9.87	-0.528	0.0820	22.09	0.751	0.3100	-9.82	-0.527	0.0789
-9.07	-0.486	0.0675	21.04	0.749	0.2949	-8.76	-0.462	0.0505
-7.75	-0.414	0.0410	20.16	0.753	0.2832	-7.69	-0.414	0.0377
-6.77	-0.364	0.0304	19.10	0.755	0.2668	-6.72	-0.362	0.0304
-5.71	-0.308	0.0260	18.05	0.753	0.2518	-5.75	-0.310	0.0240
-5.01	-0.274	0.0212	16.99	0.755	0.2312	-4.78	-0.258	0.0189
-3.77	-0.208	0.0166	16.03	0.756	0.2174	-3.80	-0.210	0.0155
-2.79	-0.150	0.0126	15.15	0.749	0.2005	-2.65	-0.151	0.0103
-1.73	-0.086	0.0091	14.09	0.726	0.1765	-1.77	-0.087	0.0083
-0.76	-0.037	0.0102	13.03	0.699	0.1528	-0.71	-0.034	0.0091
0.21	0.010	0.0101	12.15	0.664	0.1307	0.26	0.013	0.0076
0.92	0.037	0.0104	11.00	0.609	0.1032	1.32	0.061	0.0104
2.24	0.111	0.0135	10.03	0.556	0.0815	2.38	0.117	0.0105
3.22	0.171	0.0142	8.97	0.496	0.0565	3.27	0.183	0.0141
4.19	0.246	0.0216	8.35	0.464	0.0480	4.25	0.245	0.0198
			7.11	0.391	0.0363	5.31	0.306	0.0269
						6.10	0.348	0.0325

7.34	0.420	0.0420	4.16	0.234	0.0186	5.25	0.322	0.0389
8.31	0.473	0.0513	3.00	0.150	0.0124	6.05	0.369	0.0487
9.29	0.528	0.0673	2.12	0.105	0.0117	7.12	0.440	0.0596
10.35	0.588	0.0972	0.97	0.047	0.0081	8.36	0.523	0.0807
11.41	0.642	0.1205	0.09	0.002	0.0090	9.25	0.592	0.1028
12.38	0.679	0.1419	-0.97	-0.051	0.0086	10.32	0.652	0.1276
13.35	0.715	0.1655	-1.95	-0.107	0.0100	11.29	0.670	0.1493
14.06	0.738	0.1834	-2.92	-0.180	0.0135	12.25	0.660	0.1623
15.38	0.763	0.2108	-3.90	-0.229	0.0166	13.13	0.645	0.1734
16.26	0.762	0.2264	-4.96	-0.282	0.0216	14.27	0.632	0.1865
17.31	0.761	0.2410	-5.93	-0.326	0.0268	15.41	0.623	0.1992
18.36	0.758	0.2570	-6.99	-0.385	0.0343	16.38	0.618	0.2122
19.33	0.751	0.2705	-7.96	-0.431	0.0440	17.08	0.626	0.2201
20.30	0.757	0.2876	-9.02	-0.485	0.0644	18.31	0.626	0.2382
21.35	0.757	0.3027	-9.99	-0.543	0.0875	19.28	0.631	0.2503
22.32	0.748	0.3133	-11.06	-0.596	0.1112	20.24	0.626	0.2603
23.37	0.738	0.3245	-12.03	-0.633	0.1298	21.39	0.636	0.2773
24.34	0.730	0.3360	-13.00	-0.668	0.1504	22.09	0.639	0.2886
25.39	0.721	0.3449	-13.97	-0.692	0.1726	23.32	0.640	0.3026
26.36	0.720	0.3606	-15.02	-0.706	0.1904	24.38	0.645	0.3176
27.32	0.719	0.3741				25.26	0.642	0.3295
28.38	0.705	0.3826				26.31	0.649	0.3475
29.34	0.697	0.3935				27.28	0.659	0.3643
29.43	0.696	0.3941				28.16	0.652	0.3794
28.20	0.695	0.3759				29.30	0.664	0.3959
27.15	0.704	0.3618				29.04	0.661	0.3928
26.18	0.707	0.3501				28.33	0.656	0.3784
25.13	0.708	0.3365				27.02	0.652	0.3633
24.16	0.735	0.3350				26.31	0.649	0.3472
23.11	0.743	0.3229				25.17	0.646	0.3349
22.14	0.750	0.3112				24.11	0.641	0.3176
21.09	0.753	0.2964				23.15	0.640	0.3046
20.12	0.757	0.2847				22.09	0.639	0.2885
19.07	0.759	0.2670				21.12	0.632	0.2749
18.19	0.761	0.2524				20.16	0.630	0.2595
17.05	0.761	0.2363				19.28	0.629	0.2523
16.17	0.766	0.2220				18.14	0.625	0.2370
15.11	0.761	0.2029				17.08	0.627	0.2211
14.14	0.737	0.1810				16.02	0.627	0.2138
13.09	0.706	0.1572				15.15	0.634	0.1966
12.20	0.670	0.1344				14.01	0.633	0.1842
11.06	0.617	0.1070				13.13	0.651	0.1740
10.08	0.563	0.0850				12.16	0.669	0.1636
9.02	0.503	0.0581				11.11	0.677	0.1452
8.13	0.456	0.0491				10.14	0.652	0.1232
7.16	0.399	0.0394				9.25	0.597	0.1041
6.01	0.341	0.0320				8.10	0.515	0.0754
5.04	0.284	0.0242				7.12	0.451	0.0586

6.06	0.384	0.0423	7.39	0.473	0.0610	4.02	0.270	0.0248
4.99	0.323	0.0332	8.28	0.534	0.0793	3.04	0.198	0.0182
4.01	0.264	0.0264	9.17	0.602	0.1016	2.06	0.134	0.0140
3.04	0.189	0.0211	10.32	0.656	0.1277	1.00	0.068	0.0132
2.06	0.135	0.0157	11.29	0.682	0.1487	0.02	0.017	0.0120
0.91	0.073	0.0145	12.25	0.677	0.1626	-1.04	-0.046	0.0110
-0.07	0.018	0.0148	13.31	0.662	0.1772	-2.02	-0.109	0.0091
-1.04	-0.041	0.0118	14.27	0.654	0.1869	-3.08	-0.170	0.0144
-2.11	-0.106	0.0116	15.32	0.642	0.1997	-3.98	-0.245	0.0157
-2.99	-0.157	0.0138	16.20	0.639	0.2119	-5.04	-0.310	0.0248
-3.97	-0.219	0.0137	17.26	0.634	0.2242	-6.10	-0.373	0.0320
-5.04	-0.295	0.0221	18.14	0.638	0.2355	-7.08	-0.440	0.0417
-6.01	-0.354	0.0289	19.28	0.639	0.2492	-7.97	-0.498	0.0530
-7.08	-0.424	0.0399	20.33	0.638	0.2625	-9.12	-0.570	0.0769
-8.05	-0.481	0.0519	21.30	0.640	0.2752	-10.19	-0.637	0.1004
-9.03	-0.540	0.0696	22.27	0.643	0.2881	-10.90	-0.670	0.1152
-10.10	-0.615	0.0945	23.32	0.645	0.3016	-12.04	-0.684	0.1427
-11.07	-0.662	0.1186	24.38	0.648	0.3165	-13.18	-0.672	0.1584
-12.04	-0.658	0.1359	25.34	0.650	0.3296	-14.15	-0.654	0.1721
-13.09	-0.655	0.1564	26.31	0.655	0.3463	-15.20	-0.645	0.1839
-14.14	-0.638	0.1679	27.28	0.660	0.3609			
-15.20	-0.623	0.1797	28.42	0.663	0.3777	Run: 0380ga		
			29.30	0.668	0.3952	$Re = 99994.8$		
Run: 0376ar			29.04	0.665	0.3918	α	C_L	C_D
$Re = 79998.7$			28.16	0.664	0.3776	-15.10	-0.651	0.1856
	α	C_L	C_D			-13.87	-0.672	0.1688
-15.11	-0.637	0.1855	27.02	0.655	0.3577	-12.82	-0.688	0.1556
-13.88	-0.660	0.1701	26.05	0.654	0.3441	-11.86	-0.695	0.1405
-12.92	-0.678	0.1566	25.17	0.652	0.3332	-10.89	-0.677	0.1176
-11.87	-0.683	0.1393	24.11	0.648	0.3155	-9.82	-0.632	0.0966
-10.90	-0.668	0.1165	23.15	0.647	0.3023	-8.85	-0.561	0.0728
-9.92	-0.623	0.0956	22.00	0.643	0.2887	-7.78	-0.495	0.0510
-8.86	-0.543	0.0716	21.13	0.644	0.2743	-6.89	-0.442	0.0401
-7.88	-0.483	0.0536	20.16	0.639	0.2610	-5.92	-0.388	0.0332
-6.81	-0.420	0.0406	19.28	0.642	0.2511	-4.85	-0.313	0.0243
-5.84	-0.366	0.0326	18.14	0.640	0.2354	-3.79	-0.249	0.0190
-4.86	-0.305	0.0251	17.34	0.638	0.2261	-2.81	-0.165	0.0154
-3.80	-0.234	0.0193	16.11	0.642	0.2103	-1.83	-0.108	0.0151
-2.82	-0.164	0.0172	15.15	0.653	0.1985	-0.77	-0.046	0.0140
-2.11	-0.123	0.0152	14.10	0.664	0.1872	0.21	0.012	0.0133
-0.78	-0.040	0.0152	13.13	0.668	0.1740	1.19	0.069	0.0171
0.20	0.010	0.0179	12.17	0.682	0.1626	2.25	0.133	0.0187
1.17	0.074	0.0179	11.03	0.684	0.1414	3.23	0.215	0.0230
2.32	0.131	0.0204	10.14	0.659	0.1220	4.21	0.277	0.0279
3.21	0.202	0.0232	9.07	0.586	0.0943	5.27	0.352	0.0359
4.28	0.269	0.0293	8.10	0.519	0.0719	6.07	0.395	0.0429
5.35	0.341	0.0363	7.12	0.457	0.0555	7.31	0.479	0.0595
6.23	0.405	0.0470	6.32	0.411	0.0421	8.29	0.541	0.0792
			5.26	0.347	0.0347			

9.36	0.615	0.1042	2.07	0.130	0.0158	11.30	0.702	0.1521
10.33	0.672	0.1290	0.92	0.067	0.0129	12.26	0.701	0.1677
11.30	0.694	0.1494	0.03	0.010	0.0110	13.32	0.690	0.1829
12.27	0.692	0.1648	-0.94	-0.045	0.0102	14.28	0.682	0.1945
13.15	0.676	0.1753	-1.92	-0.112	0.0110	15.34	0.686	0.2112
14.29	0.665	0.1886	-2.98	-0.176	0.0137	16.40	0.718	0.2333
15.34	0.660	0.2038	-3.96	-0.255	0.0180	17.28	0.722	0.2484
16.22	0.643	0.2138	-5.03	-0.326	0.0233	18.33	0.700	0.2577
17.27	0.644	0.2259	-6.00	-0.387	0.0312	19.39	0.732	0.2820
18.32	0.646	0.2397	-7.16	-0.457	0.0417	20.25	0.655	0.2668
19.29	0.642	0.2520	-8.14	-0.517	0.0567	21.31	0.654	0.2818
20.26	0.647	0.2632	-9.02	-0.576	0.0786	22.36	0.650	0.2936
21.23	0.649	0.2780	-10.09	-0.647	0.1029	23.33	0.652	0.3071
22.28	0.645	0.2899	-11.06	-0.689	0.1238	24.30	0.655	0.3210
23.42	0.648	0.3068	-12.12	-0.699	0.1448	25.27	0.659	0.3364
24.30	0.649	0.3178	-13.08	-0.681	0.1607	26.32	0.659	0.3501
25.27	0.656	0.3338	-14.05	-0.666	0.1745	27.29	0.663	0.3661
26.32	0.656	0.3477	-14.93	-0.659	0.1834	28.34	0.664	0.3817
27.29	0.660	0.3630				29.31	0.669	0.3990
28.44	0.668	0.3802	Run: 0379ga			29.13	0.669	0.3943
29.32	0.669	0.3953	$Re = 119992.5$			28.43	0.669	0.3841
29.32	0.668	0.3988	α	C_L	C_D	27.11	0.663	0.3628
28.17	0.661	0.3746	-15.20	-0.668	0.1892	26.15	0.659	0.3471
27.03	0.657	0.3605	-13.88	-0.680	0.1718	25.09	0.657	0.3335
26.06	0.655	0.3446	-12.83	-0.700	0.1576	24.12	0.656	0.3190
25.09	0.654	0.3316	-11.95	-0.710	0.1431	23.16	0.654	0.3047
24.04	0.649	0.3167	-10.81	-0.687	0.1196	22.36	0.651	0.2927
23.16	0.648	0.3020	-9.92	-0.641	0.0999	21.05	0.654	0.2790
22.11	0.649	0.2887	-8.85	-0.565	0.0725	20.08	0.659	0.2672
21.05	0.646	0.2752	-7.88	-0.506	0.0518	19.04	0.720	0.2739
20.08	0.648	0.2619	-6.81	-0.443	0.0393	18.07	0.726	0.2609
19.38	0.645	0.2547	-5.84	-0.383	0.0302	17.10	0.724	0.2445
18.15	0.646	0.2364	-4.86	-0.325	0.0262	16.13	0.722	0.2314
17.18	0.648	0.2279	-3.79	-0.256	0.0204	15.16	0.689	0.2071
16.13	0.651	0.2132	-2.81	-0.166	0.0165	14.11	0.686	0.1912
15.08	0.658	0.1997	-1.84	-0.110	0.0137	13.14	0.690	0.1773
14.02	0.668	0.1866	-0.77	-0.046	0.0136	12.18	0.701	0.1642
13.15	0.683	0.1750	0.20	0.012	0.0156	11.12	0.702	0.1447
12.18	0.694	0.1618	1.18	0.069	0.0168	10.06	0.666	0.1222
11.04	0.693	0.1421	2.33	0.136	0.0187	9.09	0.601	0.0968
10.15	0.666	0.1217	3.23	0.230	0.0230	8.20	0.533	0.0703
9.00	0.595	0.0946	4.20	0.289	0.0291	7.13	0.468	0.0516
8.11	0.529	0.0720	5.00	0.343	0.0345	6.07	0.403	0.0400
7.13	0.462	0.0530	6.24	0.420	0.0454	5.00	0.344	0.0320
6.25	0.411	0.0418	7.31	0.488	0.0591	4.11	0.280	0.0259
5.00	0.336	0.0314	8.29	0.547	0.0799	3.05	0.212	0.0197
4.12	0.281	0.0260	9.26	0.617	0.1055	2.07	0.133	0.0163
3.05	0.207	0.0197	10.33	0.679	0.1305	0.92	0.065	0.0134

0.03	0.008	0.0120	9.62	0.605	0.1070	2.42	0.147	0.0190
-0.95	-0.050	0.0115	10.68	0.649	0.1297	1.27	0.086	0.0174
-1.84	-0.106	0.0124	11.47	0.666	0.1469	0.38	0.032	0.0167
-2.99	-0.192	0.0145	12.62	0.668	0.1674	-0.60	-0.032	0.0134
-3.97	-0.270	0.0199	13.67	0.661	0.1828	-1.66	-0.088	0.0116
-5.13	-0.342	0.0258	14.63	0.649	0.1929	-2.63	-0.143	0.0141
-6.10	-0.399	0.0326	15.69	0.629	0.2049	-3.61	-0.209	0.0143
-7.17	-0.465	0.0420	16.65	0.639	0.2192	-4.68	-0.287	0.0227
-8.14	-0.524	0.0568	17.71	0.640	0.2316	-5.75	-0.347	0.0273
-9.03	-0.586	0.0798	18.68	0.642	0.2437	-6.81	-0.413	0.0398
-10.10	-0.657	0.1046	19.73	0.647	0.2570	-7.79	-0.481	0.0552
-11.07	-0.696	0.1266	20.61	0.653	0.2691	-8.68	-0.539	0.0717
-12.04	-0.707	0.1458	21.76	0.660	0.2861	-9.74	-0.609	0.0973
-13.18	-0.695	0.1637	22.64	0.661	0.3013	-10.80	-0.631	0.1190
-14.14	-0.681	0.1774	23.69	0.662	0.3150	-11.77	-0.646	0.1345
-15.11	-0.673	0.1920	24.66	0.661	0.3229	-12.82	-0.641	0.1530
			25.62	0.661	0.3383	-13.79	-0.637	0.1644
			26.77	0.671	0.3582	-14.84	-0.622	0.1803
			27.65	0.676	0.3742			
			28.79	0.671	0.3872	Run: 0372ga		
			29.67	0.681	0.4048	$Re = 80003.6$		
			29.49	0.678	0.4023	α	C_L	C_D
			28.53	0.677	0.3892	-14.95	-0.644	0.1849
			27.47	0.671	0.3724	-13.63	-0.658	0.1665
			26.50	0.667	0.3567	-12.58	-0.666	0.1528
			25.45	0.665	0.3430	-11.61	-0.659	0.1362
			24.48	0.665	0.3249	-10.64	-0.645	0.1153
			23.51	0.657	0.3135	-9.67	-0.616	0.0984
			22.46	0.658	0.2994	-8.51	-0.539	0.0734
			21.49	0.654	0.2861	-7.62	-0.478	0.0563
			20.52	0.655	0.2703	-6.65	-0.412	0.0403
			19.73	0.648	0.2611	-5.58	-0.350	0.0301
			18.41	0.645	0.2432	-4.87	-0.307	0.0261
			17.36	0.641	0.2270	-3.54	-0.222	0.0199
			16.48	0.645	0.2209	-2.47	-0.143	0.0171
			15.43	0.652	0.2037	-1.58	-0.093	0.0146
			14.37	0.653	0.1899	-0.43	-0.024	0.0162
			13.50	0.673	0.1805	0.46	0.025	0.0187
			12.53	0.677	0.1663	1.26	0.072	0.0187
			11.47	0.671	0.1464	2.50	0.149	0.0213
			10.51	0.654	0.1261	3.48	0.217	0.0256
			9.44	0.598	0.1005	4.46	0.287	0.0316
			8.46	0.533	0.0791	5.61	0.366	0.0394
			7.49	0.470	0.0618	6.32	0.407	0.0467
			6.60	0.417	0.0451	7.57	0.489	0.0638
			5.36	0.343	0.0363	8.54	0.551	0.0830
			4.46	0.277	0.0296	9.52	0.618	0.1051
			3.40	0.205	0.0227	10.58	0.662	0.1299

11.64	0.690	0.1528	25.57	0.684	0.3448	-13.85	-0.674	0.1723
12.52	0.690	0.1674	26.54	0.685	0.3587	-14.90	-0.659	0.1838
13.40	0.684	0.1809	27.50	0.683	0.3715			
14.63	0.672	0.1947	28.65	0.685	0.3872	Run: 0373ga		
			29.53	0.690	0.4039	$Re = 119998.3$		
Run: 0369ga			29.26	0.689	0.4002	α	C_L	C_D
$Re = 99997.3$			28.38	0.687	0.3856	-14.66	-0.684	0.1880
	α	C_L	C_D			27.33	0.682	0.3699
-14.64	-0.668	0.1815				26.27	0.680	0.3536
-13.68	-0.675	0.1682				25.39	0.675	0.3396
-12.71	-0.680	0.1548				24.34	0.675	0.3243
-11.66	-0.679	0.1366				23.37	0.674	0.3113
-10.69	-0.659	0.1171				22.32	0.675	0.2975
-9.71	-0.622	0.0978				21.35	0.673	0.2840
-8.56	-0.555	0.0749				20.38	0.670	0.2683
-7.67	-0.488	0.0533				19.50	0.666	0.2573
-6.69	-0.426	0.0401				18.36	0.662	0.2400
-5.63	-0.358	0.0284				17.22	0.668	0.2274
-4.65	-0.300	0.0243				16.34	0.667	0.2161
-3.59	-0.235	0.0194				15.64	0.674	0.2074
-2.52	-0.150	0.0147				14.41	0.687	0.1917
-1.81	-0.108	0.0156				13.27	0.707	0.1784
-0.83	-0.047	0.0137				12.39	0.706	0.1629
0.24	0.013	0.0143				11.25	0.697	0.1419
1.39	0.085	0.0173				10.37	0.676	0.1224
2.46	0.151	0.0190				9.21	0.614	0.0940
3.44	0.233	0.0234				8.32	0.553	0.0721
4.50	0.304	0.0300				7.34	0.490	0.0545
5.48	0.372	0.0371				6.28	0.417	0.0385
6.46	0.430	0.0456				5.21	0.358	0.0318
7.52	0.499	0.0606				4.33	0.301	0.0264
8.50	0.565	0.0827				3.26	0.219	0.0173
9.48	0.633	0.1048				2.19	0.143	0.0145
10.54	0.681	0.1311				1.13	0.080	0.0118
11.51	0.700	0.1511				0.24	0.025	0.0106
12.48	0.708	0.1679				-0.74	-0.032	0.0088
13.53	0.696	0.1839				-1.80	-0.097	0.0091
14.59	0.685	0.1958				-2.78	-0.177	0.0120
15.64	0.677	0.2086				-3.76	-0.240	0.0154
16.43	0.664	0.2191				-4.83	-0.312	0.0220
17.48	0.661	0.2294				-5.80	-0.372	0.0272
18.62	0.663	0.2444				-6.96	-0.442	0.0397
19.50	0.665	0.2577				-7.76	-0.499	0.0558
20.47	0.669	0.2697				-8.83	-0.579	0.0777
21.53	0.674	0.2862				-9.98	-0.637	0.1024
22.23	0.673	0.2966				-10.86	-0.664	0.1215
23.64	0.678	0.3163				-11.92	-0.677	0.1404
24.52	0.681	0.3295				-12.89	-0.682	0.1579

			AR3-I100-FP1		
27.58	0.688	0.3751	Fig. 5.7		
28.64	0.691	0.3911		26.59	0.677
29.61	0.692	0.4070		27.55	0.684
29.43	0.686	0.3998	Run: 0383ar	28.61	0.684
28.46	0.689	0.3883	$Re = 59999.4$	29.66	0.690
27.32	0.686	0.3703	$\alpha \quad C_L \quad C_D$	29.40	0.686
26.44	0.686	0.3569	-14.86 -0.647 0.1871	28.43	0.688
25.38	0.680	0.3399	-13.63 -0.643 0.1644	27.38	0.684
24.42	0.679	0.3245	-12.57 -0.648 0.1504	26.59	0.676
23.45	0.677	0.3126	-11.69 -0.640 0.1318	25.35	0.676
22.40	0.683	0.3003	-10.55 -0.618 0.1136	24.39	0.676
21.43	0.677	0.2854	-9.57 -0.587 0.0922	23.42	0.676
20.46	0.677	0.2720	-8.60 -0.534 0.0720	22.36	0.670
19.67	0.680	0.2627	-7.62 -0.465 0.0520	21.40	0.665
18.35	0.673	0.2433	-6.55 -0.407 0.0413	20.43	0.666
17.30	0.692	0.2337	-5.58 -0.341 0.0310	19.38	0.663
16.42	0.696	0.2238	-4.51 -0.283 0.0255	18.41	0.657
15.37	0.720	0.2132	-3.53 -0.205 0.0200	17.35	0.650
14.41	0.739	0.2017	-2.47 -0.144 0.0180	16.39	0.651
13.44	0.723	0.1826	-1.85 -0.103 0.0189	15.42	0.659
12.47	0.720	0.1656	-0.43 -0.028 0.0169	14.37	0.660
11.33	0.709	0.1437	0.46 0.030 0.0183	13.40	0.660
10.36	0.682	0.1227	1.26 0.069 0.0183	12.43	0.658
9.38	0.623	0.0969	2.59 0.147 0.0216	11.29	0.651
8.40	0.560	0.0736	3.48 0.203 0.0258	10.41	0.635
7.42	0.492	0.0526	4.54 0.277 0.0330	9.35	0.596
6.27	0.427	0.0402	5.52 0.341 0.0421	8.37	0.532
5.29	0.368	0.0318	6.50 0.402 0.0504	7.39	0.466
4.32	0.304	0.0255	7.57 0.472 0.0669	6.32	0.400
3.34	0.227	0.0184	8.63 0.535 0.0868	5.53	0.354
2.36	0.152	0.0152	9.52 0.594 0.1085	4.28	0.276
1.20	0.082	0.0119	10.58 0.630 0.1292	3.30	0.198
0.23	0.024	0.0113	11.37 0.644 0.1458	2.33	0.142
-0.66	-0.033	0.0108	12.52 0.661 0.1646	1.17	0.080
-1.55	-0.091	0.0100	13.57 0.651 0.1829	0.37	0.031
-2.71	-0.190	0.0145	14.54 0.658 0.1932	-0.78	-0.034
-3.69	-0.253	0.0185	15.51 0.641 0.2079	-1.67	-0.092
-4.84	-0.325	0.0240	16.65 0.647 0.2230	-2.73	-0.148
-5.73	-0.384	0.0305	17.62 0.649 0.2359	-3.71	-0.209
-6.88	-0.450	0.0410	18.67 0.649 0.2494	-4.78	-0.293
-7.86	-0.512	0.0590	19.64 0.656 0.2654	-5.84	-0.347
-8.84	-0.587	0.0825	20.43 0.667 0.2759	-6.82	-0.418
-9.90	-0.642	0.1057	21.66 0.666 0.2907	-7.89	-0.480
-10.79	-0.672	0.1235	22.63 0.670 0.3058	-8.86	-0.544
-11.85	-0.687	0.1440	23.60 0.674 0.3210	-9.84	-0.599
-12.81	-0.689	0.1608	24.65 0.674 0.3332	-10.81	-0.626
-13.78	-0.688	0.1759	25.62 0.679 0.3490	-11.87	-0.638
-14.57	-0.690	0.1890		-12.92	-0.644
				-13.89	-0.643

-14.95	-0.645	0.1841	28.51	0.686	0.3916	Run: 0386ar		
			29.57	0.693	0.4082	$Re = 99999.2$		
Run: 0384ar			29.30	0.693	0.4063			
$Re = 80000.3$			28.34	0.692	0.3926	α	C_L	C_D
	α	C_L	C_D					
-14.96	-0.665	0.1897	27.28	0.690	0.3771	-14.73	-0.688	0.1886
-13.64	-0.670	0.1696	26.31	0.683	0.3603	-13.76	-0.684	0.1734
-12.68	-0.673	0.1533	25.26	0.681	0.3468	-12.79	-0.690	0.1555
-11.80	-0.666	0.1361	24.29	0.684	0.3328	-11.83	-0.686	0.1382
-10.73	-0.638	0.1166	23.32	0.683	0.3206	-10.77	-0.658	0.1171
-10.03	-0.619	0.1037	22.27	0.681	0.3042	-9.79	-0.624	0.0977
-8.70	-0.550	0.0747	21.21	0.683	0.2904	-8.73	-0.567	0.0747
-7.72	-0.484	0.0549	20.25	0.678	0.2767	-7.75	-0.497	0.0525
-6.74	-0.422	0.0413	19.19	0.674	0.2607	-6.78	-0.435	0.0391
-5.68	-0.360	0.0328	18.49	0.669	0.2515	-5.71	-0.369	0.0306
-4.97	-0.319	0.0283	17.17	0.665	0.2323	-4.73	-0.316	0.0252
-3.64	-0.232	0.0211	16.29	0.665	0.2206	-3.67	-0.248	0.0203
-2.57	-0.151	0.0192	15.50	0.669	0.2108	-2.60	-0.158	0.0149
-1.68	-0.099	0.0149	14.27	0.673	0.1933	-1.62	-0.102	0.0137
-0.62	-0.037	0.0173	13.22	0.679	0.1794	-0.56	-0.036	0.0133
0.36	0.022	0.0178	12.34	0.675	0.1637	0.33	0.021	0.0132
1.34	0.077	0.0198	11.28	0.660	0.1431	1.31	0.078	0.0163
2.40	0.140	0.0222	10.40	0.645	0.1255	2.37	0.143	0.0180
3.47	0.214	0.0260	9.16	0.596	0.0998	3.18	0.211	0.0205
4.36	0.283	0.0321	8.27	0.542	0.0800	4.42	0.299	0.0287
5.43	0.353	0.0408	7.29	0.473	0.0607	5.13	0.351	0.0341
6.40	0.412	0.0493	6.40	0.417	0.0456	6.38	0.426	0.0444
7.29	0.467	0.0623	5.16	0.341	0.0349	7.44	0.499	0.0620
8.45	0.555	0.0878	4.18	0.282	0.0283	8.51	0.572	0.0869
9.43	0.612	0.1085	3.20	0.202	0.0212	9.22	0.612	0.1017
10.48	0.644	0.1311	2.23	0.142	0.0177	10.46	0.665	0.1300
11.46	0.667	0.1512	1.07	0.074	0.0154	11.43	0.692	0.1493
12.51	0.674	0.1658	0.10	0.021	0.0135	12.49	0.705	0.1677
13.48	0.672	0.1838	-0.79	-0.035	0.0131	13.45	0.697	0.1820
14.44	0.669	0.1960	-1.86	-0.100	0.0122	14.42	0.689	0.1964
15.50	0.671	0.2096	-2.83	-0.157	0.0164	15.47	0.682	0.2105
16.47	0.666	0.2242	-3.81	-0.237	0.0186	16.53	0.678	0.2233
17.43	0.667	0.2377	-4.88	-0.308	0.0267	17.41	0.675	0.2349
18.49	0.663	0.2478	-5.94	-0.369	0.0317	18.46	0.676	0.2487
19.45	0.666	0.2631	-6.92	-0.439	0.0432	19.43	0.676	0.2615
20.42	0.671	0.2763	-7.90	-0.495	0.0575	20.40	0.683	0.2750
21.48	0.675	0.2920	-8.88	-0.562	0.0792	21.36	0.686	0.2912
22.44	0.679	0.3038	-9.94	-0.614	0.1020	22.42	0.686	0.3043
23.50	0.680	0.3195	-10.91	-0.646	0.1228	23.47	0.684	0.3197
24.55	0.679	0.3349	-11.88	-0.660	0.1412	24.44	0.685	0.3313
25.52	0.689	0.3513	-12.94	-0.674	0.1595	25.41	0.691	0.3491
26.49	0.681	0.3600	-13.99	-0.673	0.1763	26.46	0.690	0.3617
27.45	0.687	0.3763	-15.05	-0.669	0.1916	27.43	0.695	0.3798
						28.48	0.698	0.3931
						29.45	0.698	0.4084

29.45	0.692	0.4076	Run: 0385ar	29.22	0.698	0.4065		
28.31	0.696	0.3896	$Re = 119998.1$	28.25	0.695	0.3914		
27.16	0.694	0.3744	α	C_L	C_D	27.11	0.693	0.3739
26.20	0.689	0.3588	-14.87	-0.714	0.1933	26.14	0.690	0.3594
25.32	0.688	0.3465	-14.08	-0.722	0.1812	25.26	0.687	0.3449
24.26	0.685	0.3305	-13.12	-0.720	0.1635	24.21	0.686	0.3300
23.30	0.683	0.3152	-11.80	-0.697	0.1388	23.24	0.684	0.3165
22.24	0.685	0.3015	-10.82	-0.669	0.1169	22.19	0.687	0.3029
21.19	0.682	0.2875	-9.85	-0.630	0.0984	21.22	0.685	0.2893
20.22	0.680	0.2734	-8.70	-0.564	0.0744	20.25	0.687	0.2757
19.43	0.679	0.2638	-7.72	-0.501	0.0505	19.37	0.683	0.2635
18.28	0.675	0.2453	-6.83	-0.446	0.0391	18.23	0.680	0.2468
17.41	0.677	0.2366	-5.77	-0.382	0.0298	17.18	0.684	0.2337
16.26	0.685	0.2215	-4.79	-0.319	0.0249	16.21	0.688	0.2226
15.30	0.686	0.2058	-3.72	-0.252	0.0194	15.25	0.731	0.2183
14.16	0.693	0.1927	-2.74	-0.161	0.0145	14.20	0.734	0.2000
13.28	0.701	0.1771	-1.76	-0.100	0.0124	13.23	0.725	0.1816
12.31	0.701	0.1628	-0.61	-0.036	0.0129	12.26	0.717	0.1651
11.17	0.684	0.1411	0.28	0.016	0.0143	11.20	0.698	0.1432
10.28	0.659	0.1230	1.25	0.081	0.0159	10.23	0.668	0.1238
9.13	0.609	0.0983	2.41	0.151	0.0170	9.43	0.633	0.1062
8.24	0.555	0.0789	3.30	0.245	0.0232	8.28	0.561	0.0796
7.26	0.483	0.0552	4.28	0.306	0.0292	7.21	0.486	0.0542
6.38	0.433	0.0426	5.08	0.361	0.0342	6.32	0.437	0.0424
5.13	0.354	0.0325	6.32	0.439	0.0460	5.08	0.362	0.0320
4.25	0.297	0.0261	7.48	0.508	0.0632	4.19	0.301	0.0256
3.18	0.218	0.0189	8.37	0.575	0.0876	3.13	0.230	0.0189
2.11	0.143	0.0151	9.08	0.620	0.1027	2.06	0.144	0.0157
1.04	0.078	0.0128	10.41	0.675	0.1303	0.99	0.078	0.0118
0.16	0.025	0.0100	11.38	0.704	0.1514	0.10	0.020	0.0105
-0.82	-0.038	0.0100	12.35	0.717	0.1702	-0.87	-0.038	0.0105
-1.80	-0.102	0.0102	13.49	0.725	0.1898	-2.03	-0.113	0.0116
-2.95	-0.169	0.0140	14.37	0.740	0.2064	-3.01	-0.190	0.0139
-3.84	-0.249	0.0179	15.43	0.723	0.2196	-3.90	-0.264	0.0193
-5.00	-0.321	0.0243	16.39	0.685	0.2253	-4.97	-0.332	0.0247
-5.89	-0.382	0.0311	17.35	0.683	0.2369	-5.94	-0.393	0.0303
-6.78	-0.439	0.0383	18.41	0.678	0.2495	-7.10	-0.464	0.0413
-7.84	-0.510	0.0564	19.46	0.684	0.2638	-8.07	-0.524	0.0576
-8.91	-0.582	0.0789	20.43	0.688	0.2777	-8.96	-0.588	0.0810
-10.06	-0.637	0.1039	21.40	0.690	0.2926	-9.76	-0.630	0.0962
-10.95	-0.668	0.1219	22.45	0.686	0.3051	-10.82	-0.670	0.1173
-11.91	-0.686	0.1408	23.50	0.686	0.3200	-12.06	-0.702	0.1426
-12.97	-0.694	0.1602	24.38	0.688	0.3330	-12.85	-0.712	0.1576
-13.94	-0.689	0.1783	25.44	0.688	0.3490	-14.09	-0.726	0.1807
-14.81	-0.678	0.1866	26.49	0.692	0.3645	-15.05	-0.708	0.1967
			27.37	0.693	0.3781			
			28.52	0.698	0.3970			
			29.40	0.700	0.4103			

AR4-I050-FP1			26.72	0.657	0.3456	-14.59	-0.620	0.1664
Fig. 5.8			27.68	0.662	0.3607	Run: 0404ga		
Run: 0403ga			28.74	0.668	0.3798	$Re = 79998.7$		
$Re = 59998.7$			29.71	0.670	0.3960			
α	C_L	C_D	29.53	0.675	0.3962	α	C_L	C_D
-14.77	-0.610	0.1734	28.56	0.669	0.3751	-14.84	-0.630	0.1761
-13.54	-0.631	0.1554	27.51	0.662	0.3607	-13.53	-0.652	0.1611
-12.49	-0.650	0.1447	26.45	0.653	0.3396	-12.65	-0.671	0.1498
-11.62	-0.674	0.1303	25.57	0.646	0.3274	-11.60	-0.683	0.1350
-10.56	-0.671	0.1125	24.51	0.640	0.3080	-10.90	-0.690	0.1243
-9.59	-0.639	0.0912	23.55	0.638	0.2987	-9.57	-0.653	0.0961
-8.43	-0.566	0.0690	22.40	0.631	0.2779	-8.59	-0.582	0.0729
-7.54	-0.494	0.0508	21.52	0.626	0.2686	-7.61	-0.510	0.0532
-6.56	-0.434	0.0398	20.47	0.621	0.2510	-6.81	-0.461	0.0439
-5.40	-0.359	0.0296	19.50	0.626	0.2427	-5.56	-0.374	0.0308
-4.51	-0.299	0.0237	18.53	0.620	0.2279	-4.58	-0.309	0.0244
-3.44	-0.213	0.0192	17.48	0.621	0.2164	-3.51	-0.238	0.0195
-2.46	-0.151	0.0174	16.51	0.624	0.2027	-2.44	-0.151	0.0184
-1.39	-0.085	0.0166	15.55	0.632	0.1934	-1.54	-0.090	0.0172
-0.41	-0.024	0.0174	14.50	0.646	0.1784	-0.48	-0.028	0.0183
0.66	0.038	0.0177	13.53	0.656	0.1699	0.59	0.035	0.0186
1.55	0.096	0.0201	12.66	0.674	0.1559	1.48	0.091	0.0201
2.71	0.170	0.0233	11.52	0.687	0.1424	2.55	0.162	0.0222
3.60	0.237	0.0272	10.55	0.675	0.1228	3.54	0.244	0.0262
4.58	0.310	0.0350	9.48	0.626	0.1001	4.52	0.322	0.0328
5.47	0.366	0.0428	8.50	0.555	0.0769	5.41	0.378	0.0409
6.63	0.450	0.0575	7.52	0.487	0.0595	6.57	0.463	0.0540
7.79	0.528	0.0714	6.36	0.419	0.0470	7.46	0.520	0.0669
8.69	0.602	0.0955	5.47	0.358	0.0385	8.62	0.614	0.0939
9.66	0.659	0.1161	4.49	0.289	0.0289	9.42	0.656	0.1087
10.72	0.682	0.1365	3.42	0.215	0.0224	10.66	0.698	0.1335
11.69	0.679	0.1480	2.71	0.169	0.0203	11.63	0.701	0.1459
12.65	0.663	0.1611	1.37	0.082	0.0155	12.59	0.690	0.1575
13.71	0.644	0.1714	0.57	0.034	0.0147	13.64	0.671	0.1688
14.76	0.632	0.1835	-0.59	-0.036	0.0138	14.70	0.658	0.1799
15.72	0.621	0.1956	-1.66	-0.105	0.0141	15.66	0.643	0.1913
16.69	0.620	0.2080	-2.63	-0.164	0.0162	16.62	0.638	0.2028
17.65	0.617	0.2184	-3.62	-0.229	0.0157	17.68	0.633	0.2142
18.71	0.618	0.2321	-4.69	-0.308	0.0203	18.64	0.632	0.2275
19.68	0.620	0.2432	-5.67	-0.378	0.0297	19.61	0.632	0.2382
20.64	0.623	0.2569	-6.74	-0.446	0.0385	20.58	0.637	0.2521
21.52	0.625	0.2675	-7.72	-0.513	0.0532	21.64	0.639	0.2649
22.67	0.632	0.2834	-8.70	-0.586	0.0730	22.43	0.639	0.2733
23.72	0.635	0.2982	-9.77	-0.654	0.0974	23.57	0.647	0.2909
24.69	0.645	0.3146	-10.74	-0.672	0.1156	24.63	0.653	0.3075
25.66	0.653	0.3301	-11.79	-0.663	0.1353	25.59	0.661	0.3217
			-12.75	-0.643	0.1477	26.74	0.665	0.3395
			-13.72	-0.630	0.1588	27.62	0.668	0.3533

28.67	0.673	0.3694	Run: 0405ga	29.45	0.684	0.3841		
29.64	0.682	0.3882	$Re = 99998.0$	28.49	0.678	0.3664		
29.64	0.680	0.3890	α	C_L	C_D	27.34	0.674	0.3479
28.41	0.673	0.3662	-14.68	-0.639	0.1747	26.46	0.670	0.3337
27.44	0.671	0.3519	-13.63	-0.660	0.1637	25.41	0.662	0.3180
26.39	0.665	0.3343	-12.66	-0.679	0.1526	24.44	0.657	0.3011
25.42	0.661	0.3214	-11.61	-0.693	0.1362	23.47	0.653	0.2874
24.36	0.654	0.3025	-10.82	-0.698	0.1246	22.33	0.645	0.2708
23.48	0.645	0.2892	-9.67	-0.663	0.0980	21.45	0.643	0.2599
22.34	0.642	0.2731	-8.60	-0.595	0.0760	20.39	0.641	0.2452
21.46	0.638	0.2619	-7.53	-0.516	0.0518	19.60	0.639	0.2349
20.40	0.635	0.2466	-6.91	-0.474	0.0440	18.64	0.640	0.2248
19.44	0.634	0.2347	-5.57	-0.390	0.0302	17.32	0.649	0.2091
18.38	0.636	0.2224	-4.59	-0.322	0.0240	16.35	0.659	0.1964
17.33	0.639	0.2100	-3.61	-0.255	0.0199	15.39	0.670	0.1868
16.36	0.644	0.1983	-2.54	-0.157	0.0173	14.34	0.689	0.1722
15.57	0.653	0.1896	-1.55	-0.090	0.0161	13.46	0.704	0.1618
14.43	0.669	0.1750	-0.49	-0.029	0.0165	12.41	0.718	0.1485
13.47	0.687	0.1641	0.49	0.029	0.0164	11.36	0.715	0.1341
12.42	0.700	0.1493	1.47	0.095	0.0178	10.47	0.696	0.1189
11.45	0.703	0.1346	2.54	0.166	0.0202	9.41	0.660	0.1036
10.39	0.682	0.1177	3.53	0.255	0.0252	8.43	0.606	0.0844
9.42	0.636	0.0984	4.60	0.334	0.0318	7.54	0.540	0.0652
8.35	0.574	0.0781	5.58	0.408	0.0399	6.29	0.459	0.0456
7.37	0.501	0.0602	6.56	0.477	0.0529	5.40	0.391	0.0358
6.39	0.428	0.0440	7.63	0.558	0.0723	4.33	0.317	0.0269
5.41	0.368	0.0358	8.62	0.641	0.0985	3.35	0.242	0.0214
4.42	0.297	0.0281	9.42	0.683	0.1139	2.63	0.182	0.0176
3.36	0.223	0.0218	10.65	0.714	0.1364	1.21	0.089	0.0146
2.55	0.174	0.0194	11.62	0.715	0.1475	0.32	0.031	0.0126
1.31	0.091	0.0168	12.67	0.706	0.1584	-0.75	-0.027	0.0131
0.33	0.030	0.0138	13.73	0.694	0.1696	-1.82	-0.094	0.0135
-0.65	-0.034	0.0137	14.60	0.683	0.1795	-2.71	-0.154	0.0152
-1.72	-0.095	0.0140	15.65	0.659	0.1893	-3.70	-0.245	0.0175
-2.70	-0.158	0.0160	16.62	0.654	0.2020	-4.77	-0.322	0.0228
-3.68	-0.228	0.0171	17.58	0.649	0.2127	-5.57	-0.379	0.0282
-4.75	-0.313	0.0225	18.72	0.640	0.2241	-6.82	-0.464	0.0405
-5.73	-0.377	0.0295	19.60	0.641	0.2360	-7.89	-0.534	0.0565
-6.80	-0.450	0.0400	20.57	0.644	0.2494	-8.87	-0.613	0.0798
-7.79	-0.522	0.0557	21.62	0.643	0.2614	-9.94	-0.679	0.1060
-8.77	-0.596	0.0764	22.68	0.650	0.2762	-10.82	-0.698	0.1251
-9.84	-0.663	0.1023	23.65	0.652	0.2899	-11.88	-0.691	0.1418
-10.81	-0.687	0.1227	24.70	0.660	0.3070	-12.84	-0.674	0.1563
-11.77	-0.679	0.1379	25.67	0.664	0.3207	-13.80	-0.655	0.1670
-12.82	-0.663	0.1533	26.64	0.672	0.3375	-14.59	-0.638	0.1746
-13.79	-0.642	0.1650	27.61	0.676	0.3527			
-14.58	-0.632	0.1732	28.75	0.682	0.3725			
			29.63	0.686	0.3882			

Run: 0406ga			29.30	0.683	0.3839	AR4-l075-FP1
$Re = 120000.2$			28.24	0.677	0.3650	Fig. 5.9
α	C_L	C_D	27.28	0.673	0.3481	
-15.01	-0.646	0.1856	26.48	0.667	0.3366	
-13.78	-0.663	0.1680	25.34	0.664	0.3194	
-13.08	-0.675	0.1602	24.29	0.658	0.3015	
-11.77	-0.701	0.1426	23.32	0.651	0.2880	
-10.80	-0.705	0.1260	22.17	0.648	0.2720	
-9.83	-0.685	0.1061	21.29	0.644	0.2598	
-8.76	-0.630	0.0847	20.24	0.641	0.2453	
-7.78	-0.546	0.0572	19.45	0.641	0.2352	
-6.89	-0.499	0.0461	18.57	0.645	0.2248	
-5.73	-0.417	0.0309	17.16	0.651	0.2088	
-4.75	-0.356	0.0248	16.55	0.658	0.2016	
-3.68	-0.280	0.0194	15.32	0.674	0.1865	
-2.70	-0.196	0.0161	14.28	0.699	0.1744	
-1.98	-0.136	0.0148	13.31	0.716	0.1637	
-0.64	-0.036	0.0146	12.26	0.726	0.1483	
0.42	0.024	0.0150	11.29	0.723	0.1353	
1.32	0.090	0.0163	10.32	0.702	0.1184	
2.48	0.182	0.0191	9.26	0.672	0.1055	
3.37	0.268	0.0244	8.20	0.640	0.0946	
4.36	0.346	0.0302	7.30	0.569	0.0721	
5.25	0.416	0.0393	6.23	0.489	0.0485	
6.41	0.516	0.0566	5.16	0.407	0.0368	
7.49	0.594	0.0820	4.18	0.329	0.0269	
8.56	0.672	0.1076	3.19	0.251	0.0215	
9.27	0.704	0.1231	2.12	0.152	0.0148	
10.59	0.726	0.1400	1.14	0.090	0.0140	
11.47	0.726	0.1500	0.16	0.032	0.0126	
12.43	0.718	0.1608	-0.82	-0.027	0.0127	
13.40	0.704	0.1709	-1.89	-0.095	0.0130	
14.36	0.688	0.1798	-2.96	-0.169	0.0148	
15.50	0.670	0.1904	-3.86	-0.264	0.0183	
16.46	0.657	0.2021	-4.92	-0.337	0.0227	
17.43	0.647	0.2111	-5.91	-0.404	0.0288	
18.57	0.642	0.2239	-6.97	-0.476	0.0388	
19.45	0.640	0.2356	-7.96	-0.546	0.0564	
20.41	0.641	0.2480	-8.94	-0.622	0.0816	
21.47	0.643	0.2615	-10.01	-0.687	0.1067	
22.44	0.649	0.2755	-10.98	-0.707	0.1253	
23.49	0.654	0.2900	-12.03	-0.702	0.1434	
24.46	0.660	0.3068	-12.99	-0.678	0.1590	
25.43	0.665	0.3212	-13.96	-0.664	0.1708	
26.57	0.670	0.3370	-15.01	-0.641	0.1823	
27.36	0.675	0.3519				
28.51	0.680	0.3708				
29.48	0.684	0.3870				

27.34	0.690	0.3835	-13.91	-0.624	0.1729	29.32	0.700	0.4171
28.48	0.693	0.4013				30.29	0.702	0.4312
29.53	0.698	0.4200	Run: 0413ar			30.11	0.703	0.4289
30.50	0.703	0.4382	$Re = 79996.1$			29.06	0.697	0.4113
30.24	0.697	0.4306	α	C_L	C_D	28.27	0.694	0.3985
29.36	0.699	0.4183	-14.21	-0.642	0.1772	27.12	0.690	0.3774
28.22	0.695	0.3972	-12.98	-0.648	0.1601	26.07	0.684	0.3587
27.34	0.692	0.3855	-12.02	-0.659	0.1468	25.01	0.677	0.3428
26.28	0.681	0.3613	-11.06	-0.668	0.1312	24.04	0.674	0.3276
25.31	0.673	0.3469	-9.91	-0.662	0.1115	22.99	0.664	0.3114
24.25	0.670	0.3295	-9.03	-0.630	0.0939	22.11	0.658	0.2958
23.37	0.661	0.3161	-7.96	-0.564	0.0712	21.14	0.656	0.2834
22.32	0.657	0.2996	-7.24	-0.507	0.0566	20.08	0.652	0.2677
21.26	0.654	0.2867	-5.99	-0.422	0.0401	19.12	0.650	0.2547
20.29	0.650	0.2704	-5.01	-0.349	0.0308	17.97	0.647	0.2399
19.33	0.649	0.2585	-3.94	-0.286	0.0255	17.18	0.648	0.2289
18.27	0.643	0.2440	-2.95	-0.194	0.0210	16.13	0.650	0.2169
17.39	0.642	0.2335	-1.88	-0.125	0.0199	14.99	0.655	0.2028
16.25	0.642	0.2168	-0.81	-0.058	0.0195	14.37	0.659	0.1939
15.28	0.645	0.2064	0.17	0.012	0.0203	13.14	0.661	0.1784
14.49	0.643	0.1963	1.24	0.081	0.0223	12.09	0.673	0.1643
13.35	0.644	0.1809	2.13	0.146	0.0238	11.04	0.680	0.1499
12.30	0.654	0.1650	3.29	0.247	0.0286	10.25	0.679	0.1366
11.33	0.659	0.1530	4.19	0.321	0.0348	9.10	0.655	0.1122
10.28	0.661	0.1342	5.17	0.390	0.0424	8.12	0.599	0.0896
9.31	0.647	0.1166	6.25	0.469	0.0574	7.23	0.540	0.0728
8.24	0.589	0.0922	7.23	0.537	0.0736	6.06	0.448	0.0500
7.26	0.512	0.0700	8.39	0.620	0.0995	5.08	0.380	0.0399
6.19	0.442	0.0535	9.28	0.663	0.1202	4.01	0.310	0.0319
5.21	0.374	0.0430	10.25	0.681	0.1404	3.12	0.238	0.0255
4.31	0.306	0.0338	11.39	0.677	0.1571	2.04	0.149	0.0207
3.24	0.219	0.0264	12.35	0.666	0.1700	0.89	0.081	0.0193
2.08	0.148	0.0226	13.23	0.659	0.1812	0.26	0.041	0.0184
1.19	0.084	0.0214	14.29	0.659	0.1962	-1.08	-0.050	0.0173
0.39	0.039	0.0195	15.25	0.651	0.2071	-2.06	-0.115	0.0171
-0.86	-0.044	0.0207	16.39	0.651	0.2230	-3.13	-0.190	0.0188
-1.84	-0.106	0.0191	17.09	0.651	0.2305	-3.94	-0.269	0.0218
-2.91	-0.176	0.0212	18.24	0.650	0.2474	-4.83	-0.334	0.0278
-3.90	-0.261	0.0239	19.29	0.647	0.2582	-6.17	-0.433	0.0401
-4.62	-0.317	0.0294	20.26	0.652	0.2734	-7.15	-0.503	0.0549
-5.77	-0.385	0.0344	21.32	0.657	0.2869	-8.22	-0.582	0.0770
-6.93	-0.470	0.0510	22.37	0.662	0.3013	-8.94	-0.631	0.0940
-8.01	-0.545	0.0689	23.34	0.667	0.3151	-10.18	-0.668	0.1208
-8.99	-0.621	0.0943	24.39	0.672	0.3317	-11.14	-0.668	0.1372
-9.70	-0.643	0.1059	25.36	0.682	0.3492	-12.20	-0.660	0.1538
-11.01	-0.643	0.1312	26.16	0.682	0.3607	-13.16	-0.648	0.1660
-11.98	-0.635	0.1476	27.30	0.690	0.3812	-14.21	-0.646	0.1807
-13.03	-0.634	0.1611	28.27	0.693	0.3969			

Run: 0415ar		30.05	0.703	0.4283	Run: 0414ar			
$Re = 99998.0$		29.08	0.699	0.4109	$Re = 119996.7$			
α	C_L	C_D			α	C_L	C_D	
-14.28	-0.654	0.1817	27.94	0.693	0.3893	-14.41	-0.665	0.1798
-13.05	-0.666	0.1614	27.06	0.692	0.3769	-13.00	-0.682	0.1584
-12.09	-0.680	0.1484	26.09	0.689	0.3618	-12.13	-0.693	0.1455
-11.12	-0.683	0.1327	25.04	0.685	0.3461	-11.07	-0.694	0.1274
-10.07	-0.676	0.1142	24.07	0.675	0.3260	-10.10	-0.680	0.1088
-9.09	-0.647	0.0955	22.92	0.667	0.3095	-9.13	-0.644	0.0908
-8.02	-0.579	0.0726	22.04	0.659	0.2936	-8.24	-0.595	0.0754
-6.95	-0.505	0.0506	21.07	0.655	0.2818	-7.08	-0.512	0.0497
-6.06	-0.439	0.0378	20.02	0.653	0.2659	-6.10	-0.450	0.0371
-4.90	-0.364	0.0288	19.05	0.654	0.2554	-5.21	-0.397	0.0295
-4.01	-0.302	0.0245	17.91	0.650	0.2399	-4.04	-0.310	0.0235
-3.02	-0.223	0.0196	16.94	0.652	0.2277	-3.06	-0.240	0.0185
-1.95	-0.132	0.0181	16.07	0.659	0.2166	-1.98	-0.133	0.0167
-0.88	-0.065	0.0182	14.93	0.664	0.2032	-1.00	-0.067	0.0162
0.10	0.008	0.0182	14.05	0.675	0.1924	-0.11	-0.009	0.0169
1.17	0.079	0.0206	12.99	0.675	0.1788	1.05	0.085	0.0179
2.07	0.152	0.0219	12.03	0.689	0.1637	2.04	0.167	0.0199
3.15	0.265	0.0277	11.07	0.696	0.1514	3.12	0.278	0.0269
4.13	0.340	0.0341	10.01	0.689	0.1314	4.10	0.349	0.0326
5.20	0.408	0.0422	9.04	0.668	0.1141	5.17	0.419	0.0415
6.18	0.480	0.0549	8.06	0.612	0.0896	6.15	0.489	0.0538
6.99	0.534	0.0700	6.90	0.524	0.0641	7.13	0.560	0.0752
8.33	0.634	0.1005	5.91	0.457	0.0486	8.03	0.624	0.0944
9.21	0.677	0.1214	5.02	0.392	0.0386	9.18	0.687	0.1209
10.27	0.691	0.1391	3.86	0.317	0.0294	10.24	0.705	0.1409
11.33	0.695	0.1581	3.15	0.264	0.0244	11.21	0.738	0.1616
12.29	0.686	0.1711	1.80	0.144	0.0180	12.19	0.776	0.1837
13.17	0.675	0.1827	0.82	0.082	0.0166	13.25	0.784	0.2028
14.31	0.666	0.1964	-0.07	0.019	0.0158	14.28	0.702	0.2027
15.28	0.661	0.2092	-1.14	-0.057	0.0140	15.15	0.673	0.2092
16.33	0.652	0.2212	-2.12	-0.126	0.0162	16.30	0.663	0.2206
17.03	0.651	0.2304	-3.11	-0.219	0.0174	17.17	0.655	0.2315
18.17	0.649	0.2447	-4.01	-0.294	0.0219	18.23	0.653	0.2440
19.23	0.650	0.2573	-4.90	-0.365	0.0286	19.19	0.654	0.2567
20.20	0.655	0.2716	-6.33	-0.466	0.0429	20.16	0.657	0.2711
21.25	0.657	0.2845	-7.22	-0.534	0.0586	21.13	0.660	0.2833
22.31	0.664	0.3001	-8.21	-0.611	0.0816	22.27	0.663	0.2986
23.27	0.669	0.3147	-9.27	-0.665	0.1041	22.98	0.668	0.3096
24.33	0.678	0.3326	-10.24	-0.681	0.1225	24.21	0.674	0.3293
25.21	0.688	0.3496	-11.21	-0.683	0.1375	25.27	0.684	0.3473
26.27	0.688	0.3634	-12.26	-0.675	0.1539	26.15	0.689	0.3618
27.24	0.695	0.3822	-13.23	-0.662	0.1658	27.20	0.698	0.3814
28.20	0.698	0.3979	-14.28	-0.657	0.1812	27.99	0.697	0.3906
29.26	0.703	0.4175				29.31	0.710	0.4189
30.23	0.708	0.4350				30.28	0.710	0.4338

			AR4-I100-FP1		
30.02	0.704	0.4270	Fig. 5.10		
29.05	0.707	0.4140			
27.99	0.699	0.3924			
27.20	0.695	0.3790	Run: 0396cs		
26.06	0.687	0.3589	$Re = 59998.4$		
25.00	0.682	0.3425	α	C_L	C_D
24.03	0.674	0.3258	-14.61	-0.660	0.1811
22.98	0.667	0.3089	-13.56	-0.656	0.1621
21.92	0.662	0.2934	-12.59	-0.644	0.1472
21.04	0.657	0.2808	-11.54	-0.654	0.1300
19.98	0.656	0.2663	-10.57	-0.647	0.1147
19.02	0.653	0.2529	-9.51	-0.632	0.0940
17.96	0.656	0.2403	-8.53	-0.588	0.0739
16.91	0.660	0.2274	-7.55	-0.505	0.0527
16.03	0.666	0.2179	-6.83	-0.460	0.0438
14.89	0.673	0.2038	-5.41	-0.374	0.0300
14.02	0.710	0.1979	-4.52	-0.312	0.0244
13.06	0.730	0.1865	-3.44	-0.224	0.0196
11.91	0.716	0.1663	-2.46	-0.159	0.0179
11.03	0.709	0.1507	-1.39	-0.091	0.0176
9.97	0.700	0.1325	-0.41	-0.028	0.0176
9.00	0.671	0.1112	0.57	0.039	0.0185
8.02	0.618	0.0906	1.55	0.097	0.0206
6.95	0.528	0.0623	2.62	0.169	0.0234
5.97	0.464	0.0462	3.60	0.241	0.0267
4.99	0.399	0.0361	4.59	0.318	0.0344
3.92	0.322	0.0288	5.66	0.392	0.0435
2.93	0.252	0.0233	6.64	0.456	0.0573
1.86	0.145	0.0176	7.80	0.540	0.0756
0.88	0.081	0.0154	8.51	0.582	0.0899
0.07	0.031	0.0150	9.67	0.626	0.1130
-1.18	-0.067	0.0154	10.55	0.635	0.1239
-2.25	-0.138	0.0160	11.69	0.635	0.1434
-3.15	-0.248	0.0189	12.66	0.635	0.1576
-4.23	-0.331	0.0244	13.71	0.640	0.1718
-4.94	-0.384	0.0282	14.68	0.652	0.1898
-6.28	-0.476	0.0406	15.74	0.660	0.2057
-7.26	-0.550	0.0607	16.71	0.668	0.2207
-8.33	-0.623	0.0829	17.67	0.667	0.2339
-9.31	-0.671	0.1037	18.73	0.668	0.2484
-10.28	-0.690	0.1214	19.70	0.672	0.2620
-11.34	-0.695	0.1360	20.66	0.671	0.2742
-12.30	-0.685	0.1495	21.72	0.673	0.2886
-13.27	-0.675	0.1635	22.69	0.681	0.3026
-14.41	-0.667	0.1784	23.74	0.689	0.3184
			24.71	0.699	0.3381
			25.68	0.712	0.3568

-14.52	-0.653	0.1752	28.86	0.754	0.4231	Run: 0394cs
			29.82	0.745	0.4352	$Re = 99996.1$
Run: 0395cs			29.56	0.757	0.4384	
$Re = 79997.4$			28.59	0.745	0.4148	
α	C_L	C_D	27.45	0.737	0.3944	α
-14.79	-0.679	0.1850	26.48	0.722	0.3719	-0.691
-13.47	-0.672	0.1630	25.59	0.703	0.3503	0.1856
-12.86	-0.670	0.1530	24.45	0.694	0.3317	-13.64
-11.63	-0.674	0.1333	23.75	0.685	0.3175	-0.692
-10.57	-0.667	0.1147	22.43	0.686	0.3005	0.1661
-9.60	-0.644	0.0937	21.46	0.682	0.2867	-12.68
-8.53	-0.590	0.0721	20.49	0.679	0.2716	-0.689
-7.46	-0.517	0.0521	19.52	0.679	0.2584	0.1509
-6.75	-0.468	0.0416	18.56	0.680	0.2455	-11.62
-5.50	-0.383	0.0290	17.50	0.683	0.2319	-0.692
-4.52	-0.322	0.0231	16.45	0.679	0.2180	0.1335
-3.44	-0.239	0.0189	15.57	0.676	0.2038	-10.83
-2.46	-0.164	0.0177	14.51	0.668	0.1860	-0.689
-1.39	-0.095	0.0168	13.54	0.660	0.1717	0.1228
-0.50	-0.032	0.0171	12.40	0.658	0.1536	-9.59
0.57	0.037	0.0177	11.52	0.655	0.1396	-0.656
1.55	0.095	0.0193	10.47	0.648	0.1220	0.0951
2.62	0.169	0.0213	9.49	0.624	0.1031	-8.61
3.61	0.257	0.0266	8.51	0.571	0.0807	-0.605
4.59	0.326	0.0325	7.53	0.502	0.0616	0.0754
5.75	0.397	0.0421	6.46	0.422	0.0435	-10.83
6.73	0.462	0.0554	5.48	0.355	0.0337	-0.689
7.72	0.541	0.0739	4.41	0.288	0.0264	0.1228
8.70	0.605	0.0969	3.42	0.208	0.0200	-9.59
9.76	0.637	0.1139	2.35	0.137	0.0161	-0.656
10.82	0.652	0.1326	1.37	0.074	0.0154	0.0951
11.79	0.657	0.1469	0.39	0.015	0.0129	-8.61
12.75	0.661	0.1622	-0.59	-0.039	0.0133	-0.605
13.81	0.663	0.1777	-1.74	-0.108	0.0130	0.0754
14.69	0.669	0.1927	-2.64	-0.174	0.0147	-10.83
15.83	0.675	0.2087	-3.62	-0.252	0.0169	-0.689
16.62	0.679	0.2216	-4.69	-0.331	0.0227	0.2369
17.68	0.677	0.2348	-5.67	-0.398	0.0291	0.2490
18.47	0.676	0.2451	-6.75	-0.471	0.0401	0.2613
19.79	0.679	0.2619	-7.82	-0.544	0.0581	0.266
20.67	0.679	0.2752	-8.71	-0.611	0.0787	0.686
21.64	0.686	0.2902	-9.78	-0.658	0.1025	0.2765
22.78	0.689	0.3055	-10.74	-0.673	0.1202	0.687
23.75	0.693	0.3213	-11.80	-0.674	0.1370	0.2885
24.80	0.698	0.3378	-12.77	-0.672	0.1533	0.3055
25.77	0.711	0.3552	-13.73	-0.674	0.1676	0.3205
26.48	0.722	0.3718	-14.79	-0.681	0.1859	0.3344
27.71	0.740	0.3986				0.3548
						0.3750
						0.3941
						0.4165
						0.4306

29.66	0.751	0.4353	Run: 0399cs			29.49	0.747	0.4315
28.51	0.735	0.4059	$Re = 120000.9$			28.52	0.739	0.4118
27.45	0.730	0.3863	α	C_L	C_D	27.47	0.727	0.3894
26.40	0.718	0.3661	-14.87	-0.722	0.1906	26.50	0.725	0.3729
25.43	0.706	0.3487	-13.55	-0.709	0.1682	25.44	0.714	0.3547
24.46	0.698	0.3285	-12.67	-0.710	0.1532	24.47	0.700	0.3327
23.49	0.691	0.3137	-11.70	-0.717	0.1359	23.50	0.695	0.3174
22.35	0.689	0.2970	-10.64	-0.705	0.1170	22.45	0.691	0.2998
21.47	0.687	0.2858	-9.67	-0.663	0.0954	21.48	0.690	0.2884
20.41	0.683	0.2703	-8.87	-0.621	0.0794	20.43	0.695	0.2760
19.45	0.684	0.2561	-7.62	-0.529	0.0486	19.64	0.694	0.2642
18.48	0.684	0.2426	-6.90	-0.488	0.0398	18.67	0.697	0.2523
17.43	0.686	0.2299	-5.57	-0.403	0.0287	17.35	0.702	0.2345
16.46	0.693	0.2173	-4.59	-0.336	0.0240	16.39	0.702	0.2201
15.49	0.687	0.2028	-3.60	-0.267	0.0189	15.51	0.697	0.2062
14.44	0.676	0.1839	-2.52	-0.165	0.0169	14.45	0.694	0.1878
13.47	0.676	0.1708	-1.46	-0.098	0.0160	13.40	0.692	0.1747
12.50	0.673	0.1537	-0.47	-0.032	0.0164			
11.45	0.670	0.1382	0.51	0.035	0.0173			
10.39	0.659	0.1202	1.49	0.095	0.0185			
9.59	0.641	0.1061	2.56	0.183	0.0215			
8.35	0.575	0.0789	3.54	0.256	0.0258			
7.36	0.501	0.0583	4.53	0.327	0.0316			
6.38	0.427	0.0408	5.42	0.386	0.0383			
5.58	0.378	0.0331	6.40	0.453	0.0480			
4.33	0.290	0.0236	7.65	0.558	0.0766			
3.35	0.218	0.0183	8.64	0.625	0.1001			
2.36	0.130	0.0139	9.61	0.660	0.1189			
1.29	0.068	0.0130	10.76	0.682	0.1392			
0.31	0.016	0.0115	11.64	0.688	0.1537			
-0.58	-0.043	0.0114	12.61	0.686	0.1676			
-1.74	-0.115	0.0121	13.66	0.691	0.1840			
-2.81	-0.186	0.0141	14.63	0.693	0.1978			
-3.71	-0.274	0.0174	15.77	0.701	0.2160			
-4.78	-0.344	0.0221	16.39	0.702	0.2252			
-5.49	-0.395	0.0264	17.70	0.698	0.2413			
-6.92	-0.484	0.0380	18.67	0.698	0.2560			
-7.81	-0.550	0.0554	19.64	0.690	0.2668			
-8.79	-0.623	0.0783	20.69	0.691	0.2813			
-9.86	-0.669	0.1006	21.66	0.691	0.2944			
-10.83	-0.688	0.1193	22.63	0.692	0.3070			
-11.89	-0.693	0.1355	23.68	0.693	0.3228			
-12.94	-0.689	0.1518	24.74	0.702	0.3397			
-13.82	-0.696	0.1667	25.62	0.710	0.3546			
-14.88	-0.710	0.1869	26.68	0.727	0.3795			
			27.65	0.744	0.4024			
			28.79	0.744	0.4205			
			29.76	0.742	0.4332			

AR5-l100-FP1

Fig. 5.11

Run: 0420ga

 $Re = 59999.7$

α	C_L	C_D
-15.75	-0.688	0.2000
-14.43	-0.669	0.1775
-13.55	-0.659	0.1623
-12.49	-0.653	0.1459
-11.52	-0.652	0.1307
-10.56	-0.656	0.1145
-9.41	-0.650	0.0968
-8.44	-0.620	0.0763
-7.54	-0.549	0.0574
-6.38	-0.466	0.0405
-5.48	-0.401	0.0314
-4.40	-0.327	0.0257
-3.41	-0.233	0.0209
-2.34	-0.158	0.0208
-1.35	-0.091	0.0201
-0.36	-0.025	0.0207
0.62	0.042	0.0218
1.70	0.120	0.0237
2.68	0.185	0.0270
3.59	0.279	0.0344
4.75	0.364	0.0430
5.74	0.429	0.0546
6.81	0.513	0.0731

7.80	0.589	0.0956	2.50	0.182	0.0241	9.52	0.652	0.1246
8.78	0.625	0.1154	1.43	0.111	0.0209	10.84	0.654	0.1472
9.66	0.631	0.1293	0.35	0.038	0.0195	11.72	0.651	0.1603
10.80	0.630	0.1484	-0.63	-0.031	0.0184	12.86	0.657	0.1778
11.77	0.632	0.1635	-1.53	-0.098	0.0179	13.74	0.664	0.1915
12.83	0.638	0.1795	-2.69	-0.171	0.0178	14.89	0.683	0.2122
13.88	0.649	0.1953	-3.59	-0.244	0.0187	15.77	0.689	0.2270
14.85	0.664	0.2131	-4.58	-0.334	0.0239	16.56	0.694	0.2379
15.91	0.675	0.2307	-5.48	-0.397	0.0299	17.88	0.697	0.2578
16.79	0.682	0.2451	-6.64	-0.483	0.0415	18.85	0.697	0.2710
17.85	0.679	0.2589	-7.72	-0.566	0.0592	19.82	0.697	0.2847
18.81	0.684	0.2740	-8.44	-0.617	0.0759	20.78	0.698	0.2974
19.78	0.690	0.2901	-9.50	-0.652	0.0971	21.75	0.704	0.3128
20.84	0.687	0.3023	-10.82	-0.654	0.1226	22.81	0.706	0.3272
21.81	0.700	0.3206	-11.70	-0.652	0.1350	23.78	0.722	0.3482
22.86	0.701	0.3333	-12.76	-0.655	0.1525	24.84	0.749	0.3744
23.92	0.716	0.3549	-13.73	-0.663	0.1667	25.91	0.800	0.4160
24.89	0.728	0.3739	-14.70	-0.678	0.1847	26.53	0.826	0.4392
25.95	0.752	0.4032	-15.75	-0.689	0.2034	27.93	0.802	0.4503
26.84	0.783	0.4300				28.81	0.808	0.4701
27.63	0.788	0.4465	Run: 0421ga			28.55	0.811	0.4677
28.87	0.811	0.4807	$Re = 79999.2$			27.67	0.802	0.4457
28.69	0.813	0.4779	α	C_L	C_D	26.62	0.827	0.4398
27.72	0.796	0.4505	-15.82	-0.705	0.2043	25.64	0.771	0.3972
26.66	0.772	0.4205	-14.49	-0.685	0.1793	24.66	0.727	0.3619
25.60	0.741	0.3895	-13.61	-0.678	0.1636	23.51	0.716	0.3404
24.72	0.733	0.3730	-12.55	-0.672	0.1477	22.81	0.701	0.3255
23.57	0.709	0.3446	-11.59	-0.674	0.1327	21.57	0.700	0.3070
22.60	0.699	0.3293	-10.62	-0.673	0.1152	20.61	0.699	0.2945
21.81	0.696	0.3168	-9.56	-0.665	0.0976	19.55	0.701	0.2793
20.57	0.695	0.3002	-8.50	-0.629	0.0759	18.50	0.698	0.2639
19.61	0.692	0.2838	-7.60	-0.565	0.0575	17.53	0.691	0.2472
18.55	0.689	0.2694	-6.44	-0.478	0.0376	16.56	0.697	0.2362
17.67	0.683	0.2541	-5.45	-0.413	0.0282	15.51	0.685	0.2171
16.53	0.682	0.2396	-4.55	-0.345	0.0235	14.54	0.675	0.2017
15.56	0.675	0.2219	-3.39	-0.257	0.0183	13.57	0.660	0.1822
14.59	0.660	0.2059	-2.48	-0.169	0.0179	12.51	0.656	0.1683
13.53	0.644	0.1863	-1.32	-0.091	0.0172	11.54	0.652	0.1517
12.56	0.637	0.1730	-0.33	-0.024	0.0178	10.49	0.654	0.1378
11.68	0.633	0.1578	0.56	0.041	0.0189	9.61	0.651	0.1215
10.54	0.631	0.1423	1.64	0.118	0.0207	8.55	0.634	0.1023
9.66	0.634	0.1269	2.63	0.204	0.0233	7.57	0.587	0.0816
8.51	0.622	0.1080	3.62	0.299	0.0314	6.58	0.506	0.0593
7.62	0.577	0.0873	4.70	0.375	0.0383	5.41	0.425	0.0414
6.72	0.503	0.0675	5.68	0.446	0.0497	4.52	0.355	0.0326
5.56	0.421	0.0497	6.76	0.531	0.0700	3.53	0.288	0.0256
4.57	0.354	0.0405	7.75	0.605	0.0920	2.45	0.184	0.0191
3.50	0.272	0.0309	8.73	0.642	0.1122	1.37	0.110	0.0157

0.39	0.039	0.0144	11.81	0.676	0.1618
-0.33	-0.006	0.0134	12.86	0.675	0.1768
-1.59	-0.099	0.0127	13.74	0.677	0.1906
-2.75	-0.181	0.0137	13.57	0.686	0.1877
-3.66	-0.277	0.0158	12.60	0.681	0.1752
-4.64	-0.357	0.0217	11.54	0.680	0.1571
-5.72	-0.429	0.0287	10.48	0.667	0.1401
-6.71	-0.504	0.0410	9.52	0.664	0.1225
-7.78	-0.585	0.0610	8.54	0.645	0.1045
-8.77	-0.649	0.0842	7.56	0.593	0.0818
-9.83	-0.671	0.1043	6.58	0.516	0.0605
-10.80	-0.674	0.1221	5.41	0.435	0.0415
-11.76	-0.673	0.1368	4.51	0.366	0.0332
-12.73	-0.674	0.1508	3.44	0.290	0.0255
-13.79	-0.680	0.1687	2.36	0.204	0.0197
-14.49	-0.686	0.1796	1.37	0.113	0.0158
-15.82	-0.706	0.2041	0.38	0.038	0.0152
			-0.70	-0.039	0.0138
Run: 0423ga			-1.60	-0.115	0.0144
$Re = 99996.3$			-2.67	-0.202	0.0142
α	C_L	C_D	-3.67	-0.310	0.0194
-15.82	-0.710	0.2014	-4.66	-0.388	0.0241
-14.50	-0.704	0.1783	-5.47	-0.447	0.0300
-13.62	-0.689	0.1616	-6.45	-0.513	0.0409
-12.65	-0.682	0.1444	-7.80	-0.614	0.0685
-11.51	-0.685	0.1287	-8.87	-0.663	0.0888
-10.54	-0.683	0.1116	-9.75	-0.681	0.1058
-9.48	-0.670	0.0932	-10.81	-0.687	0.1226
-8.59	-0.627	0.0717	-11.77	-0.687	0.1373
-7.52	-0.558	0.0521	-12.74	-0.686	0.1514
-6.44	-0.486	0.0356	-13.80	-0.690	0.1682
-5.55	-0.424	0.0273	-14.77	-0.702	0.1838
-4.56	-0.356	0.0221	-15.73	-0.713	0.2007
-3.40	-0.270	0.0172			
-2.49	-0.168	0.0151			
-1.60	-0.115	0.0154			
-0.34	-0.025	0.0159			
0.65	0.047	0.0169			
1.63	0.125	0.0184			
2.63	0.235	0.0230			
3.62	0.313	0.0296			
4.70	0.391	0.0362			
5.68	0.461	0.0476			
6.76	0.542	0.0687			
7.75	0.617	0.0920			
8.72	0.654	0.1121			
9.87	0.667	0.1309			
10.75	0.674	0.1460			

Appendix C

Tabulated Lift and Moment Data

Appendix C contains all of the lift and moment data seen in Chapter 5. The data presented in this appendix is identified by airfoil name, figure number, and run number. The airfoil name is an identification given during testing. For example, the ‘CHK-STD-1’ refers to the Wortmann FX 63-137 *R*-4 rectangular wing. For a flat-plate wing example, in ‘AR2-l050-FP1’, ’AR2’ refers to an aspect ratio 2 wing, ’l050’ refers to a taper ratio of 0.5, and FP1 refers to the specific model number.

CHK-STD-1								
Fig. 5.1			23.14	0.884	-0.1582	-8.83	-0.204	-0.0193
Run: 0431aj			22.26	0.884	-0.1574	-7.96	-0.218	-0.0202
$Re = 39998.3$			21.11	0.874	-0.1580	-7.00	-0.240	-0.0221
α	C_L	C_M	20.15	0.876	-0.1568	-5.86	-0.262	-0.0325
-15.17	-0.219	-0.0178	19.00	0.857	-0.1558	-5.15	-0.238	-0.0535
-13.93	-0.203	-0.0189	18.38	0.848	-0.1547	-3.96	-0.011	-0.1243
-13.14	-0.203	-0.0187	17.06	0.844	-0.1527	-3.06	0.066	-0.1310
-12.00	-0.195	-0.0189	16.09	0.817	-0.1478	-1.80	0.184	-0.1408
-10.94	-0.195	-0.0196	15.30	0.805	-0.1484	-1.09	0.246	-0.1431
-9.97	-0.193	-0.0184	14.06	0.767	-0.1414	0.25	0.313	-0.1370
-8.83	-0.199	-0.0182	13.00	0.750	-0.1395	1.13	0.344	-0.1303
-7.96	-0.212	-0.0186	12.12	0.730	-0.1365	2.19	0.375	-0.1240
-7.00	-0.233	-0.0200	10.97	0.701	-0.1360	3.17	0.414	-0.1222
-5.95	-0.263	-0.0246	10.08	0.677	-0.1318	4.23	0.466	-0.1261
-4.97	-0.230	-0.0555	9.02	0.637	-0.1315	5.21	0.523	-0.1310
-3.96	-0.047	-0.1099	8.04	0.603	-0.1276	6.28	0.575	-0.1344
-2.89	0.059	-0.1249	7.07	0.567	-0.1271	7.34	0.617	-0.1368
-1.90	0.145	-0.1303	5.92	0.525	-0.1235	8.32	0.656	-0.1387
-1.10	0.185	-0.1284	5.03	0.478	-0.1213	8.94	0.676	-0.1398
0.14	0.230	-0.1124	3.96	0.417	-0.1151	10.27	0.726	-0.1422
1.12	0.271	-0.1068	2.98	0.375	-0.1123	11.24	0.750	-0.1434
2.18	0.325	-0.1082	2.00	0.322	-0.1064	12.21	0.779	-0.1451
3.16	0.377	-0.1131	0.94	0.262	-0.1068	13.36	0.803	-0.1483
4.23	0.430	-0.1168	-0.04	0.224	-0.1122	14.33	0.825	-0.1506
5.20	0.478	-0.1215	-1.10	0.192	-0.1268	15.39	0.848	-0.1533
6.27	0.533	-0.1247	-2.08	0.135	-0.1294	16.27	0.861	-0.1556
7.34	0.577	-0.1282	-3.07	0.044	-0.1237	17.25	0.879	-0.1587
8.22	0.612	-0.1286	-4.06	-0.064	-0.1081	18.30	0.886	-0.1597
9.20	0.647	-0.1327	-5.24	-0.249	-0.0486	19.36	0.891	-0.1605
10.08	0.672	-0.1325	-6.12	-0.262	-0.0234	20.32	0.888	-0.1593
11.23	0.705	-0.1365	-7.17	-0.228	-0.0192	21.38	0.893	-0.1598
12.20	0.729	-0.1381	-8.22	-0.208	-0.0186	22.26	0.895	-0.1594
13.26	0.759	-0.1407	-9.10	-0.195	-0.0187	23.31	0.896	-0.1594
14.23	0.774	-0.1443	-10.15	-0.197	-0.0196	24.11	0.905	-0.1599
15.30	0.801	-0.1483	-11.21	-0.192	-0.0191	24.11	0.898	-0.1590
16.27	0.821	-0.1510	-12.09	-0.197	-0.0182	23.05	0.898	-0.1596
17.24	0.839	-0.1535	-13.14	-0.205	-0.0190	22.08	0.891	-0.1579
18.03	0.855	-0.1540	-14.11	-0.207	-0.0187	21.12	0.899	-0.1607
19.26	0.866	-0.1575	Run: 0432aj			20.06	0.896	-0.1593
20.23	0.872	-0.1572	$Re = 60000.2$			19.36	0.892	-0.1600
21.38	0.879	-0.1584	α	C_L	C_M	18.13	0.885	-0.1583
22.34	0.877	-0.1572	-15.17	-0.226	-0.0175	16.98	0.869	-0.1569
23.31	0.882	-0.1581	-14.02	-0.216	-0.0186	15.39	0.850	-0.1531
24.28	0.890	-0.1606	-13.14	-0.212	-0.0187	14.07	0.814	-0.1488
24.19	0.883	-0.1570	-11.91	-0.198	-0.0186	13.10	0.799	-0.1476
			-10.94	-0.196	-0.0195	12.13	0.777	-0.1453
			-9.98	-0.198	-0.0196	10.98	0.744	-0.1441

10.09	0.717	-0.1421	4.16	0.540	-0.1339	-3.14	0.104	-0.1391
8.94	0.678	-0.1407	5.23	0.582	-0.1355	-4.04	0.020	-0.1323
8.05	0.648	-0.1378	6.20	0.621	-0.1371	-5.14	-0.172	-0.0792
6.99	0.605	-0.1371	7.27	0.670	-0.1397	-6.12	-0.235	-0.0333
6.01	0.564	-0.1337	8.24	0.710	-0.1412	-7.17	-0.231	-0.0232
4.95	0.508	-0.1304	9.04	0.738	-0.1422	-8.13	-0.216	-0.0205
3.97	0.455	-0.1248	10.10	0.776	-0.1431	-9.10	-0.208	-0.0192
2.90	0.420	-0.1255	11.26	0.816	-0.1449	-10.15	-0.205	-0.0182
2.19	0.376	-0.1240	12.23	0.846	-0.1463	-11.03	-0.208	-0.0177
0.95	0.334	-0.1332	13.29	0.876	-0.1484	-12.18	-0.214	-0.0170
-0.11	0.303	-0.1377	14.26	0.889	-0.1502	-13.15	-0.221	-0.0169
-1.00	0.250	-0.1431	15.40	0.900	-0.1523	-14.11	-0.229	-0.0165
-1.98	0.174	-0.1391	16.28	0.903	-0.1540			
-3.06	0.074	-0.1318	17.25	0.910	-0.1565	Run: 0436aj		
-4.05	-0.021	-0.1220	18.31	0.907	-0.1568	$Re = 90001.3$		
-5.15	-0.226	-0.0605	19.36	0.910	-0.1575	α	C_L	C_M
-6.12	-0.258	-0.0269	20.24	0.910	-0.1572	-14.91	-0.241	-0.0170
-7.17	-0.228	-0.0203	21.21	0.915	-0.1580	-13.94	-0.231	-0.0177
-8.13	-0.209	-0.0193	22.09	0.912	-0.1568	-12.97	-0.227	-0.0176
-9.10	-0.201	-0.0188	23.32	0.921	-0.1581	-12.00	-0.215	-0.0184
-10.15	-0.198	-0.0183	24.29	0.919	-0.1579	-10.94	-0.209	-0.0192
-11.12	-0.198	-0.0180	24.11	0.917	-0.1570	-9.89	-0.204	-0.0201
-12.09	-0.203	-0.0172	23.06	0.915	-0.1573	-8.92	-0.206	-0.0217
-13.23	-0.215	-0.0175	22.09	0.908	-0.1561	-7.87	-0.214	-0.0234
-14.11	-0.220	-0.0171	21.12	0.910	-0.1573	-6.90	-0.219	-0.0292
			20.15	0.914	-0.1574	-5.93	-0.204	-0.0439
Run: 0433aj			19.10	0.909	-0.1574	-4.86	-0.118	-0.0995
$Re = 80001.7$			18.31	0.902	-0.1566	-3.95	0.021	-0.1373
	α	C_L	C_M					
-15.17	-0.235	-0.0157	17.07	0.903	-0.1555	-2.87	0.139	-0.1486
-13.94	-0.226	-0.0164	16.29	0.908	-0.1549	-1.88	0.226	-0.1540
-12.88	-0.218	-0.0168	15.05	0.899	-0.1523	-0.80	0.349	-0.1625
-12.00	-0.210	-0.0171	14.08	0.888	-0.1502	0.18	0.424	-0.1610
-10.86	-0.205	-0.0178	13.03	0.870	-0.1489	1.16	0.484	-0.1560
-9.89	-0.202	-0.0186	12.05	0.844	-0.1471	2.32	0.558	-0.1538
-9.10	-0.206	-0.0190	10.99	0.808	-0.1457	3.29	0.593	-0.1442
-7.96	-0.221	-0.0213	10.02	0.782	-0.1446	4.18	0.632	-0.1403
-7.00	-0.235	-0.0253	8.95	0.739	-0.1433	5.33	0.651	-0.1391
-5.94	-0.235	-0.0401	8.07	0.703	-0.1417	6.22	0.685	-0.1407
-5.23	-0.195	-0.0692	7.00	0.658	-0.1402	7.28	0.729	-0.1427
-3.86	0.037	-0.1349	5.94	0.613	-0.1377	7.99	0.760	-0.1439
-3.05	0.099	-0.1392	4.96	0.568	-0.1357	9.32	0.816	-0.1465
-1.80	0.217	-0.1476	3.98	0.529	-0.1339	10.30	0.853	-0.1481
-0.72	0.321	-0.1534	2.92	0.505	-0.1401	11.36	1.265	-0.1431
0.26	0.390	-0.1509	1.95	0.473	-0.1431	12.43	1.338	-0.1427
1.24	0.444	-0.1471	0.89	0.427	-0.1504	13.14	1.393	-0.1429
2.22	0.488	-0.1425	-0.10	0.365	-0.1521	14.39	1.471	-0.1416
3.19	0.510	-0.1358	-1.17	0.287	-0.1531	15.46	1.525	-0.1398
			-1.80	0.225	-0.1477	16.43	1.552	-0.1356

17.40	1.573	-0.1325	Run: 0434aj	19.37	0.937	-0.1617		
18.45	1.577	-0.1295	$Re = 100001.3$	18.05	0.952	-0.1611		
19.28	0.924	-0.1672	α	C_L	C_M	17.09	0.969	-0.1602
20.25	0.927	-0.1673	-15.17	-0.243	-0.0160	16.04	0.997	-0.1578
21.30	0.920	-0.1674	-14.11	-0.233	-0.0170	15.19	1.526	-0.1430
22.27	0.927	-0.1681	-12.88	-0.226	-0.0175	14.13	1.472	-0.1443
23.15	0.932	-0.1686	-11.91	-0.214	-0.0183	13.14	1.407	-0.1456
24.02	0.929	-0.1676	-10.95	-0.210	-0.0194	12.16	1.342	-0.1456
24.02	0.928	-0.1678	-10.15	-0.205	-0.0207	11.09	1.261	-0.1469
23.15	0.928	-0.1682	-8.92	-0.201	-0.0230	10.20	1.195	-0.1466
22.09	0.927	-0.1676	-7.95	-0.200	-0.0277	9.12	1.110	-0.1473
21.30	0.928	-0.1687	-6.98	-0.172	-0.0414	8.14	1.030	-0.1466
20.16	0.925	-0.1674	-5.83	-0.148	-0.0633	7.15	0.948	-0.1470
19.10	0.928	-0.1680	-4.84	-0.004	-0.1347	6.08	0.860	-0.1459
18.05	0.931	-0.1669	-3.94	0.089	-0.1483	5.10	0.790	-0.1479
17.00	0.939	-0.1670	-2.77	0.214	-0.1571	4.12	0.723	-0.1500
16.12	0.941	-0.1643	-1.78	0.295	-0.1605	3.04	0.653	-0.1552
15.15	0.947	-0.1639	-0.79	0.399	-0.1655	2.06	0.588	-0.1592
14.12	1.461	-0.1450	0.20	0.484	-0.1651	0.91	0.513	-0.1630
13.14	1.398	-0.1473	1.17	0.534	-0.1574	0.01	0.463	-0.1681
12.25	1.331	-0.1471	2.24	0.598	-0.1526	-0.97	0.375	-0.1663
11.18	1.250	-0.1489	3.04	0.647	-0.1483	-2.04	0.296	-0.1627
10.19	1.173	-0.1488	4.29	0.730	-0.1408	-3.04	0.173	-0.1532
9.03	1.078	-0.1505	5.28	0.800	-0.1369	-4.02	0.095	-0.1490
8.13	0.989	-0.1502	6.26	0.879	-0.1352	-5.20	-0.056	-0.1144
7.02	0.728	-0.1516	7.33	0.971	-0.1355	-6.10	-0.173	-0.0483
6.04	0.682	-0.1490	8.32	1.051	-0.1360	-7.16	-0.187	-0.0330
4.98	0.652	-0.1484	9.30	1.132	-0.1371	-8.13	-0.202	-0.0237
4.10	0.640	-0.1495	10.38	1.215	-0.1380	-9.10	-0.202	-0.0209
3.03	0.590	-0.1550	11.45	1.289	-0.1392	-9.89	-0.204	-0.0193
2.06	0.563	-0.1645	12.34	1.353	-0.1395	-11.12	-0.214	-0.0175
0.90	0.473	-0.1661	13.23	1.409	-0.1406	-12.09	-0.220	-0.0162
-0.08	0.436	-0.1728	14.39	1.486	-0.1408	-13.15	-0.228	-0.0158
-1.07	0.326	-0.1696	15.46	1.535	-0.1390	-14.11	-0.235	-0.0155
-2.06	0.223	-0.1601	16.25	1.552	-0.1353			
-3.05	0.127	-0.1532	17.40	1.573	-0.1317			
-4.04	0.025	-0.1414	18.45	1.579	-0.1287			
-5.04	-0.152	-0.0853	19.33	1.148	-0.1507			
-6.11	-0.208	-0.0418	20.25	0.936	-0.1614			
-7.17	-0.221	-0.0278	21.30	0.931	-0.1614			
-8.13	-0.209	-0.0245	22.36	0.935	-0.1621			
-9.19	-0.204	-0.0226	23.41	0.935	-0.1618			
-9.98	-0.204	-0.0213	24.38	0.935	-0.1614			
-11.21	-0.212	-0.0202	24.03	0.938	-0.1612			
-12.18	-0.218	-0.0189	23.15	0.931	-0.1612			
-13.15	-0.227	-0.0185	22.09	0.931	-0.1611			
-13.85	-0.230	-0.0185	21.04	0.931	-0.1622			
			20.16	0.935	-0.1611			

AR2-1050-FP1

Fig. 5.2

Run: 0227ga

 $Re = 79997.8$

α	C_L	C_M
-13.91	-0.652	0.0649
-12.67	-0.638	0.0381
-11.79	-0.603	0.0180
-10.82	-0.560	0.0004
-9.94	-0.513	-0.0088
-8.70	-0.442	-0.0150

-7.73	-0.393	-0.0148	21.13	0.716	-0.1077	-5.69	-0.299	-0.0124
-6.75	-0.347	-0.0135	20.34	0.724	-0.1095	-4.72	-0.241	-0.0126
-5.69	-0.291	-0.0149	19.20	0.722	-0.1075	-3.75	-0.195	-0.0118
-4.72	-0.243	-0.0144	18.14	0.722	-0.1048	-2.78	-0.133	-0.0144
-4.01	-0.193	-0.0132	17.17	0.709	-0.0976	-1.89	-0.100	-0.0117
-2.78	-0.128	-0.0150	16.21	0.699	-0.0911	-0.66	-0.034	-0.0090
-1.72	-0.079	-0.0127	15.06	0.691	-0.0817	0.32	0.016	-0.0069
-0.66	-0.029	-0.0096	14.18	0.690	-0.0677	1.29	0.057	-0.0046
0.31	0.014	-0.0071	13.22	0.677	-0.0449	2.26	0.100	-0.0027
1.29	0.066	-0.0047	12.16	0.633	-0.0214	3.32	0.160	0.0007
2.35	0.110	-0.0022	11.18	0.581	-0.0057	4.38	0.219	-0.0011
3.32	0.162	0.0011	10.12	0.524	0.0016	5.35	0.273	-0.0001
4.29	0.218	0.0005	9.06	0.473	0.0026	6.33	0.325	0.0012
5.26	0.268	0.0003	8.09	0.421	0.0033	7.38	0.381	0.0010
6.41	0.327	0.0026	7.29	0.377	0.0006	8.18	0.420	0.0031
7.29	0.378	0.0019	6.32	0.329	0.0007	9.06	0.472	0.0036
8.45	0.441	0.0028	5.17	0.268	-0.0001	10.39	0.540	0.0019
9.33	0.491	0.0033	4.11	0.201	0.0007	11.45	0.595	-0.0098
10.30	0.541	0.0026	3.05	0.148	0.0001	12.16	0.642	-0.0211
11.36	0.593	-0.0081	2.08	0.105	-0.0024	13.39	0.694	-0.0507
12.42	0.649	-0.0271	1.02	0.056	-0.0052	14.36	0.705	-0.0709
13.30	0.682	-0.0502	0.14	0.011	-0.0077	15.33	0.711	-0.0846
14.36	0.687	-0.0710	-0.75	-0.033	-0.0098	16.38	0.707	-0.0935
15.15	0.691	-0.0817	-1.89	-0.088	-0.0127	17.18	0.712	-0.0966
16.38	0.700	-0.0934	-2.87	-0.129	-0.0151	18.32	0.719	-0.1040
17.44	0.708	-0.0991	-3.84	-0.189	-0.0138	19.37	0.733	-0.1070
18.32	0.723	-0.1065	-4.99	-0.250	-0.0147	20.34	0.724	-0.1075
19.37	0.719	-0.1078	-5.96	-0.298	-0.0148	21.31	0.719	-0.1073
20.25	0.717	-0.1088	-7.02	-0.355	-0.0141	22.36	0.703	-0.1022
21.30	0.702	-0.1064	-7.82	-0.401	-0.0154	23.33	0.689	-0.0994
22.36	0.688	-0.1018	-8.96	-0.460	-0.0142	24.38	0.680	-0.0980
23.32	0.683	-0.1004	-9.94	-0.514	-0.0092	25.43	0.674	-0.0954
24.38	0.678	-0.0988	-11.00	-0.565	0.0035	26.31	0.671	-0.0948
25.34	0.671	-0.0972	-11.70	-0.605	0.0182	27.37	0.674	-0.0956
26.31	0.668	-0.0976	-13.03	-0.653	0.0476	28.33	0.672	-0.0953
27.36	0.666	-0.0970	-14.08	-0.657	0.0675	29.39	0.674	-0.0949
28.07	0.669	-0.0945				30.18	0.675	-0.0949
29.39	0.671	-0.0976	Run: 0228ga			30.09	0.670	-0.0949
30.35	0.676	-0.0988	Re = 89996.9			29.39	0.668	-0.0948
30.09	0.675	-0.0975	α	C_L	C_M	28.33	0.670	-0.0950
29.21	0.673	-0.0971	-14.08	-0.664	0.0683	27.19	0.676	-0.0955
28.16	0.668	-0.0939	-13.03	-0.657	0.0490	26.14	0.674	-0.0958
27.10	0.670	-0.0963	-11.79	-0.617	0.0220	25.17	0.671	-0.0952
26.22	0.670	-0.0983	-10.73	-0.566	0.0035	24.12	0.680	-0.0978
25.08	0.685	-0.0989	-9.67	-0.504	-0.0092	23.06	0.692	-0.1002
24.20	0.669	-0.0985	-8.96	-0.465	-0.0129	22.18	0.699	-0.1021
23.15	0.674	-0.0997	-7.82	-0.404	-0.0133	21.22	0.721	-0.1080
22.18	0.701	-0.1037	-6.75	-0.351	-0.0121	20.16	0.726	-0.1074

19.11	0.727	-0.1054	-3.82	-0.195	-0.0103	17.11	0.719	-0.0941
18.32	0.724	-0.1052	-2.85	-0.135	-0.0133	16.05	0.714	-0.0891
17.35	0.716	-0.0993	-1.79	-0.090	-0.0110	15.00	0.705	-0.0791
16.12	0.706	-0.0910	-0.81	-0.039	-0.0085	14.12	0.700	-0.0643
15.07	0.695	-0.0814	0.25	0.012	-0.0066	13.15	0.687	-0.0432
14.19	0.693	-0.0667	1.22	0.055	-0.0039	12.09	0.640	-0.0197
13.22	0.683	-0.0452	2.19	0.106	-0.0016	11.29	0.597	-0.0074
12.16	0.645	-0.0217	3.25	0.161	0.0014	10.06	0.529	0.0050
11.36	0.599	-0.0092	4.22	0.223	-0.0021	8.99	0.478	0.0053
10.30	0.539	0.0019	5.19	0.270	-0.0008	8.11	0.425	0.0035
9.15	0.479	0.0034	6.26	0.332	0.0005	7.05	0.371	0.0018
8.18	0.429	0.0021	7.32	0.386	0.0012	5.99	0.314	0.0016
7.12	0.370	0.0008	8.11	0.426	0.0029	5.11	0.267	0.0006
6.41	0.329	0.0005	9.08	0.478	0.0043	4.04	0.209	0.0003
5.09	0.264	-0.0002	10.23	0.541	0.0028	3.07	0.150	0.0031
4.11	0.208	-0.0001	11.38	0.600	-0.0095	2.01	0.094	-0.0001
3.14	0.150	0.0011	12.35	0.659	-0.0289	0.95	0.047	-0.0022
2.08	0.096	-0.0023	13.24	0.688	-0.0493	0.07	0.006	-0.0047
1.11	0.052	-0.0040	14.38	0.706	-0.0699	-0.99	-0.044	-0.0068
0.05	0.008	-0.0069	15.00	0.707	-0.0795	-1.96	-0.093	-0.0094
-0.92	-0.045	-0.0088	16.31	0.713	-0.0907	-2.94	-0.143	-0.0119
-1.89	-0.095	-0.0108	17.02	0.718	-0.0943	-4.00	-0.208	-0.0093
-2.86	-0.134	-0.0136	18.25	0.729	-0.1022	-5.06	-0.263	-0.0093
-4.01	-0.197	-0.0120	19.31	0.738	-0.1043	-6.03	-0.322	-0.0083
-4.99	-0.257	-0.0122	20.27	0.731	-0.1058	-7.09	-0.378	-0.0094
-6.05	-0.311	-0.0120	21.24	0.722	-0.1051	-7.89	-0.419	-0.0101
-6.93	-0.363	-0.0121	22.38	0.700	-0.0994	-9.03	-0.480	-0.0093
-7.90	-0.417	-0.0133	23.25	0.684	-0.0964	-10.01	-0.535	-0.0028
-8.96	-0.468	-0.0121	24.31	0.684	-0.0944	-11.07	-0.588	0.0122
-9.94	-0.519	-0.0065	25.28	0.678	-0.0939	-12.04	-0.638	0.0340
-11.00	-0.577	0.0075	26.24	0.677	-0.0926	-13.10	-0.666	0.0579
-11.71	-0.625	0.0235	27.38	0.674	-0.0925	-14.07	-0.674	0.0761
-13.03	-0.661	0.0522	28.26	0.678	-0.0935			
-13.99	-0.674	0.0705	29.32	0.675	-0.0921			
			30.37	0.677	-0.0928			

Run: 0229ga

$Re = 100000.4$

α	C_L	C_M	30.11	0.678	-0.0928	α	C_L	C_M
-14.06	-0.671	0.0717	29.14	0.676	-0.0923	-14.41	-0.693	0.0763
-12.75	-0.662	0.0478	28.26	0.676	-0.0931	-13.18	-0.678	0.0528
-11.86	-0.625	0.0268	27.12	0.673	-0.0924	-12.21	-0.641	0.0309
-10.80	-0.576	0.0071	26.07	0.675	-0.0920	-11.23	-0.590	0.0105
-9.74	-0.511	-0.0067	25.10	0.673	-0.0919	-10.17	-0.533	-0.0036
-8.77	-0.464	-0.0112	24.13	0.681	-0.0950	-9.20	-0.477	-0.0084
-7.80	-0.410	-0.0112	23.34	0.693	-0.0985	-8.14	-0.422	-0.0081
-6.83	-0.357	-0.0100	22.12	0.714	-0.1031	-7.17	-0.376	-0.0069
-6.03	-0.323	-0.0091	21.06	0.727	-0.1057	-6.20	-0.331	-0.0060
-4.79	-0.255	-0.0103	20.36	0.732	-0.1074	-5.40	-0.288	-0.0067
			19.13	0.734	-0.1041	-4.16	-0.222	-0.0068
			18.07	0.725	-0.1001	-3.19	-0.152	-0.0121

-2.13	-0.103	-0.0105	14.65	0.706	-0.0721	-2.73	-0.130	-0.0057
-1.16	-0.053	-0.0083	13.78	0.698	-0.0570	-1.76	-0.086	-0.0046
-0.01	-0.001	-0.0059	12.72	0.677	-0.0345	-0.70	-0.031	-0.0026
0.88	0.049	-0.0034	11.92	0.644	-0.0177	0.27	0.012	-0.0013
1.85	0.095	-0.0015	10.77	0.578	0.0023	1.33	0.064	0.0007
2.91	0.145	0.0015	9.71	0.515	0.0095	2.21	0.097	0.0017
3.97	0.222	-0.0045	8.74	0.469	0.0082	3.36	0.155	0.0034
4.94	0.274	-0.0030	7.77	0.420	0.0068	4.42	0.218	0.0012
6.00	0.334	-0.0021	6.71	0.366	0.0043	5.40	0.268	0.0019
6.97	0.382	0.0006	5.74	0.314	0.0028	6.28	0.321	0.0010
8.03	0.437	0.0029	4.76	0.262	0.0023	7.34	0.378	0.0001
8.92	0.484	0.0050	3.70	0.202	0.0014	8.14	0.421	0.0002
9.89	0.538	0.0054	2.64	0.132	0.0068	9.46	0.496	-0.0048
11.04	0.600	-0.0059	1.67	0.084	0.0040	10.44	0.542	-0.0150
12.01	0.651	-0.0233	0.70	0.034	0.0019	11.32	0.601	-0.0338
12.89	0.686	-0.0434	-0.28	-0.015	-0.0007	12.38	0.643	-0.0533
14.04	0.699	-0.0650	-1.42	-0.065	-0.0027	13.44	0.673	-0.0713
14.74	0.700	-0.0751	-2.31	-0.109	-0.0046	14.41	0.683	-0.0853
15.71	0.708	-0.0828	-3.28	-0.166	-0.0050	15.38	0.693	-0.0962
16.94	0.719	-0.0908	-4.25	-0.232	-0.0013	16.34	0.704	-0.1055
17.91	0.725	-0.0956	-5.40	-0.288	-0.0014	17.49	0.705	-0.1131
18.96	0.734	-0.0987	-6.37	-0.342	-0.0018	18.19	0.711	-0.1176
20.02	0.730	-0.1004	-7.35	-0.392	-0.0030	19.33	0.721	-0.1217
20.90	0.727	-0.1003	-8.23	-0.438	-0.0040	20.39	0.728	-0.1243
21.95	0.711	-0.0971	-9.47	-0.500	-0.0035	21.35	0.713	-0.1212
22.92	0.698	-0.0938	-10.35	-0.551	0.0042	22.32	0.691	-0.1164
23.97	0.680	-0.0892	-11.32	-0.605	0.0195	23.37	0.677	-0.1125
25.02	0.674	-0.0872	-12.21	-0.643	0.0364	24.34	0.673	-0.1108
25.90	0.670	-0.0860	-13.44	-0.681	0.0648	25.39	0.672	-0.1086
26.95	0.666	-0.0859	-14.41	-0.695	0.0819	26.36	0.661	-0.1069
27.66	0.669	-0.0848				27.32	0.658	-0.1051
28.98	0.665	-0.0853				28.20	0.663	-0.1066
29.77	0.666	-0.0850				29.17	0.663	-0.1072
29.77	0.667	-0.0853				30.40	0.657	-0.1080
28.71	0.666	-0.0854				31.37	0.658	-0.1095
27.83	0.670	-0.0853				31.10	0.660	-0.1095
26.78	0.668	-0.0855				30.23	0.656	-0.1079
25.73	0.670	-0.0856				29.08	0.661	-0.1070
24.76	0.674	-0.0866				28.20	0.662	-0.1071
23.79	0.672	-0.0877				27.24	0.666	-0.1067
23.00	0.682	-0.0918				26.18	0.659	-0.1065
21.77	0.707	-0.0962				25.13	0.671	-0.1094
20.72	0.725	-0.1001				24.16	0.680	-0.1098
19.93	0.729	-0.0996				23.20	0.686	-0.1132
18.79	0.729	-0.0974				22.14	0.704	-0.1191
17.91	0.726	-0.0954				21.09	0.717	-0.1231
16.76	0.709	-0.0880				20.13	0.723	-0.1225
15.89	0.709	-0.0825				19.16	0.721	-0.1212

AR2-l075-FP1

Fig. 5.3

Run: 0448aj

$Re = 79998.1$

α	C_L	C_M
-12.99	-0.655	0.0661
-11.75	-0.624	0.0420
-10.78	-0.566	0.0210
-9.90	-0.521	0.0078
-8.75	-0.457	0.0012
-7.69	-0.403	-0.0003
-6.63	-0.348	-0.0005
-5.65	-0.295	-0.0031
-4.77	-0.248	-0.0027
-3.79	-0.183	-0.0067

18.37	0.716	-0.1195	-1.01	-0.050	-0.0062	15.77	0.705	-0.0932	
17.22	0.699	-0.1107	-0.13	-0.006	-0.0039	14.72	0.695	-0.0815	
16.17	0.701	-0.1029	1.11	0.051	-0.0010	13.84	0.682	-0.0686	
15.20	0.693	-0.0925	1.91	0.094	0.0015	12.78	0.645	-0.0496	
14.14	0.683	-0.0799	2.88	0.142	0.0033	11.81	0.608	-0.0321	
13.17	0.656	-0.0611	4.03	0.214	0.0008	10.66	0.555	-0.0153	
12.21	0.630	-0.0452	4.91	0.266	0.0019	9.77	0.498	-0.0032	
11.06	0.576	-0.0234	5.88	0.323	0.0023	8.71	0.444	-0.0013	
10.35	0.533	-0.0128	6.95	0.381	0.0028	7.65	0.391	-0.0006	
9.29	0.476	-0.0042	8.01	0.434	0.0033	6.68	0.344	-0.0022	
8.05	0.410	-0.0012	9.07	0.497	0.0013	5.79	0.292	-0.0008	
7.17	0.358	-0.0017	10.04	0.557	-0.0103	4.64	0.233	-0.0023	
6.19	0.313	0.0004	10.93	0.608	-0.0284	3.76	0.187	-0.0019	
5.13	0.257	0.0004	11.99	0.651	-0.0456	2.70	0.117	-0.0000	
4.16	0.212	0.0002	12.78	0.668	-0.0569	1.73	0.075	-0.0018	
3.01	0.142	0.0022	14.01	0.689	-0.0757	0.67	0.028	-0.0040	
2.04	0.093	0.0005	15.07	0.700	-0.0879	-0.30	-0.017	-0.0056	
1.06	0.048	-0.0006	15.68	0.703	-0.0930	-1.28	-0.068	-0.0081	
0.09	-0.000	-0.0028	17.00	0.709	-0.1037	-2.25	-0.115	-0.0103	
-0.88	-0.046	-0.0033	18.06	0.721	-0.1095	-3.31	-0.171	-0.0118	
-1.94	-0.096	-0.0057	19.03	0.725	-0.1134	-4.28	-0.235	-0.0070	
-2.91	-0.143	-0.0061	19.99	0.728	-0.1155	-5.26	-0.291	-0.0081	
-3.88	-0.205	-0.0039	20.96	0.721	-0.1151	-6.32	-0.349	-0.0076	
-4.95	-0.263	-0.0031	21.93	0.718	-0.1136	-7.38	-0.400	-0.0082	
-5.92	-0.311	-0.0033	22.98	0.681	-0.1047	-8.44	-0.454	-0.0088	
-6.71	-0.356	-0.0012	23.94	0.675	-0.1021	-9.32	-0.506	-0.0073	
-8.04	-0.425	-0.0003	24.73	0.677	-0.1013	-10.30	-0.561	0.0040	
-8.92	-0.469	0.0022	25.96	0.666	-0.0983	-11.36	-0.617	0.0242	
-9.90	-0.528	0.0098	26.93	0.661	-0.0985	-12.33	-0.655	0.0432	
-10.96	-0.586	0.0285	27.98	0.659	-0.0975	-13.39	-0.683	0.0601	
-11.75	-0.619	0.0433	29.04	0.663	-0.0980				
-13.08	-0.663	0.0700	30.00	0.656	-0.0973	Run: 0449aj			
			30.97	0.661	-0.0985		Re = 119996.7		
Run: 0452cs			30.71	0.658	-0.0978				
Re = 100001.4			29.83	0.655	-0.0975				
	α	C_L	C_M	28.69	0.658	-0.0975	α	C_L	C_M
-13.39	-0.686	0.0635		27.90	0.664	-0.0969	-13.35	-0.686	0.0724
-12.15	-0.648	0.0406		26.75	0.661	-0.0983	-12.02	-0.647	0.0501
-11.18	-0.599	0.0203		25.79	0.665	-0.0984	-11.05	-0.598	0.0280
-10.21	-0.552	0.0036		24.73	0.672	-0.1011	-10.08	-0.552	0.0137
-9.15	-0.489	-0.0065		23.68	0.673	-0.1021	-9.02	-0.486	0.0040
-8.17	-0.433	-0.0070		22.80	0.691	-0.1070	-8.04	-0.438	0.0033
-7.29	-0.393	-0.0066		21.84	0.711	-0.1131	-7.25	-0.396	0.0036
-6.14	-0.331	-0.0056		20.70	0.721	-0.1155	-6.01	-0.332	0.0037
-5.17	-0.275	-0.0066		19.82	0.724	-0.1157	-4.95	-0.272	0.0028
-4.11	-0.218	-0.0058		18.67	0.726	-0.1139	-3.89	-0.215	0.0026
-3.13	-0.148	-0.0108		17.79	0.716	-0.1090	-3.18	-0.165	-0.0048
-2.07	-0.100	-0.0083		16.82	0.702	-0.1015	-1.94	-0.093	-0.0044
							-0.88	-0.040	-0.0025
							0.09	0.004	-0.0009

1.06	0.055	0.0012	13.88	0.694	-0.0691	3.02	0.168	-0.0014
2.04	0.105	0.0028	12.82	0.662	-0.0497	4.17	0.232	-0.0022
3.10	0.165	-0.0001	12.20	0.636	-0.0381	5.06	0.280	-0.0015
4.16	0.233	-0.0012	10.88	0.562	-0.0138	6.12	0.335	-0.0014
5.13	0.283	-0.0004	9.90	0.505	-0.0026	7.09	0.384	-0.0005
6.02	0.333	-0.0019	8.84	0.456	-0.0010	7.80	0.422	0.0003
7.08	0.389	-0.0014	7.78	0.402	-0.0011	8.86	0.471	0.0009
8.05	0.437	-0.0008	6.90	0.353	-0.0013	10.09	0.540	-0.0054
9.20	0.493	-0.0016	5.92	0.306	-0.0007	11.07	0.597	-0.0196
10.08	0.549	-0.0106	4.86	0.251	-0.0002	12.22	0.644	-0.0368
11.06	0.602	-0.0265	3.89	0.204	-0.0008	13.19	0.681	-0.0530
12.20	0.649	-0.0451	2.83	0.130	0.0055	14.16	0.707	-0.0680
13.17	0.682	-0.0635	1.77	0.082	0.0041	15.12	0.719	-0.0811
14.14	0.703	-0.0778	1.15	0.055	0.0032	16.09	0.724	-0.0910
14.85	0.708	-0.0866	-0.17	-0.010	0.0005	17.15	0.731	-0.1000
16.16	0.716	-0.0993	-1.15	-0.064	-0.0010	18.11	0.739	-0.1057
17.22	0.723	-0.1077	-2.12	-0.110	-0.0029	19.08	0.744	-0.1101
18.10	0.727	-0.1134	-3.18	-0.177	0.0008	20.14	0.751	-0.1130
18.80	0.733	-0.1162	-3.89	-0.224	0.0043	21.10	0.746	-0.1124
20.12	0.739	-0.1190	-5.22	-0.296	0.0047	22.16	0.730	-0.1088
21.09	0.733	-0.1175	-6.28	-0.349	0.0044	22.86	0.720	-0.1060
22.14	0.723	-0.1154	-7.16	-0.398	0.0040	24.09	0.702	-0.1003
23.11	0.702	-0.1094	-7.96	-0.438	0.0033	25.14	0.688	-0.0948
23.90	0.689	-0.1042	-9.19	-0.498	0.0041	26.19	0.680	-0.0928
24.95	0.677	-0.1012	-10.17	-0.558	0.0152	27.16	0.672	-0.0903
26.18	0.678	-0.1004	-11.23	-0.614	0.0353	28.13	0.672	-0.0900
27.06	0.669	-0.0983	-12.20	-0.658	0.0544	29.00	0.670	-0.0900
27.94	0.673	-0.0984	-13.26	-0.687	0.0734	30.15	0.669	-0.0899
28.99	0.669	-0.0981				31.11	0.667	-0.0899
30.14	0.666	-0.0978	Run: 0450cs			30.94	0.666	-0.0898
31.19	0.662	-0.0982	$Re = 139997.0$			29.88	0.667	-0.0893
30.84	0.667	-0.0986	α	C_L	C_M	28.92	0.667	-0.0895
29.96	0.665	-0.0978	-13.33	-0.697	0.0722	27.95	0.672	-0.0897
28.82	0.668	-0.0979	-12.19	-0.668	0.0526	26.90	0.673	-0.0914
28.11	0.669	-0.0982	-11.04	-0.613	0.0290	25.93	0.678	-0.0924
26.88	0.675	-0.0992	-10.07	-0.562	0.0133	24.96	0.684	-0.0949
25.92	0.676	-0.0997	-8.92	-0.497	0.0022	23.91	0.688	-0.0970
24.95	0.677	-0.1003	-8.03	-0.450	0.0019	22.95	0.706	-0.1019
23.90	0.686	-0.1031	-7.15	-0.413	0.0024	21.98	0.732	-0.1086
22.84	0.695	-0.1069	-6.00	-0.344	0.0029	20.84	0.746	-0.1129
21.97	0.726	-0.1151	-4.94	-0.293	0.0034	19.96	0.750	-0.1124
20.83	0.735	-0.1180	-3.97	-0.233	0.0032	18.82	0.743	-0.1090
19.95	0.738	-0.1173	-2.99	-0.160	-0.0039	17.94	0.733	-0.1032
18.80	0.734	-0.1150	-2.02	-0.101	-0.0058	16.88	0.727	-0.0969
17.92	0.724	-0.1106	-0.96	-0.047	-0.0035	15.83	0.722	-0.0877
17.13	0.716	-0.1056	0.01	0.001	-0.0015	14.86	0.715	-0.0759
15.81	0.715	-0.0949	1.16	0.052	0.0013	13.98	0.700	-0.0623
14.85	0.711	-0.0840	1.87	0.089	0.0030	13.19	0.674	-0.0481

12.21	0.633	-0.0304	-0.63	-0.026	-0.0058	12.10	0.638	-0.0385
10.89	0.556	-0.0080	-0.01	-0.000	-0.0046	11.31	0.604	-0.0256
9.91	0.501	0.0005	1.23	0.061	-0.0020	10.16	0.544	-0.0079
8.94	0.445	-0.0002	2.38	0.118	-0.0001	9.10	0.485	-0.0036
7.79	0.395	-0.0004	3.26	0.157	0.0018	8.13	0.437	-0.0013
6.82	0.342	-0.0011	4.23	0.219	0.0004	7.06	0.378	-0.0017
5.94	0.299	-0.0011	5.30	0.281	-0.0006	6.00	0.326	-0.0003
4.79	0.234	-0.0011	6.27	0.329	0.0003	5.12	0.272	-0.0017
3.90	0.184	-0.0009	7.33	0.391	-0.0001	4.15	0.219	0.0005
2.75	0.112	0.0059	8.30	0.446	-0.0008	3.08	0.156	0.0009
1.87	0.068	0.0043	9.36	0.498	-0.0025	2.11	0.107	-0.0012
0.90	0.019	0.0021	10.42	0.555	-0.0098	1.05	0.057	-0.0027
-0.16	-0.035	0.0001	11.31	0.604	-0.0230	0.08	0.012	-0.0049
-0.96	-0.071	-0.0012	12.28	0.651	-0.0411	-0.89	-0.037	-0.0065
-2.11	-0.129	-0.0032	13.34	0.684	-0.0589	-1.95	-0.083	-0.0092
-3.08	-0.204	0.0064	14.31	0.709	-0.0723	-2.92	-0.140	-0.0104
-4.14	-0.259	0.0067	15.36	0.711	-0.0857	-3.90	-0.200	-0.0085
-5.12	-0.310	0.0064	16.33	0.710	-0.0945	-4.96	-0.255	-0.0083
-6.18	-0.361	0.0054	17.39	0.716	-0.1009	-5.93	-0.304	-0.0100
-7.24	-0.409	0.0044	18.35	0.719	-0.1075	-6.99	-0.363	-0.0091
-8.03	-0.448	0.0034	19.41	0.719	-0.1097	-7.97	-0.415	-0.0086
-9.18	-0.508	0.0016	20.38	0.726	-0.1122	-8.94	-0.470	-0.0039
-10.16	-0.568	0.0137	21.43	0.730	-0.1133	-10.09	-0.537	0.0108
-11.22	-0.627	0.0321	22.40	0.726	-0.1132	-10.97	-0.575	0.0262
-12.01	-0.659	0.0472	23.19	0.727	-0.1124	-11.94	-0.614	0.0414
-13.25	-0.696	0.0702	24.33	0.719	-0.1096	-12.74	-0.639	0.0514
			25.38	0.692	-0.1015	-13.97	-0.669	0.0708
			26.35	0.693	-0.1019	-15.03	-0.680	0.0824
			27.31	0.689	-0.1005			
			28.37	0.680	-0.0994			
			29.42	0.679	-0.1008			

AR2-I100-FP1

Fig. 5.4

Run: 0441ga

$Re = 79999.8$

α	C_L	C_M
-15.03	-0.675	0.0807
-13.80	-0.659	0.0661
-12.82	-0.637	0.0514
-11.86	-0.609	0.0379
-10.80	-0.560	0.0203
-9.82	-0.516	0.0043
-8.94	-0.463	-0.0048
-7.70	-0.400	-0.0091
-6.73	-0.344	-0.0091
-5.67	-0.286	-0.0095
-4.96	-0.257	-0.0084
-3.81	-0.194	-0.0073
-2.75	-0.126	-0.0099
-1.69	-0.081	-0.0081

Run: 0439ga	α	C_L	C_M		
$Re = 99998.7$					
29.42	0.679	-0.1001	-14.98	-0.688	0.0809
29.07	0.674	-0.1001	-13.75	-0.674	0.0680
28.10	0.675	-0.0982	-12.78	-0.648	0.0536
27.31	0.682	-0.1004	-11.81	-0.617	0.0403
26.35	0.691	-0.1008	-10.66	-0.570	0.0221
25.21	0.695	-0.1024	-9.78	-0.519	0.0071
24.06	0.704	-0.1036	-8.98	-0.471	-0.0037
23.10	0.723	-0.1125	-7.74	-0.407	-0.0076
22.13	0.731	-0.1120	-6.77	-0.355	-0.0072
21.17	0.727	-0.1130	-5.71	-0.297	-0.0074
20.11	0.718	-0.1108	-4.74	-0.247	-0.0069
19.06	0.717	-0.1085	-3.68	-0.204	-0.0058
18.18	0.712	-0.1050	-2.70	-0.135	-0.0100
17.12	0.721	-0.0997	-1.73	-0.085	-0.0084
16.15	0.708	-0.0930	-0.67	-0.031	-0.0059
15.10	0.710	-0.0831	0.30	0.014	-0.0038
14.13	0.700	-0.0696			
13.07	0.670	-0.0540			

1.36	0.060	-0.0019	10.12	0.548	-0.0079	3.31	0.166	0.0019
2.34	0.113	0.0006	9.15	0.493	-0.0035	4.20	0.238	-0.0054
3.40	0.164	0.0025	8.17	0.442	-0.0030	5.26	0.297	-0.0042
4.19	0.224	-0.0017	7.11	0.391	-0.0029	6.23	0.350	-0.0037
5.43	0.293	-0.0018	6.14	0.331	-0.0022	7.12	0.399	-0.0034
6.32	0.344	-0.0014	5.17	0.284	-0.0030	8.35	0.463	-0.0028
7.46	0.398	-0.0017	4.20	0.232	-0.0029	9.24	0.513	-0.0023
8.35	0.455	-0.0020	3.04	0.157	0.0021	10.39	0.576	-0.0097
9.06	0.489	-0.0020	2.25	0.108	0.0003	11.36	0.628	-0.0240
10.47	0.572	-0.0105	1.10	0.054	-0.0015	12.24	0.672	-0.0393
11.45	0.621	-0.0248	0.13	0.007	-0.0035	13.39	0.711	-0.0563
12.24	0.659	-0.0397	-0.93	-0.037	-0.0050	14.27	0.735	-0.0697
13.48	0.695	-0.0591	-1.99	-0.091	-0.0074	15.33	0.746	-0.0830
14.18	0.712	-0.0688	-2.88	-0.145	-0.0075	16.12	0.750	-0.0903
15.41	0.735	-0.0861	-3.94	-0.211	-0.0047	17.26	0.744	-0.0993
16.47	0.732	-0.0946	-4.91	-0.265	-0.0056	18.32	0.741	-0.1044
17.43	0.731	-0.1017	-5.88	-0.311	-0.0059	19.28	0.744	-0.1087
18.40	0.733	-0.1077	-6.95	-0.373	-0.0059	20.25	0.741	-0.1087
19.37	0.730	-0.1097	-8.01	-0.427	-0.0063	21.39	0.742	-0.1089
20.42	0.733	-0.1113	-8.63	-0.467	-0.0036	22.27	0.740	-0.1075
21.21	0.734	-0.1112	-9.95	-0.535	0.0136	23.32	0.732	-0.1051
22.36	0.728	-0.1102	-10.75	-0.570	0.0242	24.29	0.729	-0.1036
23.41	0.729	-0.1094	-11.90	-0.623	0.0440	25.26	0.720	-0.1008
24.47	0.719	-0.1054	-12.96	-0.659	0.0581	26.40	0.714	-0.0990
25.34	0.710	-0.1031	-13.93	-0.680	0.0721	27.36	0.697	-0.0940
26.13	0.694	-0.0982	-14.98	-0.686	0.0832	28.33	0.700	-0.0949
27.10	0.686	-0.0961				29.30	0.696	-0.0940
28.15	0.689	-0.0973	Run: 0442ga			29.12	0.693	-0.0929
29.47	0.686	-0.0975	Re = 119998.1			28.07	0.689	-0.0927
29.47	0.681	-0.0970	α	C_L	C_M	27.01	0.698	-0.0943
28.24	0.683	-0.0966	-15.07	-0.702	0.0775	26.13	0.696	-0.0943
27.36	0.680	-0.0968	-13.84	-0.681	0.0630	25.08	0.703	-0.0961
26.31	0.693	-0.0976	-12.78	-0.655	0.0479	24.11	0.712	-0.0980
25.16	0.701	-0.1000	-11.90	-0.626	0.0356	23.06	0.736	-0.1065
24.46	0.698	-0.0999	-10.75	-0.576	0.0182	22.09	0.741	-0.1084
23.15	0.726	-0.1085	-9.87	-0.531	0.0042	21.04	0.748	-0.1102
22.09	0.732	-0.1104	-8.80	-0.463	-0.0092	20.07	0.739	-0.1093
21.21	0.733	-0.1113	-7.83	-0.412	-0.0096	19.11	0.738	-0.1076
20.25	0.734	-0.1120	-6.86	-0.361	-0.0089	18.14	0.744	-0.1046
19.19	0.729	-0.1101	-5.88	-0.307	-0.0083	17.00	0.749	-0.0978
18.40	0.726	-0.1069	-4.82	-0.254	-0.0078	16.12	0.746	-0.0912
17.35	0.728	-0.1021	-3.76	-0.203	-0.0068	15.42	0.746	-0.0841
16.20	0.732	-0.0925	-2.79	-0.135	-0.0108	14.10	0.724	-0.0665
15.41	0.733	-0.0859	-1.73	-0.085	-0.0104	13.04	0.697	-0.0508
14.09	0.717	-0.0693	-0.67	-0.034	-0.0079	12.07	0.660	-0.0361
13.12	0.689	-0.0535	0.04	0.002	-0.0063	11.09	0.608	-0.0191
12.15	0.650	-0.0374	1.19	0.059	-0.0032	10.39	0.572	-0.0111
11.36	0.617	-0.0253	2.25	0.111	-0.0006	9.06	0.495	-0.0046

8.09	0.442	-0.0052	5.25	0.299	-0.0061	5.96	0.339	-0.0080
7.11	0.394	-0.0051	6.23	0.356	-0.0055	5.08	0.285	-0.0081
6.05	0.338	-0.0048	7.29	0.413	-0.0046	4.10	0.235	-0.0082
5.08	0.288	-0.0052	8.35	0.466	-0.0042	3.04	0.151	0.0008
4.11	0.237	-0.0058	9.23	0.518	-0.0030	2.07	0.105	-0.0008
3.04	0.158	0.0017	10.29	0.579	-0.0094	1.01	0.048	-0.0033
2.07	0.110	-0.0001	11.27	0.628	-0.0208	0.03	0.005	-0.0051
1.01	0.058	-0.0022	12.24	0.676	-0.0373	-1.03	-0.051	-0.0073
0.22	0.018	-0.0040	13.30	0.708	-0.0528	-2.00	-0.102	-0.0092
-0.93	-0.038	-0.0061	14.35	0.735	-0.0676	-2.80	-0.160	-0.0012
-1.99	-0.095	-0.0089	15.41	0.752	-0.0813	-4.04	-0.228	-0.0023
-2.97	-0.165	-0.0030	16.29	0.761	-0.0902	-5.01	-0.281	-0.0028
-3.94	-0.214	-0.0045	16.99	0.755	-0.0956	-6.07	-0.331	-0.0037
-4.91	-0.271	-0.0054	18.31	0.753	-0.1046	-6.78	-0.369	-0.0041
-5.97	-0.323	-0.0062	19.28	0.751	-0.1083	-7.92	-0.429	-0.0050
-7.04	-0.381	-0.0071	20.33	0.751	-0.1095	-8.99	-0.483	-0.0029
-8.01	-0.429	-0.0077	21.30	0.752	-0.1096	-9.78	-0.531	0.0075
-8.98	-0.485	-0.0035	22.27	0.751	-0.1087	-11.02	-0.591	0.0244
-10.04	-0.545	0.0104	23.32	0.739	-0.1051	-12.08	-0.635	0.0396
-11.10	-0.593	0.0258	24.29	0.723	-0.1007	-13.05	-0.665	0.0541
-11.98	-0.633	0.0401	25.34	0.714	-0.0982	-14.11	-0.691	0.0673
-13.04	-0.662	0.0542	26.31	0.717	-0.0977	-15.07	-0.703	0.0795
-14.10	-0.688	0.0675	27.10	0.713	-0.0968			
-15.07	-0.699	0.0784	28.32	0.698	-0.0919			
			29.29	0.692	-0.0912			
Run: 0443ga			29.38	0.689	-0.0910	Run: 0444ga		
Re = 139994.6			28.24	0.697	-0.0915	Re = 159991.6		
α	C_L	C_M	27.09	0.699	-0.0927	α	C_L	C_M
-15.07	-0.707	0.0774	26.13	0.704	-0.0935	-15.02	-0.708	0.0782
-13.84	-0.686	0.0622	25.07	0.706	-0.0946	-13.97	-0.693	0.0648
-13.05	-0.665	0.0520	24.11	0.708	-0.0959	-12.82	-0.658	0.0484
-11.90	-0.629	0.0352	23.06	0.740	-0.1061	-11.85	-0.627	0.0340
-10.84	-0.578	0.0180	22.09	0.751	-0.1090	-10.79	-0.579	0.0169
-9.87	-0.528	0.0033	21.04	0.749	-0.1098	-9.82	-0.527	0.0025
-9.07	-0.486	-0.0060	20.16	0.753	-0.1106	-8.76	-0.462	-0.0067
-7.75	-0.414	-0.0083	19.10	0.755	-0.1091	-7.69	-0.414	-0.0067
-6.77	-0.364	-0.0075	18.05	0.753	-0.1033	-6.72	-0.362	-0.0063
-5.71	-0.308	-0.0070	16.99	0.755	-0.0966	-5.75	-0.310	-0.0062
-5.01	-0.274	-0.0064	16.03	0.756	-0.0888	-4.78	-0.258	-0.0053
-3.77	-0.208	-0.0060	15.15	0.749	-0.0800	-3.80	-0.210	-0.0051
-2.79	-0.150	-0.0057	14.09	0.726	-0.0649	-2.65	-0.151	-0.0042
-1.73	-0.086	-0.0111	13.03	0.699	-0.0503	-1.77	-0.087	-0.0126
-0.76	-0.037	-0.0085	12.15	0.664	-0.0366	-0.71	-0.034	-0.0102
0.21	0.010	-0.0060	11.00	0.609	-0.0189	0.26	0.013	-0.0077
0.92	0.037	-0.0045	10.03	0.556	-0.0088	1.32	0.061	-0.0052
2.24	0.111	-0.0007	8.97	0.496	-0.0078	2.38	0.117	-0.0023
3.22	0.171	-0.0005	8.35	0.464	-0.0084	3.27	0.183	-0.0076
4.19	0.246	-0.0066	7.11	0.391	-0.0082	4.25	0.245	-0.0105
						5.31	0.306	-0.0104
						6.10	0.348	-0.0094

7.34	0.420	-0.0088	4.16	0.234	-0.0108	5.25	0.322	0.0095
8.31	0.473	-0.0084	3.00	0.150	0.0000	6.05	0.369	0.0112
9.29	0.528	-0.0071	2.12	0.105	-0.0003	7.12	0.440	0.0103
10.35	0.588	-0.0125	0.97	0.047	-0.0025	8.36	0.523	0.0070
11.41	0.642	-0.0251	0.09	0.002	-0.0041	9.25	0.592	-0.0050
12.38	0.679	-0.0393	-0.97	-0.051	-0.0063	10.32	0.652	-0.0312
13.35	0.715	-0.0538	-1.95	-0.107	-0.0057	11.29	0.670	-0.0537
14.06	0.738	-0.0638	-2.92	-0.180	0.0006	12.25	0.660	-0.0655
15.38	0.763	-0.0799	-3.90	-0.229	0.0006	13.13	0.645	-0.0711
16.26	0.762	-0.0898	-4.96	-0.282	-0.0003	14.27	0.632	-0.0742
17.31	0.761	-0.0981	-5.93	-0.326	-0.0012	15.41	0.623	-0.0749
18.36	0.758	-0.1048	-6.99	-0.385	-0.0027	16.38	0.618	-0.0746
19.33	0.751	-0.1075	-7.96	-0.431	-0.0045	17.08	0.626	-0.0755
20.30	0.757	-0.1101	-9.02	-0.485	-0.0045	18.31	0.626	-0.0755
21.35	0.757	-0.1095	-9.99	-0.543	0.0084	19.28	0.631	-0.0759
22.32	0.748	-0.1074	-11.06	-0.596	0.0256	20.24	0.626	-0.0742
23.37	0.738	-0.1030	-12.03	-0.633	0.0396	21.39	0.636	-0.0751
24.34	0.730	-0.1006	-13.00	-0.668	0.0538	22.09	0.639	-0.0737
25.39	0.721	-0.0973	-13.97	-0.692	0.0676	23.32	0.640	-0.0755
26.36	0.720	-0.0970	-15.02	-0.706	0.0801	24.38	0.645	-0.0774
27.32	0.719	-0.0961				25.26	0.642	-0.0765
28.38	0.705	-0.0927				26.31	0.649	-0.0786
29.34	0.697	-0.0908				27.28	0.659	-0.0804
29.43	0.696	-0.0902				28.16	0.652	-0.0803
28.20	0.695	-0.0895				29.30	0.664	-0.0846
27.15	0.704	-0.0923				29.04	0.661	-0.0825
26.18	0.707	-0.0924				28.33	0.656	-0.0833
25.13	0.708	-0.0939				27.02	0.652	-0.0793
24.16	0.735	-0.1006				26.31	0.649	-0.0793
23.11	0.743	-0.1051				25.17	0.646	-0.0757
22.14	0.750	-0.1072				24.11	0.641	-0.0751
21.09	0.753	-0.1096				23.15	0.640	-0.0747
20.12	0.757	-0.1094				22.09	0.639	-0.0750
19.07	0.759	-0.1081				21.12	0.632	-0.0751
18.19	0.761	-0.1033				20.16	0.630	-0.0740
17.05	0.761	-0.0965				19.28	0.629	-0.0750
16.17	0.766	-0.0892				18.14	0.625	-0.0747
15.11	0.761	-0.0783				17.08	0.627	-0.0749
14.14	0.737	-0.0648				16.02	0.627	-0.0736
13.09	0.706	-0.0500				15.15	0.634	-0.0758
12.20	0.670	-0.0364				14.01	0.633	-0.0733
11.06	0.617	-0.0208				13.13	0.651	-0.0710
10.08	0.563	-0.0109				12.16	0.669	-0.0641
9.02	0.503	-0.0115				11.11	0.677	-0.0489
8.13	0.456	-0.0117				10.14	0.652	-0.0258
7.16	0.399	-0.0114				9.25	0.597	-0.0065
6.01	0.341	-0.0114				8.10	0.515	0.0080
5.04	0.284	-0.0115				7.12	0.451	0.0099

6.06	0.384	0.0102	7.39	0.473	0.0101	4.02	0.270	0.0060
4.99	0.323	0.0092	8.28	0.534	0.0074	3.04	0.198	0.0064
4.01	0.264	0.0085	9.17	0.602	-0.0052	2.06	0.134	0.0065
3.04	0.189	0.0092	10.32	0.656	-0.0316	1.00	0.068	0.0039
2.06	0.135	0.0070	11.29	0.682	-0.0556	0.02	0.017	0.0020
0.91	0.073	0.0043	12.25	0.677	-0.0683	-1.04	-0.046	-0.0012
-0.07	0.018	0.0027	13.31	0.662	-0.0750	-2.02	-0.109	-0.0035
-1.04	-0.041	-0.0009	14.27	0.654	-0.0781	-3.08	-0.170	-0.0058
-2.11	-0.106	-0.0035	15.32	0.642	-0.0787	-3.98	-0.245	-0.0025
-2.99	-0.157	-0.0055	16.20	0.639	-0.0779	-5.04	-0.310	-0.0044
-3.97	-0.219	-0.0064	17.26	0.634	-0.0780	-6.10	-0.373	-0.0034
-5.04	-0.295	-0.0060	18.14	0.638	-0.0776	-7.08	-0.440	-0.0046
-6.01	-0.354	-0.0066	19.28	0.639	-0.0774	-7.97	-0.498	-0.0047
-7.08	-0.424	-0.0063	20.33	0.638	-0.0767	-9.12	-0.570	0.0012
-8.05	-0.481	-0.0065	21.30	0.640	-0.0748	-10.19	-0.637	0.0219
-9.03	-0.540	-0.0021	22.27	0.643	-0.0759	-10.90	-0.670	0.0394
-10.10	-0.615	0.0182	23.32	0.645	-0.0752	-12.04	-0.684	0.0673
-11.07	-0.662	0.0446	24.38	0.648	-0.0765	-13.18	-0.672	0.0782
-12.04	-0.658	0.0633	25.34	0.650	-0.0764	-14.15	-0.654	0.0820
-13.09	-0.655	0.0745	26.31	0.655	-0.0783	-15.20	-0.645	0.0842
-14.14	-0.638	0.0787	27.28	0.660	-0.0795			
-15.20	-0.623	0.0798	28.42	0.663	-0.0814			
			29.30	0.668	-0.0831			
Run: 0376ar			29.04	0.665	-0.0821			
Re = 79998.7			28.16	0.664	-0.0799			
	α	C_L	C_M			α	C_L	C_M
-15.11	-0.637	0.0816	27.02	0.655	-0.0781	-15.10	-0.651	0.0839
-13.88	-0.660	0.0800	26.05	0.654	-0.0777	-13.87	-0.672	0.0816
-12.92	-0.678	0.0739	25.17	0.652	-0.0761	-12.82	-0.688	0.0762
-11.87	-0.683	0.0622	24.11	0.648	-0.0752	-11.86	-0.695	0.0644
-10.90	-0.668	0.0373	23.15	0.647	-0.0751	-10.89	-0.677	0.0407
-9.92	-0.623	0.0139	22.00	0.643	-0.0762	-9.82	-0.632	0.0177
-8.86	-0.543	-0.0038	21.13	0.644	-0.0755	-8.85	-0.561	-0.0014
-7.88	-0.483	-0.0064	20.16	0.639	-0.0765	-7.78	-0.495	-0.0049
-6.81	-0.420	-0.0059	19.28	0.642	-0.0773	-6.89	-0.442	-0.0041
-5.84	-0.366	-0.0048	18.14	0.640	-0.0781	-5.92	-0.388	-0.0027
-4.86	-0.305	-0.0055	17.34	0.638	-0.0780	-4.85	-0.313	-0.0023
-3.80	-0.234	-0.0044	16.11	0.642	-0.0786	-3.79	-0.249	-0.0014
-2.82	-0.164	-0.0067	15.15	0.653	-0.0792	-2.81	-0.165	-0.0065
-2.11	-0.123	-0.0050	14.10	0.664	-0.0775	-1.83	-0.108	-0.0041
-0.78	-0.040	-0.0015	13.13	0.668	-0.0741	-0.77	-0.046	-0.0014
0.20	0.010	0.0017	12.17	0.682	-0.0673	0.21	0.012	0.0013
1.17	0.074	0.0040	11.03	0.684	-0.0495	1.19	0.069	0.0043
2.32	0.131	0.0069	10.14	0.659	-0.0290	2.25	0.133	0.0072
3.21	0.202	0.0059	9.07	0.586	-0.0030	3.23	0.215	0.0040
4.28	0.269	0.0072	8.10	0.519	0.0077	4.21	0.277	0.0051
5.35	0.341	0.0086	7.12	0.457	0.0083	5.27	0.352	0.0065
6.23	0.405	0.0091	6.32	0.411	0.0067	6.07	0.395	0.0077
			5.26	0.347	0.0071	7.31	0.479	0.0098
						8.29	0.541	0.0079

9.36	0.615	-0.0079	2.07	0.130	0.0068	11.30	0.702	-0.0531
10.33	0.672	-0.0330	0.92	0.067	0.0043	12.26	0.701	-0.0666
11.30	0.694	-0.0553	0.03	0.010	0.0020	13.32	0.690	-0.0742
12.27	0.692	-0.0680	-0.94	-0.045	-0.0005	14.28	0.682	-0.0778
13.15	0.676	-0.0742	-1.92	-0.112	-0.0033	15.34	0.686	-0.0805
14.29	0.665	-0.0786	-2.98	-0.176	-0.0054	16.40	0.718	-0.0870
15.34	0.660	-0.0792	-3.96	-0.255	-0.0002	17.28	0.722	-0.0882
16.22	0.643	-0.0777	-5.03	-0.326	-0.0006	18.33	0.700	-0.0845
17.27	0.644	-0.0775	-6.00	-0.387	-0.0016	19.39	0.732	-0.0894
18.32	0.646	-0.0768	-7.16	-0.457	-0.0033	20.25	0.655	-0.0728
19.29	0.642	-0.0757	-8.14	-0.517	-0.0039	21.31	0.654	-0.0713
20.26	0.647	-0.0745	-9.02	-0.576	0.0029	22.36	0.650	-0.0695
21.23	0.649	-0.0740	-10.09	-0.647	0.0253	23.33	0.652	-0.0682
22.28	0.645	-0.0727	-11.06	-0.689	0.0496	24.30	0.655	-0.0690
23.42	0.648	-0.0721	-12.12	-0.699	0.0687	25.27	0.659	-0.0688
24.30	0.649	-0.0726	-13.08	-0.681	0.0787	26.32	0.659	-0.0695
25.27	0.656	-0.0732	-14.05	-0.666	0.0822	27.29	0.663	-0.0707
26.32	0.656	-0.0742	-14.93	-0.659	0.0842	28.34	0.664	-0.0719
27.29	0.660	-0.0752				29.31	0.669	-0.0736
28.44	0.668	-0.0778	Run: 0379ga			29.13	0.669	-0.0728
29.32	0.669	-0.0781	$Re = 119992.5$			28.43	0.669	-0.0722
29.32	0.668	-0.0788	α	C_L	C_M	27.11	0.663	-0.0705
28.17	0.661	-0.0761	-15.20	-0.668	0.0873	26.15	0.659	-0.0693
27.03	0.657	-0.0750	-13.88	-0.680	0.0838	25.09	0.657	-0.0693
26.06	0.655	-0.0739	-12.83	-0.700	0.0786	24.12	0.656	-0.0688
25.09	0.654	-0.0734	-11.95	-0.710	0.0668	23.16	0.654	-0.0688
24.04	0.649	-0.0726	-10.81	-0.687	0.0430	22.36	0.651	-0.0697
23.16	0.648	-0.0719	-9.92	-0.641	0.0198	21.05	0.654	-0.0710
22.11	0.649	-0.0730	-8.85	-0.565	-0.0002	20.08	0.659	-0.0732
21.05	0.646	-0.0729	-7.88	-0.506	-0.0025	19.04	0.720	-0.0871
20.08	0.648	-0.0749	-6.81	-0.443	-0.0012	18.07	0.726	-0.0891
19.38	0.645	-0.0755	-5.84	-0.383	-0.0002	17.10	0.724	-0.0890
18.15	0.646	-0.0773	-4.86	-0.325	0.0013	16.13	0.722	-0.0874
17.18	0.648	-0.0775	-3.79	-0.256	0.0021	15.16	0.689	-0.0807
16.13	0.651	-0.0783	-2.81	-0.166	-0.0060	14.11	0.686	-0.0778
15.08	0.658	-0.0790	-1.84	-0.110	-0.0041	13.14	0.690	-0.0738
14.02	0.668	-0.0779	-0.77	-0.046	-0.0009	12.18	0.701	-0.0660
13.15	0.683	-0.0746	0.20	0.012	0.0022	11.12	0.702	-0.0496
12.18	0.694	-0.0677	1.18	0.069	0.0049	10.06	0.666	-0.0242
11.04	0.693	-0.0496	2.33	0.136	0.0082	9.09	0.601	-0.0022
10.15	0.666	-0.0290	3.23	0.230	0.0022	8.20	0.533	0.0087
9.00	0.595	-0.0035	4.20	0.289	0.0039	7.13	0.468	0.0071
8.11	0.529	0.0072	5.00	0.343	0.0048	6.07	0.403	0.0049
7.13	0.462	0.0073	6.24	0.420	0.0074	5.00	0.344	0.0034
6.25	0.411	0.0055	7.31	0.488	0.0102	4.11	0.280	0.0028
5.00	0.336	0.0045	8.29	0.547	0.0097	3.05	0.212	0.0019
4.12	0.281	0.0040	9.26	0.617	-0.0053	2.07	0.133	0.0085
3.05	0.207	0.0028	10.33	0.679	-0.0310	0.92	0.065	0.0054

0.03	0.008	0.0031	9.62	0.605	-0.0087	2.42	0.147	0.0045
-0.95	-0.050	0.0005	10.68	0.649	-0.0324	1.27	0.086	0.0016
-1.84	-0.106	-0.0023	11.47	0.666	-0.0484	0.38	0.032	-0.0002
-2.99	-0.192	-0.0007	12.62	0.668	-0.0638	-0.60	-0.032	-0.0040
-3.97	-0.270	0.0033	13.67	0.661	-0.0699	-1.66	-0.088	-0.0070
-5.13	-0.342	0.0024	14.63	0.649	-0.0714	-2.63	-0.143	-0.0092
-6.10	-0.399	0.0009	15.69	0.629	-0.0713	-3.61	-0.209	-0.0100
-7.17	-0.465	-0.0010	16.65	0.639	-0.0717	-4.68	-0.287	-0.0108
-8.14	-0.524	-0.0023	17.71	0.640	-0.0725	-5.75	-0.347	-0.0113
-9.03	-0.586	0.0044	18.68	0.642	-0.0733	-6.81	-0.413	-0.0115
-10.10	-0.657	0.0255	19.73	0.647	-0.0739	-7.79	-0.481	-0.0105
-11.07	-0.696	0.0511	20.61	0.653	-0.0740	-8.68	-0.539	-0.0006
-12.04	-0.707	0.0695	21.76	0.660	-0.0749	-9.74	-0.609	0.0237
-13.18	-0.695	0.0814	22.64	0.661	-0.0753	-10.80	-0.631	0.0438
-14.14	-0.681	0.0857	23.69	0.662	-0.0746	-11.77	-0.646	0.0575
-15.11	-0.673	0.0888	24.66	0.661	-0.0753	-12.82	-0.641	0.0665
			25.62	0.661	-0.0751	-13.79	-0.637	0.0701
			26.77	0.671	-0.0775	-14.84	-0.622	0.0719
			27.65	0.676	-0.0787			
			28.79	0.671	-0.0806	Run: 0372ga		
			29.67	0.681	-0.0814	$Re = 80003.6$		

α	C_L	C_M	α	C_L	C_M
-14.84	-0.621	0.0699	28.53	0.677	-0.0800
-13.53	-0.634	0.0674	27.47	0.671	-0.0782
-12.47	-0.640	0.0625	26.50	0.667	-0.0761
-11.51	-0.640	0.0532	25.45	0.665	-0.0745
-10.54	-0.625	0.0374	24.48	0.665	-0.0751
-9.56	-0.592	0.0167	23.51	0.657	-0.0731
-8.50	-0.522	-0.0044	22.46	0.658	-0.0747
-7.52	-0.460	-0.0116	21.49	0.654	-0.0741
-6.46	-0.401	-0.0121	20.52	0.655	-0.0738
-5.48	-0.334	-0.0114	19.73	0.648	-0.0738
-4.50	-0.272	-0.0107	18.41	0.645	-0.0725
-3.44	-0.210	-0.0101	17.36	0.641	-0.0725
-2.37	-0.136	-0.0090	16.48	0.645	-0.0707
-1.40	-0.082	-0.0071	15.43	0.652	-0.0728
-0.33	-0.020	-0.0033	14.37	0.653	-0.0708
0.56	0.034	-0.0004	13.50	0.673	-0.0690
1.27	0.074	0.0012	12.53	0.677	-0.0618
2.69	0.153	0.0044	11.47	0.671	-0.0489
3.66	0.213	0.0073	10.51	0.654	-0.0289
4.64	0.277	0.0076	9.44	0.598	-0.0057
5.71	0.350	0.0080	8.46	0.533	0.0071
6.60	0.407	0.0085	7.49	0.470	0.0090
7.66	0.470	0.0105	6.60	0.417	0.0071
8.64	0.535	0.0070	5.36	0.343	0.0074
			4.46	0.277	0.0077
			3.40	0.205	0.0067

11.64	0.690	-0.0546	25.57	0.684	-0.0734	-13.85	-0.674	0.0760
12.52	0.690	-0.0648	26.54	0.685	-0.0739	-14.90	-0.659	0.0771
13.40	0.684	-0.0705	27.50	0.683	-0.0738			
14.63	0.672	-0.0740	28.65	0.685	-0.0753	Run: 0373ga		
			29.53	0.690	-0.0764	$Re = 119998.3$		
Run: 0369ga			29.26	0.689	-0.0760	α	C_L	C_M
$Re = 99997.3$			28.38	0.687	-0.0750	-14.66	-0.684	0.0820
	α	C_L	C_M					
-14.64	-0.668	0.0770	27.33	0.682	-0.0737	-13.60	-0.693	0.0783
-13.68	-0.675	0.0749	26.27	0.680	-0.0725	-12.55	-0.690	0.0713
-12.71	-0.680	0.0697	25.39	0.675	-0.0716	-11.58	-0.684	0.0616
-11.66	-0.679	0.0594	24.34	0.675	-0.0717	-10.79	-0.672	0.0502
-10.69	-0.659	0.0428	23.37	0.674	-0.0714	-9.64	-0.632	0.0268
-9.71	-0.622	0.0236	22.32	0.675	-0.0730	-8.57	-0.566	0.0036
-8.56	-0.555	0.0004	21.35	0.673	-0.0733	-7.50	-0.491	-0.0066
-7.67	-0.488	-0.0088	20.38	0.670	-0.0734	-6.62	-0.432	-0.0059
-6.69	-0.426	-0.0087	19.50	0.666	-0.0734	-5.55	-0.369	-0.0047
-5.63	-0.358	-0.0077	18.36	0.662	-0.0737	-4.84	-0.326	-0.0039
-4.65	-0.300	-0.0066	17.22	0.668	-0.0747	-3.51	-0.243	-0.0022
-3.59	-0.235	-0.0054	16.34	0.667	-0.0750	-2.44	-0.162	-0.0052
-2.52	-0.150	-0.0098	15.64	0.674	-0.0753	-1.55	-0.094	-0.0074
-1.81	-0.108	-0.0085	14.41	0.687	-0.0752	-0.49	-0.029	-0.0040
-0.83	-0.047	-0.0058	13.27	0.707	-0.0723	0.49	0.029	-0.0005
0.24	0.013	-0.0026	12.39	0.706	-0.0651	1.47	0.086	0.0025
1.39	0.085	0.0016	11.25	0.697	-0.0502	2.53	0.156	0.0062
2.46	0.151	0.0047	10.37	0.676	-0.0336	3.52	0.248	0.0003
3.44	0.233	0.0020	9.21	0.614	-0.0077	4.58	0.317	0.0016
4.50	0.304	0.0022	8.32	0.553	0.0052	5.29	0.364	0.0029
5.48	0.372	0.0040	7.34	0.490	0.0059	6.54	0.445	0.0058
6.46	0.430	0.0058	6.28	0.417	0.0036	7.69	0.510	0.0090
7.52	0.499	0.0082	5.21	0.358	0.0023	8.58	0.575	0.0067
8.50	0.565	0.0047	4.33	0.301	0.0007	9.29	0.626	-0.0046
9.48	0.633	-0.0118	3.26	0.219	0.0019	10.62	0.690	-0.0329
10.54	0.681	-0.0368	2.19	0.143	0.0042	11.59	0.711	-0.0514
11.51	0.700	-0.0551	1.13	0.080	0.0016	12.56	0.720	-0.0622
12.48	0.708	-0.0662	0.24	0.025	-0.0009	13.61	0.722	-0.0707
13.53	0.696	-0.0731	-0.74	-0.032	-0.0039	14.40	0.726	-0.0742
14.59	0.685	-0.0759	-1.80	-0.097	-0.0069	15.64	0.734	-0.0799
15.64	0.677	-0.0759	-2.78	-0.177	-0.0049	16.60	0.715	-0.0783
16.43	0.664	-0.0748	-3.76	-0.240	-0.0041	17.66	0.720	-0.0786
17.48	0.661	-0.0742	-4.83	-0.312	-0.0054	18.61	0.670	-0.0688
18.62	0.663	-0.0739	-5.80	-0.372	-0.0068	19.58	0.675	-0.0686
19.50	0.665	-0.0735	-6.96	-0.442	-0.0081	20.46	0.675	-0.0670
20.47	0.669	-0.0730	-7.76	-0.499	-0.0077	21.61	0.681	-0.0667
21.53	0.674	-0.0729	-8.83	-0.579	0.0062	22.66	0.681	-0.0662
22.23	0.673	-0.0722	-9.98	-0.637	0.0308	23.63	0.682	-0.0651
23.64	0.678	-0.0724	-10.86	-0.664	0.0485	24.59	0.685	-0.0659
24.52	0.681	-0.0739	-11.92	-0.677	0.0628	25.56	0.688	-0.0655
			-12.89	-0.682	0.0718	26.62	0.688	-0.0660

			AR3-I100-FP1		
27.58	0.688	-0.0661	Fig. 5.7		
28.64	0.691	-0.0667		26.59	0.677
29.61	0.692	-0.0679		27.55	0.684
29.43	0.686	-0.0662	Run: 0383ar	28.61	0.684
28.46	0.689	-0.0661	$Re = 59999.4$	29.66	0.690
27.32	0.686	-0.0654	$\alpha \quad C_L \quad C_M$	29.40	0.686
26.44	0.686	-0.0644	-14.86 -0.647 0.0643	28.43	0.688
25.38	0.680	-0.0638	-13.63 -0.643 0.0589	27.38	0.684
24.42	0.679	-0.0638	-12.57 -0.648 0.0537	26.59	0.676
23.45	0.677	-0.0638	-11.69 -0.640 0.0443	25.35	0.676
22.40	0.683	-0.0662	-10.55 -0.618 0.0294	24.39	0.676
21.43	0.677	-0.0665	-9.57 -0.587 0.0113	23.42	0.676
20.46	0.677	-0.0675	-8.60 -0.534 -0.0058	22.36	0.670
19.67	0.680	-0.0691	-7.62 -0.465 -0.0133	21.40	0.665
18.35	0.673	-0.0693	-6.55 -0.407 -0.0125	20.43	0.666
17.30	0.692	-0.0731	-5.58 -0.341 -0.0110	19.38	0.663
16.42	0.696	-0.0739	-4.51 -0.283 -0.0087	18.41	0.657
15.37	0.720	-0.0763	-3.53 -0.205 -0.0105	17.35	0.650
14.41	0.739	-0.0759	-2.47 -0.144 -0.0070	16.39	0.651
13.44	0.723	-0.0688	-1.85 -0.103 -0.0053	15.42	0.659
12.47	0.720	-0.0601	-0.43 -0.028 -0.0009	14.37	0.660
11.33	0.709	-0.0457	0.46 0.030 0.0026	13.40	0.660
10.36	0.682	-0.0273	1.26 0.069 0.0049	12.43	0.658
9.38	0.623	-0.0040	2.59 0.147 0.0087	11.29	0.651
8.40	0.560	0.0081	3.48 0.203 0.0127	10.41	0.635
7.42	0.492	0.0073	4.54 0.277 0.0124	9.35	0.596
6.27	0.427	0.0045	5.52 0.341 0.0147	8.37	0.532
5.29	0.368	0.0026	6.50 0.402 0.0164	7.39	0.466
4.32	0.304	0.0012	7.57 0.472 0.0178	6.32	0.400
3.34	0.227	0.0017	8.63 0.535 0.0104	5.53	0.354
2.36	0.152	0.0068	9.52 0.594 -0.0068	4.28	0.276
1.20	0.082	0.0035	10.58 0.630 -0.0277	3.30	0.198
0.23	0.024	0.0006	11.37 0.644 -0.0383	2.33	0.142
-0.66	-0.033	-0.0025	12.52 0.661 -0.0494	1.17	0.080
-1.55	-0.091	-0.0057	13.57 0.651 -0.0551	0.37	0.031
-2.71	-0.190	-0.0004	14.54 0.658 -0.0580	-0.78	-0.034
-3.69	-0.253	-0.0011	15.51 0.641 -0.0597	-1.67	-0.092
-4.84	-0.325	-0.0030	16.65 0.647 -0.0621	-2.73	-0.148
-5.73	-0.384	-0.0045	17.62 0.649 -0.0632	-3.71	-0.209
-6.88	-0.450	-0.0065	18.67 0.649 -0.0647	-4.78	-0.293
-7.86	-0.512	-0.0068	19.64 0.656 -0.0663	-5.84	-0.347
-8.84	-0.587	0.0079	20.43 0.667 -0.0674	-6.82	-0.418
-9.90	-0.642	0.0310	21.66 0.666 -0.0662	-7.89	-0.480
-10.79	-0.672	0.0490	22.63 0.670 -0.0681	-8.86	-0.544
-11.85	-0.687	0.0633	23.60 0.674 -0.0673	-9.84	-0.599
-12.81	-0.689	0.0725	24.65 0.674 -0.0679	-10.81	-0.626
-13.78	-0.688	0.0775	25.62 0.679 -0.0682	-11.87	-0.638
-14.57	-0.690	0.0812		-12.92	-0.644
				-13.89	-0.643
					0.0614

-14.95	-0.645	0.0654	28.51	0.686	-0.0691		Run: 0386ar	
			29.57	0.693	-0.0704		$Re = 99999.2$	
Run: 0384ar			29.30	0.693	-0.0699			
$Re = 80000.3$			28.34	0.692	-0.0683			
α	C_L	C_M	27.28	0.690	-0.0678		α	C_L
-14.96	-0.665	0.0689	26.31	0.683	-0.0667		-14.73	-0.688
-13.64	-0.670	0.0646	25.26	0.681	-0.0660		-13.76	-0.684
-12.68	-0.673	0.0578	24.29	0.684	-0.0663		-12.79	-0.690
-11.80	-0.666	0.0488	23.32	0.683	-0.0659		-11.83	-0.686
-10.73	-0.638	0.0335	22.27	0.681	-0.0672		-10.77	-0.658
-10.03	-0.619	0.0219	21.21	0.683	-0.0670		-9.79	-0.624
-8.70	-0.550	-0.0030	20.25	0.678	-0.0675		-8.73	-0.567
-7.72	-0.484	-0.0104	19.19	0.674	-0.0667		-7.75	-0.497
-6.74	-0.422	-0.0100	18.49	0.669	-0.0672		-6.78	-0.435
-5.68	-0.360	-0.0086	17.17	0.665	-0.0654		-5.71	-0.369
-4.97	-0.319	-0.0071	16.29	0.665	-0.0637		-4.73	-0.316
-3.64	-0.232	-0.0055	15.50	0.669	-0.0629		-3.67	-0.248
-2.57	-0.151	-0.0071	14.27	0.673	-0.0601		-2.60	-0.158
-1.68	-0.099	-0.0053	13.22	0.679	-0.0568		-1.62	-0.102
-0.62	-0.037	-0.0011	12.34	0.675	-0.0501		-0.56	-0.036
0.36	0.022	0.0029	11.28	0.660	-0.0399		0.33	0.021
1.34	0.077	0.0060	10.40	0.645	-0.0281		2.37	0.143
2.40	0.140	0.0094	9.16	0.596	-0.0058		3.18	0.211
3.47	0.214	0.0106	8.27	0.542	0.0100		4.42	0.299
4.36	0.283	0.0104	7.29	0.473	0.0150		5.13	0.351
5.43	0.353	0.0133	6.40	0.417	0.0131		6.38	0.426
6.40	0.412	0.0150	5.16	0.341	0.0115		7.44	0.499
7.29	0.467	0.0166	4.18	0.282	0.0095		8.51	0.572
8.45	0.555	0.0082	3.20	0.202	0.0115		9.22	0.612
9.43	0.612	-0.0100	2.23	0.142	0.0095		10.46	0.665
10.48	0.644	-0.0295	1.07	0.074	0.0061		11.43	0.692
11.46	0.667	-0.0423	0.10	0.021	0.0031		12.49	0.705
12.51	0.674	-0.0514	-0.79	-0.035	-0.0003		13.45	0.697
13.48	0.672	-0.0575	-1.86	-0.100	-0.0038		14.42	0.689
14.44	0.669	-0.0609	-2.83	-0.157	-0.0065		15.47	0.682
15.50	0.671	-0.0625	-3.81	-0.237	-0.0042		16.53	0.678
16.47	0.666	-0.0644	-4.88	-0.308	-0.0061		17.41	0.675
17.43	0.667	-0.0659	-5.94	-0.369	-0.0077		18.46	0.676
18.49	0.663	-0.0661	-6.92	-0.439	-0.0093		19.43	0.676
19.45	0.666	-0.0664	-7.90	-0.495	-0.0089		20.40	0.683
20.42	0.671	-0.0675	-8.88	-0.562	0.0012		21.36	0.686
21.48	0.675	-0.0662	-9.94	-0.614	0.0221		22.42	0.686
22.44	0.679	-0.0667	-10.91	-0.646	0.0398		23.47	0.684
23.50	0.680	-0.0651	-11.88	-0.660	0.0519		24.44	0.685
24.55	0.679	-0.0660	-12.94	-0.674	0.0616		25.41	0.691
25.52	0.689	-0.0672	-13.99	-0.673	0.0665		26.46	0.690
26.49	0.681	-0.0664	-15.05	-0.669	0.0702		27.43	0.695
27.45	0.687	-0.0675					28.48	0.698
							29.45	0.698
								-0.0682

29.45	0.692	-0.0676	Run: 0385ar	29.22	0.698	-0.0605		
28.31	0.696	-0.0672	$Re = 119998.1$	28.25	0.695	-0.0592		
27.16	0.694	-0.0661	α	C_L	C_M	27.11	0.693	-0.0586
26.20	0.689	-0.0649	-14.87	-0.714	0.0727	26.14	0.690	-0.0578
25.32	0.688	-0.0645	-14.08	-0.722	0.0687	25.26	0.687	-0.0578
24.26	0.685	-0.0649	-13.12	-0.720	0.0619	24.21	0.686	-0.0577
23.30	0.683	-0.0646	-11.80	-0.697	0.0492	23.24	0.684	-0.0581
22.24	0.685	-0.0657	-10.82	-0.669	0.0354	22.19	0.687	-0.0598
21.19	0.682	-0.0657	-9.85	-0.630	0.0190	21.22	0.685	-0.0602
20.22	0.680	-0.0674	-8.70	-0.564	-0.0002	20.25	0.687	-0.0624
19.43	0.679	-0.0670	-7.72	-0.501	-0.0073	19.37	0.683	-0.0624
18.28	0.675	-0.0674	-6.83	-0.446	-0.0059	18.23	0.680	-0.0627
17.41	0.677	-0.0665	-5.77	-0.382	-0.0044	17.18	0.684	-0.0626
16.26	0.685	-0.0664	-4.79	-0.319	-0.0030	16.21	0.688	-0.0619
15.30	0.686	-0.0644	-3.72	-0.252	-0.0013	15.25	0.731	-0.0657
14.16	0.693	-0.0623	-2.74	-0.161	-0.0079	14.20	0.734	-0.0608
13.28	0.701	-0.0582	-1.76	-0.100	-0.0053	13.23	0.725	-0.0541
12.31	0.701	-0.0515	-0.61	-0.036	-0.0012	12.26	0.717	-0.0460
11.17	0.684	-0.0398	0.28	0.016	0.0023	11.20	0.698	-0.0349
10.28	0.659	-0.0285	1.25	0.081	0.0063	10.23	0.668	-0.0221
9.13	0.609	-0.0098	2.41	0.151	0.0107	9.43	0.633	-0.0099
8.24	0.555	0.0061	3.30	0.245	0.0056	8.28	0.561	0.0079
7.26	0.483	0.0123	4.28	0.306	0.0074	7.21	0.486	0.0131
6.38	0.433	0.0103	5.08	0.361	0.0093	6.32	0.437	0.0106
5.13	0.354	0.0079	6.32	0.439	0.0130	5.08	0.362	0.0078
4.25	0.297	0.0062	7.48	0.508	0.0160	4.19	0.301	0.0062
3.18	0.218	0.0059	8.37	0.575	0.0057	3.13	0.230	0.0050
2.11	0.143	0.0081	9.08	0.620	-0.0048	2.06	0.144	0.0104
1.04	0.078	0.0048	10.41	0.675	-0.0255	0.99	0.078	0.0066
0.16	0.025	0.0020	11.38	0.704	-0.0379	0.10	0.020	0.0034
-0.82	-0.038	-0.0016	12.35	0.717	-0.0474	-0.87	-0.038	-0.0002
-1.80	-0.102	-0.0051	13.49	0.725	-0.0560	-2.03	-0.113	-0.0044
-2.95	-0.169	-0.0083	14.37	0.740	-0.0636	-3.01	-0.190	-0.0023
-3.84	-0.249	-0.0033	15.43	0.723	-0.0653	-3.90	-0.264	-0.0001
-5.00	-0.321	-0.0055	16.39	0.685	-0.0624	-4.97	-0.332	-0.0021
-5.89	-0.382	-0.0071	17.35	0.683	-0.0630	-5.94	-0.393	-0.0037
-6.78	-0.439	-0.0084	18.41	0.678	-0.0630	-7.10	-0.464	-0.0061
-7.84	-0.510	-0.0097	19.46	0.684	-0.0629	-8.07	-0.524	-0.0070
-8.91	-0.582	0.0029	20.43	0.688	-0.0626	-8.96	-0.588	0.0055
-10.06	-0.637	0.0246	21.40	0.690	-0.0619	-9.76	-0.630	0.0186
-10.95	-0.668	0.0387	22.45	0.686	-0.0594	-10.82	-0.670	0.0356
-11.91	-0.686	0.0507	23.50	0.686	-0.0582	-12.06	-0.702	0.0517
-12.97	-0.694	0.0608	24.38	0.688	-0.0584	-12.85	-0.712	0.0601
-13.94	-0.689	0.0666	25.44	0.688	-0.0582	-14.09	-0.726	0.0694
-14.81	-0.678	0.0682	26.49	0.692	-0.0586	-15.05	-0.708	0.0737
			27.37	0.693	-0.0593			
			28.52	0.698	-0.0601			
			29.40	0.700	-0.0609			

AR4-I050-FP1			26.72	0.657	-0.0714	-14.59	-0.620	0.0692
Fig. 5.8			27.68	0.662	-0.0735	Run: 0404ga		
Run: 0403ga			28.74	0.668	-0.0755	$Re = 79998.7$		
$Re = 59998.7$			29.71	0.670	-0.0776	α	C_L	C_M
α	C_L	C_M	29.53	0.675	-0.0769	-14.84	-0.630	0.0720
-14.77	-0.610	0.0673	28.56	0.669	-0.0750	-13.53	-0.652	0.0745
-13.54	-0.631	0.0692	27.51	0.662	-0.0721	-12.65	-0.671	0.0734
-12.49	-0.650	0.0684	26.45	0.653	-0.0708	-11.60	-0.683	0.0665
-11.62	-0.674	0.0622	25.57	0.646	-0.0687	-10.90	-0.690	0.0570
-10.56	-0.671	0.0469	24.51	0.640	-0.0680	-9.57	-0.653	0.0230
-9.59	-0.639	0.0195	23.55	0.638	-0.0665	-8.59	-0.582	-0.0006
-8.43	-0.566	-0.0035	22.40	0.631	-0.0661	-7.61	-0.510	-0.0078
-7.54	-0.494	-0.0093	21.52	0.626	-0.0643	-6.81	-0.461	-0.0082
-6.56	-0.434	-0.0096	20.47	0.621	-0.0654	-5.56	-0.374	-0.0065
-5.40	-0.359	-0.0094	19.50	0.626	-0.0646	-4.58	-0.309	-0.0063
-4.51	-0.299	-0.0084	18.53	0.620	-0.0654	-3.51	-0.238	-0.0064
-3.44	-0.213	-0.0110	17.48	0.621	-0.0647	-2.44	-0.151	-0.0088
-2.46	-0.151	-0.0094	16.51	0.624	-0.0658	-1.54	-0.090	-0.0067
-1.39	-0.085	-0.0068	15.55	0.632	-0.0652	-0.48	-0.028	-0.0041
-0.41	-0.024	-0.0042	14.50	0.646	-0.0675	0.59	0.035	-0.0015
0.66	0.038	-0.0017	13.53	0.656	-0.0660	1.48	0.091	0.0012
1.55	0.096	0.0007	12.66	0.674	-0.0639	2.55	0.162	0.0048
2.71	0.170	0.0039	11.52	0.687	-0.0516	3.54	0.244	0.0045
3.60	0.237	0.0053	10.55	0.675	-0.0323	4.52	0.322	0.0046
4.58	0.310	0.0054	9.48	0.626	-0.0074	5.41	0.378	0.0059
5.47	0.366	0.0072	8.50	0.555	0.0051	6.57	0.463	0.0084
6.63	0.450	0.0080	7.52	0.487	0.0081	7.46	0.520	0.0095
7.79	0.528	0.0073	6.36	0.419	0.0063	8.62	0.614	-0.0008
8.69	0.602	-0.0017	5.47	0.358	0.0070	9.42	0.656	-0.0147
9.66	0.659	-0.0232	4.49	0.289	0.0050	10.66	0.698	-0.0454
10.72	0.682	-0.0463	3.42	0.215	0.0059	11.63	0.701	-0.0571
11.69	0.679	-0.0587	2.71	0.169	0.0045	12.59	0.690	-0.0652
12.65	0.663	-0.0653	1.37	0.082	0.0005	13.64	0.671	-0.0682
13.71	0.644	-0.0670	0.57	0.034	-0.0014	14.70	0.658	-0.0687
14.76	0.632	-0.0662	-0.59	-0.036	-0.0047	15.66	0.643	-0.0672
15.72	0.621	-0.0652	-1.66	-0.105	-0.0074	16.62	0.638	-0.0662
16.69	0.620	-0.0653	-2.63	-0.164	-0.0091	17.68	0.633	-0.0653
17.65	0.617	-0.0651	-3.62	-0.229	-0.0095	18.64	0.632	-0.0652
18.71	0.618	-0.0655	-4.69	-0.308	-0.0089	19.61	0.632	-0.0645
19.68	0.620	-0.0647	-5.67	-0.378	-0.0096	20.58	0.637	-0.0643
20.64	0.623	-0.0653	-6.74	-0.446	-0.0101	21.64	0.639	-0.0634
21.52	0.625	-0.0643	-7.72	-0.513	-0.0086	22.43	0.639	-0.0637
22.67	0.632	-0.0659	-8.70	-0.586	0.0012	23.57	0.647	-0.0642
23.72	0.635	-0.0669	-9.77	-0.654	0.0295	24.63	0.653	-0.0652
24.69	0.645	-0.0680	-10.74	-0.672	0.0525	25.59	0.661	-0.0664
25.66	0.653	-0.0698	-11.79	-0.663	0.0662	26.74	0.665	-0.0681
			-12.75	-0.643	0.0701	27.62	0.668	-0.0692
			-13.72	-0.630	0.0699			

28.67	0.673	-0.0707	Run: 0405ga	29.45	0.684	-0.0663		
29.64	0.682	-0.0729	$Re = 99998.0$	28.49	0.678	-0.0654		
29.64	0.680	-0.0733	α	C_L	C_M	27.34	0.674	-0.0634
28.41	0.673	-0.0705	-14.68	-0.639	0.0730	26.46	0.670	-0.0633
27.44	0.671	-0.0691	-13.63	-0.660	0.0758	25.41	0.662	-0.0612
26.39	0.665	-0.0679	-12.66	-0.679	0.0751	24.44	0.657	-0.0611
25.42	0.661	-0.0663	-11.61	-0.693	0.0681	23.47	0.653	-0.0607
24.36	0.654	-0.0655	-10.82	-0.698	0.0578	22.33	0.645	-0.0607
23.48	0.645	-0.0639	-9.67	-0.663	0.0276	21.45	0.643	-0.0606
22.34	0.642	-0.0641	-8.60	-0.595	0.0019	20.39	0.641	-0.0619
21.46	0.638	-0.0634	-7.53	-0.516	-0.0070	19.60	0.639	-0.0624
20.40	0.635	-0.0646	-6.91	-0.474	-0.0070	18.64	0.640	-0.0635
19.44	0.634	-0.0647	-5.57	-0.390	-0.0054	17.32	0.649	-0.0652
18.38	0.636	-0.0654	-4.59	-0.322	-0.0043	16.35	0.659	-0.0674
17.33	0.639	-0.0655	-3.61	-0.255	-0.0035	15.39	0.670	-0.0686
16.36	0.644	-0.0670	-2.54	-0.157	-0.0098	14.34	0.689	-0.0696
15.57	0.653	-0.0679	-1.55	-0.090	-0.0073	13.46	0.704	-0.0663
14.43	0.669	-0.0697	-0.49	-0.029	-0.0046	12.41	0.718	-0.0588
13.47	0.687	-0.0673	0.49	0.029	-0.0018	11.36	0.715	-0.0455
12.42	0.700	-0.0609	1.47	0.095	0.0017	10.47	0.696	-0.0288
11.45	0.703	-0.0473	2.54	0.166	0.0054	9.41	0.660	-0.0111
10.39	0.682	-0.0268	3.53	0.255	0.0017	8.43	0.606	0.0025
9.42	0.636	-0.0071	4.60	0.334	0.0024	7.54	0.540	0.0088
8.35	0.574	0.0051	5.58	0.408	0.0049	6.29	0.459	0.0055
7.37	0.501	0.0082	6.56	0.477	0.0078	5.40	0.391	0.0033
6.39	0.428	0.0057	7.63	0.558	0.0092	4.33	0.317	0.0009
5.41	0.368	0.0042	8.62	0.641	-0.0043	3.35	0.242	0.0010
4.42	0.297	0.0031	9.42	0.683	-0.0199	2.63	0.182	0.0047
3.36	0.223	0.0042	10.65	0.714	-0.0461	1.21	0.089	0.0018
2.55	0.174	0.0052	11.62	0.715	-0.0569	0.32	0.031	-0.0011
1.31	0.091	0.0019	12.67	0.706	-0.0642	-0.75	-0.027	-0.0036
0.33	0.030	-0.0011	13.73	0.694	-0.0685	-1.82	-0.094	-0.0065
-0.65	-0.034	-0.0038	14.60	0.683	-0.0700	-2.71	-0.154	-0.0085
-1.72	-0.095	-0.0062	15.65	0.659	-0.0677	-3.70	-0.245	-0.0025
-2.70	-0.158	-0.0080	16.62	0.654	-0.0663	-4.77	-0.322	-0.0035
-3.68	-0.228	-0.0064	17.58	0.649	-0.0650	-5.57	-0.379	-0.0046
-4.75	-0.313	-0.0060	18.72	0.640	-0.0632	-6.82	-0.464	-0.0070
-5.73	-0.377	-0.0061	19.60	0.641	-0.0623	-7.89	-0.534	-0.0071
-6.80	-0.450	-0.0076	20.57	0.644	-0.0618	-8.87	-0.613	0.0057
-7.79	-0.522	-0.0073	21.62	0.643	-0.0605	-9.94	-0.679	0.0359
-8.77	-0.596	0.0026	22.68	0.650	-0.0605	-10.82	-0.698	0.0575
-9.84	-0.663	0.0302	23.65	0.652	-0.0606	-11.88	-0.691	0.0696
-10.81	-0.687	0.0558	24.70	0.660	-0.0614	-12.84	-0.674	0.0747
-11.77	-0.679	0.0682	25.67	0.664	-0.0621	-13.80	-0.655	0.0743
-12.82	-0.663	0.0733	26.64	0.672	-0.0632	-14.59	-0.638	0.0719
-13.79	-0.642	0.0728	27.61	0.676	-0.0644			
-14.58	-0.632	0.0714	28.75	0.682	-0.0659			
			29.63	0.686	-0.0673			

Run: 0406ga			29.30	0.683	-0.0612	AR4-l075-FP1
$Re = 120000.2$			28.24	0.677	-0.0603	Fig. 5.9
α	C_L	C_M	27.28	0.673	-0.0592	
-15.01	-0.646	0.0763	26.48	0.667	-0.0584	
-13.78	-0.663	0.0790	25.34	0.664	-0.0573	
-13.08	-0.675	0.0793	24.29	0.658	-0.0573	
-11.77	-0.701	0.0743	23.32	0.651	-0.0564	
-10.80	-0.705	0.0614	22.17	0.648	-0.0572	
-9.83	-0.685	0.0390	21.29	0.644	-0.0574	
-8.76	-0.630	0.0130	20.24	0.641	-0.0589	
-7.78	-0.546	-0.0036	19.45	0.641	-0.0597	
-6.89	-0.499	-0.0038	18.57	0.645	-0.0613	
-5.73	-0.417	-0.0026	17.16	0.651	-0.0637	
-4.75	-0.356	-0.0015	16.55	0.658	-0.0654	
-3.68	-0.280	-0.0011	15.32	0.674	-0.0686	
-2.70	-0.196	-0.0048	14.28	0.699	-0.0706	
-1.98	-0.136	-0.0087	13.31	0.716	-0.0673	
-0.64	-0.036	-0.0044	12.26	0.726	-0.0590	
0.42	0.024	-0.0015	11.29	0.723	-0.0451	
1.32	0.090	0.0024	10.32	0.702	-0.0277	
2.48	0.182	0.0046	9.26	0.672	-0.0124	
3.37	0.268	0.0003	8.20	0.640	-0.0017	
4.36	0.346	0.0014	7.30	0.569	0.0087	
5.25	0.416	0.0045	6.23	0.489	0.0052	
6.41	0.516	0.0093	5.16	0.407	0.0015	
7.49	0.594	0.0080	4.18	0.329	-0.0017	
8.56	0.672	-0.0105	3.19	0.251	-0.0018	
9.27	0.704	-0.0256	2.12	0.152	0.0044	
10.59	0.726	-0.0467	1.14	0.090	0.0018	
11.47	0.726	-0.0559	0.16	0.032	-0.0012	
12.43	0.718	-0.0639	-0.82	-0.027	-0.0038	
13.40	0.704	-0.0678	-1.89	-0.095	-0.0066	
14.36	0.688	-0.0693	-2.96	-0.169	-0.0074	
15.50	0.670	-0.0673	-3.86	-0.264	0.0004	
16.46	0.657	-0.0652	-4.92	-0.337	-0.0004	
17.43	0.647	-0.0626	-5.91	-0.404	-0.0019	
18.57	0.642	-0.0610	-6.97	-0.476	-0.0045	
19.45	0.640	-0.0594	-7.96	-0.546	-0.0046	
20.41	0.641	-0.0586	-8.94	-0.622	0.0103	
21.47	0.643	-0.0571	-10.01	-0.687	0.0399	
22.44	0.649	-0.0569	-10.98	-0.707	0.0622	
23.49	0.654	-0.0569	-12.03	-0.702	0.0758	
24.46	0.660	-0.0573	-12.99	-0.678	0.0800	
25.43	0.665	-0.0579	-13.96	-0.664	0.0801	
26.57	0.670	-0.0589	-15.01	-0.641	0.0761	
27.36	0.675	-0.0595				
28.51	0.680	-0.0607				
29.48	0.684	-0.0618				

27.34	0.690	-0.0734	-13.91	-0.624	0.0687	29.32	0.700	-0.0720
28.48	0.693	-0.0760				30.29	0.702	-0.0742
29.53	0.698	-0.0781	Run: 0413ar			30.11	0.703	-0.0740
30.50	0.703	-0.0811	$Re = 79996.1$			29.06	0.697	-0.0714
30.24	0.697	-0.0797	α	C_L	C_M	28.27	0.694	-0.0702
29.36	0.699	-0.0783	-14.21	-0.642	0.0716	27.12	0.690	-0.0678
28.22	0.695	-0.0759	-12.98	-0.648	0.0713	26.07	0.684	-0.0662
27.34	0.692	-0.0739	-12.02	-0.659	0.0689	25.01	0.677	-0.0647
26.28	0.681	-0.0713	-11.06	-0.668	0.0607	24.04	0.674	-0.0639
25.31	0.673	-0.0697	-9.91	-0.662	0.0434	22.99	0.664	-0.0619
24.25	0.670	-0.0686	-9.03	-0.630	0.0211	22.11	0.658	-0.0612
23.37	0.661	-0.0657	-7.96	-0.564	0.0002	21.14	0.656	-0.0615
22.32	0.657	-0.0657	-7.24	-0.507	-0.0063	20.08	0.652	-0.0620
21.26	0.654	-0.0646	-5.99	-0.422	-0.0064	19.12	0.650	-0.0620
20.29	0.650	-0.0649	-5.01	-0.349	-0.0051	17.97	0.647	-0.0625
19.33	0.649	-0.0649	-3.94	-0.286	-0.0038	17.18	0.648	-0.0631
18.27	0.643	-0.0649	-2.95	-0.194	-0.0081	16.13	0.650	-0.0643
17.39	0.642	-0.0646	-1.88	-0.125	-0.0058	14.99	0.655	-0.0643
16.25	0.642	-0.0649	-0.81	-0.058	-0.0030	14.37	0.659	-0.0642
15.28	0.645	-0.0639	0.17	0.012	0.0001	13.14	0.661	-0.0639
14.49	0.643	-0.0641	1.24	0.081	0.0032	12.09	0.673	-0.0628
13.35	0.644	-0.0624	2.13	0.146	0.0063	11.04	0.680	-0.0574
12.30	0.654	-0.0615	3.29	0.247	0.0049	10.25	0.679	-0.0498
11.33	0.659	-0.0570	4.19	0.321	0.0056	9.10	0.655	-0.0254
10.28	0.661	-0.0460	5.17	0.390	0.0081	8.12	0.599	-0.0025
9.31	0.647	-0.0265	6.25	0.469	0.0096	7.23	0.540	0.0077
8.24	0.589	-0.0025	7.23	0.537	0.0088	6.06	0.448	0.0085
7.26	0.512	0.0090	8.39	0.620	-0.0092	5.08	0.380	0.0069
6.19	0.442	0.0094	9.28	0.663	-0.0307	4.01	0.310	0.0048
5.21	0.374	0.0083	10.25	0.681	-0.0502	3.12	0.238	0.0050
4.31	0.306	0.0068	11.39	0.677	-0.0601	2.04	0.149	0.0062
3.24	0.219	0.0084	12.35	0.666	-0.0634	0.89	0.081	0.0036
2.08	0.148	0.0057	13.23	0.659	-0.0642	0.26	0.041	0.0019
1.19	0.084	0.0035	14.29	0.659	-0.0643	-1.08	-0.050	-0.0019
0.39	0.039	0.0016	15.25	0.651	-0.0640	-2.06	-0.115	-0.0049
-0.86	-0.044	-0.0019	16.39	0.651	-0.0645	-3.13	-0.190	-0.0079
-1.84	-0.106	-0.0048	17.09	0.651	-0.0634	-3.94	-0.269	-0.0033
-2.91	-0.176	-0.0071	18.24	0.650	-0.0631	-4.83	-0.334	-0.0047
-3.90	-0.261	-0.0064	19.29	0.647	-0.0620	-6.17	-0.433	-0.0070
-4.62	-0.317	-0.0069	20.26	0.652	-0.0621	-7.15	-0.503	-0.0068
-5.77	-0.385	-0.0086	21.32	0.657	-0.0617	-8.22	-0.582	0.0040
-6.93	-0.470	-0.0090	22.37	0.662	-0.0618	-8.94	-0.631	0.0218
-8.01	-0.545	-0.0027	23.34	0.667	-0.0625	-10.18	-0.668	0.0511
-8.99	-0.621	0.0212	24.39	0.672	-0.0636	-11.14	-0.668	0.0633
-9.70	-0.643	0.0367	25.36	0.682	-0.0655	-12.20	-0.660	0.0696
-11.01	-0.643	0.0584	26.16	0.682	-0.0661	-13.16	-0.648	0.0715
-11.98	-0.635	0.0651	27.30	0.690	-0.0683	-14.21	-0.646	0.0720
-13.03	-0.634	0.0681	28.27	0.693	-0.0699			

Run: 0415ar			30.05	0.703	-0.0654	Run: 0414ar		
$Re = 99998.0$			29.08	0.699	-0.0634	$Re = 119996.7$		
α	C_L	C_M	27.94	0.693	-0.0622	α	C_L	C_M
-14.28	-0.654	0.0721	27.06	0.692	-0.0612	-14.41	-0.665	0.0779
-13.05	-0.666	0.0724	26.09	0.689	-0.0607	-13.00	-0.682	0.0780
-12.09	-0.680	0.0697	25.04	0.685	-0.0593	-12.13	-0.693	0.0742
-11.12	-0.683	0.0618	24.07	0.675	-0.0584	-11.07	-0.694	0.0637
-10.07	-0.676	0.0470	22.92	0.667	-0.0568	-10.10	-0.680	0.0466
-9.09	-0.647	0.0258	22.04	0.659	-0.0561	-9.13	-0.644	0.0266
-8.02	-0.579	0.0021	21.07	0.655	-0.0561	-8.24	-0.595	0.0092
-6.95	-0.505	-0.0065	20.02	0.653	-0.0575	-7.08	-0.512	-0.0019
-6.06	-0.439	-0.0059	19.05	0.654	-0.0580	-6.10	-0.450	-0.0012
-4.90	-0.364	-0.0043	17.91	0.650	-0.0589	-5.21	-0.397	-0.0003
-4.01	-0.302	-0.0034	16.94	0.652	-0.0604	-4.04	-0.310	0.0006
-3.02	-0.223	-0.0035	16.07	0.659	-0.0621	-3.06	-0.240	0.0015
-1.95	-0.132	-0.0076	14.93	0.664	-0.0629	-1.98	-0.133	-0.0064
-0.88	-0.065	-0.0046	14.05	0.675	-0.0646	-1.00	-0.067	-0.0035
0.10	0.008	-0.0010	12.99	0.675	-0.0636	-0.11	-0.009	-0.0007
1.17	0.079	0.0029	12.03	0.689	-0.0628	1.05	0.085	0.0043
2.07	0.152	0.0067	11.07	0.696	-0.0571	2.04	0.167	0.0079
3.15	0.265	0.0026	10.01	0.689	-0.0449	3.12	0.278	0.0016
4.13	0.340	0.0048	9.04	0.668	-0.0277	4.10	0.349	0.0039
5.20	0.408	0.0078	8.06	0.612	-0.0046	5.17	0.419	0.0070
6.18	0.480	0.0102	6.90	0.524	0.0082	6.15	0.489	0.0102
6.99	0.534	0.0108	5.91	0.457	0.0066	7.13	0.560	0.0105
8.33	0.634	-0.0100	5.02	0.392	0.0044	8.03	0.624	-0.0020
9.21	0.677	-0.0322	3.86	0.317	0.0019	9.18	0.687	-0.0284
10.27	0.691	-0.0480	3.15	0.264	0.0007	10.24	0.705	-0.0455
11.33	0.695	-0.0585	1.80	0.144	0.0050	11.21	0.738	-0.0557
12.29	0.686	-0.0626	0.82	0.082	0.0020	12.19	0.776	-0.0651
13.17	0.675	-0.0628	-0.07	0.019	-0.0012	13.25	0.784	-0.0717
14.31	0.666	-0.0622	-1.14	-0.057	-0.0050	14.28	0.702	-0.0638
15.28	0.661	-0.0613	-2.12	-0.126	-0.0083	15.15	0.673	-0.0588
16.33	0.652	-0.0606	-3.11	-0.219	-0.0052	16.30	0.663	-0.0568
17.03	0.651	-0.0594	-4.01	-0.294	-0.0047	17.17	0.655	-0.0548
18.17	0.649	-0.0581	-4.90	-0.365	-0.0060	18.23	0.653	-0.0534
19.23	0.650	-0.0567	-6.33	-0.466	-0.0084	19.19	0.654	-0.0518
20.20	0.655	-0.0569	-7.22	-0.534	-0.0079	20.16	0.657	-0.0513
21.25	0.657	-0.0561	-8.21	-0.611	0.0084	21.13	0.660	-0.0502
22.31	0.664	-0.0567	-9.27	-0.665	0.0340	22.27	0.663	-0.0500
23.27	0.669	-0.0566	-10.24	-0.681	0.0520	22.98	0.668	-0.0501
24.33	0.678	-0.0582	-11.21	-0.683	0.0630	24.21	0.674	-0.0508
25.21	0.688	-0.0593	-12.26	-0.675	0.0692	25.27	0.684	-0.0517
26.27	0.688	-0.0603	-13.23	-0.662	0.0707	26.15	0.689	-0.0529
27.24	0.695	-0.0614	-14.28	-0.657	0.0706	27.20	0.698	-0.0543
28.20	0.698	-0.0629				27.99	0.697	-0.0545
29.26	0.703	-0.0642				29.31	0.710	-0.0571
30.23	0.708	-0.0662				30.28	0.710	-0.0583

			AR4-I100-FP1		
30.02	0.704	-0.0571	Fig. 5.10		
29.05	0.707	-0.0565			26.56 0.719 -0.0838
27.99	0.699	-0.0549			27.71 0.736 -0.0877
27.20	0.695	-0.0541	Run: 0396cs		28.85 0.743 -0.0899
26.06	0.687	-0.0527	$Re = 59998.4$		29.64 0.740 -0.0907
25.00	0.682	-0.0518	$\alpha \quad C_L \quad C_M$		29.56 0.741 -0.0903
24.03	0.674	-0.0509	-14.61 -0.660 0.0736		28.58 0.723 -0.0862
22.98	0.667	-0.0499	-13.56 -0.656 0.0707		27.70 0.723 -0.0856
21.92	0.662	-0.0499	-12.59 -0.644 0.0664		26.83 0.721 -0.0841
21.04	0.657	-0.0497	-11.54 -0.654 0.0608		25.59 0.698 -0.0790
19.98	0.656	-0.0513	-10.57 -0.647 0.0507		24.54 0.694 -0.0776
19.02	0.653	-0.0522	-9.51 -0.632 0.0315		23.56 0.678 -0.0741
17.96	0.656	-0.0543	-8.53 -0.588 0.0101		22.51 0.682 -0.0747
16.91	0.660	-0.0561	-7.55 -0.505 -0.0022		21.54 0.676 -0.0733
16.03	0.666	-0.0579	-6.83 -0.460 -0.0037		20.49 0.672 -0.0743
14.89	0.673	-0.0594	-5.41 -0.374 -0.0030		19.78 0.671 -0.0740
14.02	0.710	-0.0650	-4.52 -0.312 -0.0028		18.47 0.677 -0.0744
13.06	0.730	-0.0661	-3.44 -0.224 -0.0059		17.50 0.670 -0.0710
11.91	0.716	-0.0609	-2.46 -0.159 -0.0049		16.53 0.669 -0.0711
11.03	0.709	-0.0536	-1.39 -0.091 -0.0028		15.56 0.667 -0.0673
9.97	0.700	-0.0405	-0.41 -0.028 -0.0004		14.51 0.656 -0.0644
9.00	0.671	-0.0206	0.57 0.039 0.0018		13.54 0.646 -0.0600
8.02	0.618	-0.0007	1.55 0.097 0.0043		12.48 0.641 -0.0572
6.95	0.528	0.0101	2.62 0.169 0.0069		11.43 0.640 -0.0509
5.97	0.464	0.0074	3.60 0.241 0.0071		10.55 0.639 -0.0406
4.99	0.399	0.0047	4.59 0.318 0.0064		9.40 0.617 -0.0225
3.92	0.322	0.0024	5.66 0.392 0.0085		8.51 0.565 -0.0038
2.93	0.252	0.0009	6.64 0.456 0.0082		7.62 0.499 0.0067
1.86	0.145	0.0075	7.80 0.540 0.0014		6.37 0.418 0.0073
0.88	0.081	0.0044	8.51 0.582 -0.0096		5.47 0.351 0.0074
0.07	0.031	0.0017	9.67 0.626 -0.0316		4.49 0.286 0.0053
-1.18	-0.067	-0.0031	10.55 0.635 -0.0418		3.42 0.206 0.0080
-2.25	-0.138	-0.0062	11.69 0.635 -0.0536		2.44 0.144 0.0060
-3.15	-0.248	0.0016	12.66 0.635 -0.0583		1.37 0.080 0.0041
-4.23	-0.331	0.0003	13.71 0.640 -0.0611		0.39 0.020 0.0017
-4.94	-0.384	-0.0012	14.68 0.652 -0.0653		-0.59 -0.036 -0.0003
-6.28	-0.476	-0.0042	15.74 0.660 -0.0685		-1.66 -0.100 -0.0025
-7.26	-0.550	-0.0026	16.71 0.668 -0.0715		-2.73 -0.168 -0.0040
-8.33	-0.623	0.0147	17.67 0.667 -0.0733		-3.71 -0.234 -0.0048
-9.31	-0.671	0.0388	18.73 0.668 -0.0741		-4.69 -0.316 -0.0016
-10.28	-0.690	0.0567	19.70 0.672 -0.0748		-5.50 -0.365 -0.0022
-11.34	-0.695	0.0683	20.66 0.671 -0.0744		-6.83 -0.458 -0.0026
-12.30	-0.685	0.0747	21.72 0.673 -0.0742		-7.73 -0.525 0.0004
-13.27	-0.675	0.0775	22.69 0.681 -0.0752		-8.71 -0.595 0.0145
-14.41	-0.667	0.0778	23.74 0.689 -0.0766		-9.86 -0.637 0.0391
			24.71 0.699 -0.0787		-10.83 -0.650 0.0560
			25.68 0.712 -0.0815		-11.71 -0.647 0.0646
					-12.77 -0.652 0.0697
					-13.73 -0.653 0.0732

-14.52	-0.653	0.0758	28.86	0.754	-0.0861	Run: 0394cs
			29.82	0.745	-0.0859	$Re = 99996.1$
Run: 0395cs			29.56	0.757	-0.0871	α
$Re = 79997.4$			28.59	0.745	-0.0849	C_L
α	C_L	C_M	27.45	0.737	-0.0816	C_M
-14.79	-0.679	0.0777	26.48	0.722	-0.0792	-14.87
-13.47	-0.672	0.0743	25.59	0.703	-0.0752	-13.64
-12.86	-0.670	0.0718	24.45	0.694	-0.0736	-12.68
-11.63	-0.674	0.0644	23.75	0.685	-0.0722	-11.62
-10.57	-0.667	0.0522	22.43	0.686	-0.0724	-10.83
-9.60	-0.644	0.0325	21.46	0.682	-0.0712	-9.59
-8.53	-0.590	0.0103	20.49	0.679	-0.0723	-8.61
-7.46	-0.517	0.0000	19.52	0.679	-0.0725	-7.63
-6.75	-0.468	-0.0008	18.56	0.680	-0.0729	-6.65
-5.50	-0.383	-0.0005	17.50	0.683	-0.0721	-5.49
-4.52	-0.322	-0.0001	16.45	0.679	-0.0707	-4.60
-3.44	-0.239	-0.0032	15.57	0.676	-0.0685	-3.53
-2.46	-0.164	-0.0048	14.51	0.668	-0.0659	-2.45
-1.39	-0.095	-0.0028	13.54	0.660	-0.0622	-1.47
-0.50	-0.032	-0.0004	12.40	0.658	-0.0595	-0.58
0.57	0.037	0.0020	11.52	0.655	-0.0533	-0.036
1.55	0.095	0.0045	10.47	0.648	-0.0421	0.49
2.62	0.169	0.0071	9.49	0.624	-0.0245	0.030
3.61	0.257	0.0050	8.51	0.571	-0.0048	0.0020
4.59	0.326	0.0058	7.53	0.502	0.0055	0.0049
5.75	0.397	0.0074	6.46	0.422	0.0056	0.0063
6.73	0.462	0.0085	5.48	0.355	0.0049	0.257
7.72	0.541	0.0036	4.41	0.288	0.0032	0.0018
8.70	0.605	-0.0135	3.42	0.208	0.0055	-0.100
9.76	0.637	-0.0314	2.35	0.137	0.0055	-0.0034
10.82	0.652	-0.0467	1.37	0.074	0.0038	-0.0008
11.79	0.657	-0.0543	0.39	0.015	0.0014	0.0017
12.75	0.661	-0.0594	-0.59	-0.039	-0.0006	0.0017
13.81	0.663	-0.0623	-1.74	-0.108	-0.0027	0.0017
14.69	0.669	-0.0650	-2.64	-0.174	-0.0044	0.0017
15.83	0.675	-0.0678	-3.62	-0.252	-0.0020	0.0017
16.62	0.679	-0.0699	-4.69	-0.331	0.0004	0.0017
17.68	0.677	-0.0712	-5.67	-0.398	-0.0002	0.0017
18.47	0.676	-0.0718	-6.75	-0.471	-0.0004	0.0017
19.79	0.679	-0.0719	-7.82	-0.544	0.0022	0.0017
20.67	0.679	-0.0714	-8.71	-0.611	0.0170	0.0017
21.64	0.686	-0.0720	-9.78	-0.658	0.0414	0.0017
22.78	0.689	-0.0717	-10.74	-0.673	0.0575	0.0017
23.75	0.693	-0.0723	-11.80	-0.674	0.0674	0.0017
24.80	0.698	-0.0739	-12.77	-0.672	0.0722	0.0017
25.77	0.711	-0.0758	-13.73	-0.674	0.0748	0.0017
26.48	0.722	-0.0787	-14.79	-0.681	0.0784	0.0017
27.71	0.740	-0.0830				0.0017

29.66	0.751	-0.0790	Run: 0399cs	29.49	0.747	-0.0718		
28.51	0.735	-0.0761	$Re = 120000.9$	28.52	0.739	-0.0709		
27.45	0.730	-0.0742	α	C_L	C_M	27.47	0.727	-0.0683
26.40	0.718	-0.0725	-14.87	-0.722	0.0915	26.50	0.725	-0.0682
25.43	0.706	-0.0700	-13.55	-0.709	0.0854	25.44	0.714	-0.0661
24.46	0.698	-0.0690	-12.67	-0.710	0.0801	24.47	0.700	-0.0645
23.49	0.691	-0.0678	-11.70	-0.717	0.0713	23.50	0.695	-0.0635
22.35	0.689	-0.0684	-10.64	-0.705	0.0553	22.45	0.691	-0.0640
21.47	0.687	-0.0681	-9.67	-0.663	0.0380	21.48	0.690	-0.0645
20.41	0.683	-0.0695	-8.87	-0.621	0.0211	20.43	0.695	-0.0673
19.45	0.684	-0.0696	-7.62	-0.529	0.0087	19.64	0.694	-0.0672
18.48	0.684	-0.0705	-6.90	-0.488	0.0088	18.67	0.697	-0.0672
17.43	0.686	-0.0693	-5.57	-0.403	0.0083	17.35	0.702	-0.0671
16.46	0.693	-0.0695	-4.59	-0.336	0.0075	16.39	0.702	-0.0668
15.49	0.687	-0.0669	-3.60	-0.267	0.0064	15.51	0.697	-0.0647
14.44	0.676	-0.0650	-2.52	-0.165	-0.0031	14.45	0.694	-0.0639
13.47	0.676	-0.0626	-1.46	-0.098	-0.0016	13.40	0.692	-0.0621
12.50	0.673	-0.0596	-0.47	-0.032	0.0008			
11.45	0.670	-0.0525	0.51	0.035	0.0035			
10.39	0.659	-0.0413	1.49	0.095	0.0064			
9.59	0.641	-0.0283	2.56	0.183	0.0045			
8.35	0.575	-0.0048	3.54	0.256	0.0021			
7.36	0.501	0.0053	4.53	0.327	0.0035			
6.38	0.427	0.0040	5.42	0.386	0.0051			
5.58	0.378	0.0029	6.40	0.453	0.0067			
4.33	0.290	0.0014	7.65	0.558	0.0036			
3.35	0.218	0.0020	8.64	0.625	-0.0146			
2.36	0.130	0.0060	9.61	0.660	-0.0309			
1.29	0.068	0.0040	10.76	0.682	-0.0470			
0.31	0.016	0.0018	11.64	0.688	-0.0543			
-0.58	-0.043	-0.0003	12.61	0.686	-0.0588			
-1.74	-0.115	-0.0031	13.66	0.691	-0.0607			
-2.81	-0.186	-0.0035	14.63	0.693	-0.0621			
-3.71	-0.274	0.0032	15.77	0.701	-0.0647			
-4.78	-0.344	0.0031	16.39	0.702	-0.0659			
-5.49	-0.395	0.0030	17.70	0.698	-0.0659			
-6.92	-0.484	0.0025	18.67	0.698	-0.0666			
-7.81	-0.550	0.0039	19.64	0.690	-0.0660			
-8.79	-0.623	0.0196	20.69	0.691	-0.0657			
-9.86	-0.669	0.0426	21.66	0.691	-0.0645			
-10.83	-0.688	0.0585	22.63	0.692	-0.0638			
-11.89	-0.693	0.0694	23.68	0.693	-0.0630			
-12.94	-0.689	0.0753	24.74	0.702	-0.0641			
-13.82	-0.696	0.0798	25.62	0.710	-0.0651			
-14.88	-0.710	0.0851	26.68	0.727	-0.0684			
			27.65	0.744	-0.0711			
			28.79	0.744	-0.0718			
			29.76	0.742	-0.0717			

AR5-l100-FP1

Fig. 5.11

Run: 0420ga

 $Re = 59999.7$

α	C_L	C_M
-15.75	-0.688	0.0848
-14.43	-0.669	0.0796
-13.55	-0.659	0.0763
-12.49	-0.653	0.0723
-11.52	-0.652	0.0680
-10.56	-0.656	0.0599
-9.41	-0.650	0.0451
-8.44	-0.620	0.0237
-7.54	-0.549	0.0060
-6.38	-0.466	0.0024
-5.48	-0.401	0.0021
-4.40	-0.327	0.0027
-3.41	-0.233	-0.0017
-2.34	-0.158	-0.0005
-1.35	-0.091	0.0008
-0.36	-0.025	0.0027
0.62	0.042	0.0044
1.70	0.120	0.0062
2.68	0.185	0.0080
3.59	0.279	0.0054
4.75	0.364	0.0057
5.74	0.429	0.0059
6.81	0.513	0.0022

7.80	0.589	-0.0160	2.50	0.182	0.0076	9.52	0.652	-0.0503
8.78	0.625	-0.0361	1.43	0.111	0.0061	10.84	0.654	-0.0628
9.66	0.631	-0.0488	0.35	0.038	0.0048	11.72	0.651	-0.0665
10.80	0.630	-0.0596	-0.63	-0.031	0.0032	12.86	0.657	-0.0699
11.77	0.632	-0.0644	-1.53	-0.098	0.0017	13.74	0.664	-0.0723
12.83	0.638	-0.0673	-2.69	-0.171	0.0002	14.89	0.683	-0.0763
13.88	0.649	-0.0710	-3.59	-0.244	-0.0004	15.77	0.689	-0.0779
14.85	0.664	-0.0745	-4.58	-0.334	0.0035	16.56	0.694	-0.0791
15.91	0.675	-0.0782	-5.48	-0.397	0.0034	17.88	0.697	-0.0810
16.79	0.682	-0.0801	-6.64	-0.483	0.0035	18.85	0.697	-0.0806
17.85	0.679	-0.0809	-7.72	-0.566	0.0097	19.82	0.697	-0.0804
18.81	0.684	-0.0824	-8.44	-0.617	0.0243	20.78	0.698	-0.0795
19.78	0.690	-0.0834	-9.50	-0.652	0.0473	21.75	0.704	-0.0800
20.84	0.687	-0.0823	-10.82	-0.654	0.0656	22.81	0.706	-0.0800
21.81	0.700	-0.0842	-11.70	-0.652	0.0705	23.78	0.722	-0.0833
22.86	0.701	-0.0843	-12.76	-0.655	0.0751	24.84	0.749	-0.0882
23.92	0.716	-0.0873	-13.73	-0.663	0.0785	25.91	0.800	-0.0987
24.89	0.728	-0.0899	-14.70	-0.678	0.0828	26.53	0.826	-0.1047
25.95	0.752	-0.0963	-15.75	-0.689	0.0863	27.93	0.802	-0.1011
26.84	0.783	-0.1032				28.81	0.808	-0.1032
27.63	0.788	-0.1054	Run: 0421ga			28.55	0.811	-0.1036
28.87	0.811	-0.1118	$Re = 79999.2$			27.67	0.802	-0.1016
28.69	0.813	-0.1114	α	C_L	C_M	26.62	0.827	-0.1058
27.72	0.796	-0.1070	-15.82	-0.705	0.0872	25.64	0.771	-0.0943
26.66	0.772	-0.1008	-14.49	-0.685	0.0821	24.66	0.727	-0.0846
25.60	0.741	-0.0939	-13.61	-0.678	0.0790	23.51	0.716	-0.0828
24.72	0.733	-0.0911	-12.55	-0.672	0.0759	22.81	0.701	-0.0801
23.57	0.709	-0.0862	-11.59	-0.674	0.0718	21.57	0.700	-0.0806
22.60	0.699	-0.0838	-10.62	-0.673	0.0629	20.61	0.699	-0.0811
21.81	0.696	-0.0834	-9.56	-0.665	0.0487	19.55	0.701	-0.0824
20.57	0.695	-0.0835	-8.50	-0.629	0.0260	18.50	0.698	-0.0814
19.61	0.692	-0.0832	-7.60	-0.565	0.0093	17.53	0.691	-0.0808
18.55	0.689	-0.0825	-6.44	-0.478	0.0045	16.56	0.697	-0.0807
17.67	0.683	-0.0816	-5.45	-0.413	0.0043	15.51	0.685	-0.0781
16.53	0.682	-0.0803	-4.55	-0.345	0.0045	14.54	0.675	-0.0755
15.56	0.675	-0.0779	-3.39	-0.257	0.0028	13.57	0.660	-0.0724
14.59	0.660	-0.0735	-2.48	-0.169	-0.0017	12.51	0.656	-0.0704
13.53	0.644	-0.0706	-1.32	-0.091	0.0000	11.54	0.652	-0.0669
12.56	0.637	-0.0670	-0.33	-0.024	0.0019	10.49	0.654	-0.0618
11.68	0.633	-0.0638	0.56	0.041	0.0036	9.61	0.651	-0.0525
10.54	0.631	-0.0584	1.64	0.118	0.0058	8.55	0.634	-0.0346
9.66	0.634	-0.0500	2.63	0.204	0.0054	7.57	0.587	-0.0151
8.51	0.622	-0.0331	3.62	0.299	0.0018	6.58	0.506	-0.0005
7.62	0.577	-0.0136	4.70	0.375	0.0027	5.41	0.425	0.0006
6.72	0.503	0.0016	5.68	0.446	0.0033	4.52	0.355	0.0004
5.56	0.421	0.0040	6.76	0.531	-0.0005	3.53	0.288	0.0003
4.57	0.354	0.0040	7.75	0.605	-0.0185	2.45	0.184	0.0057
3.50	0.272	0.0040	8.73	0.642	-0.0390	1.37	0.110	0.0050

0.39	0.039	0.0037	11.81	0.676	-0.0680
-0.33	-0.006	0.0026	12.86	0.675	-0.0704
-1.59	-0.099	0.0004	13.74	0.677	-0.0719
-2.75	-0.181	-0.0016	13.57	0.686	-0.0737
-3.66	-0.277	0.0044	12.60	0.681	-0.0709
-4.64	-0.357	0.0049	11.54	0.680	-0.0687
-5.72	-0.429	0.0046	10.48	0.667	-0.0607
-6.71	-0.504	0.0049	9.52	0.664	-0.0514
-7.78	-0.585	0.0129	8.54	0.645	-0.0355
-8.77	-0.649	0.0355	7.56	0.593	-0.0140
-9.83	-0.671	0.0553	6.58	0.516	-0.0005
-10.80	-0.674	0.0671	5.41	0.435	-0.0012
-11.76	-0.673	0.0730	4.51	0.366	-0.0014
-12.73	-0.674	0.0765	3.44	0.290	-0.0018
-13.79	-0.680	0.0798	2.36	0.204	0.0008
-14.49	-0.686	0.0819	1.37	0.113	0.0043
-15.82	-0.706	0.0876	0.38	0.038	0.0026
			-0.70	-0.039	0.0001
Run:	0423ga		-1.60	-0.115	-0.0019
$Re = 99996.3$			-2.67	-0.202	-0.0021
α	C_L	C_M	-3.67	-0.310	0.0061
-15.82	-0.710	0.0893	-4.66	-0.388	0.0066
-14.50	-0.704	0.0872	-5.47	-0.447	0.0064
-13.62	-0.689	0.0823	-6.45	-0.513	0.0063
-12.65	-0.682	0.0790	-7.80	-0.614	0.0202
-11.51	-0.685	0.0742	-8.87	-0.663	0.0421
-10.54	-0.683	0.0653	-9.75	-0.681	0.0588
-9.48	-0.670	0.0496	-10.81	-0.687	0.0700
-8.59	-0.627	0.0271	-11.77	-0.687	0.0764
-7.52	-0.558	0.0109	-12.74	-0.686	0.0797
-6.44	-0.486	0.0079	-13.80	-0.690	0.0823
-5.55	-0.424	0.0078	-14.77	-0.702	0.0863
-4.56	-0.356	0.0071	-15.73	-0.713	0.0898
-3.40	-0.270	0.0060			
-2.49	-0.168	-0.0020			
-1.60	-0.115	-0.0008			
-0.34	-0.025	0.0017			
0.65	0.047	0.0038			
1.63	0.125	0.0062			
2.63	0.235	0.0008			
3.62	0.313	0.0006			
4.70	0.391	0.0008			
5.68	0.461	0.0018			
6.76	0.542	-0.0016			
7.75	0.617	-0.0204			
8.72	0.654	-0.0398			
9.87	0.667	-0.0546			
10.75	0.674	-0.0627			

Appendix D

LRN-FB Drawings

Information presented in this appendix contains CAD drawings of the machined components of the LRN-FB. Documentation is provided to assist future researchers in the event that a component needs to be remanufactured. Table D.1 below lists details of the machined components used. The heading 'Quantity' represents the number of parts needed to construct a complete balance. All components except for the sting were machined from aluminum, more specifically AL-6061.

Table D.1: LRN-FB machining list

Part	Quantity	Figure / Page
MILL		
Rig Base	1	Fig. D.1 / Pg. 182
Lift Base	1	Fig. D.2 / Pg. 183
Drag Base	1	Fig. D.3 / Pg. 184
Absolute Optical Encoder Plate	1	Fig. D.4 / Pg. 185
Top Roller Bearing Base	1	Fig. D.5 / Pg. 186
Lift Mounting Bracket	8	Fig. D.6 / Pg. 187
Drag Mounting Bracket	8	Fig. D.7 / Pg. 188
Encoder Mounting Bracket	4	Fig. D.8 / Pg. 189
Load Cell Bracket Mounting Bracket	2	Fig. D.9 / Pg. 190
Lift Pivot Arm	4	Fig. D.10 / Pg. 191
Drag Pivot Arm	4	Fig. D.11 / Pg. 192
Encoder Base Arm	4	Fig. D.12 / Pg. 193
DC Motor Mount	1	Fig. D.13 / Pg. 194

Table D.1: Continued.

Part	Quantity	Figure / Page
Worm Shaft Mounting Bracket	1	Fig. D.14 / Pg. 195
Lift Carriage Stiffener	4	Fig. D.20 / Pg. 201
Drag Carriage Stiffener	4	Fig. D.21 / Pg. 202
Lift Load Cell Base Mounting 1	1	Fig. D.22 / Pg. 203
Lift Load Cell Base Mounting 2	1	Fig. D.23 / Pg. 204
Drag Load Cell Base Mounting 1	1	Fig. D.24 / Pg. 205
Drag Load Cell Base Mounting 2	1	Fig. D.25 / Pg. 206
Pre-Loading Mounting Bracket	2	Fig. D.26 / Pg. 207
Pre-Loading Mount 1	1	Fig. D.27 / Pg. 208
Pre-Loading Mount 2	1	Fig. D.28 / Pg. 209
Pre-Loading L-Shape Bracket	1	Fig. D.29 / Pg. 210
Pre-Loading Corner Bracket	5	Fig. D.30 / Pg. 211
Pre-Loading L-Shape Bracket	2	Fig. D.31 / Pg. 212
<hr/>		
LATHE		
Lower Tapered Bearing Fitting	1	Fig. D.15 / Pg. 196
Flexural Pivot Fitting	1	Fig. D.16 / Pg. 197
Torque Sensor-Flexural Pivot Fitting	1	Fig. D.17 / Pg. 198
Worm Gear-Torque Sensor Connector Fitting	1	Fig. D.18 / Pg. 199
Worm Gear-Optical Encoder Fitting	1	Fig. D.19 / Pg. 200
Main Sting (connected to flexure)	1	Fig. D.32 / Pg. 213
Secondary Sting	1	Fig. D.33 / Pg. 214

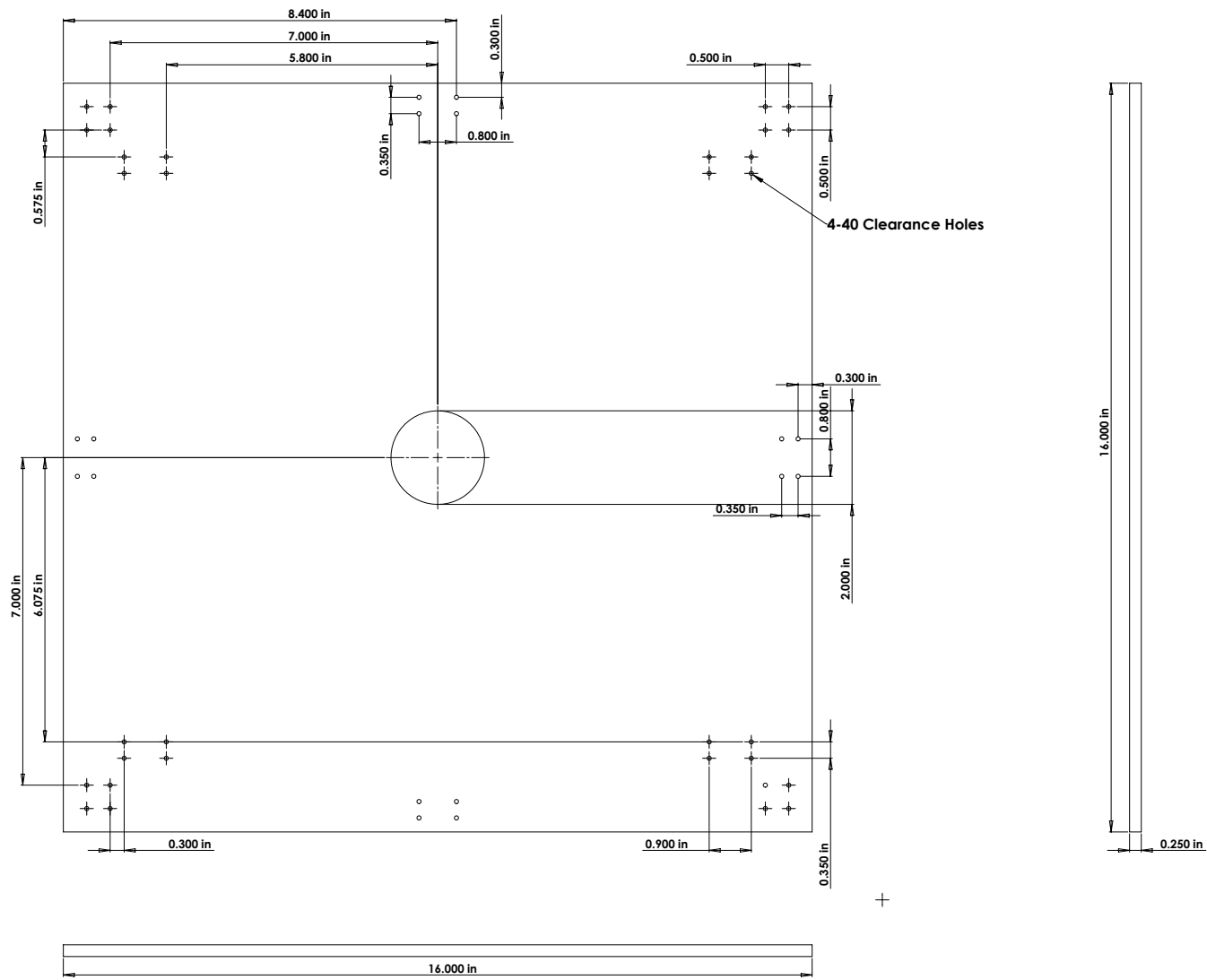


Fig. D.1: LRN-FB rig base.

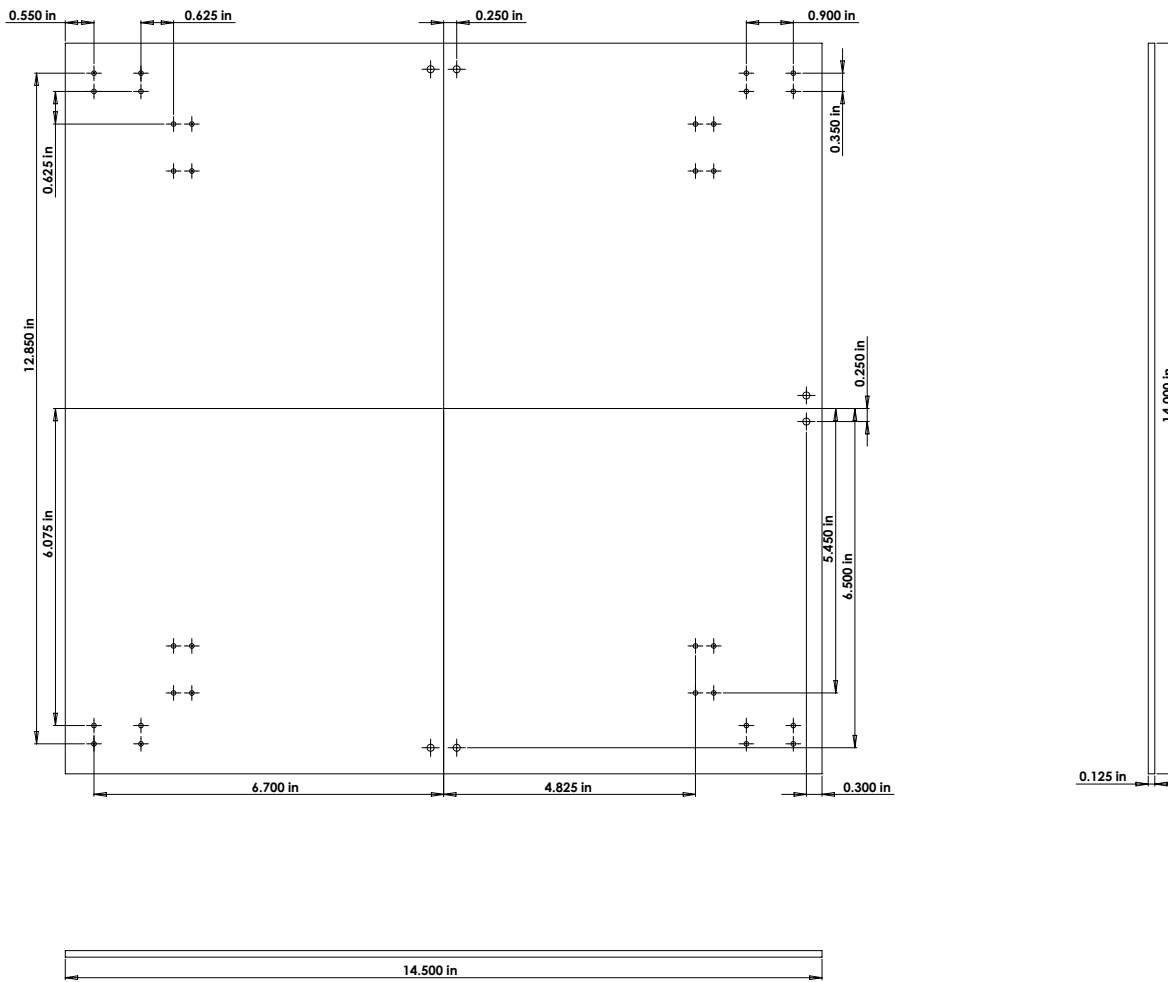


Fig. D.2: LRN-FB lift base.

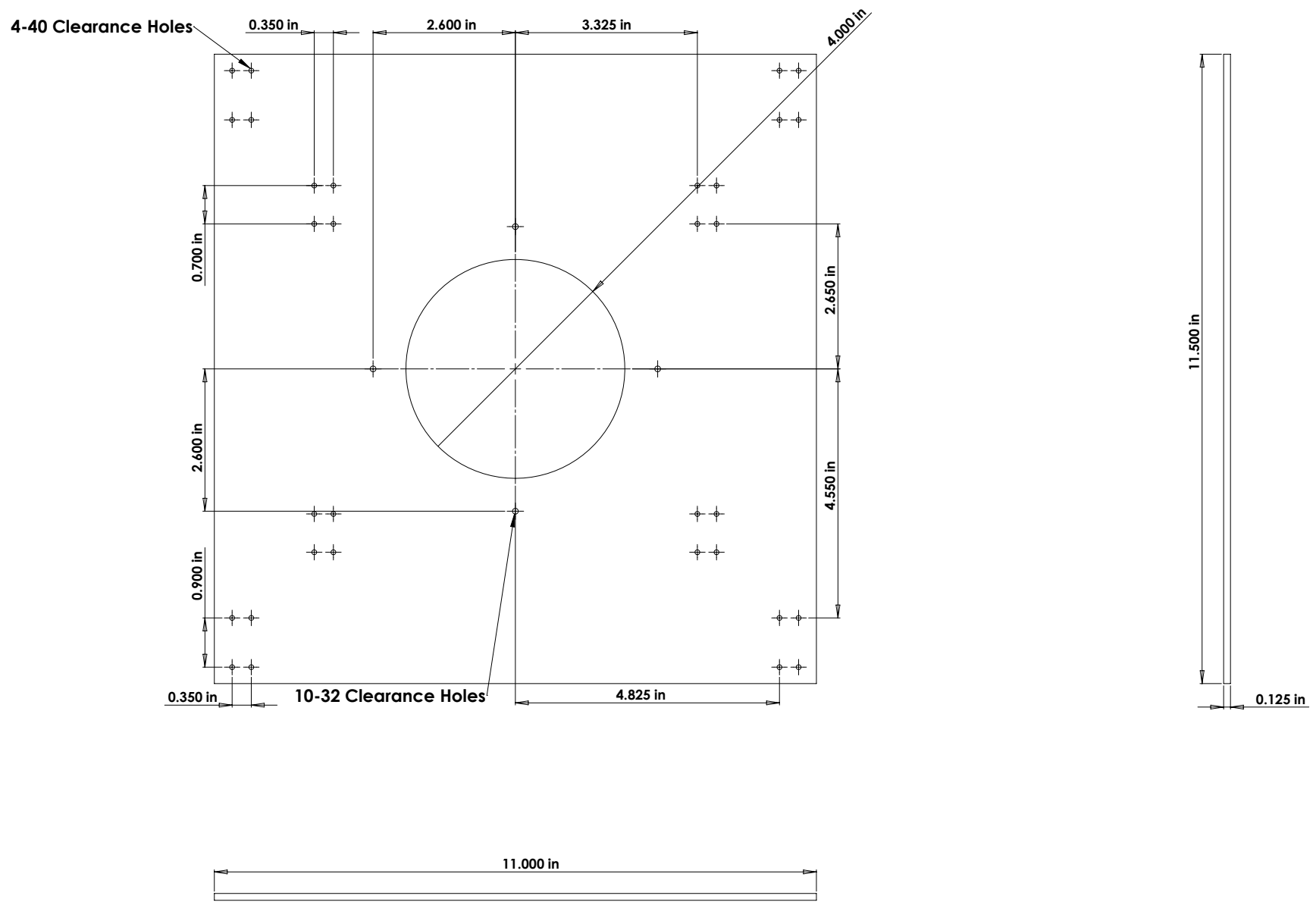


Fig. D.3: LRN-FB drag base.

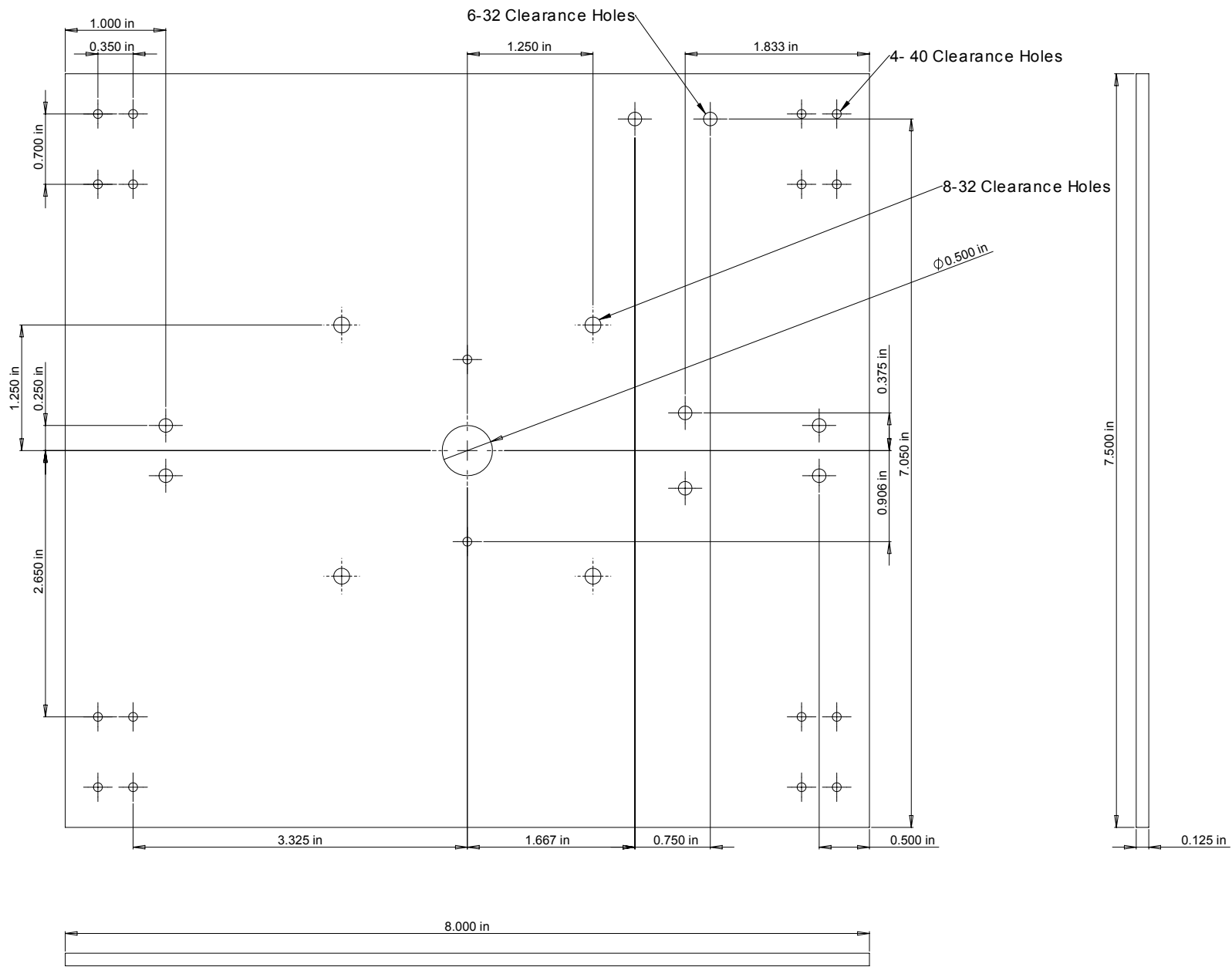


Fig. D.4: LRN-FB absolute optical encoder base.

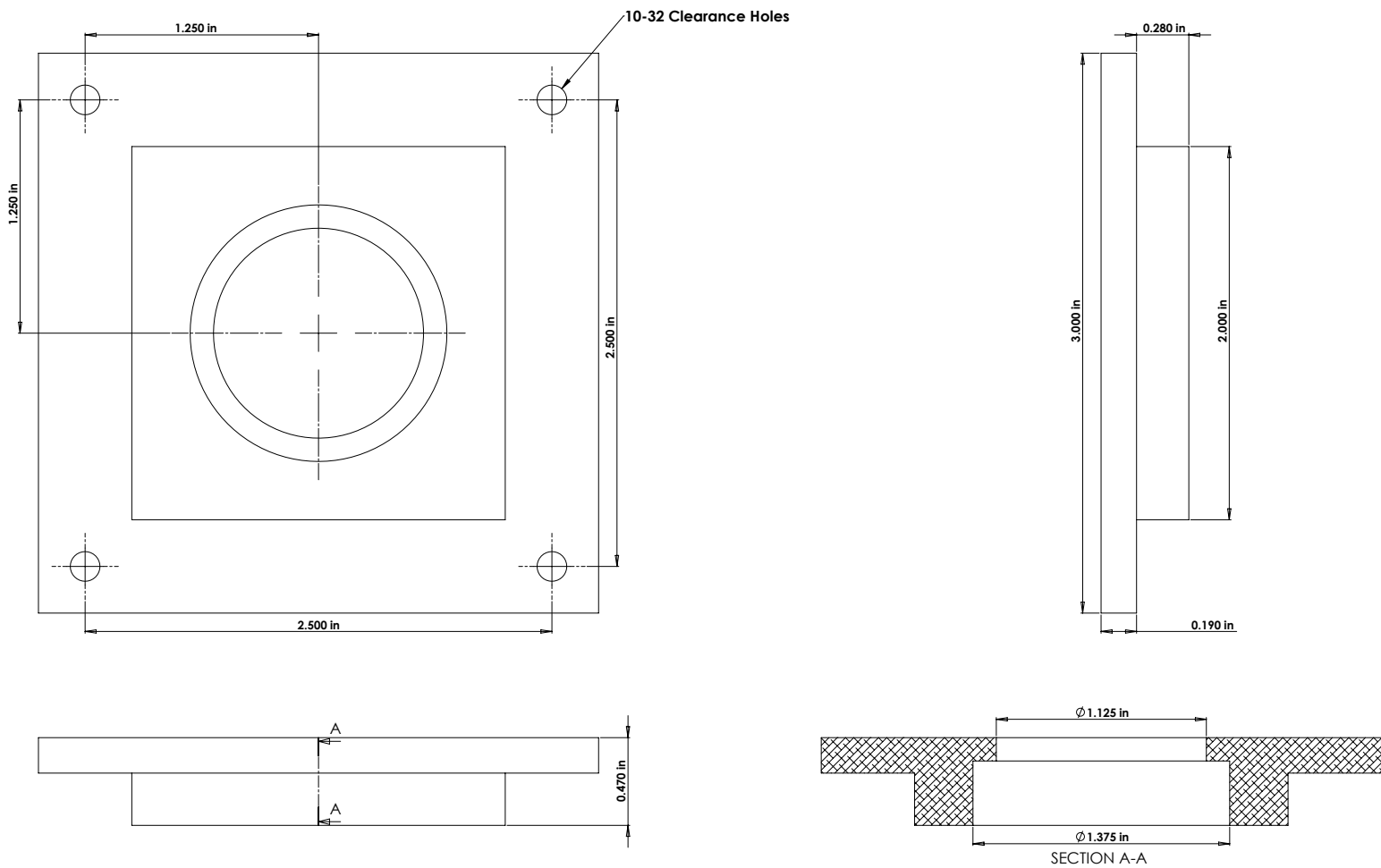


Fig. D.5: LRN-FB top roller-bearing base.

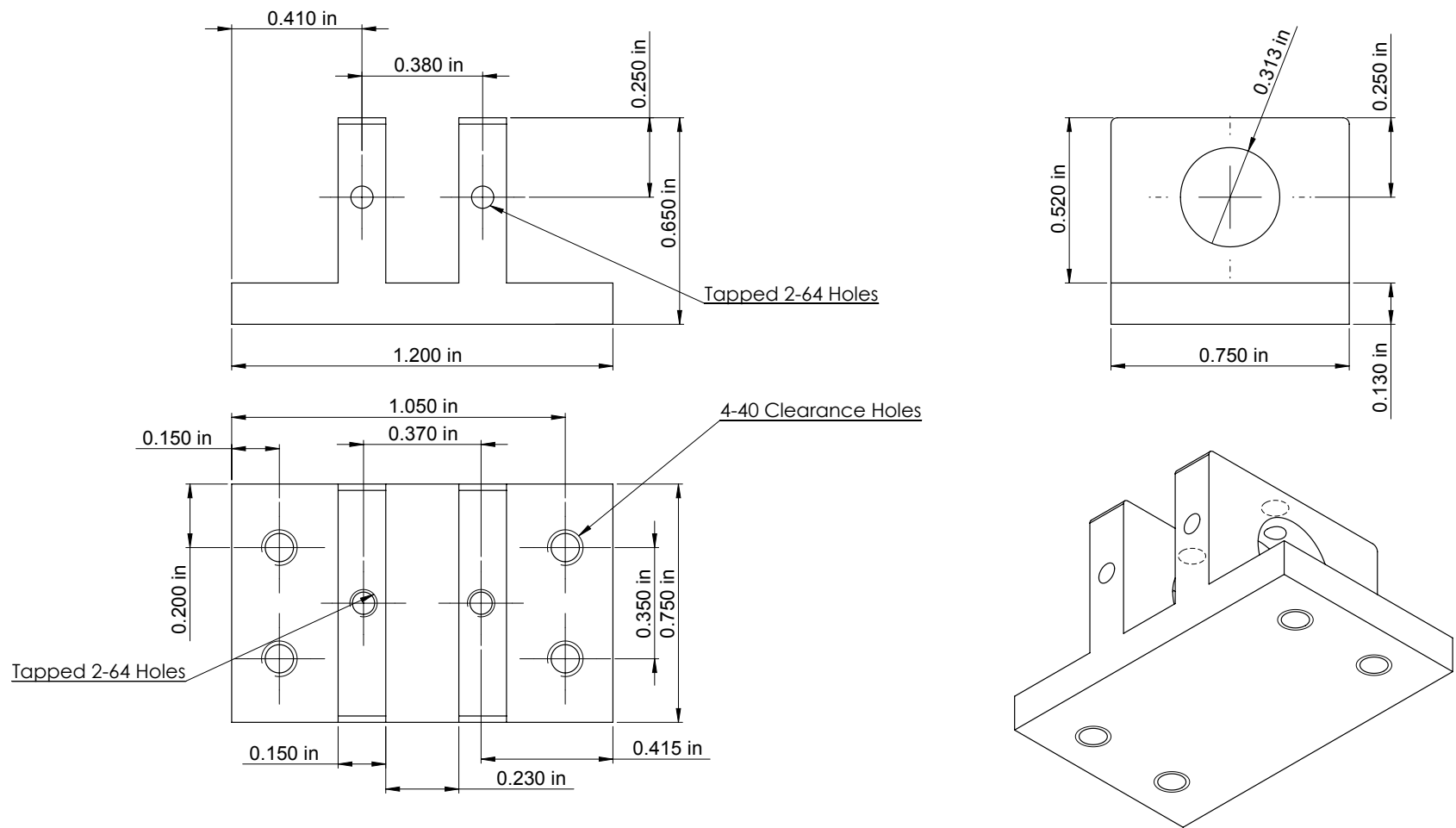


Fig. D.6: LRN-FB lift mounting bracket.

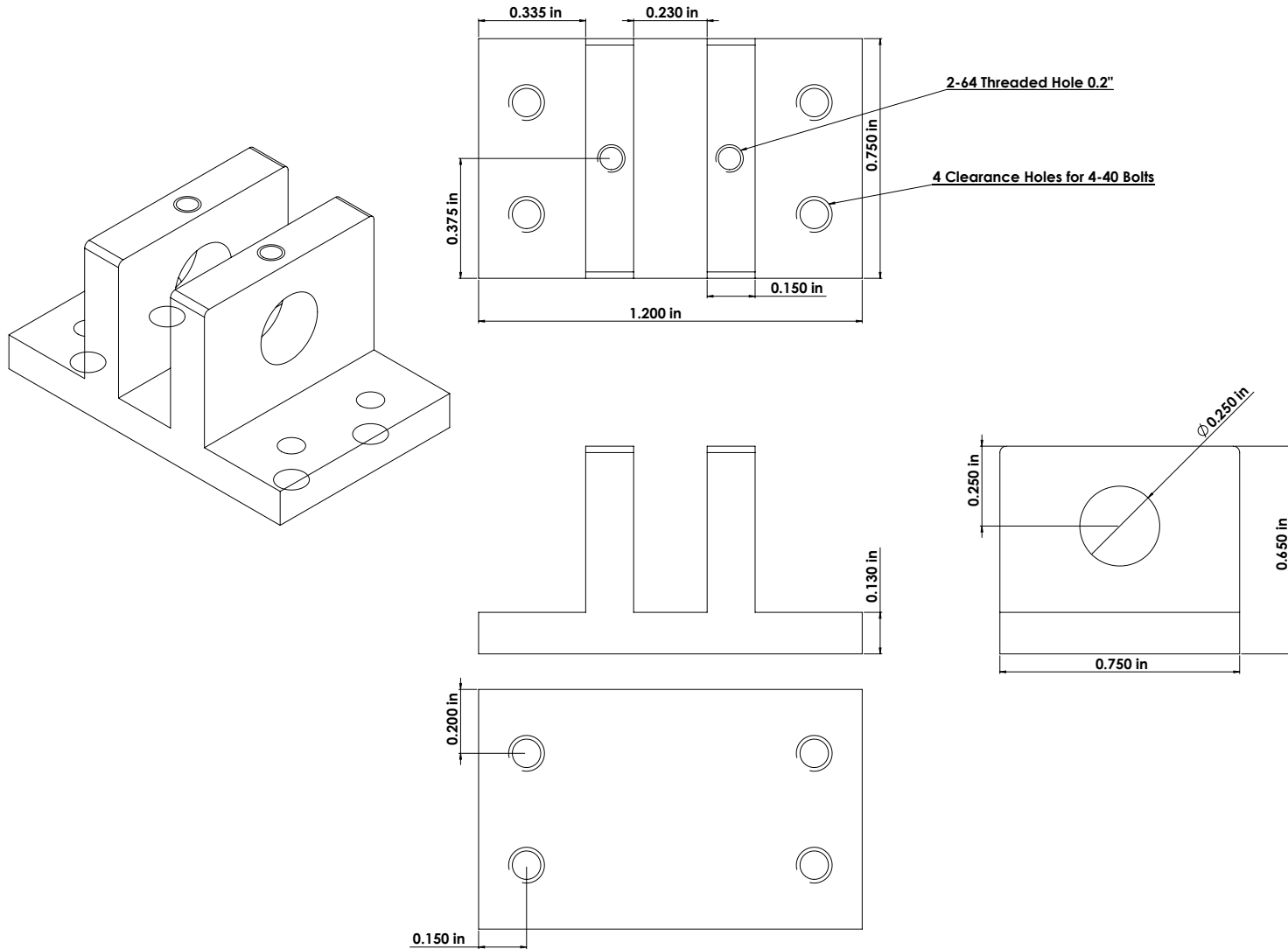


Fig. D.7: LRN-FB drag mounting bracket.

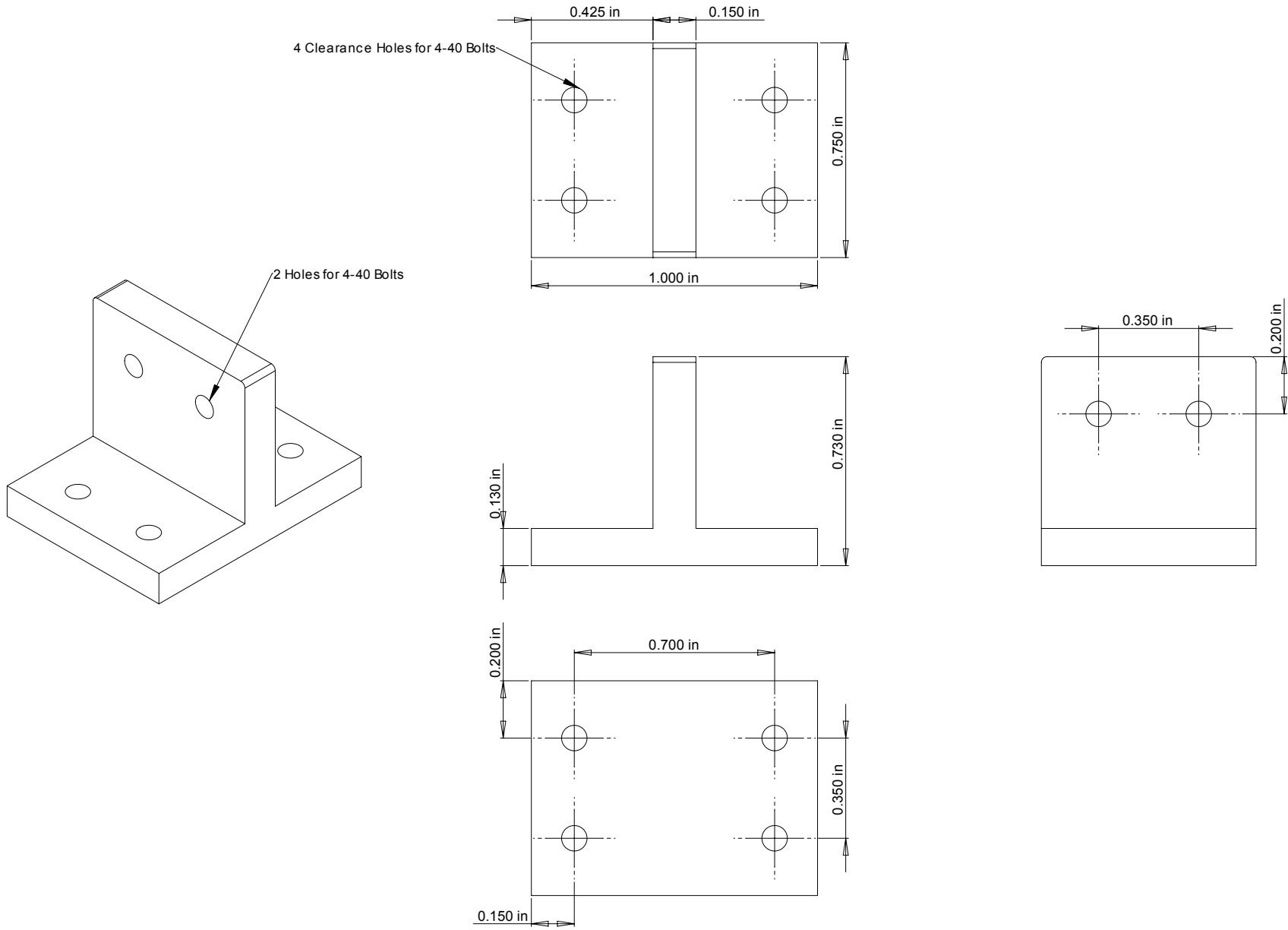


Fig. D.8: LRN-FB encoder mounting bracket.

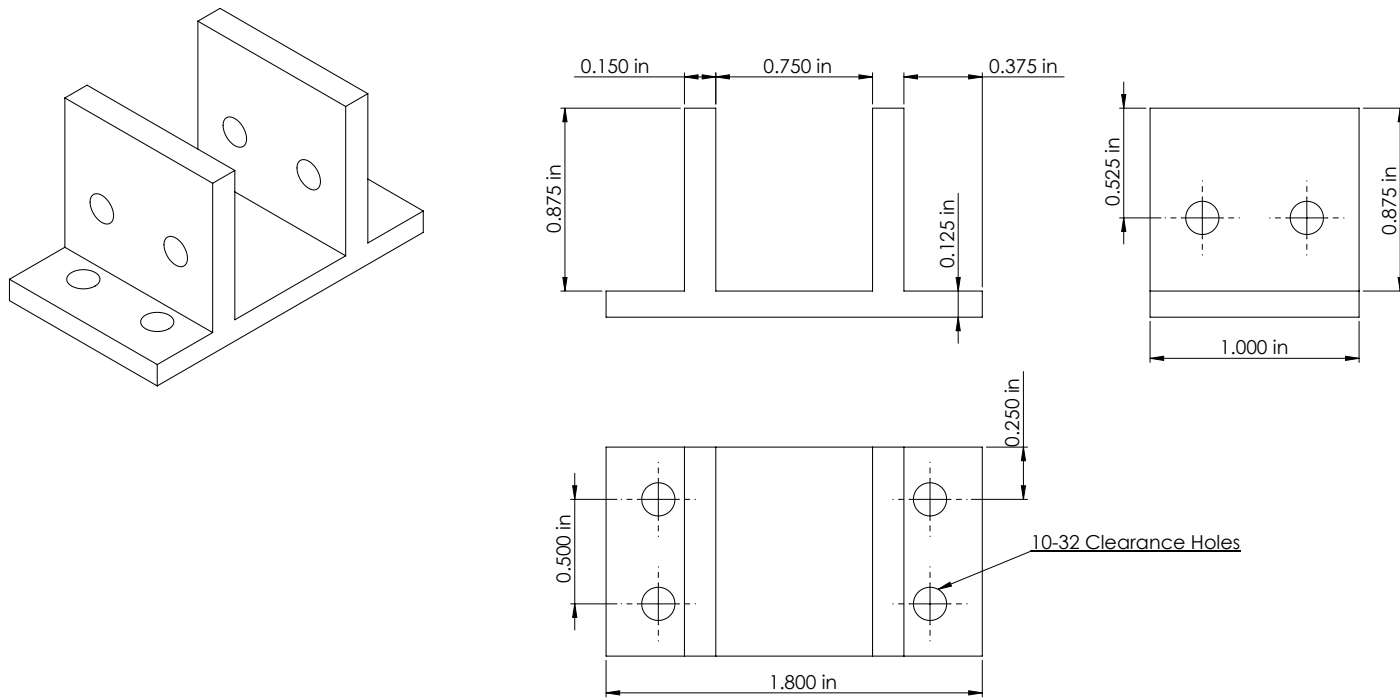


Fig. D.9: LRN-FB load cell bracket mounting bracket.

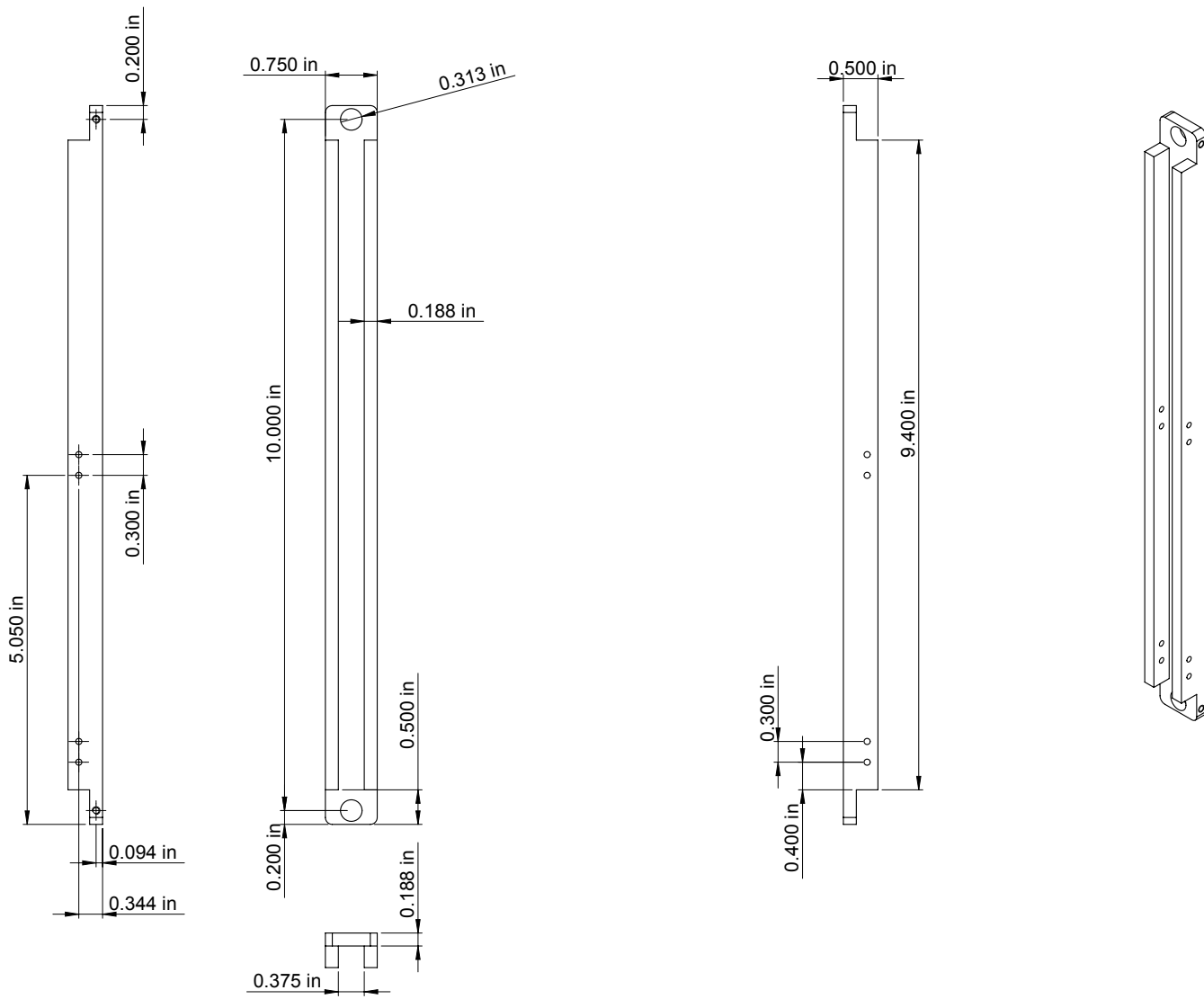


Fig. D.10: LRN-FB lift pivot arm.

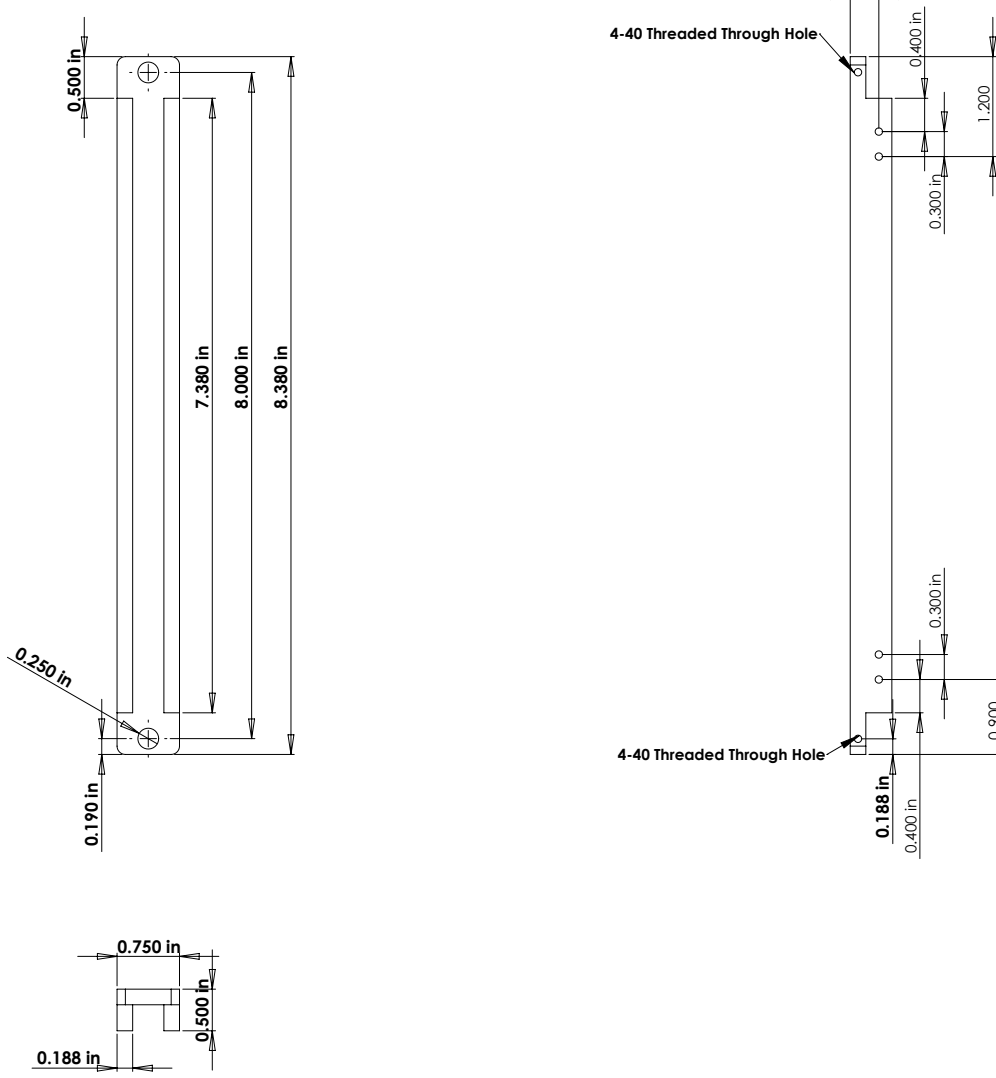


Fig. D.11: LRN-FB drag pivot arm.

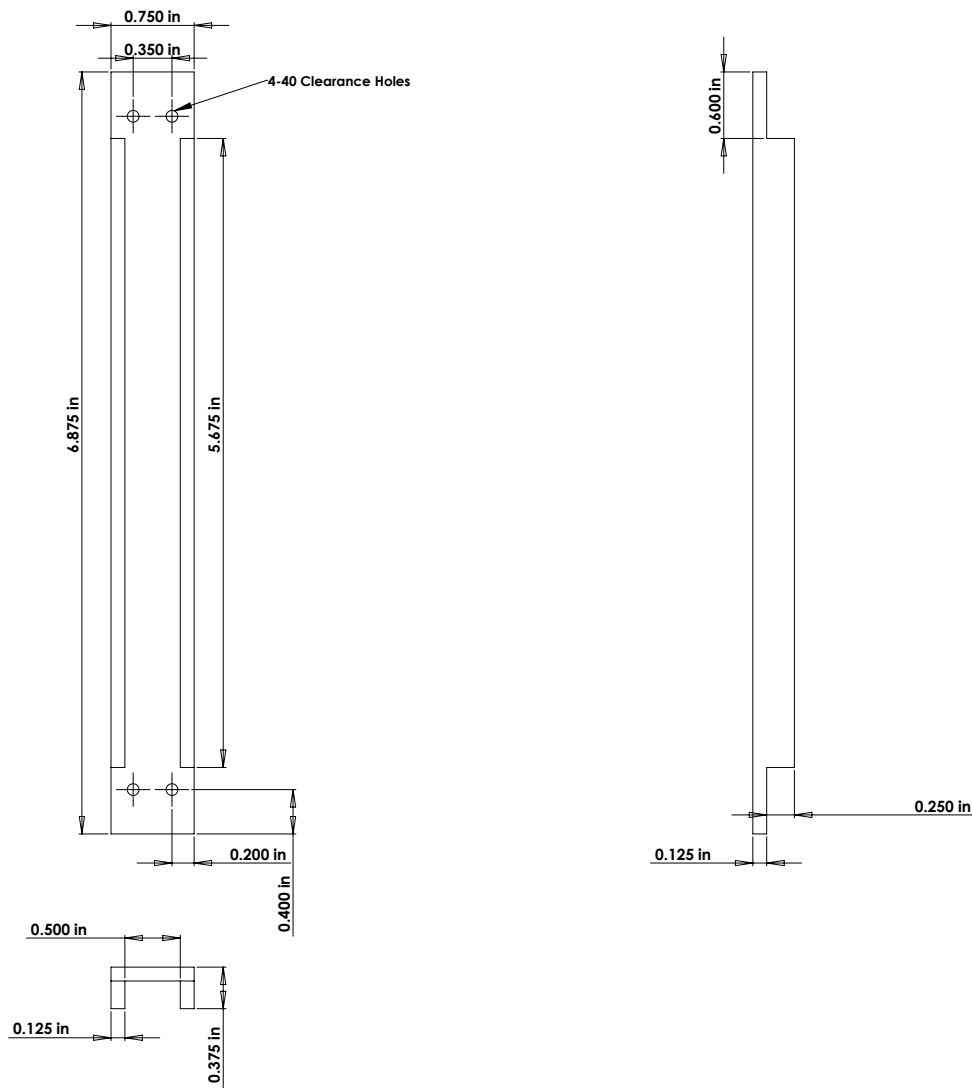


Fig. D.12: LRN-FB encoder base arm.

194

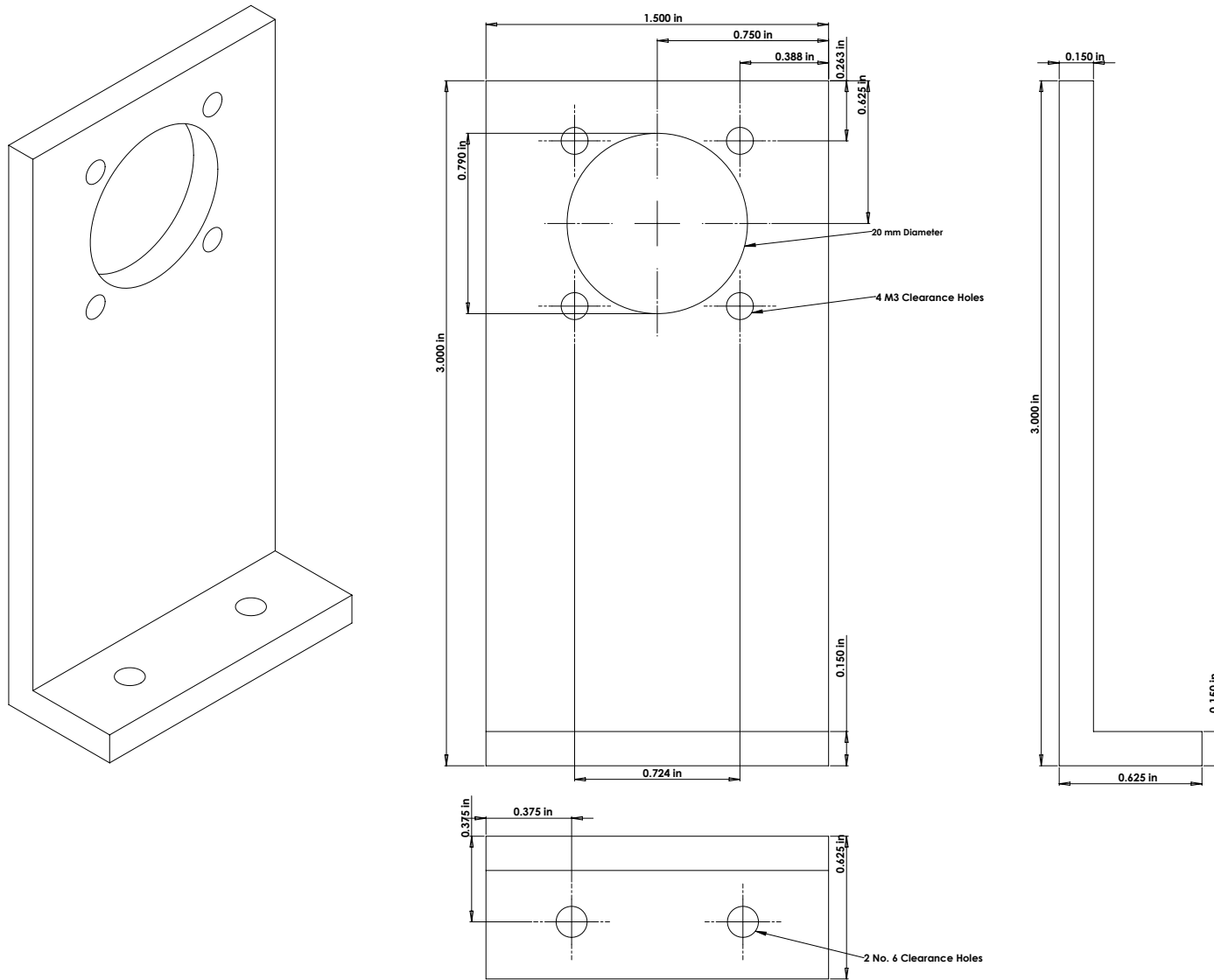


Fig. D.13: LRN-FB DC motor mount.

195

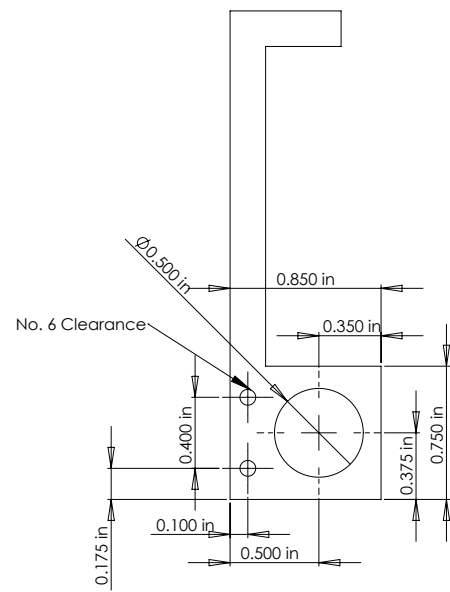
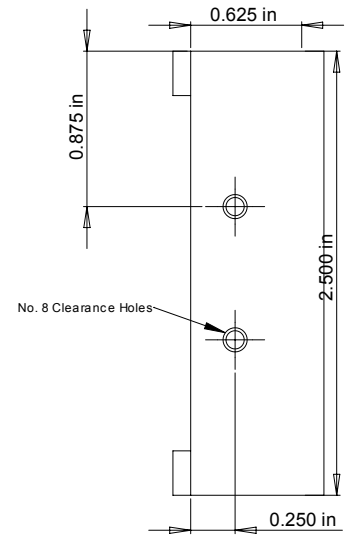
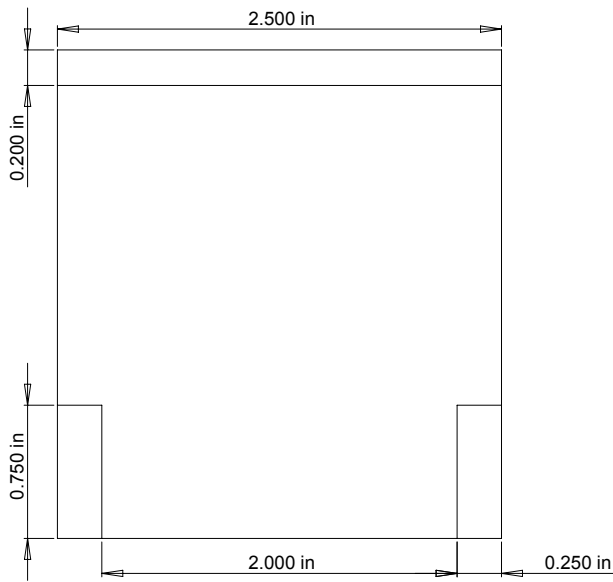
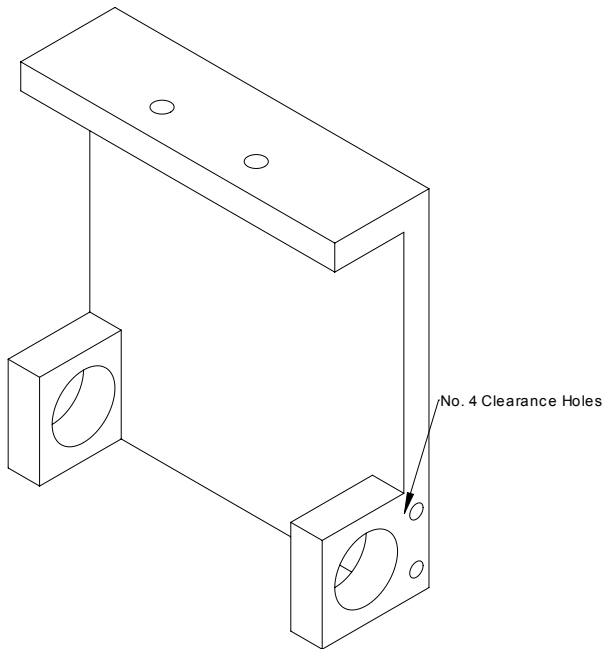


Fig. D.14: LRN-FB worm shaft mounting bracket.

961

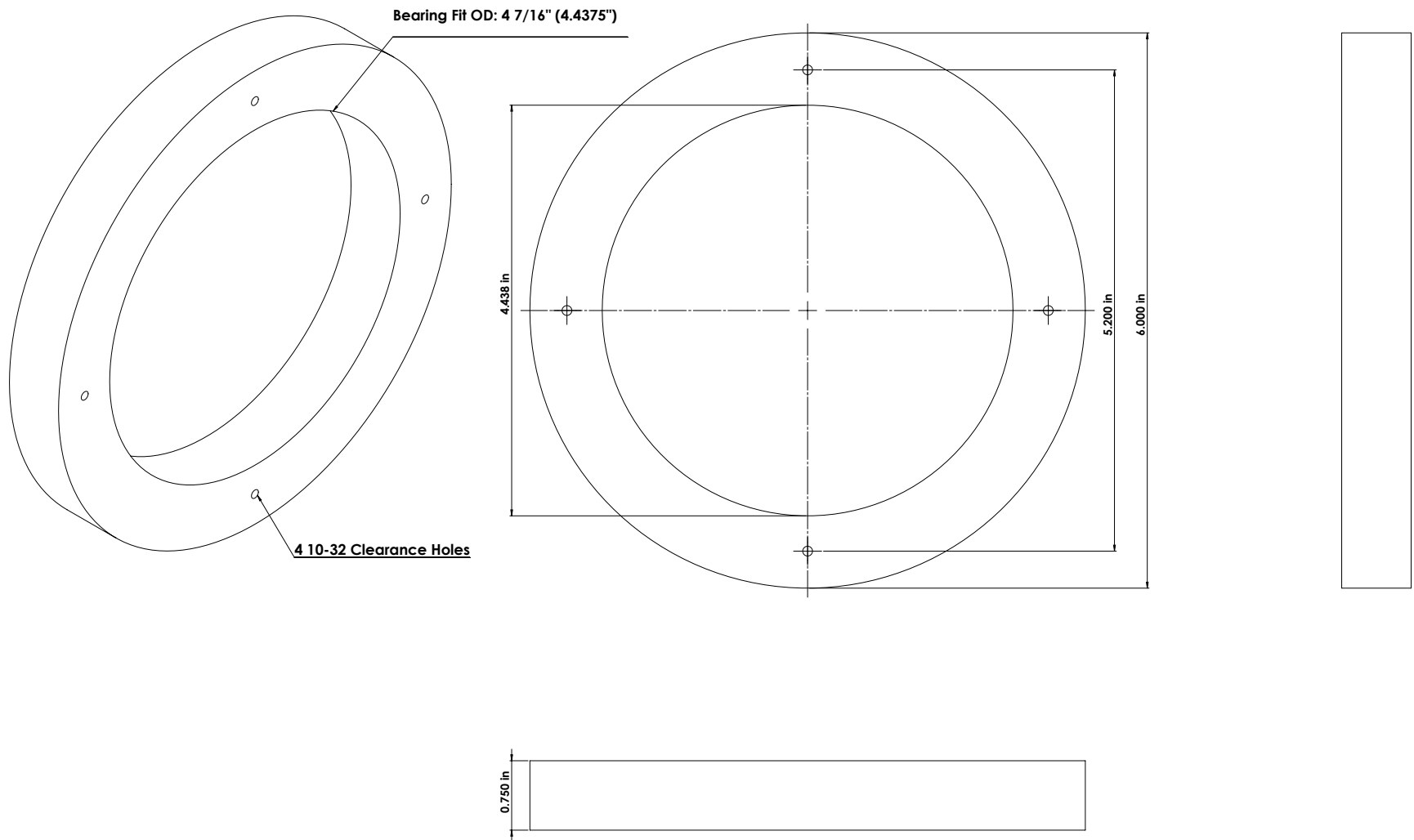


Fig. D.15: LRN-FB lower tapered bearing fitting.

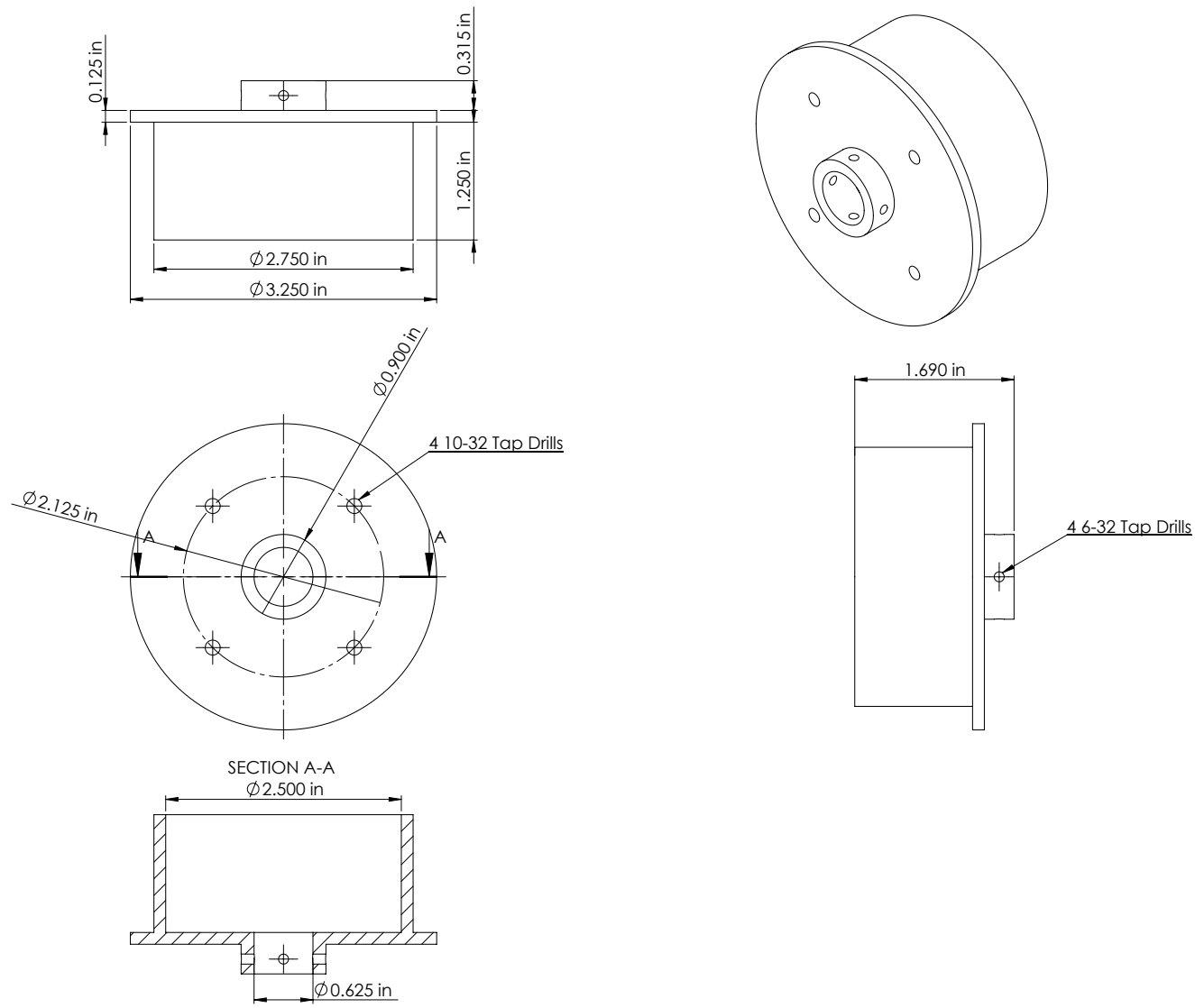


Fig. D.16: LRN-FB flex-pivot fitting.

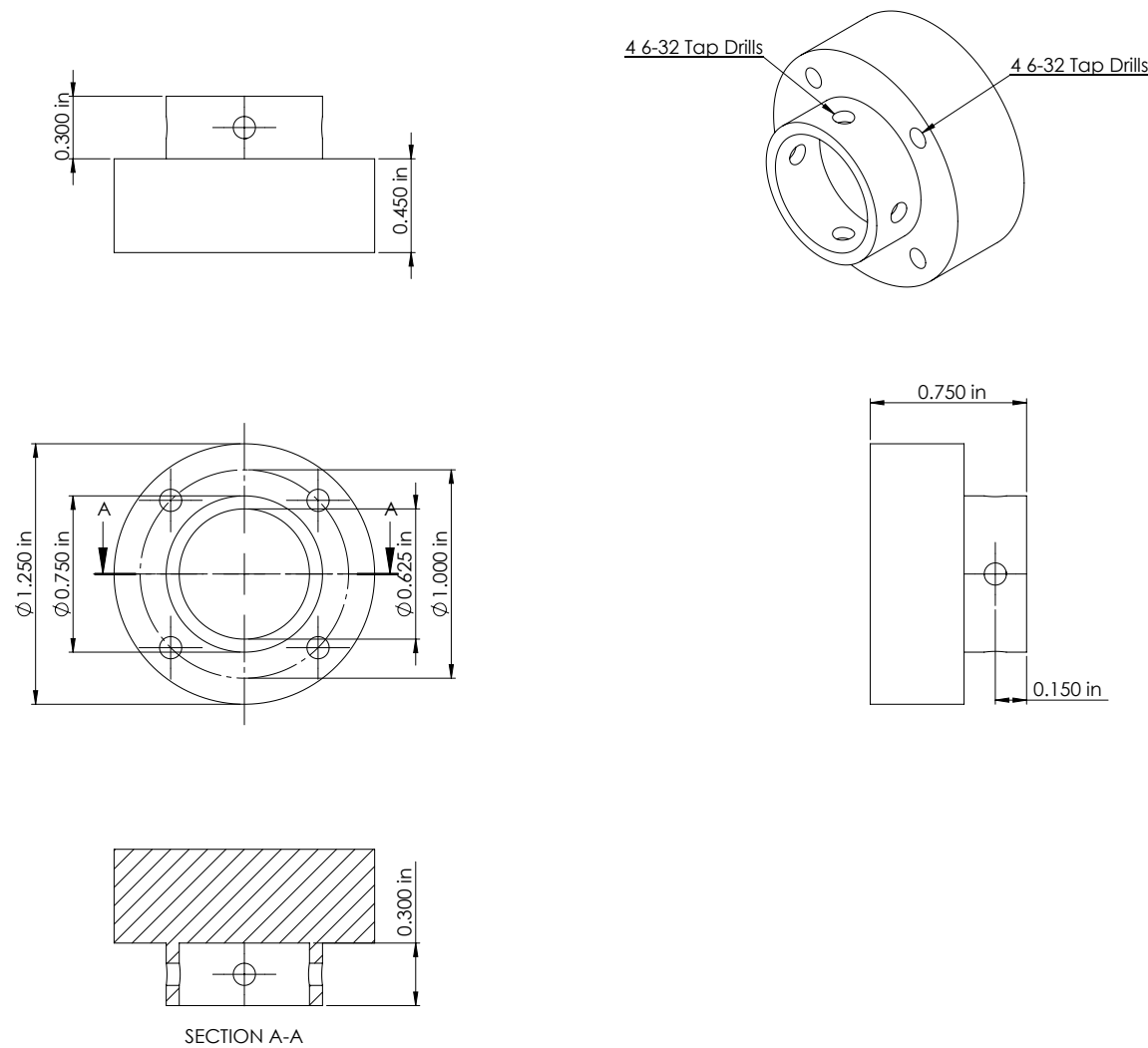


Fig. D.17: LRN-FB torque sensor to flex-pivot fitting.

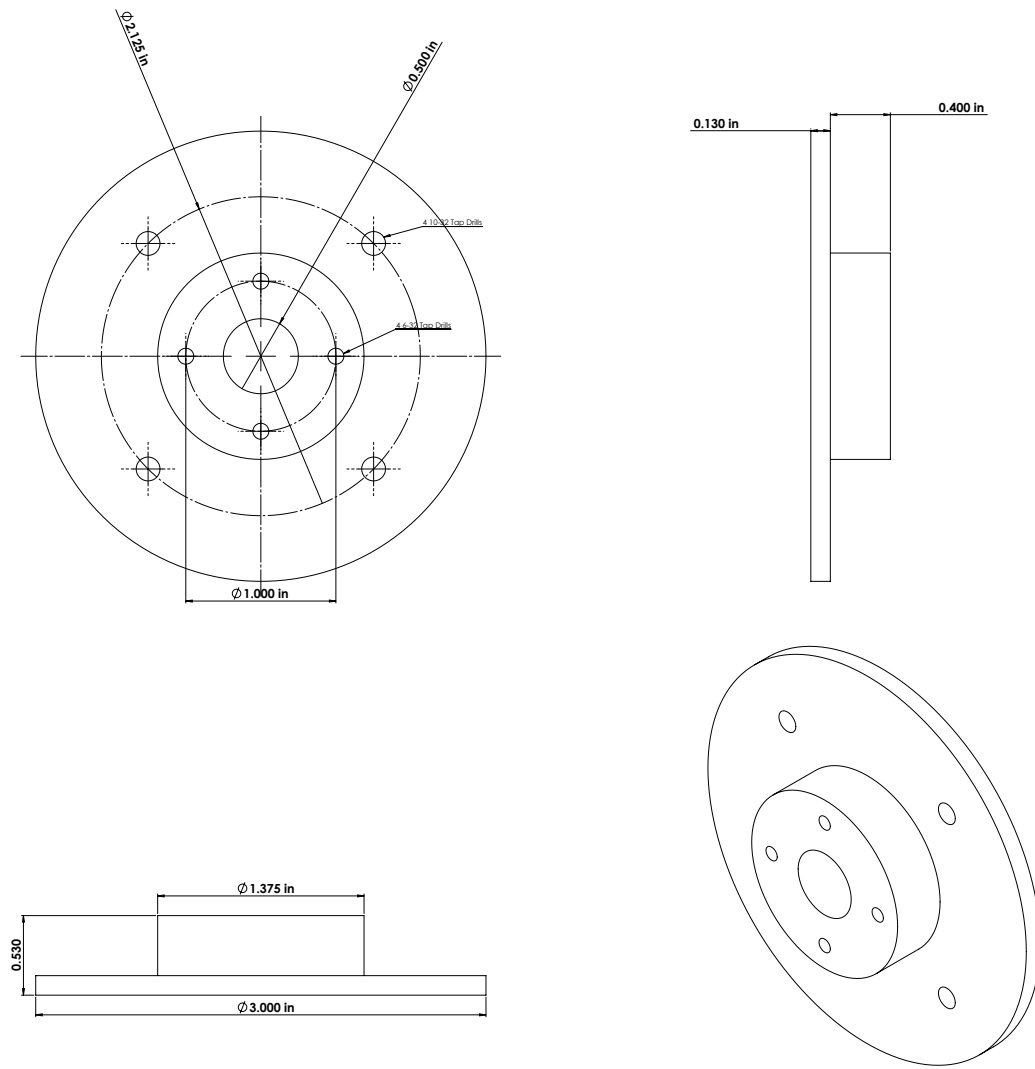


Fig. D.18: LRN-FB worm gear to torque sensor fitting.

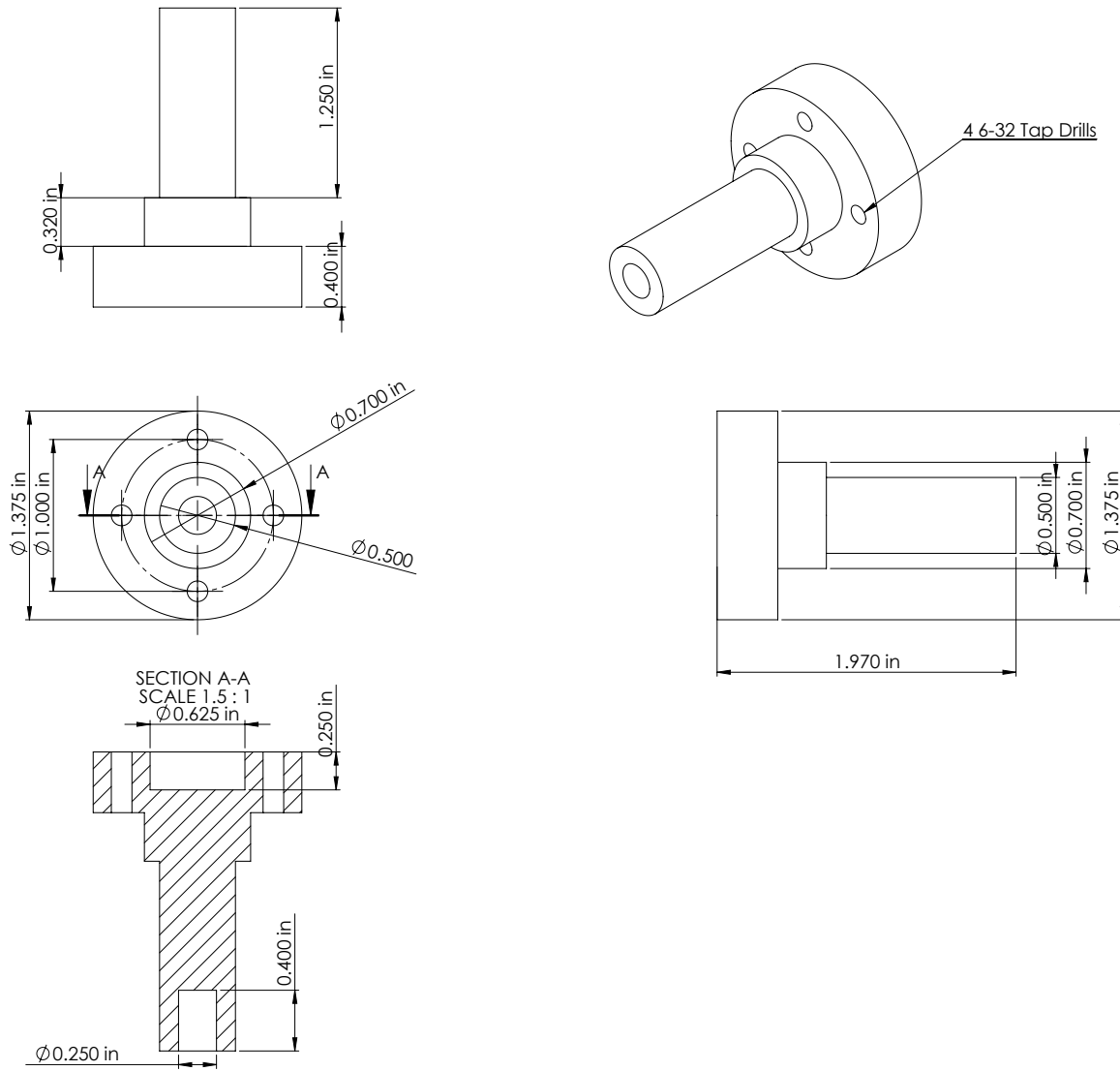


Fig. D.19: LRN-FB worm gear to optical encoder fitting.

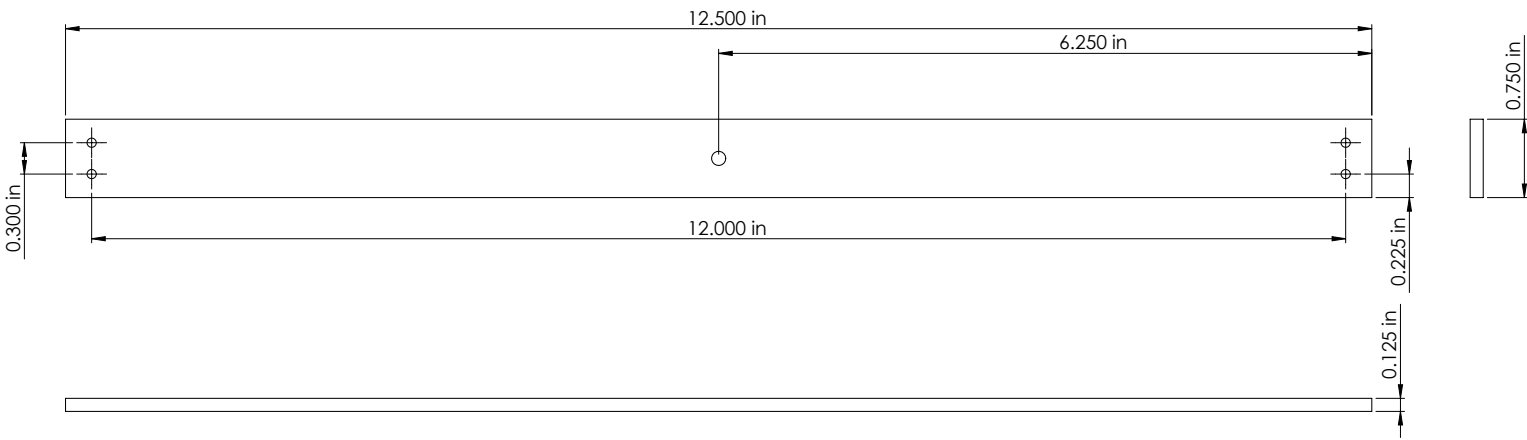


Fig. D.20: LRN-FB lift platform stiffener.

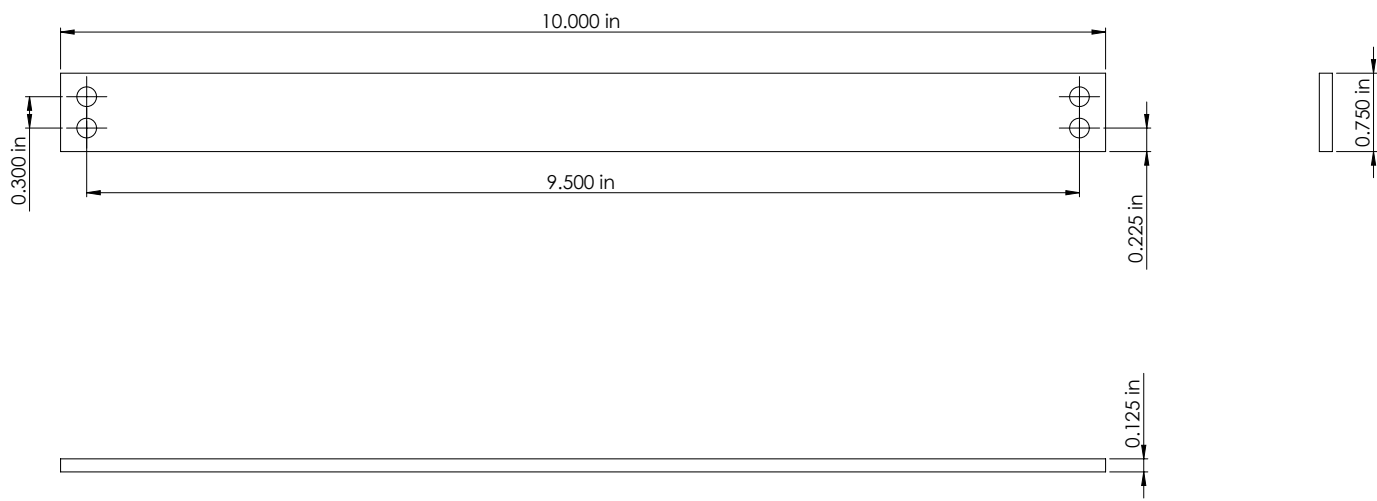


Fig. D.21: LRN-FB drag platform stiffener.

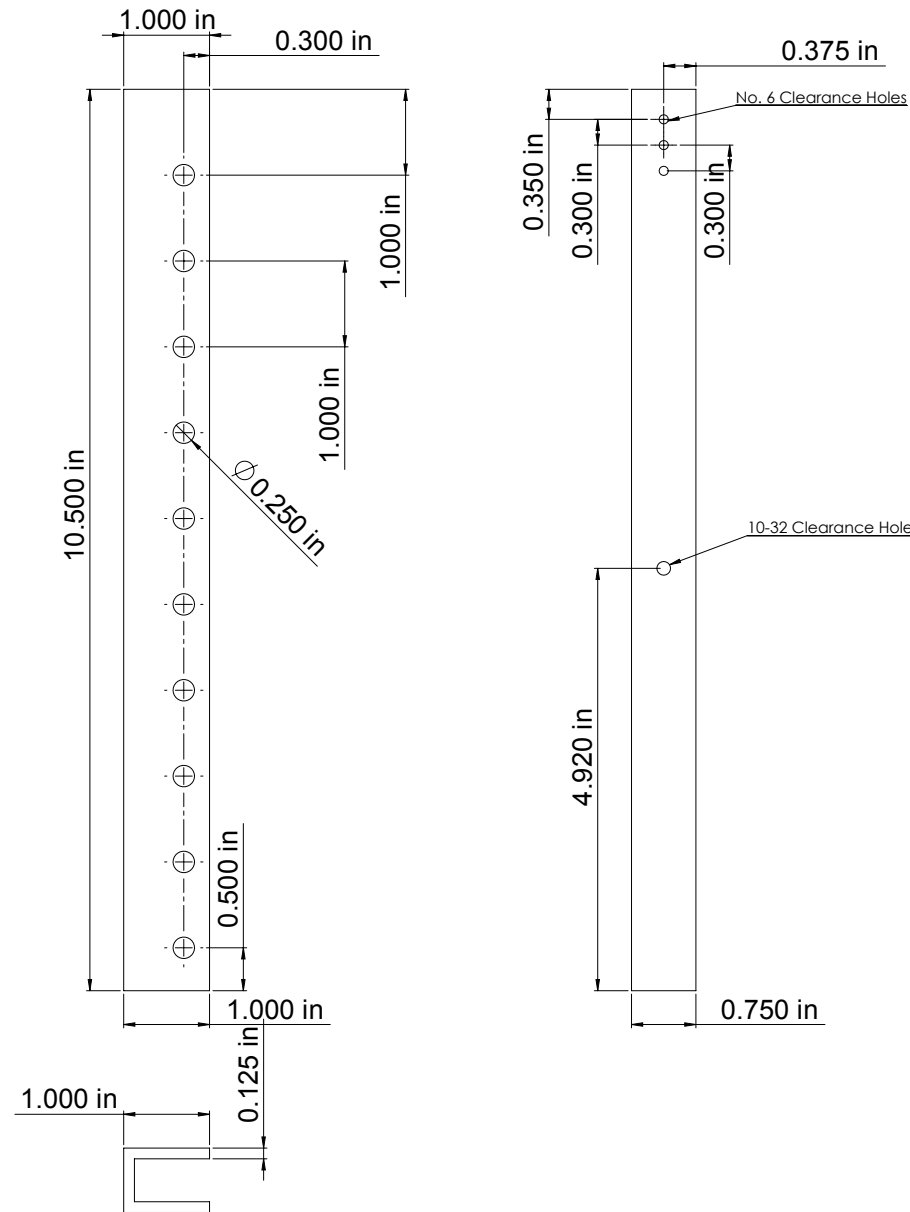


Fig. D.22: LRN-FB lift load cell base mounting 1.

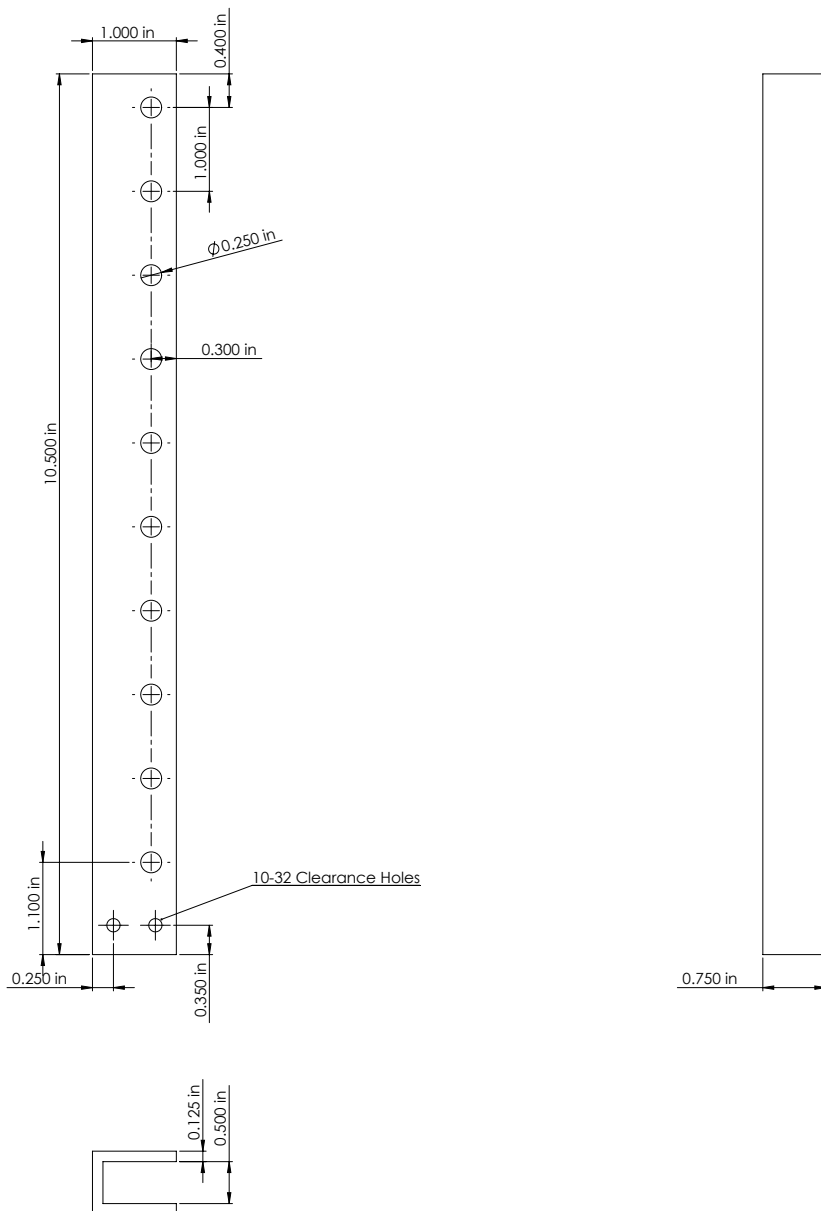


Fig. D.23: LRN-FB lift load cell base mounting 2.

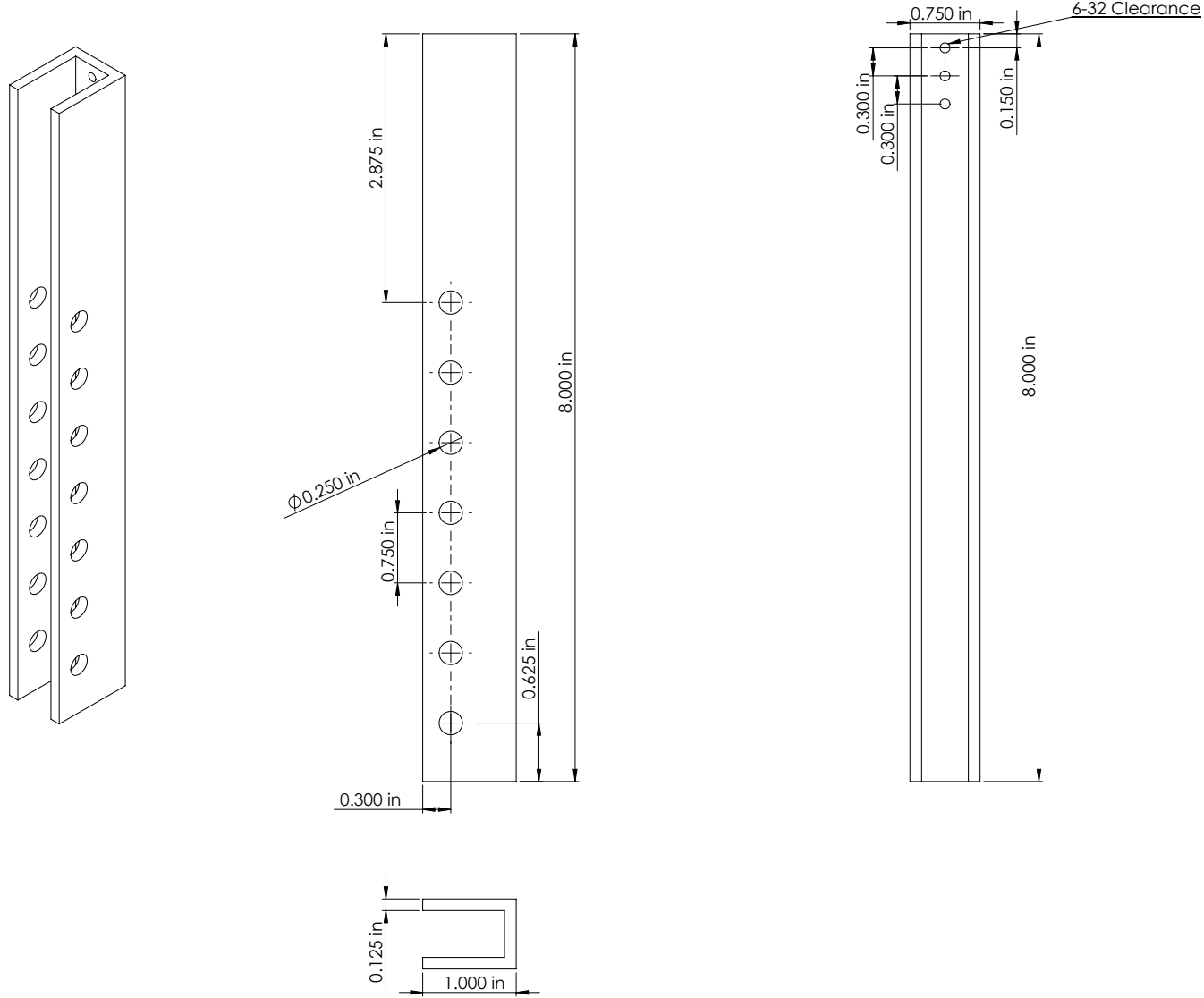


Fig. D.24: LRN-FB drag load cell base mounting 1.

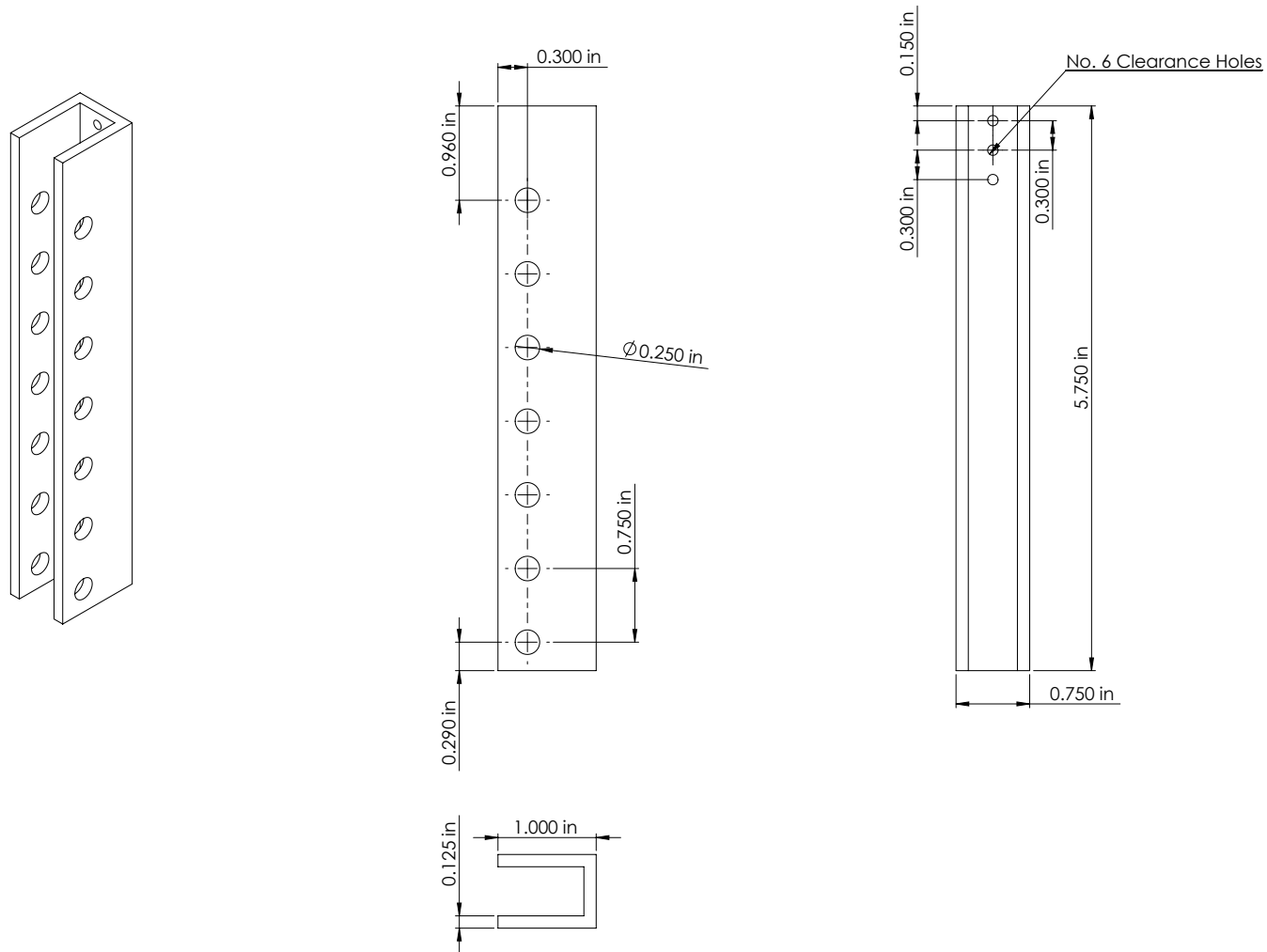


Fig. D.25: LRN-FB drag load cell base mounting 2.

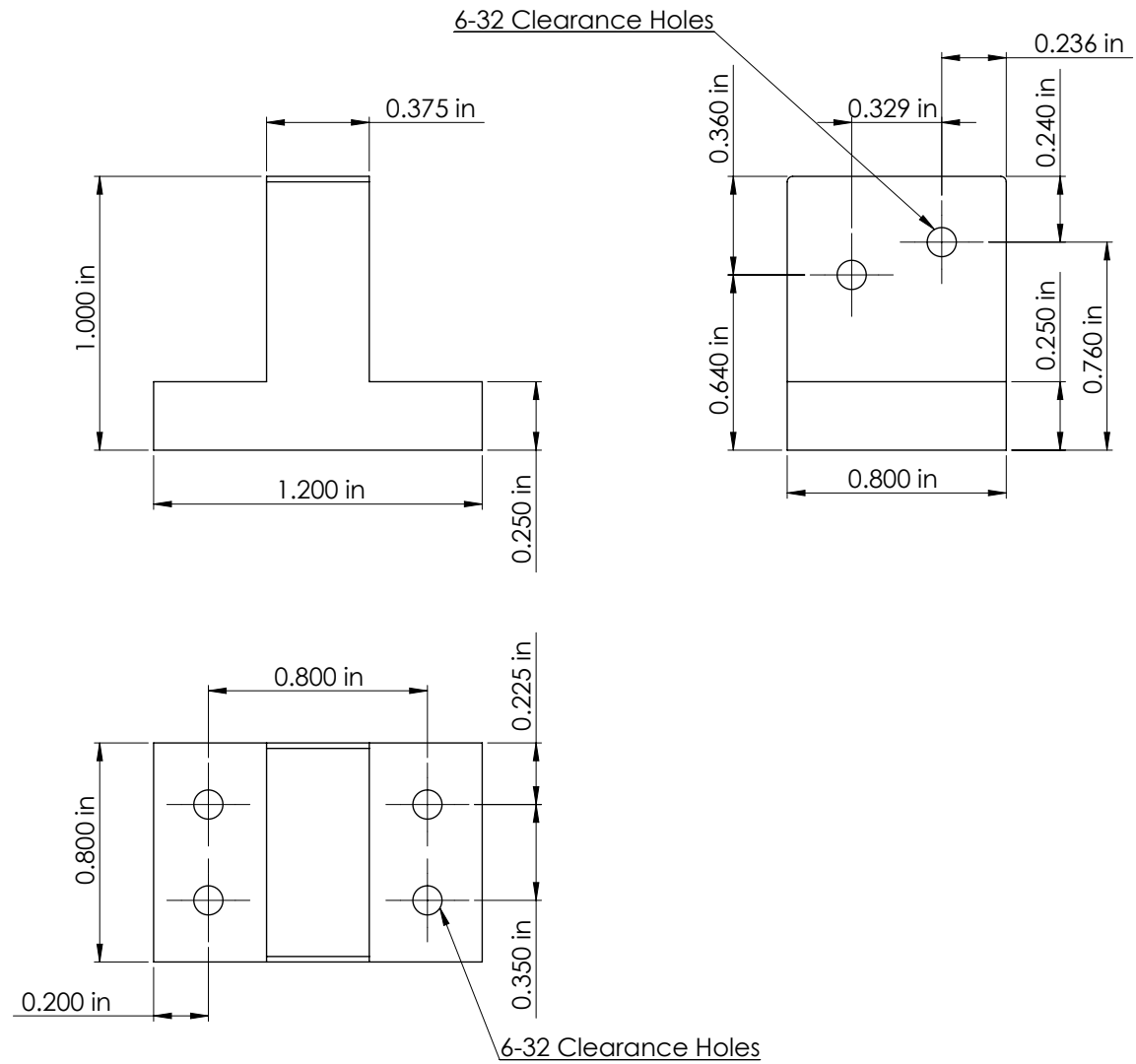
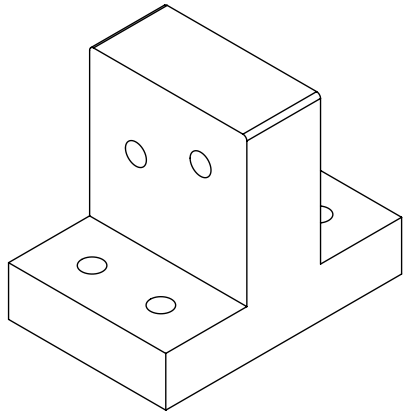


Fig. D.26: LRN-FB pre-loading mounting bracket.

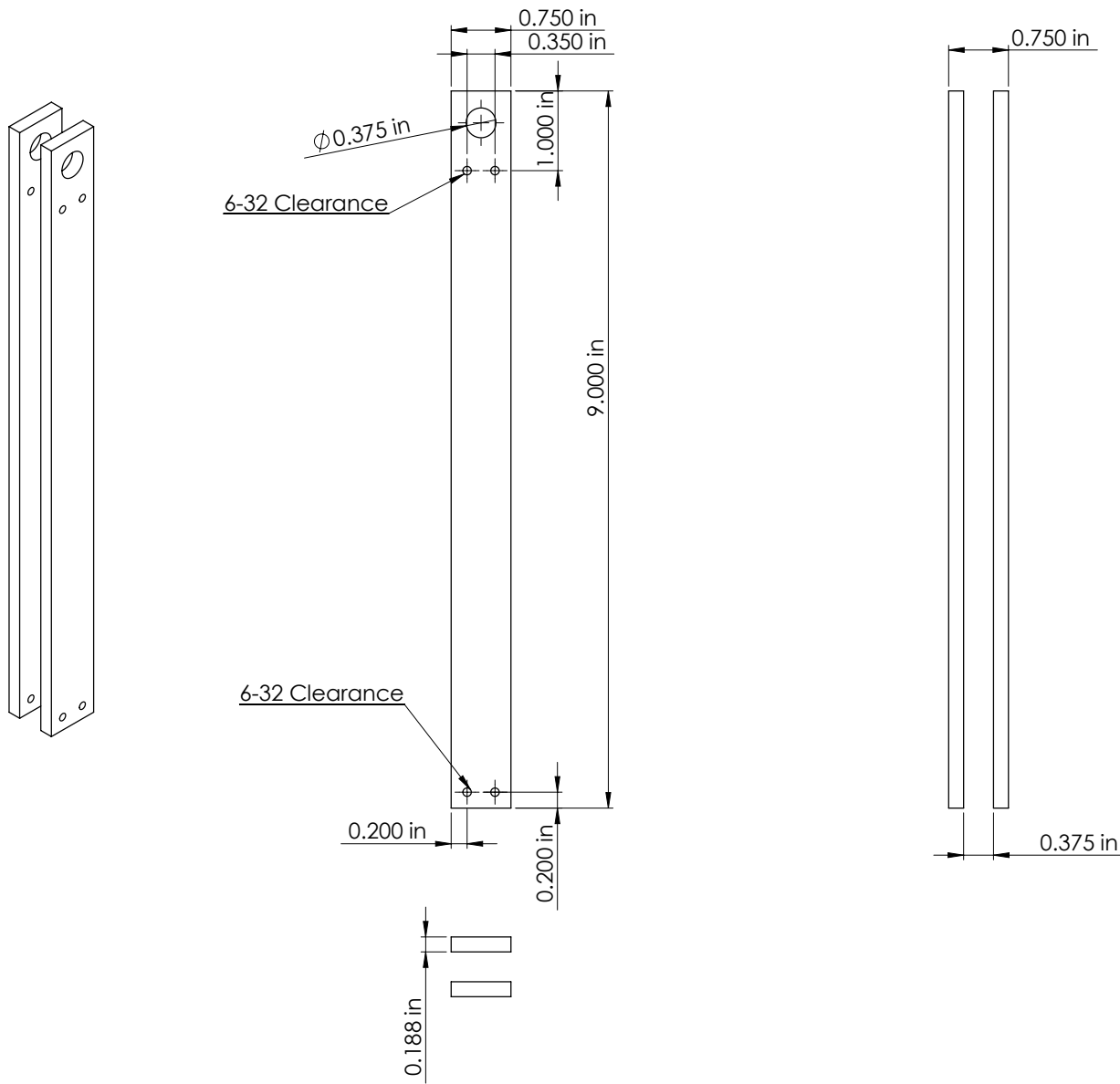


Fig. D.27: LRN-FB pre-loading mount 1.

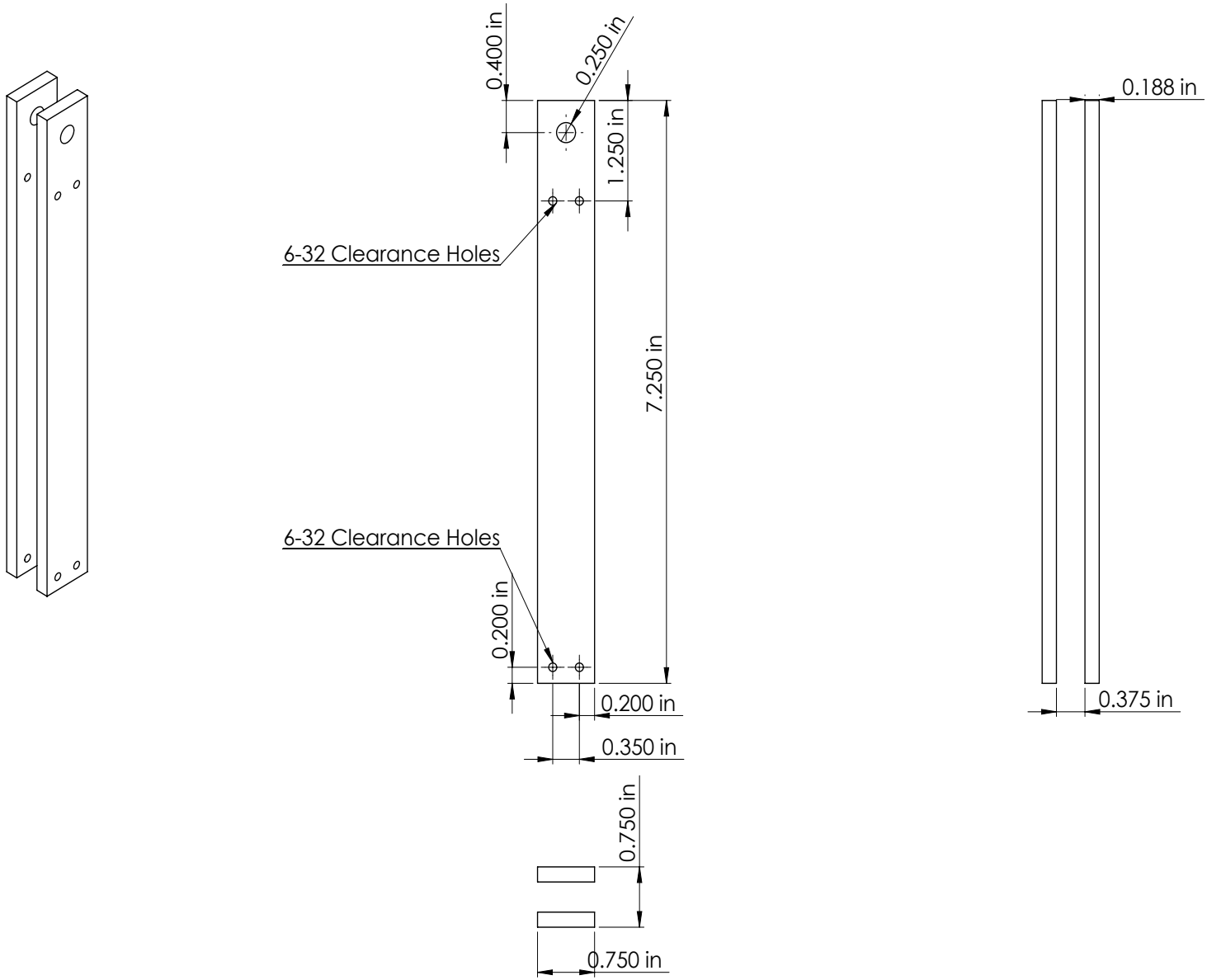


Fig. D.28: LRN-FB pre-loading mount 2.

210

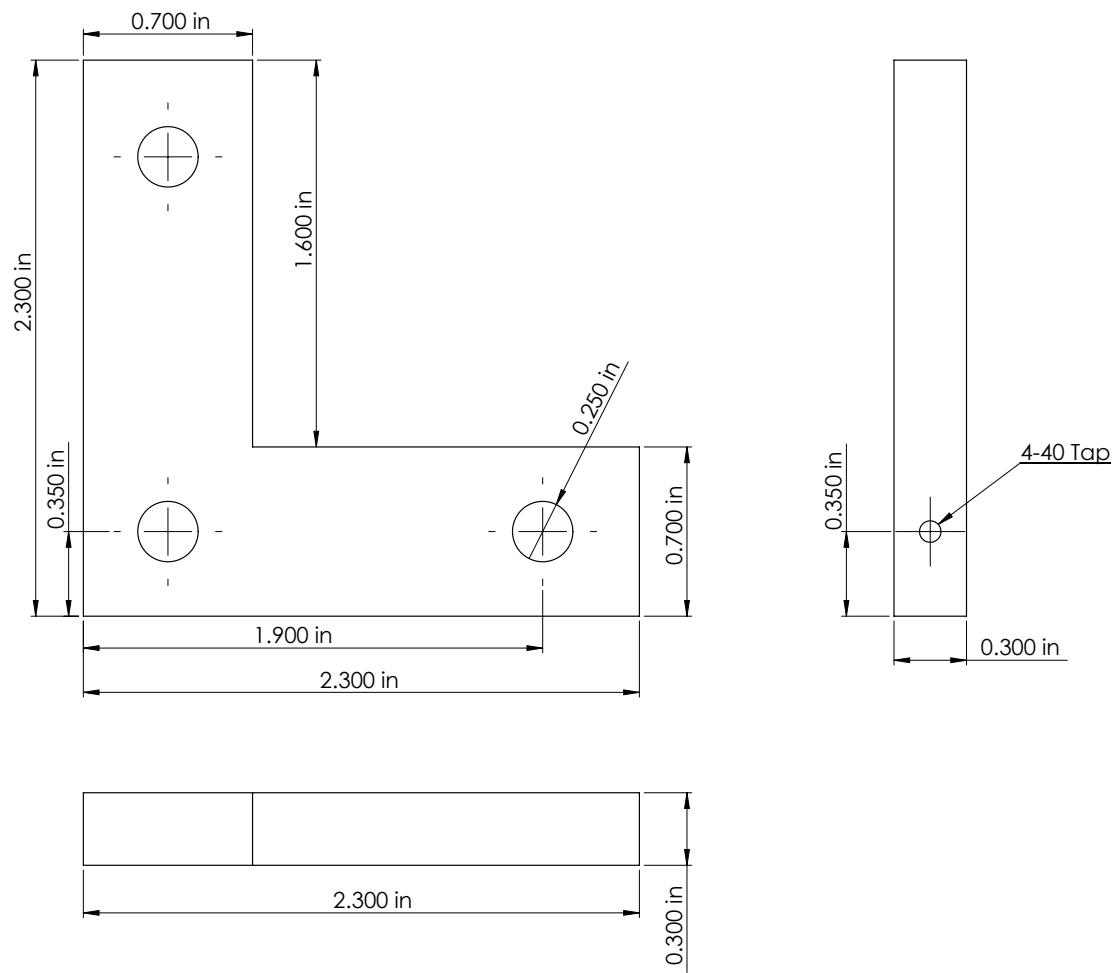
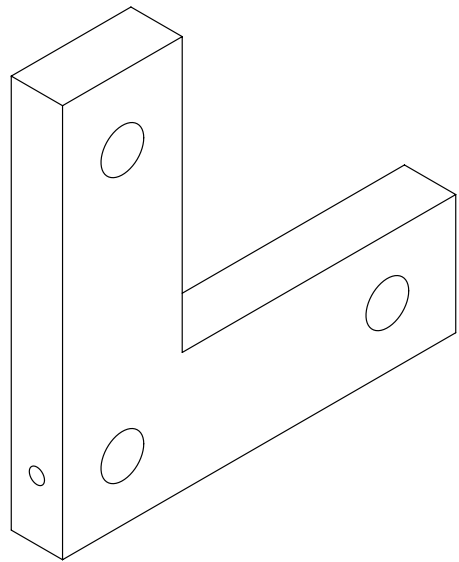


Fig. D.29: LRN-FB pre-loading l-shape bracket.

211

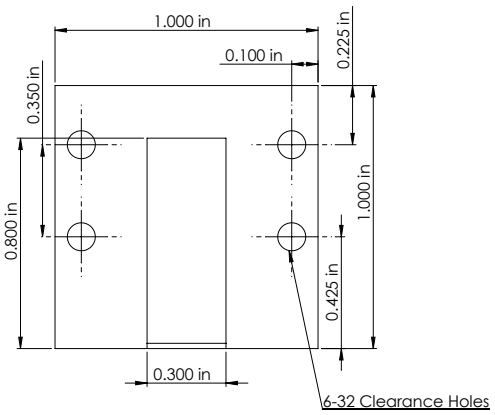
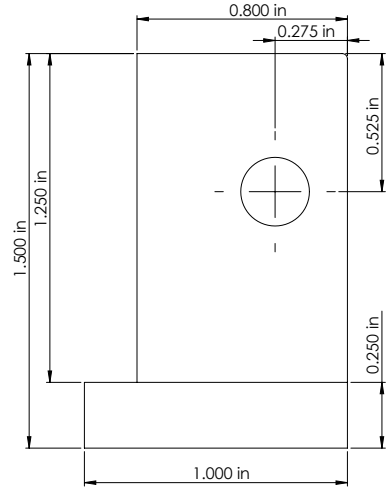
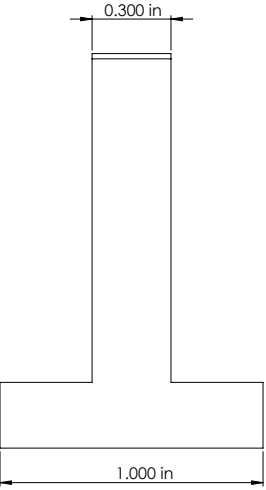
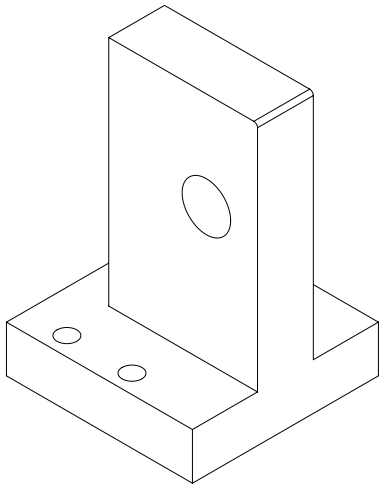


Fig. D.30: LRN-FB lift platform locking bracket.

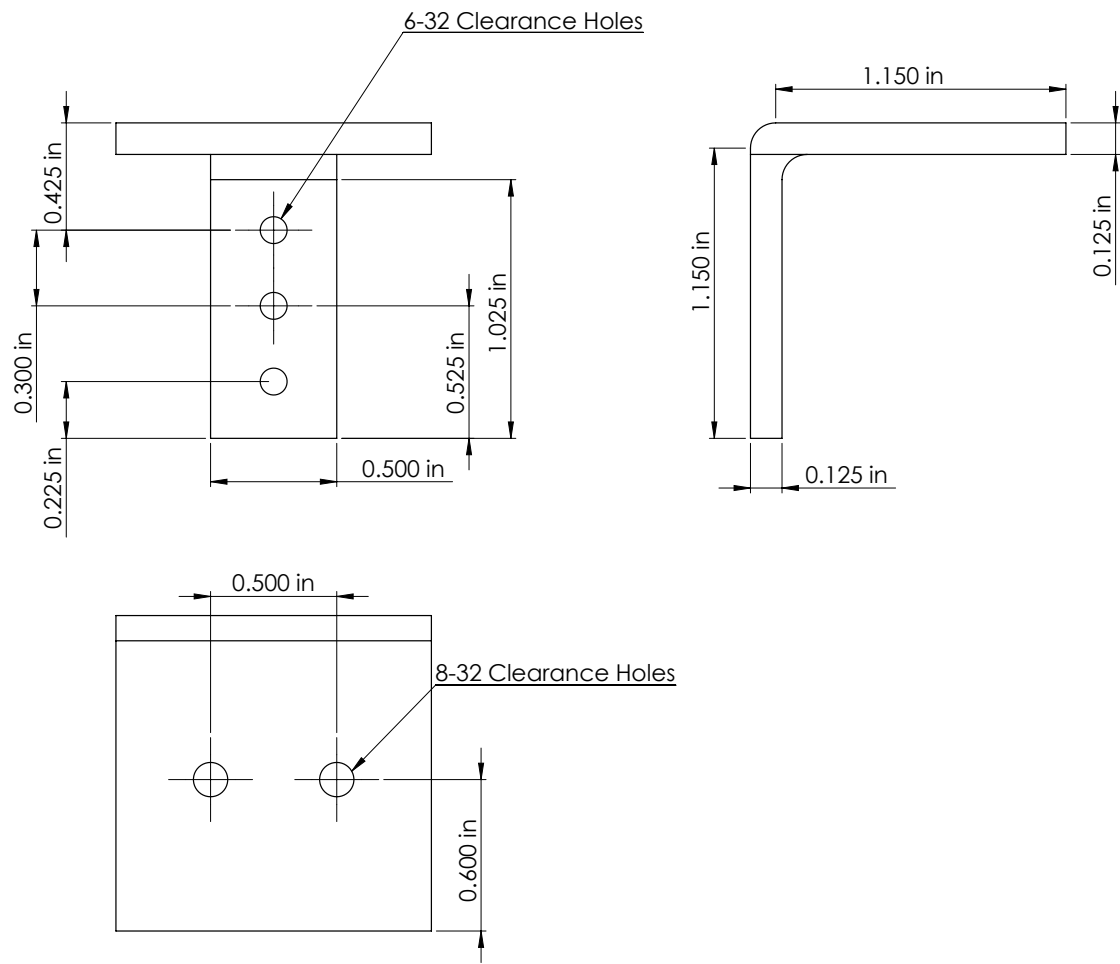
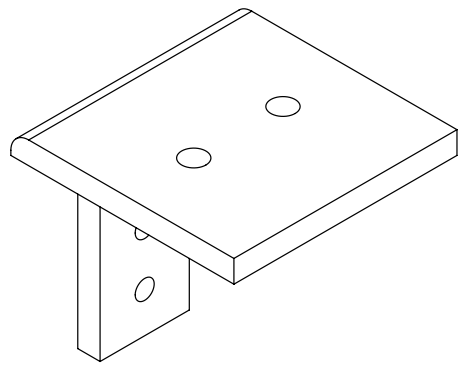


Fig. D.31: LRN-FB pre-loading corner bracket.

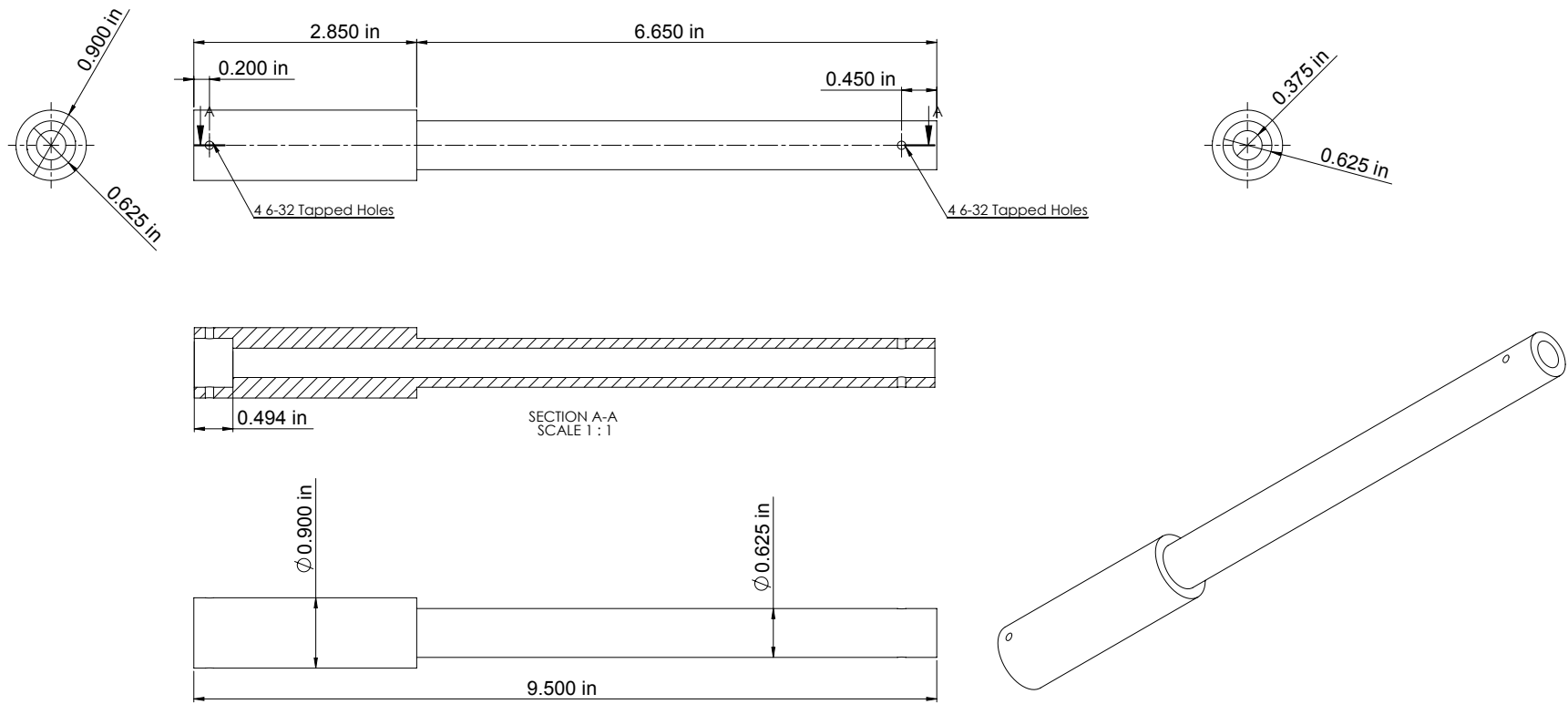


Fig. D.32: LRN-FB main sting (connected to flexure).

214

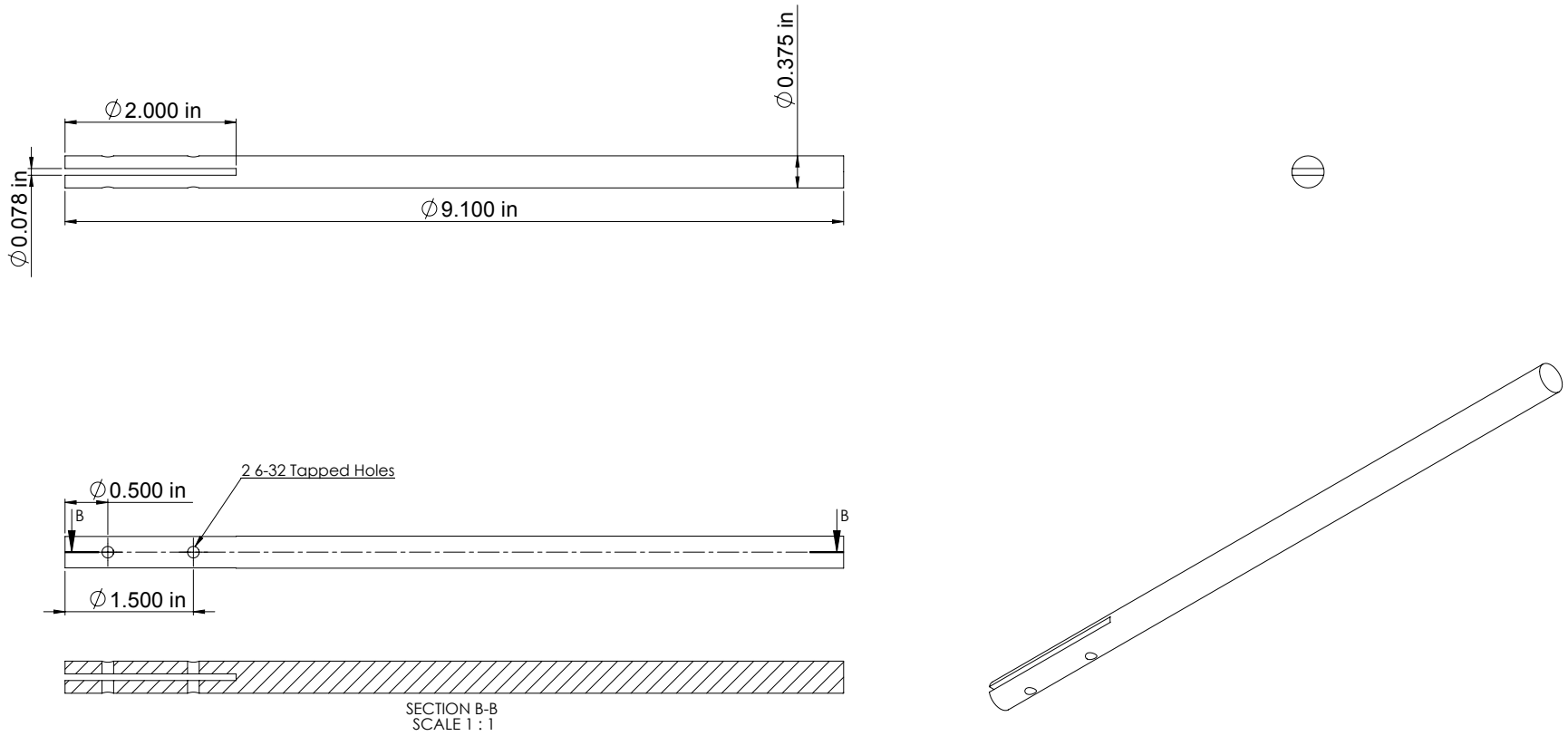


Fig. D.33: LRN-FB secondary sting.

References

- ¹ T. J. Mueller and J. D. DeLaurier. Aerodynamics of Small Vehicles. *Annual Review of Fluid Mechanics*, 35:89–111, Jan. 2003.
- ² S. Lupo, H. Nyberg, A. Karlsson, and K. Mohnseni. Xwing – A 3D Viscous Design Tool for Wings. AIAA Paper 2008-0173, Reno, NV, Jan. 2008.
- ³ P. Cosyn and J. Vierendeels. Numerical Investigation of Low-Aspect-Ratio Wings at Low Reynolds Numbers. *Journal of Aircraft*, 43(3):713–722, May–June 2006.
- ⁴ W. G. Bastedo Jr. and T. J. Mueller. Spanwise Variation of Laminar Separation Bubbles on Wings at Low Reynolds Numbers. *Journal of Aircraft*, 23(9):687–694, Sept. 1986.
- ⁵ A. Pelletier and T. J. Mueller. Low Reynolds Number Aerodynamics of Low-Aspect-Ratio Thin/Flat/Cambered-Plate Wings. *Journal of Aircraft*, 37(5):825–832, Sept.–Oct. 2000.
- ⁶ G. E. Torres and T. J. Mueller. Low-Aspect-Ratio Wing Aerodynamics at Low Reynolds Numbers. *Journal of Aircraft*, 42(5):865–873, May 2004.
- ⁷ E. V. Laitone. Wind Tunnel Tests of Wings at Reynolds Numbers below 70,000. *Experiments in Fluids*, 23(5):405–409, 1997.
- ⁸ M. Shields and K. Mohseni. Effects of Sideslip on the Aerodynamics of Low-Aspect-Ratio Low-Reynolds-Number Wings. *AIAA Journal*, 50(1):85–99, Jan. 2012.
- ⁹ M. Okamoto and A. Azuma. Aerodynamic Characteristics at Low Reynolds Number for Wings of Various Plansforms. *Journal of Aircraft*, 49(6):1135–1150, June 2011.
- ¹⁰ M. S. Selig, J. F. Donovan, and D. B. Fraser. *Airfoils at Low Speeds*. Soartech 8, SoarTech Publications, Virginia Beach, VA, 1989.
- ¹¹ M. S. Selig, J. J. Guglielmo, A. P. Broeren, and P. Giguère. *Summary of Low-Speed Airfoil Data*, volume 1. SoarTech Publications, Virginia Beach, VA, 1995.
- ¹² M. S. Selig, C. A. Lyon, P. Giguère, C. N. Ninham, and J. J. Guglielmo. *Summary of Low-Speed Airfoil Data*, volume 2. SoarTech Publications, Virginia Beach, VA, 1996.
- ¹³ C. A. Lyon, A. P. Broeren, P. Giguère, A. Gopalarathnam, and M. S. Selig. *Summary of Low-Speed Airfoil Data*, volume 3. SoarTech Publications, Virginia Beach, VA, 1997.
- ¹⁴ M. S. Selig and B. D. McGranahan. *Wind Tunnel Aerodynamic Tests of Six Airfoils for Use on Small Wind Turbines*. National Renewable Energy Laboratory, NREL/SR-500-35515, Golden, CO, 2004.

- ¹⁵ F. M. White. *Viscous Fluid Flow*. McGraw-Hill, New York, NY, third edition, 2005.
- ¹⁶ G. K. Batchelor. *An Introduction to Fluid Dynamics*. Cambridge University Press, 1967.
- ¹⁷ A. M. Kuethe and C. Y. Chow. *Foundations of Aerodynamics, Fifth Ed.* John Wiley and Sons, New York, 1998.
- ¹⁸ P. B. S. Lissaman. Low-Reynolds-Number Airfoils. *Annual Review of Fluid Mechanics*, 15, 1983.
- ¹⁹ M. S. Selig. Low Reynolds Number Airfoil Design. Number RTO/AVT-VKI-104. von Karman Institute for Fluid Dynamics (VKI) Lecture Series, Nov. 2003.
- ²⁰ H. P. Horton. *Laminar Separation Bubbles in Two and Three-Dimensional Incompressible Flow*. PhD thesis, Univ. of London, UK, 1968.
- ²¹ J. H. McMasters and M. L. Henderson. Low-Speed Single-Element Airfoil Synthesis. 6(2):1–21, 1980.
- ²² B. H. Carmichael. Low Reynolds Number Airfoil Survey. NASA Contractor Report 165803, Nov. 1981.
- ²³ A. Gopalarathnam and M. S. Selig. Design of Low Reynolds Number Airfoils with Trips. *Journal of Aircraft*, 40(4):768–775, July–August 2003.
- ²⁴ R. Ricci, S. Montelpare, and E. Silvi. Study of Acoustic Disturbances Effect on Laminar Separation Bubble by IR Thermography. *Experimental Thermal and Fluid Science*, 31(4):349–359, 2007.
- ²⁵ R. Eppler. Direkte Berechnung von Tragflügelprofilen aus der Druckverteilung. Inginieur-Archive 1, 1981. Translated as “Direct Calculation of Airfoils from Pressure Distribution,” NASA TT F-15, 417, 1974.
- ²⁶ R. Eppler and D. M. Somers. Low Speed Airfoil Design and Analysis. NASA CP 2045, 1979.
- ²⁷ R. Eppler and D. M. Somers. A Computer Program for the Design and Analysis of Low-Speed Airfoils. NASA TM 80210, August 1980.
- ²⁸ M. Drela. Low-Reynolds-Number Airfoil Design for the M.I.T. Deadalus Prototype: A Case Study. *Journal of Aircraft*, 25(8):724–732, 1988.
- ²⁹ M. Drela. XFOIL: An Analysis and Design System for Low Reynolds Number Airfoils. In T. J. Mueller, editor, *Low Reynolds Number Aerodynamics*, volume 54 of *Lecture Notes in Engineering*, pages 1–12. Springer-Verlag, New York, June 1988.
- ³⁰ M. S. Selig. Generalized Multipoint Inverse Airfoil Design. 30(11):2618–2625, 1992.
- ³¹ M. S. Selig. *Multi-Point Inverse Design of Isolated Airfoils and Airfoils in Cascade in Incompressible Flow*. PhD thesis, Dept. of Aerospace Engineering, Pennsylvania State Univ., University Park, PA, May 1992.
- ³² A. E. Winklemann and J. B. Barlow. A Flowfield Model for a Rectangular Planform Wing. *AIAA Journal*, 18(3):1006–1008, Aug. 1980.
- ³³ L. Prandtl. Applications of Modern Hydrodynamics to Aeronautics. TR 116, 1921.

- ³⁴ F. W. Lanchester. *Aerodynamics*. Constable & Co. Ltd., London, 1918.
- ³⁵ E. C. Polhamus. Predictions of Vortex-Lift Characteristics by a Leading-Edge Suction Analogy. *Journal of Aircraft*, 8(3):713–722, May–June 1971.
- ³⁶ E. C. Polhamus. A Concept of the Vortex Lift of Sharp-Edge Delta Wings Based on a Leading-Edge-Suction Analogy. NASA TN D-3767, Dec. 1966.
- ³⁷ M. Gad-el-Hak. Control of Low-Speed Airfoil Aerodynamics. *AIAA Journal*, 28(9):1537–1552, Sept. 1990.
- ³⁸ J. C. Kellogg. Case Study: Micro Tactical Expendable Rigid-Wing Micro Air Vehicle. In Thomas J. Mueller, James C. Kellogg, Peter G. Ifju, and Sergey V. Shkarayev, editors, *Introduction to the Design of Fixed-Wing Micro Air Vehicles*, pages 151–184. AIAA Educational Series, AIAA, Reston, VA, 2006.
- ³⁹ J. M. Grassmeyer and M. T. Keenon. Development of the Black Widow Micro Air Vehicle. AIAA Paper 2001-0127, Reno, NV, Jan. 2001.
- ⁴⁰ P. G. Ifju, D. A. Jenkins, S. Ettinger, Y. Lian, W. Shyy, and M. R. Waszak. Flexible-Wing-Based Micro Air Vehicles. AIAA Paper 2002-0705, Reno, NV, Jan. 2002.
- ⁴¹ Y. Lian and W. Shyy. Three Dimensional Fluid Structure Interactions of a Membrane Wing for MAV Applications. AIAA Paper 2003-1726, Norfolk, VA, April 2003.
- ⁴² R. Albertani. *Experimental Aerodynamic of Elastic Deformation Characterization of Low Aspect Ratio Finite Wings Applied to Micro Air Vehicles*. PhD thesis, Dept. of Mechanical and Aerospace Engineering, University of Florida, Gainesville, FL, 2005.
- ⁴³ R. Albertani, B. Stanford, J. Hubner, and P. Ifju. Aerodynamic Characterization and Deformation Measurements of a Flexible Wing Micro Air Vehicle. *Experimental Mechanics*, 47(5):625–635, 2007.
- ⁴⁴ W. Null and S. Shkarayev. Effects of Camber on the Aerodynamics of Adaptive-Wing Micro Air Vehicles. *Journal of Aircraft*, 42(6):1537–1542, Nov.–Dec. 2005.
- ⁴⁵ W. Null, A. Noseck, and S. Shkarayev. Effects of Propulsive-Induced Flow on the Aerodynamics of Micro Air Vehicles. AIAA Paper 2005-4616, Toronto, Ontario, June 2005.
- ⁴⁶ S. Shkarayev, J.-M. Moschetta, and B. Bataille. Aerodynamic Design of Micro Air Vehicles for Vertical Flight. *Journal of Aircraft*, 45(5):1715–1724, Sept.–Oct. 2008.
- ⁴⁷ K. Ailinger. Micro Air Vehicle (MAV) Development at NRL. Arlington, VA, June 1997. Association of Unmanned Vehicle Systems International Conference 1997 (AUVSI '97).
- ⁴⁸ J. C. Kellogg, C. Bovais, J. Foch, R. Gardner, D. Gordon, R. Hartley, B. Kamgar-Parsi, H. McFarlene, F. Pipitone, R. Ramamurthy, R. Sciambi, W. Spears, D. Scrull, and C. Sullivan. The NRL Micro Tactical Expendable (MITE) Air Vehicle. *The Aeronautical Journal*, pages 431–441, 106(1062), August 2002.
- ⁴⁹ J.-M. Moschetta and C. Thipyopas. Aerodynamic Performance of a Biplane Micro Air Vehicle. *Journal of Aircraft*, 44(1):291–299, 2007.

- ⁵⁰ T. J. Mueller. Aerodynamic Measurements at Low Reynolds Numbers for Fixed Wing Micro-Air Vehicles. Rhode-St-Genèse, Belgium, Sept. 1999. RTO AVT/VKI Special Course.
- ⁵¹ M. Shields and K. Mohnseni. Experimental Complications Inherent to Low Reynolds Number Wind Tunnel Testing. AIAA Paper 2011-0873, Orlando, FL, Jan. 2011.
- ⁵² S. M. Kaplan, A. Altman, and M. Ol. Wake Vorticity Measurements for Low Aspect Ratio Wings at Low Reynolds Numbers. *Journal of Aircraft*, 44(1):241–251, 2007.
- ⁵³ D. J. Pines and F. Bohorquez. Challenges Facing Future Micro-Air-Vehicle Development. *Journal of Aircraft*, 43(2):290–305, March–April 2006.
- ⁵⁴ M. S. Selig, R. W. Deters, and G. A. Williamson. Wind Tunnel Testing Airfoils at Low Reynolds Numbers. AIAA Paper 2011-0875, Jan. 2011.
- ⁵⁵ J. B. Barlow, W. H. Rae Jr., and A. Pope. *Low-Speed Wind Tunnel Testing*. John Wiley and Sons, New York, 3rd edition, 1999.
- ⁵⁶ Anonymous. Setra[®] Sensing Solutions - Model 239 Differential Pressure Transducer. http://http://www.setra.com/ProductDetails/model_239.htm, Accessed April 2012.
- ⁵⁷ Anonymous. MSK Instruments - 220DD Baratron[®] Differential Capacitance Manometer. <http://www.mksinst.com/product/product.aspx?ProductID=158>, Accessed Feb. 2012.
- ⁵⁸ Anonymous. MSK Instruments - 221B Baratron[®] Differential Capacitance Manometer. <http://www.mksinst.com/product/product.aspx?ProductID=160>, Accessed Feb. 2012.
- ⁵⁹ S. S. W. Lam. A FORTRAN Program for the Calculation of the Calibration Coefficient of a Six-Component Strain Gauge Balance. Flight Mechanics Technical Memorandum 410, Aeronautical Research Laboratory, Defence Science and Technology Organisation, Melbourne, Australia, 1989.
- ⁶⁰ S. Y. F. Leung and Y. Y. Link. Comparison and Analysis of Strain Gauge Balance Calibration Matrix Mathematical Models. DSTO 857, Aeronautical and Maritime Research Laboratory, Defence Science and Technology Organisation, Melbourne, Australia, 1999.
- ⁶¹ M. A. Ramaswamy, T. Srinivas, and V. S. Holla. A Simple Method for Wind Tunnel Balance Calibration Including Non-Linear Interaction Terms. Technical Report A88-36483 14-35, Williamsburg, VA,, June 1987.
- ⁶² Anonymous. Realize,[®] Inc. Rapid Prototyping, Rapid Prototypes, Stereolithography. <http://www.realizeinc.com/>, Accessed Feb. 2012.
- ⁶³ J. F. Marchman. Aerodynamic Testing at Low Reynolds Numbers. *Journal of Aircraft*, 24(2):107–114, Feb. 1987.
- ⁶⁴ M. S. Selig. UIUC APA - LSATs. http://www.ae.illinois.edu/m-selig/uiuc_lsat.html, Accessed Feb. 2012.
- ⁶⁵ M. Drela. XFOIL Subsonic Airfoil Development System. <http://web.mit.edu/drela/Public/web/xfoil/>, Accessed March 2012.
- ⁶⁶ R. C. Pankhurst and D. W. Holder. *Wind-Tunnel Technique*. Pitman Publishing Corporation, 1952.

- ⁶⁷ E. C. Maskell. A Theory of the Blockage Effects on Bluff Bodies and Stalled Wings in a Closed Wind Tunnel. ARC R&M 3400, 1965.
- ⁶⁸ S. C. Noe. Force Balance Measurements of Wind-Turbine Airfoil Performance with Simulated Leading-Edge Ice Accretions. Master's thesis, University of Illinois at Urbana-Champaign, Department of Aerospace Engineering, 1996.
- ⁶⁹ S. Kline and F. A. McClintock. Describing Uncertainty in Single-Sample Experiments. *Mechanical Engineering*, 75:3–8, 1953.
- ⁷⁰ H. W. Coleman and W. G. Steele Jr. *Experimentation and Uncertainty Analysis for Engineers*. John Wiley and Sons, New York, 1989.
- ⁷¹ M. S. Selig. The Design of Airfoils at Low Reynolds Numbers. AIAA Paper 1985-0074, Reno, NV, Jan. 1985.
- ⁷² D. Althaus. *Profilpolaren für den Modellflug (Windkanalmessungen an Profile im Kritischen Reynoldszahlbereich)*. Necker-Verlag, Villingen-Schwenningen, Germany, 1980.
- ⁷³ B. W. McCormick. *Aerodynamics Aeronautics and Flight Mechanics, Second Ed.* John Wiley & Sons, New York, 1995.